BIOSYNTHESIS OF AMINO ACIDS AND THEIR DERIVED CHEMICALS FROM RENEWABLE FEEDSTOCK

EDITED BY: Liming Liu, Yi-Rui Wu, Congqiang Zhang and K. Madhavan Nampoothiri

PUBLISHED IN: Frontiers in Bioengineering and Biotechnology

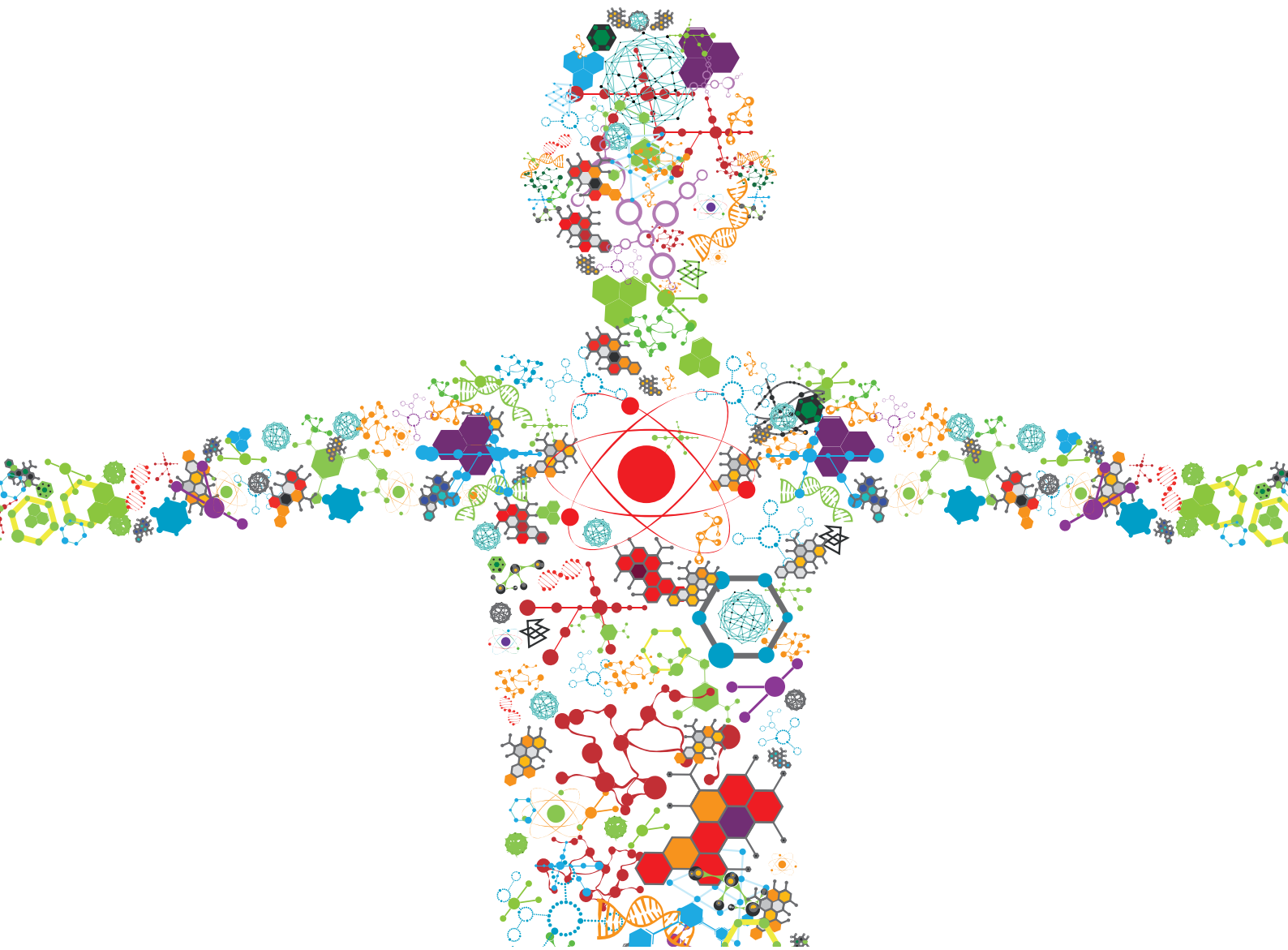

frontiers Research Topics

frontiers

ISSN 1664-8714
ISBN 978-2-88974-145-8
DOI 10.3389/978-2-88974-145-8

About Frontiers

Frontiers is more than just an open-access publisher of scholarly articles: it is a pioneering approach to the world of academia, radically improving the way scholarly research is managed. The grand vision of Frontiers is a world where all people have an equal opportunity to seek, share and generate knowledge. Frontiers provides immediate and permanent online open access to all its publications, but this alone is not enough to realize our grand goals.

Frontiers Journal Series

The Frontiers Journal Series is a multi-tier and interdisciplinary set of open-access, online journals, promising a paradigm shift from the current review, selection and dissemination processes in academic publishing. All Frontiers journals are driven by researchers for researchers; therefore, they constitute a service to the scholarly community. At the same time, the Frontiers Journal Series operates on a revolutionary invention, the tiered publishing system, initially addressing specific communities of scholars, and gradually climbing up to broader public understanding, thus serving the interests of the lay society, too.

Dedication to Quality

Each Frontiers article is a landmark of the highest quality, thanks to genuinely collaborative interactions between authors and review editors, who include some of the world's best academicians. Research must be certified by peers before entering a stream of knowledge that may eventually reach the public - and shape society; therefore, Frontiers only applies the most rigorous and unbiased reviews.
Frontiers revolutionizes research publishing by freely delivering the most outstanding research, evaluated with no bias from both the academic and social point of view. By applying the most advanced information technologies, Frontiers is catapulting scholarly publishing into a new generation.

What are Frontiers Research Topics?

Frontiers Research Topics are very popular trademarks of the Frontiers Journals Series: they are collections of at least ten articles, all centered on a particular subject. With their unique mix of varied contributions from Original Research to Review Articles, Frontiers Research Topics unify the most influential researchers, the latest key findings and historical advances in a hot research area! Find out more on how to host your own Frontiers Research Topic or contribute to one as an author by contacting the Frontiers Editorial Office: frontiersin.org/about/contact

BIOSYNTHESIS OF AMINO ACIDS AND THEIR DERIVED CHEMICALS FROM RENEWABLE FEEDSTOCK

Topic Editors:
Liming Liu, Jiangnan University, China
Yi-Rui Wu, Shantou University, China
Congqiang Zhang, Technology and Research (A*STAR), Singapore
K. Madhavan Nampoothiri, National Institute for Interdisciplinary Science and Technology (CSIR), India

Citation: Liu, L., Wu, Y.-R., Zhang, C., Nampoothiri, K. M., eds. (2022). Biosynthesis of Amino Acids and Their Derived Chemicals From Renewable Feedstock. Lausanne: Frontiers Media SA. doi: 10.3389/978-2-88974-145-8

Table of Contents

frontiers in Bioengineering and Biotechnology

EDITORIAL
published: 13 October 2021
doi: 10.3389/fbioe.2021.770002

Editorial: Biosynthesis of Amino Acids and Their Derived Chemicals From Renewable Feedstock

Yi-Rui Wu[1,2]*, *K. Madhavan Nampoothiri*[3], *Congqiang Zhang*[4] and *Liming Liu*[5]

[1]Department of Biology, Shantou University, Shantou, China, [2]Beijing Tidetron Bioworks Company, Beijing, China, [3]National Institute for Interdisciplinary Science and Technology (CSIR), Thiruvananthapuram, India, [4]Singapore Institute of Food and Biotechnology Innovation (SIFBI), Agency for Science, Technology and Research, Singapore, Singapore, [5]State Key Laboratory of Food Science and Technology, Jiangnan University, Wuxi, China

Keywords: amino acids, biomanufacturing, metabolic engineering, microbial fermentation, renewable feedstock

Editorial on the Research Topic

Biosynthesis of Amino Acids and their Derived Chemicals from Renewable Feedstock

This research topic aimed to introduce the current advancements in the biosynthesis of amino acids and their derived products from renewable feedstocks. Authors were invited to contribute original research and review articles that provided a comprehensive discussion and analysis of the current success and future outlooks for biosynthesis of various amino acids and derived chemicals. A total of 12 manuscripts were submitted, and 11 were accepted for publication after a thorough and rigorous peer review process. The papers were selected in such a way to give a flavor of a variety of topics related to the production of amino acids and their derived products, including biological and chemical catalytic production, design and construction of new molecular pathways for amino acid production, application of metabolic engineering and synthetic biology strategies, as well as the utilization of non-food renewable feedstock such as rice straw. We believed that the papers in this research topic would bring readers the latest advances in these fields.

Bioproduction of 5-aminovalerate (5AVA) from renewable feedstock could support a sustainable biorefinery process to produce bioplastics. The paper by Cheng et al. developed a promising artificial pathway for the efficient 5AVA synthesis by establishing a 2-keto-6-aminocaproate-mediated pathway. Introduction of L-lysine α-oxidase from *Scomber japonicas*, α-ketoacid decarboxylase from *Lactococcus lactis* and aldehyde dehydrogenase from *Escherichia coli* could finally achieved the biosynthesis of 5AVA from L-lysine with the high titre through the fed-batch fermentation. Another paper by Cheng et al. further presented an efficient biobased co-production of 5AVA and δ-valerolactam in *E. coli* from L-lysine. With the optimized cultivation conditions, the titers of 5AVA and δ-valerolactam were improved, and their ratio was identified to be affected by pH values. The paper by Sasikumar et al. established the production of 5AVA and putrescine from the biomass-derived sugars by using the engineered *Corynebacterium glutamicum* strain. It was indicated that with the heterologous introduction of genes $xylA_{Xc}$ and $xylB_{Cg}$, the modified strain could co-produce putrescine and 5-AVA by consuming a blend of glucose and xylose. Further investigation by using alkali-hydrolases pretreated rice straw hydrolysate (RSH) as the raw material also yielded the generation of putrescine and 5AVA. The paper by Brito et al. demonstrated another study involved in the methanol-based production of 5AVA using genetically modified *Bacillus methanolicus*. Five different metabolic pathways were evaluated, whereof two directly converted L-lysine to 5AVA and three used cadaverine as an intermediate. The results indicated the proof-of-concept 5AVA production from methanol at 50°C, enabled by two pathways out of the five tested with the

OPEN ACCESS

Edited and reviewed by:
Georg M. Guebitz,
University of Natural Resources and Life Sciences Vienna, Austria

***Correspondence:**
Yi-Rui Wu
wuyr@stu.edu.cn
wuyr@creapep.com

Specialty section:
This article was submitted to Industrial Biotechnology, a section of the journal Frontiers in Bioengineering and Biotechnology

Received: *03 September 2021*
Accepted: *21 September 2021*
Published: *13 October 2021*

Citation:
Wu Y-R Nampoothiri KM, Zhang C and Liu L (2021) Editorial: Biosynthesis of Amino Acids and Their Derived Chemicals From Renewable Feedstock. Front. Bioeng. Biotechnol. 9:770002. doi: 10.3389/fbioe.2021.770002

highest titer, representing the first report of 5AVA production from methanol in the methylotrophic bacteria.

Protocatechuic acid (PCA) was a strong antioxidant and could also be used as a potential platform for polymer building blocks. The paper by Englund Örn et al. presented the production of PCA from glucose through the shikimate pathway by heterologously expressing 3-dehydroshikimate dehydratase encoded gene in *E. coli*. With the overproduction of phenylalanine to relieve the allosteric inhibition of 3-deoxy-7-phosphoheptulonate synthase by the aromatic amino acids, the engineered strain was shown to achieve a highest PCA yield during cultivation in fed-batch mode using a feed of glucose and ammonium salt. As another trifunctional building block, L-2-hydroxyglutarate (L-2HG) was also highly attractive for the chemical and pharmaceutical industries. The paper by Prell et al. demonstrated the natural biosynthesis of L-2HG by metabolically engineering *C. glutamicum* through the construction of a gene cassette involved in a six-step synthetic pathway. The modified strain with media adaptation was observed to produce L-2HG in a micro-cultivation system, and a high titer of L-2HG was finally achieved via a glucose-based process in a 2 L bioreactor.

L-Carnitine was a bioactive compound derived from L-lysine and S-adenosyl-L-methionine. The paper by Kugler et al. described the metabolic engineering of *E. coli* for L-carnitine production by introducing and optimizing a four-step pathway from the fungus *Neurospora crassa*. The engineered strain was investigated to produce L-carnitine by supplementing L-Nε-trimethyllysine for biotransformation. The work provided a proof of concept as the first report for the *de novo* L-carnitine production in the engineered bacteria.

The paper by Ren et al. presented *Saccharopolyspora erythraea* as an excellent host to produce valuable heterologous polyketides. The recombinant strain AbΔery was genetically generated by knocking out the erythromycin biosynthesis gene cluster via the CRISPR-Cas9 system, and three heterologous genes driven by strong promoters were subsequently introduced to produce novel polyketide by using L-tyrosine and methylmalonyl-CoA as the substrates. With the final product of (E)-4-hydroxy-6-(4-hydroxystyryl)-3,5-dimethyl-2H-pyrone identified by LC-MS, the engineered strain AbΔery could potentially serve as a precious heterologous host to boost the synthesis of other valuable polyketone compounds.

The paper by E et al. investigated the effect of biochar on an enhanced production of L-histidine from glucose by *E. coli*. The optimal biochar concentration was demonstrated, and too high-concentration treatment was found to inhibit the yield. A regulatory protein (HisG) was further identified to be responsible for the improved L-histidine production through the protein docking analysis and gene overexpression.

Corynebacterium glutamicum was a model Gram-positive bacterium that had been extensively engineered to produce amino acids and other chemicals. The review paper from Zhang et al. summarized the recent progress on the metabolic engineering of *C. glutamicum* towards various chemicals production, and also discussed potential manners to broaden its substrate spectrum to those non-food sustainable carbon sources such as xylose, methanol, arabinose, glycerol, etc. The review paper from Liu et al. also provided examples to illustrate the latest progress on the microbial synthesis of 5-hydroxytryptophan (5-HTP) in the manner of the directed evolution and metabolic engineering.

AUTHOR CONTRIBUTIONS

All authors listed have made a substantial, direct, and intellectual contribution to the work and approved it for publication.

ACKNOWLEDGMENTS

We would like to thank all the authors and reviewers who contributed to this Research Topic. This publication would not be possible without the participation of our expert reviewers, who provided constructive feedback and criticism throughout the review process.

Author Disclaimer: This editorial summarized the papers submitted to our research topic and was not an endorsement by the authors' agency or institution of the view or position of the paper's authors.

Conflict of Interest: Y-RW is also employed by Beijing Tidetron Bioworks Company.

The remaining authors declare that the research was conducted in the absence of any commercial or financial relationships that could be construed as a potential conflict of interest.

Publisher's Note: All claims expressed in this article are solely those of the authors and do not necessarily represent those of their affiliated organizations, or those of the publisher, the editors, and the reviewers. Any product that may be evaluated in this article, or claim that may be made by its manufacturer, is not guaranteed or endorsed by the publisher.

frontiers in Bioengineering and Biotechnology

REVIEW
published: 10 December 2020
doi: 10.3389/fbioe.2020.606047

Recent Progress on Chemical Production From Non-food Renewable Feedstocks Using *Corynebacterium glutamicum*

Bin Zhang[1,2], Yan Jiang[1,2], Zhimin Li[1,2], Fei Wang[1,2] and Xiao-Yu Wu[1,2]*

[1] College of Bioscience and Bioengineering, Jiangxi Agricultural University, Nanchang, China, [2] Jiangxi Engineering Laboratory for the Development and Utilization of Agricultural Microbial Resources, Jiangxi Agricultural University, Nanchang, China

Due to the non-renewable nature of fossil fuels, microbial fermentation is considered a sustainable approach for chemical production using glucose, xylose, menthol, and other complex carbon sources represented by lignocellulosic biomass. Among these, xylose, methanol, arabinose, glycerol, and other alternative feedstocks have been identified as superior non-food sustainable carbon substrates that can be effectively developed for microbe-based bioproduction. *Corynebacterium glutamicum* is a model gram-positive bacterium that has been extensively engineered to produce amino acids and other chemicals. Recently, in order to reduce production costs and avoid competition for human food, *C. glutamicum* has also been engineered to broaden its substrate spectrum. Strengthening endogenous metabolic pathways or assembling heterologous ones enables *C. glutamicum* to rapidly catabolize a multitude of carbon sources. This review summarizes recent progress in metabolic engineering of *C. glutamicum* toward a broad substrate spectrum and diverse chemical production. In particularly, utilization of lignocellulosic biomass-derived complex hybrid carbon source represents the futural direction for non-food renewable feedstocks was discussed.

Keywords: *Corynebacterium glutamicum*, renewable feedstocks, metabolic engineering, chemical, fermentation

OPEN ACCESS

Edited by:
Yi-Rui Wu,
Shantou University, China

Reviewed by:
Wenming Zhang,
Nanjing Tech University, China
K. Madhavan Nampoothiri,
National Institute for Interdisciplinary Science and Technology (CSIR), India

****Correspondence:***
Bin Zhang
zhangbin2919@jxau.edu.cn

Specialty section:
This article was submitted to Industrial Biotechnology, a section of the journal Frontiers in Bioengineering and Biotechnology

Received: *14 September 2020*
Accepted: *31 October 2020*
Published: *10 December 2020*

Citation:
Zhang B, Jiang Y, Li Z, Wang F and Wu X-Y (2020) Recent Progress on Chemical Production From Non-food Renewable Feedstocks Using Corynebacterium glutamicum. Front. Bioeng. Biotechnol. 8:606047. doi: 10.3389/fbioe.2020.606047

INTRODUCTION

Since isolation in 1957, *Corynebacterium glutamicum* has been intensively applied for biobased chemical production due to its ability to secrete amino acids, which are traditionally used as drugs or health products (Kogure and Inui, 2018; Wu et al., 2019). These amino acids and their derived chemicals are worth billions of dollars per year. Development of engineered strains with higher production performance is an active field that has attracted numerous researchers (Lee and Wendisch, 2017b; Li et al., 2017; D'Este et al., 2018; Zhang et al., 2018a,b). In particular, most amino acids, including L-glutamate, L-lysine, L-arginine, L-valine, and L-ornithine, have achieved industrial-scale production due to rapid development of gene-editing and fermentation-manipulation techniques. These amino acids are used in human nutrition, food additives, and drug preparation, applications that benefit from the use of biologically safe *C. glutamicum* (Lee and Wendisch, 2017a). In addition to amino acids, *C. glutamicum* has also been extensively modulated to produce a multitude of valuable products, including bulk chemicals, natural products,

polymers, proteins, and biofuels (Becker et al., 2018b; Shanmugam et al., 2018, 2019; Wendisch et al., 2018). This vigorous development has benefited from fossil fuel depletion and anthropogenic climate change caused by the emission of toxic gases generated from oil decomposition, which traditionally served as the major source of manufactured chemicals (Sun et al., 2018). However, biobased production of metabolites using *C. glutamicum* consumes large amounts of glucose, obtained from the hydrolysis reaction of starch, creating competition for food with humans. Hence, it is critical to exploit alternative renewable carbon sources, such as agricultural wastes, industrial wastes, and others for the cultivation of industrial model strains. In the past few years, research efforts have shifted toward biobased production of metabolites from non-food renewable feedstocks. Here are summarized recent advances in the utilization of alternative C-resources, including xylose, arabinose, methanol, glycerol, and mannitol, to produce high-value chemicals using *C. glutamicum* (**Figure 1**).

BIOCONVERSION OF SINGLE-CARBON SOURCES TO VALUABLE CHEMICALS

Xylose

Xylose, a pentose, is the major constituent of lignocellulose biomass, and was deemed to be the second most abundant biological resource, after glucose (Elmore et al., 2020). High-value utilization of xylose is shifting from bioenergy to a broader range of chemicals. Engineering microbes to produce biobased chemicals from xylose provides a potential alternative to threatening human food security by continuing to use glucose. In *C. glutamicum*, the absence of xylose isomerase means there is no established endogenous metabolic pathway for xylose assimilation. To overcome this obstacle, *xylA*, which encodes xylose isomerase and originates from various microorganisms, has been amplified and employed to reconstruct the xylose utilization metabolic pathway in *C. glutamicum* (Zhao et al., 2018). Heterologous expression of *xylA* from *Xanthomonas campestris* converts imported xylose into xylulose, demonstrating better performance than *xylA* from other microbial species. Tandem expression of *X. campestris xylAB* operon by employing a plasmid or chromosomal insertion of gene copy approach enables impressive conversion of xylose to chemicals in *C. glutamicum* (**Table 1**). For instance, we previously demonstrated plasmid-based expression of *X. campestris xylAB* operon in the L-ornithine-producing strain *C. glutamicum* SO26 that significantly improved the yield of L-ornithine. By adjusting the expression of the *xylAB* operon, we achieved an L-ornithine titer of 18.9 g/L, representing the highest L-ornithine production titer from xylose recorded to date (Zhang et al., 2019). In contrast to the xylose isomerase (XI) pathway, the Weimberg (WMB) pathway, consisting of multistep reactions catalyzed by enzymes including xylose dehydrogenase, xylonolactonase, xylonate dehydratase, 2-keto-3-deoxy-D-xylonate dehydratase, and α-ketoglutarate semialdehyde dehydrogenase, was introduced into *C. glutamicum* to progressively convert xylose to α-ketoglutarate (**Figure 1**; Zhao et al., 2018; Choi et al., 2019). The enzymes involved in the WMB pathway are encoded by genes listed as belonging to the *xylXABCD* operon in *Caulobacter crescentus*. Heterologous expression of the *xylXABCD* operon allowed *C. glutamicum* to utilize xylose without loss of carbon; however, cell growth was hindered by inferior metabolic flux. To overcome this growth inhibition, the mutated strain *C. glutamicum* WMB2evo was selected by adaptive laboratory evolution, providing a 3.7-fold increase in growth rate compared to the original strain (Radek et al., 2017). Results from comparative genomics analysis suggest that mutations in IolR, which upregulated the expression of *iolT1*, significantly improved xylose transport and contributed to increased cell growth (Radek et al., 2017). It is universally acknowledged that reinforcing the xylose uptake system markedly increases conversion from xylose to valuable chemicals. Currently, two transmembrane proteins capable of transporting xylose, XylE (Yim et al., 2016) and AraE (Chen Z. et al., 2017), are applied to boost xylose utilization, which promotes the accumulation of metabolites. *C. glutamicum* ATCC 31831, possessing the endogenic arabinose transporter AraE, and *C. glutamicum* ATCC 13032, which lacks this transporter, were simultaneously modulated to produce xylonic acid from xylose; as a result, engineered *C. glutamicum* ATCC 31831 produced approximately 10% more xylonic acid than engineered *C. glutamicum* ATCC 13032 (Sundar et al., 2020). During 120 h of fermentation, 75% xylose consumption in the engineered *C. glutamicum* ATCC 31831 strain likewise outstripped the 60% xylose consumption observed in the AraE-absent *C. glutamicum* ATCC 13032 strain. It can be widely accepted that *C. glutamicum* ATCC 31831 is a superior host for the conversion from xylose to valued chemicals. A robust uptake system exerts the crucial role in xylose utilization by using *C. glutamicum*. Although xylose is the second abundant carbon source next to glucose, the fermentation of pure xylose to produce compounds has been little investigated. This probably due to xylose generally derives from complex carbon sources, frequently obtained by the pretreatment of cellulose, rather than pure sugars like glucose.

Methanol

Methanol is an attractive alternative feedstock that can be easily obtained from the oxidation of methane. Ongoing development of natural gas, the main source of methane, and use of exploitation technology enable the steady conversion from methane to methanol, continuously reducing the price of methanol (Zhao et al., 2018). Consequently, microbes engineered to convert methanol to valuable metabolites have received considerable attention regarding their comparable cost to glucose-based processes. In microbes, the ribulose monophosphate (RuMP) pathway demonstrates advantages in generating ATP and NAD(P)H, which are frequently used for methanol assimilation, a process in which methanol is converted to fructose 6-phosphate, catalyzed by methanol dehydrogenase (encoded by *mdh*), 3-hexulose-6-phosphate synthase (encoded by *hps*), and 6-phospho-3-hexuloisomerase (encoded by *phi*) (**Figure 1**; Zhao et al., 2018). In addition to natural occurrence in methylotrophic microorganisms, the

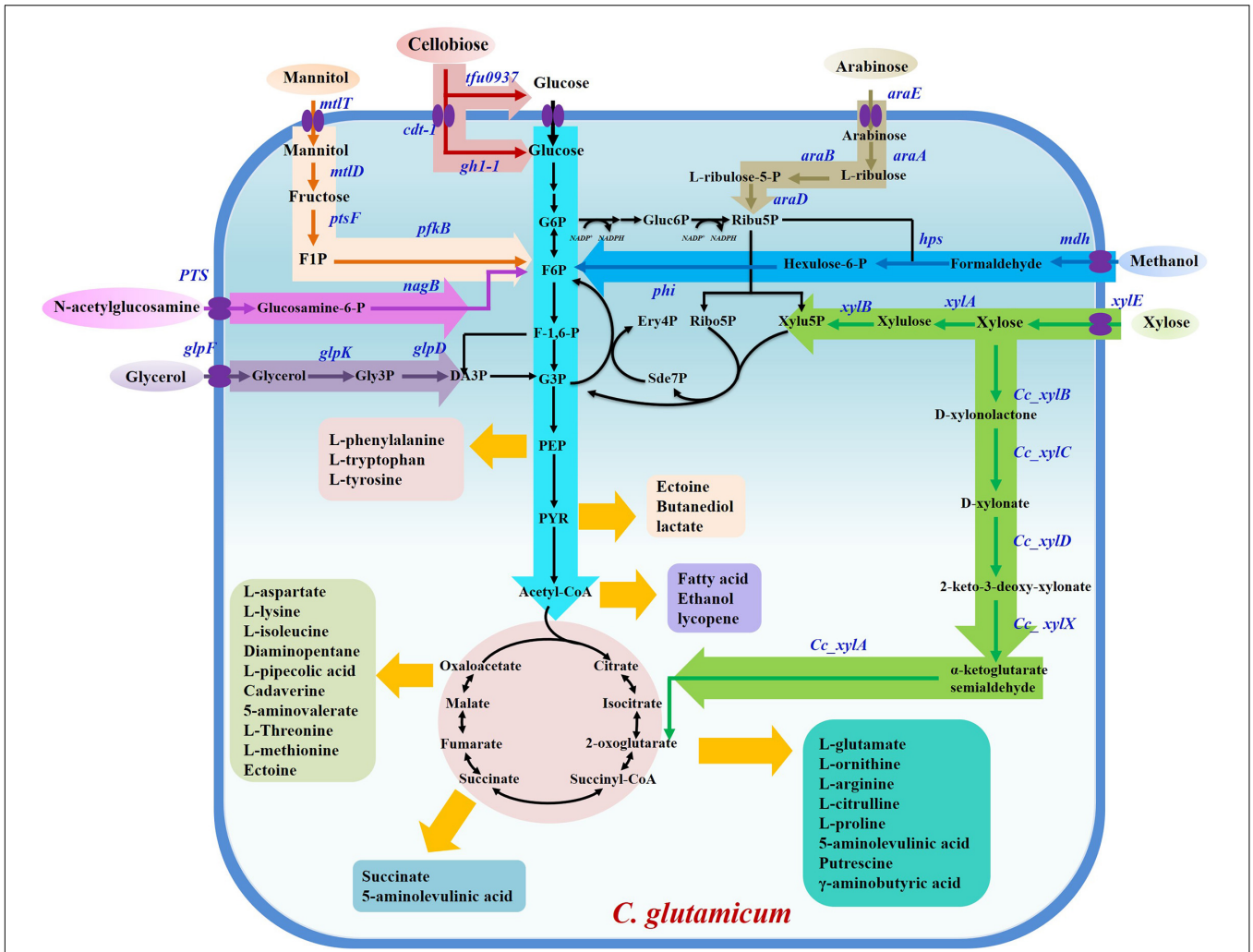

FIGURE 1 | Overview of non-food renewable carbon resource utilization and chemicals production in *C. glutamicum*. G6P, glucose-6-phosphate; F6P, fructose-6-phosphate; F-1,6-P, fructose-1,6-diphosphate; G3P, glyceraldehyde-3-phosphate; DA3P, dihydroxyacetone-3-phosphate; PEP, phosphoenolpyruvate; PYR, pyruvate; Gluc6P, gluconate-6-phosphate; Ribu5P, L-ribulose-5-phosphate; Ribo5P, ribose-5-phosphate; Xylu5P, xylulose-5-phosphate; Ery4P, erythritol-4-phosphate; Sde7P, sedoheptulose-7-phosphate; F1P, fructose-1-phosphate; Gly3P, glycerol-3-phosphate.

RuMP pathway has been completely assembled in synthetic methylotrophs and is feasible for the conversion of methanol to metabolites (Antoniewicz, 2019). In *C. glutamicum*, despite the existence of an endogenous metabolic pathway in which the four reactions catalyzed by AdhE, Ald, FdhF, and MshC convert methanol to CO_2, this strain requires an auxiliary carbon source to maintain cell growth (Witthoff et al., 2013). In order to continuously utilize methanol, the RuMP pathway was introduced to *C. glutamicum* by heterogeneous expression of Mdh from *Bacillus methanolicus* and Hps and Phi from *Bacillus subtilis* that produced an average methanol consumption rate of 1.7 mM/h in a glucose-methanol-containing medium (Witthoff et al., 2015). Simultaneously, a non-methylotrophic strain was successfully modulated to produce ^{13}C-label cadaverine from methanol, though high amounts of methanol added to the fermentation medium were toxic to *C. glutamicum* cells (Lessmeier et al., 2015). Accordingly, to enhance the methanol tolerance of *C. glutamicum*, adaptive laboratory evolution was applied to screen mutant strains that exhibited tolerance to high methanol content (Lessmeier and Wendisch, 2015; Wang et al., 2020). Comparative genome analysis of these mutant strains indicated that the amino acid substitution of A165T in MetY and a shortened Cat are crucial factors for improving methanol tolerance (Lessmeier and Wendisch, 2015). In addition, adaptive laboratory evolution was also applied to screen mutant strains capable of increased methanol-dependent cell growth in methanol-xylose-containing medium (Tuyishime et al., 2018). In these mutant strains, the carbon atom in methanol was used to synthesize cell materials, co-factors, and intermediates, which were subsequently converted to L-glutamate through interference with the biosynthesis of the cell wall (Tuyishime et al., 2018). Results from transcriptome analysis illustrate that increased methanol concentrations readjusted the metabolic flux distribution of

TABLE 1 | Directly conversion from xylose to chemicals by using *C. glutamicum*.

Strains (*C. glutamicum*)	Products	Modulations	Titer (g/L)	Yield (g/g)	Cultivation	References
ATCC 31831 pVWEx1-*xylB*	Xylonic acid	Overexpression of *xylB*	56.32	0.94	Shake flask; Batch	Sundar et al., 2020
SL-1A pIEARKT	Ethylene Glycol	Heterologous overexpression of D-tagatose 3-epimerase, L-fuculose kinase, and YqhD reductase	5.80	0.31	Shake flask; Batch	Lee et al., 2019
SL-3 pIEAKD pZ8-AY	Glycolate	Heterologous overexpression of D-tagatose 3-epimerase, L-fuculose kinase	19.20	0.96	BioLector; Batch	Lee et al., 2020
SO29	L-ornithine	Heterologous overexpression of *xylAB* operon	18.90	0.40	Shake flask; Batch	Zhang et al., 2019
SAR3	Sarcosine	Heterologous expression of *dpkA* and overexpression of *xylAB* operon	8.7	0.25*	Shake flask; Batch	Mindt et al., 2019b
HalT1 (pECXT99A-*xylAB*)	Halogenated tryptophan	Heterologous expression of *rebH* and *rebF*; overexpression of *xylAB* operon	0.034	ND	Shake flask; Batch	Veldmann et al., 2019
BETALYS	Carotenoids	Deletion of *crtR*, *cg0719*, *cg0718*, and *cg0717*	0.007	0.0007*	Shake flask; Batch	Henke et al., 2018
Ecto5	Ectoine	Overexpression of *ectABC* operon and overexpression of *xylAB* operon	0.4	ND	Shake flask; Batch	Perez-Garcia et al., 2017
BL-1 pXylAB	Succinate	Deletions of the *pqo*, *pta-ack*, *sdhCAB*, and *cat*; overexpression of *xylAB* operon	7.22	0.18	Shake flask; Batch	Jo et al., 2017
MH15	3-Hydroxypropionic acid	Overexpression of AraE and *xylAB* operon	35.4	0.44	Shake flask; Batch	Chen Z. et al., 2017
Cg-xr3	Xylitol	Introduction of pentose transport and xylitol synthesis pathway	6.2	0.96	Shake flask; Batch	Dhar et al., 2016
DAP-Xyl2	1,5-Diaminopentane	Overexpression of *tkt* and *fbp*; attenuation of *icd*; deletion of *act* and *lysE*	103	0.55	Bioreactor; Fed-batch	Buschke et al., 2013
PUT21	Putrescine	Overexpression of *xylA* and *xylB* from different host	3.78	ND	Shake flask; Batch	Meiswinkel et al., 2013a

**These values were not described in the main text of the original reference and thus estimated from the figure or graph.*

the glycolysis pathway, amino acid biosynthesis pathway, oxidative phosphorylation reactions, ribosome biosynthesis, and parts of the tricarboxylic acid cycle in *C. glutamicum* (Wang et al., 2020). Moreover, mechanistic analysis of mutant strains obtained by adaptive laboratory evolution of methanol-glucose co-utilizing strains demonstrated that improved expression of *mdh-hxlAB*, improved supplementation of riboflavin, and S288N mutation in MetY contribute to the distinct methanol-dependent growth of *C. glutamicum* (Hennig et al., 2020). Inspired by research on methanol bioconversion, a similar study claimed that methyl acetate can be easily obtained from the carbonylation of methanol and CO and that this was utilized by *C. glutamicum* through the introduction of a highly active esterase (Choo et al., 2016). In practice, current progress consistently indicated that cell growth of *C. glutamicum* was hindered by the cytotoxicity of methanol and formaldehyde, which restricted the conversion from methanol to chemicals. In addition to using engineered *C. glutamicum* to improve utilization efficiency and tolerance of methanol, the range of synthetic chemicals produced should also be further expanded.

Glycerol

Glycerol, a carbon-containing waste resulting from the biodiesel production process, has been widely applied in microbial fermentation owing to its high-reduction property, which frequently leads to higher maximum theoretical yields for producing chemicals (Xiberras et al., 2019). Recently, global markets witnessed remarkable growth in the biodiesel industry that subsequently stimulated research toward utilization of byproduct glycerol (Vivek et al., 2017). Due to its abundance, high-reduction ability, non-toxicity, and low cost, glycerol is regarded as a favorable carbon substrate for numerous industrial microbes, including *Escherichia coli* (Westbrook et al., 2019), *Saccharomyces cerevisiae* (Xiberras et al., 2019), *B. subtilis* (Fan et al., 2018), and *Pseudomonas* species (Pobletecastro et al., 2020) to produce various types of metabolites. Glycerol is typically not treated as a carbon resource for *C. glutamicum*-based bioprocesses due to the absence of glycerol oxidation pathway enzymes in this strain. In practice, *glpK*-encoded glycerol kinase and *glpD*-encoded glycerol-3-phosphate dehydrogenase from *E. coli* are introduced into *C. glutamicum* to obtain engineered strains capable of metabolizing glycerol (Rittmann et al., 2008).

In order to further improve glycerol utilization, heterogeneous expression of *glpF*, which encodes a glycerol facilitator from *E. coli*, was developed, accelerating the growth of *C. glutamicum* on glycerol. These strategies have been intensively applied to developing engineered *C. glutamicum* to convert glycerol into chemicals. For instance, overexpression of *E. coli_glpFKD* in corresponding *C. glutamicum* strains produced 3.5 ± 0.8 mM, 23.0 ± 2.3 mM, 17.9 ± 0.4 mM, and 23.6 ± 0.9 mM of L-glutamate, L-lysine, L-ornithine, and L-arginine, respectively (Rittmann et al., 2008; Meiswinkel et al., 2013b). Additionally, plasmid-based overexpression of *E. coli_glpFKD* in engineered *C. glutamicum* produced 11 ± 1 mM L-pipecolic acid at a yield of 0.14 ± 0.02 g/g glycerol (Pérez-García et al., 2017), 0.6 ± 0.0 g/L ectoine at a yield of 0.055 ± 0.003 g/g glycerol (Perez-Garcia et al., 2017), and 38.4 g/L succinate at a yield of 1.02 g/g glycerol (Wang et al., 2016), indicating that the majority of chemicals can be produced from glycerol in manipulated strains. Although rapid progress has been made in modulation of *C. glutamicum* to convert glycerol to chemicals, there are still uncertainties: At first, crude glycerol obtained from biodiesel production bioprocesses contains growth inhibitors that limit its application for the majority of industrial microorganisms (Vivek et al., 2017). Second, poor metabolic flux to the pentose phosphate pathway, using glycerol as carbon resource, results in inadequate cofactor NADPH regeneration, hindering the biosynthesis of chemicals including amino acids, fatty acids, and others, which requires NADPH to drive multistep enzyme reactions (Xiberras et al., 2019). In conclusion, if these obstacles can be addressed, microbial fermentation will be a promising approach for converting glycerol to metabolites.

Arabinose

Arabinose is the second most abundant pentose, following xylose, in plant cellulose biomass, and is intensively used as a carbon feedstock for industrial microbes. Assimilation of arabinose requires three enzyme actions and a membrane protein. First, arabinose isomerase (encoded by *araA*) catalyzes L-arabinose to synthesize L-ribulose. Second, ribulokinase (encoded by *araB*) catalyzes L-ribulose to synthesize L-ribulose-5-P. Third, ribulose-5-phosphate 4-epimerase (encoded by *araD*) catalyzes L-ribulose-5-P to synthesize D-xylulose-5-P, and this terminal metabolite is able to enter the pentose phosphate pathway (Gopinath et al., 2012; Zhao et al., 2018; Choi et al., 2019). AraE, a membrane channel protein that functions as a xylose transporter, was able to simultaneously transport L-arabinose. *C. glutamicum* strains, with the exception of *C. glutamicum* ATCC31831, cannot utilize arabinose due to lack of this metabolic pathway (Zhao et al., 2018; Choi et al., 2019). By heterogeneously assembling the arabinose metabolic pathway from *E. coli*, researchers engineered *C. glutamicum* to produce succinic acid from arabinose (Kawaguchi et al., 2008). Subsequently, *C. glutamicum* ATCC31831 with the ability to grow on L-arabinose was discovered by random screening. Analysis of the genome of this strain suggested that genes associated with arabinose utilization were included in the *araBAD* operon, which is negatively controlled by the transcription factor AraR (Kuge et al., 2015). In addition, simultaneous utilization of L-arabinose and D-glucose in *C. glutamicum* ATCC31831 indicated that carbon metabolism repression was ineffective against arabinose in this strain (Kawaguchi et al., 2009). Hence, development of recombinant *C. glutamicum* strains for converting arabinose to chemicals has received extensive attention. Heterologous expression of the *E. coli araBAD* operon in *C. glutamicum* HalT1 enabled fermentation production of 7-Cl-Trp and Trp at a titer of 52 ± 1 mg/L and 2.4 ± 0.1 g/L, respectively (Veldmann et al., 2019). Co-expression of *the E. coli araBAD* operon and *X. campestris xylA* endowed engineered *C. glutamicum* with the ability to simultaneously utilize arabinose and xylose as well as improve the production titers of L-lysine, L-glutamate, L-ornithine, and putrescine (Meiswinkel et al., 2013a). Despite the existence of endogenous arabinose metabolic pathways in *C. glutamicum* ATCC31831, researchers prefer heterologous expression of the *araBAD* operon from *E. coli* to construct engineered *C. glutamicum* strains (Meiswinkel et al., 2013a; Pérez-García et al., 2017). Because hydrolyzed cellulose is composed of glucose, xylose, arabinose, and other sugars, it can be acknowledged that the arduous feasibility of mixed sugar fermentation is the main bottleneck for the utilization of arabinose (Jojima et al., 2015; Mindt et al., 2019b).

Mannose or Mannitol

In addition to xylose and arabinose, mannose is another feedstock, making up approximately 20% of the sugar composition in lignocellulose hydrolyzate. Engineering recombinant strains to convert mannose to valuable chemicals has captured widespread attention. Mannose catabolism relies largely on the branching metabolism of the glycolytic pathway, similar to other sugars. In this metabolic pathway, mannose is transported into the cytoplasm, accompanied by acquisition of the phosphoryl group from phosphoenolpyruvate to generate mannose-6-phosphate. Subsequently, phosphomannose isomerase is employed to catalyze mannose-6-phosphate to synthesize fructose-6-phosphate, which is an intermediate in the glycolytic pathway. In *C. glutamicum*, a well-established native mannose metabolic pathway consists of glucose or fructose permeases (encoded by *ptsG* or *ptsF*), as well as phosphomannose isomerase (encoded by *manA*), which has been applied for the biosynthesis of various organic acids from mannose (Sasaki et al., 2011). Under anaerobic conditions, co-overexpression of *manA* and *ptsF* not only accelerated utilization of mannose but also broke down carbon metabolite repression, enabling simultaneous metabolism of glucose and mannose in *C. glutamicum* (Sasaki et al., 2011). Currently, engineered *C. glutamicum* to utilize mannose requires deforestation to prepare raw materials that are unsustainable; therefore, attention has been transferred to its reductive format, mannitol, which can be easily obtained from hydrolysis of marine plants.

Similar to mannose, the catabolic pathway of mannitol involves two transmembrane transport systems and two enzymatic reactions; mannitol can also be processed in *C. glutamicum* (**Figure 1**). First, it is transported from extracellular to intracellular space using the transmembrane protein MtlT and converted to fructose by mannitol dehydrogenase (encoded by *mtlD*) (Peng et al., 2011).

Subsequently, fructose is transported twice across the cell membrane to produce fructose-1-phosphate by employing a non-specific PTS transport system composed of an EI (encoded by *ptsIH*) and an EII (encoded by *ptsF*) membrane protein. Moreover, fructose-1-phosphate is applied to generate fructose-1,6-bisphosphate under the catalysis of phosphofructokinase (encoded by *pfkB*), which enters the glycolysis pathway (Laslo et al., 2012). Therefore, it is reasonable to speculate that sufficient expression of mannitol transporter and mannitol dehydrogenase is a critical factor for the utilization of mannitol in *C. glutamicum*. In general, *C. glutamicum* is unable to utilize mannitol until the negative regulator MtlR is removed; this regulator severely represses the expression of *mtlTD* operon (Peng et al., 2011). Accordingly, deletion of MtlR was performed in the lysine-producing strain *C. glutamicum* Lys12 to generate the recombinant strain *C. glutamicum* SEA-1, which is capable of producing 8.5 mM L-lysine from mannitol (Hoffmann et al., 2018). However, the recombinant *C. glutamicum* SEA-1 strain could only metabolically convert mannitol as long as the cell growth rate and biosynthesis of intracellular cofactor NADPH were much lower than in the parent *C. glutamicum* Lys12 strain cultured on glucose (Hoffmann et al., 2018). Fructose was found in the fermentation broth of strain *C. glutamicum* SEA-1, along with secondary growth observed in the fermentation process, indicating that fructose was incompletely converted to fructose-1-phosphate and secreted into the extracellular space. Thus, there are important factors, such as low expression of related enzymes, inefficient fructose uptake system, and insufficient supply of cofactor NADPH, that restrict biotransformation from mannitol to chemicals in MtlR-stripped *C. glutamicum*. Further regulatory mechanism analyses of mannitol metabolism, rational design and modification of related gene targets, and adoption of appropriate metabolic engineering approaches to optimize the metabolic flux of mannitol catabolism and fructose metabolism pathways are crucial for improving mannitol utilization efficiency.

N-Acetylglucosamine

N-Acetylglucosamine is an amino sugar that serves as a monomer for chitin, a polymer widely present in the exoskeleton of crustaceans. Cooked shrimp serves as food for humans, particularly in China, producing several million tons of shellfish waste, of which chitin makes up approximately half of the dry weight. Simple disposal of these wastes not only wastes biological resources but also causes environmental pollution, detracting from sustainable development of the national economy. Engineering microbes to utilize abundant polysaccharides from crustacean exoskeletons in order to produce chemicals has attracted extensive attention from researchers. Generally, the metabolic pathway of N-acetylglucosamine consists of a specific transport system and two enzyme actions, catalyzed by N-acetylglucosamine-6-phosphatedeacetylase (encoded by *nagA*) and glucosamine-6P deaminase (encoded by *nagB*), converting N-acetylglucosamine to fructose-6-phosphate that enters the glycolytic pathway (Matano et al., 2016). In *C. glutamicum*, the absence of a specific uptake system prevents the utilization of extracellular N-acetylglucosamine, requiring heterogeneous expression of *nagE* from *Corynebacterium glycinophilum*; this expression enables prompt transportation and feasible assimilation of N-acetylglucosamine. Co-expression of exogenous *nagA*, *nagB*, and *nagE* generated *C. glutamicum* capable of producing various chemicals, including L-lysine (Sgobba et al., 2018), L-citrulline (Eberhardt et al., 2014), lycopene (Matano et al., 2014), putrescine (Uhde et al., 2013), 7-chloro-L-tryptophan (Veldmann et al., 2019), 5-aminovalerate (Jorge et al., 2017b), gamma-aminobutyric acid (Jorge et al., 2017a), ectoine (Perez-Garcia et al., 2017), and L-pipecolic acid (Pérez-García et al., 2017) from N-acetylglucosamine. Consequently, N-acetylglucosamine is a promising alternative carbon source for *C. glutamicum*, although further investigation is required to accelerate the conversion from N-acetylglucosamine to bulk chemicals at the industrial scale. Additionally, the solid nature of chitin is unfavorable in preprocessing, as it hinders industrial application of amino sugars.

Cellobiose

Cellobiose, a disaccharide formed by the connection of two glucose molecules, is a carbon feedstock generated by degradation of cellulose through a synergistic reaction between endoglucanase and cellobiohydrolase (Li et al., 2020). Currently, direct utilization of cellobiose requires a β-glucosidase that catalyzes breakage of β-1,4-glucoside bonds and converts cellobiose to glucose. Due to the absence of a cellobiose transporter and low permeability of cellobiose, expression of β-glucosidase in microorganisms invariably requires secretion or surface display in order for the enzyme to contact the substrate. Traditionally, secreted expression or surface display of β-glucosidase has been applied for biorefinery chemical production in a multitude of industrial strains, including *Clostridium thermocellum* (Dash et al., 2019), *S. cerevisiae* (Yun et al., 2018), *Pseudomonas putida* (Dvoøák and de Lorenzo, 2018), *E. coli* (Satowa et al., 2020), and *C. glutamicum* (Adachi et al., 2013). *C. glutamicum* displays high β-glucosidase activity derived from *Saccharophagus degradans*, successfully displaying β-glucosidase fused with the C-terminus of the anchor protein PorC. On the surface, *C. glutamicum* enables simultaneous saccharification and fermentation, producing three-fold more L-lysine than a β-glucosidase-secretory *C. glutamicum* strain (Adachi et al., 2013). Co-expression of endoglucanase and β-glucosidase, either secretory or surface-displaying, in *C. glutamicum* DM1729 directly converts cellulose to L-lysine (Anusree et al., 2016). However, due to insufficient β-glucosidase activity, the yield of L-lysine and the cellobiose consumption rate of this engineered *C. glutamicum* were underdeveloped. To address limitations on enzyme activity, Tfu0937 from *Thermobifida fusca*, which shares high β-glucosidase activity with *E. coli*, was codon-optimized and introduced into *C. glutamicum*. Fusion with the CgR0949 signal sequence resulted in a Tfu0937-secreting strain that produced 9.7 g/L lysine, an improvement of approximately eight-fold compared to the original β-glucosidase-displaying strains (1.08 g/L) (Matsuura et al., 2019). Additionally, intracellular utilization of cellobiose in *C. glutamicum* is feasible through heterologous expression of codon-optimized *cdt-1*, which encodes a cellobiose transporter, and the *gh1-1* gene

from *Neurospora crassa* (Lee et al., 2016). By adaptive evolution, this mutant strain was also applied for the co-utilization of cellobiose and xylose.

DIRECT BIOCONVERSION FROM PLANT BIOMASS HYDROLYZATES TO CHEMICALS

Lignocellulosic biomass is generally regarded as agricultural waste, stored in huge amounts of organic carbon sources. Although many cellulosic ethanol factories are gradually coming into operation, lignocellulosic biomass is still underutilized and poses major environmental problems in some economically disadvantaged areas. Thus, there is an urgent need to improve the utilization of lignocellulosic biomass, which is a promising alternative raw material for the biobased production of chemicals. Pretreated by high-temperature acid hydrolysis, lignocellulosic materials such as corn stalk, rice straw, cassava bagasse, and wheat bran can be converted into corresponding hydrolyzates containing various monosaccharides (glucose, xylose, arabinose, etc.) that can be used to provide nutrition for microbes.

Corn Straw Hydrolyzate

Corn is an economic and food crop that is widely planted in numerous countries. Billions of tons of corn straw biomass are generated annually by harvesting corn. Most corn straw is incinerated, and only a fraction is applied for feeding animals, causing an extreme waste of resources and environmental pollution. To address these problems, corn straw has been preprocessed by mixing with dilute sulfuric acid and mild treatment at high temperature to generate exploitable corn straw hydrolyzate, which contains multitudinous carbohydrates, including glucose, xylose, arabinose, and mannose, which are favorable substrates for microbial fermentation (Choi et al., 2019). However, hydrolyzate generated from dilute-acid pretreatment process invariably contains fermentation inhibitors, including furfural, 5-hydroxymethylfurfural (HMF), and phenolic aldehydes, that affect the growth of microbes such as *C. glutamicum*. Hence, improving the tolerance of *C. glutamicum* to these inhibitors was investigated by adaptive evolutionary analysis to obtain a mutant strain capable of rapid growth on corn straw hydrolyzate (Wang et al., 2018). Exploration of tolerance mechanisms using a transcriptome analysis approach found that overexpression of *CGS9114_RS01115*, which encodes an alcohol dehydrogenase, as well as numerous oxidoreductase genes, accelerated conversion of these aldehyde inhibitors in *C. glutamicum* (Zhou et al., 2019). Meanwhile, excess biotin, which is unavoidable in lignocellulosic hydrolyzate produced by the pretreatment process, results in a rigid cell membrane that hampers secretion of L-glutamate, restricting cellulosic L-glutamate production (Wen et al., 2018). This unfavorable phenomenon can be reversed by extrinsic addition of osmotic agents, such as Tween 40, ethambutol, and penicillin, a step that not only improves the yield of L-glutamate but also promotes accumulation of L-arginine and L-ornithine during fermentation (Chen M. et al., 2015; Jiang et al., 2020). In addition, the uptake system of biotin is reinforced by overexpression of the *bioYMN* operon, which encodes biotin transporter, reducing biotin content in corn straw hydrolyzate and stimulating faster cell growth and multiplicative cellulosic L-glutamate production (Han et al., 2019). Moreover, to increase the transport of L-glutamate, MscCG, the primary L-glutamate transporter, was truncated, which stimulated L-glutamate production in biotin-rich corn stover hydrolyzates (Wen and Bao, 2019; Kawasaki and Martinac, 2020). Reducing biotin concentration in corn stover hydrolyzates is indispensable for cellulosic L-glutamate production. In addition to L-glutamate, L-lysine is a bulk amino acid that is in tremendous global demand and can be produced from corn straw hydrolyzate. For instance, fermentation cultivation of *C. glutamicum* SIIM B253 in high-glucose corn straw hydrolyzate resulted in L-lysine accumulation at a titer of 7.4 g/L. By modulating nutrient concentration, fermentation conditions, and simultaneous saccharification and fermentation processes, the yield of L-lysine was further elevated to 33.8 g/L, representing the highest yield of cellulosic L-lysine (Chen et al., 2019). As illustrated in these examples, *C. glutamicum*-based cellulosic biomass utilization has focused on the assimilation of glucose in corn straw hydrolyzate. Xylose serves as the second most abundant carbon feedstock in corn straw hydrolyzate, though *C. glutamicum* does not contain its own xylose metabolic machinery. Heterologous assimilation of xylose metabolic pathways from *X. campestris* were processed in strain SAZ3 that then produced 98.6 g/L of succinate by two-stage fermentations of glucose and xylose in corn straw hydrolyzate (Mao et al., 2018). However, despite extensive investigations aims at engineering *C. glutamicum* strains to produce valuable chemicals from corn straw hydrolyzate, multitude of problems, including the complexity of nutrients, generation of fermentation inhibitors, complex pretreatment process, and limited sugar yield, still restrict the large-scale application of corn straw hydrolyzate. In summary, corn straw hydrolyzate is an alternative renewable feedstock with huge potential in the field of microbial fermentation if those drawbacks could be addressed.

Other Cellulose Hydrolyzates

There are many food crops grown on Earth. In addition to corn straw, cellulose hydrolyzate prepared from crop residues such as cassava bagasse, straw stalk, and wheat bran are also applied for the cultivation of industrial microbes. Among these, cassava bagasse is a residuum generated from the starch extraction process and frequently identified as widespread waste, occupying a high proportion of disposal capacity (Padi and Chimphango, 2020). Engineering microbes for bioconversion of cassava bagasse has aroused intense interest in the past few decades (Sugumaran et al., 2014). Currently, the enzymatic hydrolysis products of cassava bagasse contains amounts of glucose and trace amounts of xylose, arabinose, and acids has been resoundingly used for the bioproduction of various bulk chemicals, including alcohols (Huang et al., 2019), organic acids (Wang and Yang, 2013), and fatty acids (Chen J. et al., 2015). For example, an immobilized *C. glutamicum* cell device, using a mixture of substrates and alkalis, has been discovered and can produce succinic acid

from cassava bagasse (Shi et al., 2014). After immobilization in a porous polyurethane filler, *C. glutamicum* can be used for cyclic utilization of hydrolyzate generated by the two-step enzymatic hydrolysis of cassava bagasse, producing 22.5 g/L succinic acid for each round of fermentation (Shi et al., 2014). Additionally, enzymatic hydrolysis of cassava bagasse (contains (w/w) 50.3% starch, and 12.2% fiber, and 6.5% moisture) recovers approximately half the mass of glucose (0.53 g glucose/g cassava bagasse), which can then be utilized by engineered *C. glutamicum*. This produced 18.5 g/L of 5-aminolevulinic acid during fed-batch fermentation, exhibiting 90.1% thrift on the cost of carbon material (Chen et al., 2020). In addition to cassava, rice is another widely planted food crop that generates a hundred billion tons of waste straw in the harvested phase. Traditionally, incineration disposal of rice straw has resulted in extensive haze and waste of resources. Acid treatment of rice straw generates 42 g/L of carbohydrate, containing 40 mM glucose, 166 mM xylose, and 66 mM arabinose, which can be utilized by engineered *C. glutamicum* containing a heterogeneously assembled xylose and arabinose metabolic pathway and produced 96 mM of L-glutamate during 100 h of fermentation cultivation (Gopinath et al., 2011). Similarly, acid treatment of wheat bran generates 41 g/L of carbohydrate, containing 125 mM glucose, 62 mM xylose, and 64 mM arabinose, was also can be utilized by engineered *C. glutamicum* to produce L-glutamate (Gopinath et al., 2011). Inspired by this example, biobased production of *N*-ethylglycine from rice straw hydrolyzate was enabled in engineered *C. glutamicum* by introducing a mutant DpkA from *P. putida* (Mindt et al., 2019a). Moreover, small quantities of plant biomass hydrolyzates, such as those derived from sorghum, softwood lignin, and *Miscanthus*, also deserve attention in the fermentation field. Biobased production of 5-aminovaleric acid (Joo et al., 2017) and biogasoline isopentenol (Sasaki et al., 2019) from *Miscanthus* hydrolyzate, as well as *cis*-muconic acid from depolymerized small aromatics of softwood lignin (Becker et al., 2018a), is feasible. Biomass hydrolyzates provide an alternative to glucose, creating enormous potential to alleviate the problem of industrial fermentation competing with humans for food.

CONCLUSION AND PERSPECTIVES

In this review, non-food carbon sources for the fermentation cultivation of *C. glutamicum* and chemical production were summarized. These feedstocks, including xylose, methanol, arabinose, glycerol, mannitol, N-acetylglucosamine, cellobiose, and cellulose hydrolyzates, provide alternative and renewable substrates to produce biobased chemicals. Microbial fermentation using these substrates is expected to alleviate the problem of food competition between industrial fermentation and human nutrition. However, there are still many technical bottlenecks in the practical application of these carbon sources. First, the tolerance of *C. glutamicum* to toxic materials, such as methanol and cellulose hydrolyzate, requires additional improvement to meet the demands of industrial fermentation. Fermentation inhibitors, including furfurals and phenolic aldehydes generated in the dilute-acid hydrolysis process of cellulose, are crucial factors restricting cellulose conversion. In addition to fermentation inhibitors, some nutrients may themselves hinder biosynthesis and secretion of target chemicals. Second, the instability of allogenically assembled metabolic pathways frequently restricts the biosynthesis of chemicals. These metabolic pathways disrupt the original metabolic balance, resulting in low growth and relatively low substrate utilization rates. Dynamic regulation of allochthonous metabolic pathways and chromosome insertion of genes involved in substrate utilization provide an effective solution for unstable pathway engineering. Third, the abundance and outlook of the alternative feedstock are important factors to consider when evaluating the technological index. As sea levels rise, land desertifies, the total human population of the earth increases, and the area of arable land decreases; biomass from terrestrial plants will no longer be the ideal substrate source. Utilization of marine biomass in the form of mannitol, mannose, and trehalose is one alternative, owing to the heavy specific proportion of these substrates in oceans. Meanwhile, stimulated by the development of sea-rice (Chen R. et al., 2017) and sand rice (Genievskaya et al., 2017), the utilization of rice straw hydrolyzate will also play an important role in industrial fermentation in the future.

AUTHOR CONTRIBUTIONS

All authors listed have made a substantial, direct and intellectual contribution to the work, and approved it for publication. BZ wrote and submitted this manuscript. YJ and ZL revised the "Bioconversion of Single-Carbon Sources to Valuable Chemicals" section. FW and X-YW revised the "Direct Bioconversion from Plant Biomass Hydrolysates to Chemicals" section.

FUNDING

This work was supported by the National Natural Science Foundation of China (No. 32000057) and Jiangxi Provincial Natural Science Foundation (No. 20202BAB213023), and Jiangxi Key R&D Program (No. 20171ACF60006).

ACKNOWLEDGMENTS

We would like to thank Editage (www.editage.cn) for English language editing.

REFERENCES

Adachi, N., Takahashi, C., Onomurota, N., Yamaguchi, R., Tanaka, T., and Kondo, A. (2013). Direct L-lysine production from cellobiose by *Corynebacterium glutamicum* displaying beta-glucosidase on its cell surface. *Appl. Microbiol. Biotechnol.* 97, 7165–7172. doi: 10.1007/s00253-013-5009-4

Antoniewicz, M. R. (2019). Synthetic methylotrophy: strategies to assimilate methanol for growth and chemicals production.

Curr. Opin. Biotechnol. 59, 165–174. doi: 10.1016/j.copbio.2019.07.001

Anusree, M., Wendisch, V. F., and Nampoothiri, K. M. (2016). Co-expression of endoglucanase and β-glucosidase in *Corynebacterium glutamicum* DM1729 towards direct lysine fermentation from cellulose. *Bioresour. Technol.* 213, 239–244. doi: 10.1016/j.biortech.2016.03.019

Becker, J., Kuhl, M., Kohlstedt, M., Starck, S., and Wittmann, C. (2018a). Metabolic engineering of *Corynebacterium glutamicum* for the production of *cis*, *cis*-muconic acid from lignin. *Microb. Cell Fact.* 17:115. doi: 10.1186/s12934-018-0963-2

Becker, J., Rohles, C. M., and Wittmann, C. (2018b). Metabolically engineered *Corynebacterium glutamicum* for bio-based production of chemicals, fuels, materials, and healthcare products. *Metab. Eng.* 50, 122–141. doi: 10.1016/j.ymben.2018.07.008

Buschke, N., Becker, J., Schafer, R., Kiefer, P., Biedendieck, R., and Wittmann, C. (2013). Systems metabolic engineering of xylose-utilizing *Corynebacterium glutamicum* for production of 1,5-diaminopentane. *Biotechnol. J.* 8, 557–570. doi: 10.1002/biot.201200367

Chen, J., Liu, X., Wei, D., and Chen, G. (2015). High yields of fatty acid and neutral lipid production from cassava bagasse hydrolysate (CBH) by heterotrophic *Chlorella protothecoides*. *Bioresour. Technol.* 191, 281–290. doi: 10.1016/j.biortech.2015.04.116

Chen, J., Wang, Y., Guo, X., Rao, D., Zhou, W., Zheng, P., et al. (2020). Efficient bioproduction of 5-aminolevulinic acid, a promising biostimulant and nutrient, from renewable bioresources by engineered *Corynebacterium glutamicum*. *Biotechnol. Biofuels* 13:41. doi: 10.1186/s13068-020-01685-0

Chen, M., Chen, X., Wan, F., Zhang, B., Chen, J., and Xiong, Y. (2015). Effect of Tween 40 and DtsR1 on l-arginine overproduction in *Corynebacterium crenatum*. *Microb. Cell Fact.* 14:119. doi: 10.1186/s12934-015-0310-9

Chen, R., Cheng, Y., Han, S., Van Handel, B., Dong, L., Li, X., et al. (2017). Whole genome sequencing and comparative transcriptome analysis of a novel seawater adapted, salt-resistant rice cultivar - sea rice 86. *BMC Genomics* 18:655. doi: 10.1186/s12864-017-4037-3

Chen, Z., Huang, J., Wu, Y., Wu, W., Zhang, Y., and Liu, D. (2017). Metabolic engineering of *Corynebacterium glutamicum* for the production of 3-hydroxypropionic acid from glucose and xylose. *Metab. Eng.* 39, 151–158. doi: 10.1016/j.ymben.2016.11.009

Chen, Z., Liu, G., Zhang, J., and Bao, J. (2019). A preliminary study on l-lysine fermentation from lignocellulose feedstock and techno-economic evaluation. *Bioresour. Technol.* 271, 196–201. doi: 10.1016/j.biortech.2018.09.098

Choi, J. W., Jeon, E. J., and Jeong, K. J. (2019). Recent advances in engineering *Corynebacterium glutamicum* for utilization of hemicellulosic biomass. *Curr. Opin. Biotechnol.* 57, 17–24. doi: 10.1016/j.copbio.2018.11.004

Choo, S., Um, Y., Han, S. O., and Woo, H. M. (2016). Engineering of *Corynebacterium glutamicum* to utilize methyl acetate, a potential feedstock derived by carbonylation of methanol with CO. *J. Biotechnol.* 224, 47–50. doi: 10.1016/j.jbiotec.2016.03.011

D'Este, M., Alvarado-Morales, M., and Angelidaki, I. (2018). Amino acids production focusing on fermentation technologies - a review. *Biotechnol. Adv.* 36, 14–25. doi: 10.1016/j.biotechadv.2017.09.001

Dash, S., Olson, D. G., Chan, S. H. J., Amadornoguez, D., Lynd, L. R., and Maranas, C. D. (2019). Thermodynamic analysis of the pathway for ethanol production from cellobiose in *Clostridium thermocellum*. *Metab. Eng.* 55, 161–169. doi: 10.1016/j.ymben.2019.06.006

Dhar, K. S., Wendisch, V. F., and Nampoothiri, K. M. (2016). Engineering of *Corynebacterium glutamicum* for xylitol production from lignocellulosic pentose sugars. *J. Biotechnol.* 230, 63–71. doi: 10.1016/j.jbiotec.2016.05.011

Dvoøák, P., and de Lorenzo, V. (2018). Refactoring the upper sugar metabolism of *Pseudomonas putida* for co-utilization of cellobiose, xylose, and glucose. *Metab. Eng.* 48, 94–108. doi: 10.1016/j.ymben.2018.05.019

Eberhardt, D., Jensen, J. V., and Wendisch, V. F. (2014). L-citrulline production by metabolically engineered *Corynebacterium glutamicum* from glucose and alternative carbon sources. *AMB Express* 4:85. doi: 10.1186/s13568-014-0085-0

Elmore, J. R., Dexter, G. N., Salvachúa, D., O'Brien, M., and Guss, A. M. J. M. E. (2020). Engineered *Pseudomonas putida* simultaneously catabolizes five major components of lignocellulosic biomass: glucose, xylose, arabinose, coumaric acid, and acetic acid. *Metab. Eng.* 62, 62–71. doi: 10.1016/j.ymben.2020.08.001

Fan, X., Wu, H., Jia, Z., Li, G., Li, Q., Chen, N., et al. (2018). Metabolic engineering of *Bacillus subtilis* for the co-production of uridine and acetoin. *Appl. Microbiol. Biotechnol.* 102, 8753–8762. doi: 10.1007/s00253-018-9316-7

Genievskaya, Y., Abugalieva, S., Zhubanysheva, A., and Turuspekov, Y. (2017). Morphological description and DNA barcoding study of sand rice (*Agriophyllum squarrosum*, Chenopodiaceae) collected in Kazakhstan. *BMC Plant Biol.* 17(Suppl. 1):177. doi: 10.1186/s12870-017-1132-1

Gopinath, V., Meiswinkel, T. M., Wendisch, V. F., and Nampoothiri, K. M. (2011). Amino acid production from rice straw and wheat bran hydrolysates by recombinant pentose-utilizing *Corynebacterium glutamicum*. *Appl. Microbiol. Biotechnol.* 92, 985–996. doi: 10.1007/s00253-011-3478-x

Gopinath, V., Murali, A., Dhar, K. S., and Nampoothiri, K. M. (2012). *Corynebacterium glutamicum* as a potent biocatalyst for the bioconversion of pentose sugars to value-added products. *Appl. Microbiol. Biotechnol.* 93, 95–106. doi: 10.1007/s00253-011-3686-4

Han, X., Li, L., and Bao, J. (2019). Microbial extraction of biotin from lignocellulose biomass and its application on glutamic acid production. *Bioresour. Technol.* 288:121523. doi: 10.1016/j.biortech.2019.121523

Henke, N. A., Wiebe, D., Perezgarcia, F., Peterswendisch, P., and Wendisch, V. F. (2018). Coproduction of cell-bound and secreted value-added compounds: simultaneous production of carotenoids and amino acids by *Corynebacterium glutamicum*. *Bioresour. Technol.* 247, 744–752. doi: 10.1016/j.biortech.2017.09.167

Hennig, G., Haupka, C., Brito, L. F., Ruckert, C., Cahoreau, E., Heux, S., et al. (2020). Methanol-essential growth of *Corynebacterium glutamicum*: adaptive laboratory evolution overcomes limitation due to methanethiol assimilation pathway. *Int. J. Mol. Sci.* 21:3617. doi: 10.3390/ijms21103617

Hoffmann, S. L., Jungmann, L., Schiefelbein, S., Peyriga, L., Cahoreau, E., Portais, J. C., et al. (2018). Lysine production from the sugar alcohol mannitol: design of the cell factory *Corynebacterium glutamicum* SEA-3 through integrated analysis and engineering of metabolic pathway fluxes. *Metab. Eng.* 47, 475–487. doi: 10.1016/j.ymben.2018.04.019

Huang, J., Du, Y., Bao, T., Lin, M., Wang, J., and Yang, S. (2019). Production of *n*-butanol from cassava bagasse hydrolysate by engineered *Clostridium tyrobutyricum* overexpressing *adhE2*: kinetics and cost analysis. *Bioresour. Technol.* 292:121969. doi: 10.1016/j.biortech.2019.121969

Jiang, Y., Huang, M., Chen, X., and Zhang, B. (2020). Proteome analysis guided genetic engineering of *Corynebacterium glutamicum* S9114 for Tween 40-triggered improvement in L-ornithine production. *Microb. Cell Fact.* 19:2. doi: 10.1186/s12934-019-1272-0

Jo, S., Yoon, J., Lee, S., Um, Y., Han, S. O., and Woo, H. M. (2017). Modular pathway engineering of *Corynebacterium glutamicum* to improve xylose utilization and succinate production. *J. Biotechnol.* 258, 69–78. doi: 10.1016/j.jbiotec.2017.01.015

Jojima, T., Noburyu, R., Sasaki, M., Tajima, T., Suda, M., Yukawa, H., et al. (2015). Metabolic engineering for improved production of ethanol by *Corynebacterium glutamicum*. *Appl. Microbiol. Biotechnol.* 99, 1165–1172. doi: 10.1007/s00253-014-6223-4

Joo, J. C., Oh, Y. H., Yu, J. H., Hyun, S. M., Khang, T. U., Kang, K. H., et al. (2017). Production of 5-aminovaleric acid in recombinant *Corynebacterium glutamicum* strains from a miscanthus hydrolysate solution prepared by a newly developed miscanthus hydrolysis process. *Bioresour. Technol.* 245, 1692–1700. doi: 10.1016/j.biortech.2017.05.131

Jorge, J. M. P., Nguyen, A. Q., Pérez-García, F., Kind, S., and Wendisch, V. F. (2017a). Improved fermentative production of gamma-aminobutyric acid via the putrescine route: systems metabolic engineering for production from glucose, amino sugars, and xylose. *Biotechnol. Bioeng.* 114, 862–873. doi: 10.1002/bit.26211

Jorge, J. M. P., Pérez-García, F., and Wendisch, V. F. (2017b). A new metabolic route for the fermentative production of 5-aminovalerate from glucose and alternative carbon sources. *Bioresour. Technol.* 245(Pt B), 1701–1709. doi: 10.1016/j.biortech.2017.04.108

Kawaguchi, H., Sasaki, M., Vertes, A. A., Inui, M., and Yukawa, H. (2008). Engineering of an l-arabinose metabolic pathway in *Corynebacterium glutamicum*. *Appl. Microbiol. Biotechnol.* 77, 1053–1062. doi: 10.1007/s00253-007-1244-x

Kawaguchi, H., Sasaki, M., Vertes, A. A., Inui, M., and Yukawa, H. (2009). Identification and functional analysis of the gene cluster for l-arabinose utilization in *Corynebacterium glutamicum*. *Appl. Environ. Microbiol.* 75, 3419–3429. doi: 10.1128/AEM.02912-08

Kawasaki, H., and Martinac, B. (2020). Mechanosensitive channels of *Corynebacterium glutamicum* functioning as exporters of l-glutamate and other valuable metabolites. *Curr. Opin. Chem. Biol.* 59, 77–83. doi: 10.1016/j.cbpa.2020.05.005

Kogure, T., and Inui, M. (2018). Recent advances in metabolic engineering of *Corynebacterium glutamicum* for bioproduction of value-added aromatic chemicals and natural products. *Appl. Microbiol. Biotechnol.* 102, 8685–8705. doi: 10.1007/s00253-018-9289-6

Kuge, T., Teramoto, H., and Inui, M. (2015). AraR, an l-arabinose-responsive transcriptional regulator in *Corynebacterium glutamicum* ATCC 31831, exerts different degrees of repression depending on the location of its binding sites within the three target promoter regions. *J. Bacteriol.* 197, 3788–3796. doi: 10.1128/jb.00314-15

Laslo, T., von Zaluskowski, P., Gabris, C., Lodd, E., Ruckert, C., Dangel, P., et al. (2012). Arabitol metabolism of *Corynebacterium glutamicum* and its regulation by AtlR. *J. Bacteriol.* 194, 941–955. doi: 10.1128/Jb.06064-11

Lee, J., Saddler, J. N., Um, Y., and Woo, H. M. (2016). Adaptive evolution and metabolic engineering of a cellobiose- and xylose- negative *Corynebacterium glutamicum* that co-utilizes cellobiose and xylose. *Microb. Cell Fact.* 15:20. doi: 10.1186/s12934-016-0420-z

Lee, J. H., and Wendisch, V. F. (2017a). Biotechnological production of aromatic compounds of the extended shikimate pathway from renewable biomass. *J. Biotechnol.* 257, 211–221. doi: 10.1016/j.jbiotec.2016.11.016

Lee, J. H., and Wendisch, V. F. (2017b). Production of amino acids - genetic and metabolic engineering approaches. *Bioresour. Technol.* 245(Pt B), 1575–1587. doi: 10.1016/j.biortech.2017.05.065

Lee, S. S., Choi, J. I., and Woo, H. M. (2019). Bioconversion of xylose to ethylene glycol and glycolate in engineered *Corynebacterium glutamicum*. *ACS Omega* 4, 21279–21287. doi: 10.1021/acsomega.9b02805

Lee, S. S., Park, J., Heo, Y. B., and Woo, H. M. (2020). Case study of xylose conversion to glycolate in *Corynebacterium glutamicum*: current limitation and future perspective of the CRISPR-Cas systems. *Enzyme Microb. Technol.* 132:109395. doi: 10.1016/j.enzmictec.2019.109395

Lessmeier, L., Pfeifenschneider, J., Carnicer, M., Heux, S., Portais, J. C., and Wendisch, V. F. (2015). Production of carbon-13-labeled cadaverine by engineered *Corynebacterium glutamicum* using carbon-13-labeled methanol as co-substrate. *Appl. Microbiol. Biotechnol.* 99, 10163–10176. doi: 10.1007/s00253-015-6906-5

Lessmeier, L., and Wendisch, V. F. (2015). Identification of two mutations increasing the methanol tolerance of *Corynebacterium glutamicum*. *BMC Microbiol.* 15:216. doi: 10.1186/s12866-015-0558-6

Li, J., Zhang, Y., Li, J., Sun, T., and Tian, C. (2020). Metabolic engineering of the cellulolytic thermophilic fungus *Myceliophthora thermophila* to produce ethanol from cellobiose. *Biotechnol. Biofuels* 13:23. doi: 10.1186/s13068-020-1661-y

Li, Y., Wei, H., Wang, T., Xu, Q., Zhang, C., Fan, X., et al. (2017). Current status on metabolic engineering for the production of l-aspartate family amino acids and derivatives. *Bioresour. Technol.* 245(Pt B), 1588–1602. doi: 10.1016/j.biortech.2017.05.145

Mao, Y., Li, G., Chang, Z., Tao, R., Cui, Z., Wang, Z., et al. (2018). Metabolic engineering of *Corynebacterium glutamicum* for efficient production of succinate from lignocellulosic hydrolysate. *Biotechnol. Biofuels* 11:95. doi: 10.1186/s13068-018-1094-z

Matano, C., Kolkenbrock, S., Hamer, S. N., Sgobba, E., Moerschbacher, B. M., and Wendisch, V. F. (2016). *Corynebacterium glutamicum* possesses β-N-acetylglucosaminidase. *BMC Microbiol.* 16:177. doi: 10.1186/s12866-016-0795-3

Matano, C., Uhde, A., Youn, J. W., Maeda, T., Clermont, L., Marin, K., et al. (2014). Engineering of *Corynebacterium glutamicum* for growth and L-lysine and lycopene production from N-acetyl-glucosamine. *Appl. Microbiol. Biotechnol.* 98, 5633–5643. doi: 10.1007/s00253-014-5676-9

Matsuura, R., Kishida, M., Konishi, R., Hirata, Y., Adachi, N., Segawa, S., et al. (2019). Metabolic engineering to improve 1,5-diaminopentane production from cellobiose using ß-glucosidase-secreting *Corynebacterium glutamicum*. *Biotechnol. Bioeng.* 116, 2640–2651. doi: 10.1002/bit.27082

Meiswinkel, T. M., Gopinath, V., Lindner, S. N., Nampoothiri, K. M., and Wendisch, V. F. (2013a). Accelerated pentose utilization by *Corynebacterium glutamicum* for accelerated production of lysine, glutamate, ornithine and putrescine. *Microb. Biotechnol.* 6, 131–140. doi: 10.1111/1751-7915.12001

Meiswinkel, T. M., Rittmann, D., Lindner, S. N., and Wendisch, V. F. (2013b). Crude glycerol-based production of amino acids and putrescine by *Corynebacterium glutamicum*. *Bioresour. Technol.* 145, 254–258. doi: 10.1016/j.biortech.2013.02.053

Mindt, M., Hannibal, S., Heuser, M., Risse, J. M., Sasikumar, K., Nampoothiri, K. M., et al. (2019a). Fermentative production of N-alkylated glycine derivatives by recombinant *Corynebacterium glutamicum* using a mutant of imine reductase DpkA from *Pseudomonas putida*. *Front. Bioeng. Biotechnol.* 7:232. doi: 10.3389/fbioe.2019.00232

Mindt, M., Heuser, M., and Wendisch, V. F. (2019b). Xylose as preferred substrate for sarcosine production by recombinant *Corynebacterium glutamicum*. *Bioresour. Technol.* 281, 135–142. doi: 10.1016/j.biortech.2019.02.084

Padi, R. K., and Chimphango, A. F. A. (2020). Feasibility of commercial waste biorefineries for cassava starch industries: techno-economic assessment. *Bioresour. Technol.* 297:122461. doi: 10.1016/j.biortech.2019.122461

Peng, X., Okai, N., Vertes, A. A., Inatomi, K., Inui, M., and Yukawa, H. (2011). Characterization of the mannitol catabolic operon of *Corynebacterium glutamicum*. *Appl. Microbiol. Biotechnol.* 91, 1375–1387. doi: 10.1007/s00253-011-3352-x

Pérez-García, F., Max Risse, J., Friehs, K., and Wendisch, V. F. (2017). Fermentative production of L-pipecolic acid from glucose and alternative carbon sources. *Biotechnol. J.* 12:1600646. doi: 10.1002/biot.201600646

Perez-Garcia, F., Ziert, C., Risse, J. M., and Wendisch, V. F. (2017). Improved fermentative production of the compatible solute ectoine by *Corynebacterium glutamicum* from glucose and alternative carbon sources. *J. Biotechnol.* 258, 59–68. doi: 10.1016/j.jbiotec.2017.04.039

Pobletecastro, I., Wittmann, C., and Nikel, P. I. (2020). Biochemistry, genetics and biotechnology of glycerol utilization in *Pseudomonas* species. *Microb. Biotechnol.* 13, 32–53. doi: 10.1111/1751-7915.13400

Radek, A., Tenhaef, N., Muller, M. F., Brusseler, C., Wiechert, W., Marienhagen, J., et al. (2017). Miniaturized and automated adaptive laboratory evolution: evolving *Corynebacterium glutamicum* towards an improved d-xylose utilization. *Bioresour. Technol.* 245, 1377–1385. doi: 10.1016/j.biortech.2017.05.055

Rittmann, D., Lindner, S. N., and Wendisch, V. F. (2008). Engineering of a glycerol utilization pathway for amino acid production by *Corynebacterium glutamicum*. *Appl. Environ. Microbiol.* 74, 6216–6222. doi: 10.1128/AEM.00963-08

Sasaki, M., Teramoto, H., Inui, M., and Yukawa, H. (2011). Identification of mannose uptake and catabolism genes in *Corynebacterium glutamicum* and genetic engineering for simultaneous utilization of mannose and glucose. *Appl. Microbiol. Biotechnol.* 89, 1905–1916. doi: 10.1007/s00253-010-3002-8

Sasaki, Y., Eng, T., Herbert, R. A., Trinh, J., Chen, Y., Rodriguez, A., et al. (2019). Engineering *Corynebacterium glutamicum* to produce the biogasoline isopentenol from plant biomass hydrolysates. *Biotechnol. Biofuels* 12:41. doi: 10.1186/s13068-019-1381-3

Satowa, D., Fujiwara, R., Uchio, S., Nakano, M., Otomo, C., Hirata, Y., et al. (2020). Metabolic engineering of *E. coli* for improving mevalonate production to promote NADPH regeneration and enhance acetyl-CoA supply. *Biotechnol. Bioeng.* 117, 2153–2164. doi: 10.1002/bit.27350

Sgobba, E., Blobaum, L., and Wendisch, V. F. (2018). Production of food and feed additives from non-food-competing feedstocks: valorizing N-acetylmuramic acid for amino acid and carotenoid fermentation with *Corynebacterium glutamicum*. *Front. Microbiol.* 9:2046. doi: 10.3389/fmicb.2018.02046

Shanmugam, S., Sun, C., Chen, Z., and Wu, Y. R. (2019). Enhanced bioconversion of hemicellulosic biomass by microbial consortium for biobutanol production with bioaugmentation strategy. *Bioresour. Technol.* 279, 149–155. doi: 10.1016/j.biortech.2019.01.121

Shanmugam, S., Sun, C., Zeng, X., and Wu, Y. R. (2018). High-efficient production of biobutanol by a novel *Clostridium* sp. strain WST with uncontrolled pH strategy. *Bioresour. Technol.* 256, 543–547. doi: 10.1016/j.biortech.2018.02.077

Shi, X., Chen, Y., Ren, H., Liu, D., Zhao, T., Zhao, N., et al. (2014). Economically enhanced succinic acid fermentation from cassava bagasse hydrolysate using *Corynebacterium glutamicum* immobilized in porous polyurethane filler. *Bioresour. Technol.* 174, 190–197. doi: 10.1016/j.biortech.2014.09.137

Sugumaran, K. R., Jothi, P., and Ponnusami, V. (2014). Bioconversion of industrial solid waste-Cassava bagasse for pullulan production in solid state fermentation. *Carbohydr. Polym.* 99, 22–30. doi: 10.1016/j.carbpol.2013.08.039

Sun, C., Zhang, S., Xin, F., Shanmugam, S., and Wu, Y. R. (2018). Genomic comparison of *Clostridium* species with the potential of utilizing red algal biomass for biobutanol production. *Biotechnol. Biofuels* 11:42. doi: 10.1186/s13068-018-1044-9

Sundar, M. S. L., Susmitha, A., Rajan, D., Hannibal, S., Sasikumar, K., Wendisch, V. F., et al. (2020). Heterologous expression of genes for bioconversion of xylose to xylonic acid in *Corynebacterium glutamicum* and optimization of the bioprocess. *AMB Express* 10:68. doi: 10.1186/s13568-020-01003-9

Tuyishime, P., Wang, Y., Fan, L., Zhang, Q., Li, Q., Zheng, P., et al. (2018). Engineering *Corynebacterium glutamicum* for methanol-dependent growth and glutamate production. *Metab. Eng.* 49, 220–231. doi: 10.1016/j.ymben.2018.07.011

Uhde, A., Youn, J. W., Maeda, T., Clermont, L., Matano, C., Krämer, R., et al. (2013). Glucosamine as carbon source for amino acid-producing *Corynebacterium glutamicum*. *Appl. Microbiol. Biotechnol.* 97, 1679–1687. doi: 10.1007/s00253-012-4313-8

Veldmann, K. H., Minges, H., Sewald, N., Lee, J. H., and Wendisch, V. F. (2019). Metabolic engineering of *Corynebacterium glutamicum* for the fermentative production of halogenated tryptophan. *J. Biotechnol.* 291, 7–16. doi: 10.1016/j.jbiotec.2018.12.008

Vivek, N., Sindhu, R., Madhavan, A., Anju, A. J., Castro, E., Faraco, V., et al. (2017). Recent advances in the production of value added chemicals and lipids utilizing biodiesel industry generated crude glycerol as a substrate – metabolic aspects, challenges and possibilities: an overview. *Bioresour. Technol.* 239, 507–517. doi: 10.1016/j.biortech.2017.05.056

Wang, C., Cai, H., Chen, Z., and Zhou, Z. (2016). Engineering a glycerol utilization pathway in *Corynebacterium glutamicum* for succinate production under O2 deprivation. *Biotechnol. Lett.* 38, 1791–1797. doi: 10.1007/s10529-016-2166-4

Wang, X., Khushk, I., Xiao, Y., Gao, Q., and Bao, J. (2018). Tolerance improvement of *Corynebacterium glutamicum* on lignocellulose derived inhibitors by adaptive evolution. *Appl. Microbiol. Biotechnol.* 102, 377–388. doi: 10.1007/s00253-017-8627-4

Wang, Y., Fan, L., Tuyishime, P., Liu, J., Zhang, K., Gao, N., et al. (2020). Adaptive laboratory evolution enhances methanol tolerance and conversion in engineered *Corynebacterium glutamicum*. *Commun. Biol.* 3:217. doi: 10.1038/s42003-020-0954-9

Wang, Z., and Yang, S. (2013). Propionic acid production in glycerol/glucose co-fermentation by *Propionibacterium freudenreichii* subsp. *shermanii*. *Bioresour. Technol.* 137, 116–123. doi: 10.1016/j.biortech.2013.03.012

Wen, J., and Bao, J. (2019). Engineering *Corynebacterium glutamicum* triggers glutamic acid accumulation in biotin-rich corn stover hydrolysate. *Biotechnol. Biofuels* 12:86. doi: 10.1186/s13068-019-1428-5

Wen, J., Xiao, Y., Liu, T., Gao, Q., and Bao, J. (2018). Rich biotin content in lignocellulose biomass plays the key role in determining cellulosic glutamic acid accumulation by *Corynebacterium glutamicum*. *Biotechnol. Biofuels* 11:132. doi: 10.1186/s13068-018-1132-x

Wendisch, V. F., Mindt, M., and Pérez-García, F. (2018). Biotechnological production of mono- and diamines using bacteria: recent progress, applications, and perspectives. *Appl. Microbiol. Biotechnol.* 102, 3583–3594. doi: 10.1007/s00253-018-8890-z

Westbrook, A. W., Miscevic, D., Kilpatrick, S., Bruder, M., Mooyoung, M., and Chou, C. P. (2019). Strain engineering for microbial production of value-added chemicals and fuels from glycerol. *Biotechnol. Adv.* 37, 538–568. doi: 10.1016/j.biotechadv.2018.10.006

Witthoff, S., Muhlroth, A., Marienhagen, J., and Bott, M. (2013). C1 metabolism in *Corynebacterium glutamicum*: an endogenous pathway for oxidation of methanol to carbon dioxide. *Appl. Environ. Microbiol.* 79, 6974–6983. doi: 10.1128/AEM.02705-13

Witthoff, S., Schmitz, K., Niedenfuhr, S., Noh, K., Noack, S., Bott, M., et al. (2015). Metabolic engineering of *Corynebacterium glutamicum* for methanol metabolism. *Appl. Environ. Microbiol.* 81, 2215–2225. doi: 10.1128/AEM.03110-14

Wu, X. Y., Guo, X. Y., Zhang, B., Jiang, Y., and Ye, B. C. (2019). Recent advances of L-ornithine biosynthesis in metabolically engineered *Corynebacterium glutamicum*. *Front. Bioeng. Biotechnol.* 7:440. doi: 10.3389/fbioe.2019.00440

Xiberras, J., Klein, M., and Nevoigt, E. (2019). Glycerol as a substrate for *Saccharomyces cerevisiae* based bioprocesses - Knowledge gaps regarding the central carbon catabolism of this 'non-fermentable' carbon source. *Biotechnol. Adv.* 37:107378. doi: 10.1016/j.biotechadv.2019.03.017

Yim, S. S., Choi, J. W., Lee, S. H., and Jeong, K. J. (2016). Modular optimization of a hemicellulose-utilizing pathway in *Corynebacterium glutamicum* for consolidated bioprocessing of hemicellulosic biomass. *ACS Synth. Biol.* 5, 334–343. doi: 10.1021/acssynbio.5b00228

Yun, E. J., Oh, E. J., Liu, J. J., Yu, S., Kim, D., Kwak, S., et al. (2018). Promiscuous activities of heterologous enzymes lead to unintended metabolic rerouting in *Saccharomyces cerevisiae* engineered to assimilate various sugars from renewable biomass. *Biotechnol. Biofuels* 11:140. doi: 10.1186/s13068-018-1135-7

Zhang, B., Gao, G., Chu, X. H., and Ye, B. C. (2019). Metabolic engineering of *Corynebacterium glutamicum* S9114 to enhance the production of L-ornithine driven by glucose and xylose. *Bioresour. Technol.* 284, 204–213. doi: 10.1016/j.biortech.2019.03.122

Zhang, B., Ren, L. Q., Yu, M., Zhou, Y., and Ye, B. C. (2018a). Enhanced L-ornithine production by systematic manipulation of L-ornithine metabolism in engineered *Corynebacterium glutamicum* S9114. *Bioresour. Technol.* 250, 60–68. doi: 10.1016/j.biortech.2017.11.017

Zhang, B., Yu, M., Wei, W. P., and Ye, B. C. (2018b). Optimization of L-ornithine production in recombinant *Corynebacterium glutamicum* S9114 by cg3035 overexpression and manipulating the central metabolic pathway. *Microb. Cell Fact.* 17:91. doi: 10.1186/s12934-018-0940-9

Zhao, N., Qian, L., Luo, G., and Zheng, S. (2018). Synthetic biology approaches to access renewable carbon source utilization in *Corynebacterium glutamicum*. *Appl. Microbiol. Biotechnol.* 102, 9517–9529. doi: 10.1007/s00253-018-9358-x

Zhou, P., Khushk, I., Gao, Q., and Bao, J. (2019). Tolerance and transcriptional analysis of *Corynebacterium glutamicum* on biotransformation of toxic furaldehyde and benzaldehyde inhibitory compounds. *J. Ind. Microbiol. Biotechnol.* 46, 951–963. doi: 10.1007/s10295-019-02171-9

Conflict of Interest: The authors declare that the research was conducted in the absence of any commercial or financial relationships that could be construed as a potential conflict of interest.

frontiers in Bioengineering and Biotechnology

ORIGINAL RESEARCH
published: 07 January 2021
doi: 10.3389/fbioe.2020.605096

Effect of Biochar on the Production of L-Histidine From Glucose Through *Escherichia coli* Metabolism

Yang E[1], Jun Meng[1], Heqing Cai[2], Caibin Li[2], Sainan Liu[1], Luming Sun[1] and Yanxiang Liu[2]**

[1] Liaoning Biochar Engineering & Technology Research Center, Shenyang Agricultural University, Shenyang, China, [2] Guizhou Tobacco Company in Bijie Company, Bijie, China

The organic compounds from biochar play a role of hormone analogs, stimulating the expression of metabolites by controlling related gene and protein. In this experiment, we reported the L-histidine biosysthesis was promoted by biochar treatment in *E. coli* unlike genetic engineering of the traditional method. The related results indicated the most optimal concentration was found to be 3%, and 7% is the lethal dose. *E. coli* was inhibited in the high-concentration treatment. On the other hand, docking technology was usually used as drug screening, basing on Lock-and-key model of protein in order to better understand mechanisms. So the organic compounds of biochar from GC-MS analysis that acted as ligands were connected to HisG protein controlling L-histidine biosysthesis in *E. coli*. The result showed that the three organic molecules interacted with HisG protein by hydrogen bond. So we considered that these three compounds play regulatory roles in L-histidine biosysthesis, and the *his*G *gene* expression fully supports this conclusion.

Keywords: biochar, L-histidine, *E. coli*, biosynthesis, organic compounds

OPEN ACCESS

Edited by:
Yi-Rui Wu,
Shantou University, China

Reviewed by:
Jianming Xue,
New Zealand Forest Research Institute Limited (Scion), New Zealand
Dengmiao Cheng,
Dongguan University of Technology, China

****Correspondence:***
Yang E
eyang@syau.edu.cn
Yanxiang Liu
1759235829@qq.com

Specialty section:
This article was submitted to Industrial Biotechnology, a section of the journal Frontiers in Bioengineering and Biotechnology

Received: *11 September 2020*
Accepted: *02 December 2020*
Published: *07 January 2021*

Citation:
E Y, Meng J, Cai H, Li C, Liu S, Sun L and Liu Y (2021) Effect of Biochar on the Production of L-Histidine From Glucose Through Escherichia coli Metabolism. Front. Bioeng. Biotechnol. 8:605096. doi: 10.3389/fbioe.2020.605096

INTRODUCTION

L-histidine is an essential proteinogenic amino acid in plants and animals. Therefore, amino acids are widely used in the medical and agriculture industries. Many studies have indicated that several diseases are related to a lack of histidine (Kulis-Horn et al., 2014). Appropriate histidine levels in the diet (12 mg) can effectively prevent obesity and metabolic disorders (Kasaoka et al., 2004; Tuttle et al., 2012). In cancer therapy, all methods focus on enhancing the body's natural defense mechanisms (Maus et al., 2014). Recent studies have shown that suitable dietary supplementation of histidine can boost the effectiveness of the immune system (Kanarek et al., 2018).

The traditional biosynthetic pathway of histidine includes 10 enzymatic reactions that convert phosphoribosyl-1-pyrophosphate into histidine (Lazcano et al., 1996; Ikeda, 2003). The process mainly depends on the degradation of natural protein resources. There are many challenges in increasing histidine content. Therefore, artificially synthesized histidine is being developed rapidly (Shibasaki et al., 2008; Mitsuhashi, 2014). However, the chemical synthesis of histidine produces a racemic mixture with unnatural compounds, which may not be beneficial for health. As a result, administrative agencies have ruled that histidine production is not up to standard. Therefore, microbial producers and fermentation processes have become the focus of research.

Agricultural processes produce waste in massive amounts (Shi, 2011). This waste contains large amounts of fiber and lignin. Agricultural biomass is subjected to thermal treatment under an oxygen-limited atmosphere, yielding a carbon-rich, solid product known as biochar (Lehmann, 2009; Meng, 2013). Many different biomass and preparation processes can be used to produce biochar for different purposes. However, there is a challenge in obtaining suitable biochar precursors for specific purposes. Current research suggests that biochar can provide a suitable environment for plants and microorganisms (Yang et al., 2015). The most notable functions of biochar are (1) sorption in both organic and inorganic compounds, (2) changing the cation exchange capability, (3) providing hormone analogs for plants, (4) altering soil pH, and (5) providing a place and irritant substance for microbial growth (Chan et al., 2007; Yang et al., 2019; Hong et al., 2020). Biochar contains several organic compounds with various biological functions. For example, 2-Acetyl-5-methylfuran from biochar can promote rice seedling growth by playing the role of a hormone analog (Yang et al., 2019). Moreover, Yuan et al. (2017) reported that organic molecules from biochar, including 14 candidate compounds, have a positive effect on the cold tolerance of rice seedlings. Many studies have reported that biochar can benefit microbial growth (Lehmann, 2009). The traditional biosynthetic pathway of L-histidine mainly depends on bacteria, such as *Salmonella typhimurium*, *Escherichia (E.) coli*, and *Corynebacterium glutamicum* (Lazcano et al., 1996; Jung et al., 2010). A previous study indicated that biochar could change the microbial community (Yang et al., 2015). However, there is no reports that the biochar can promote the bacteria producing the L-histidine. Therefore, *E. coli* was selected as a representative bacterium of the biosynthetic pathway in L-histidine in order to study influence of biochar on bio-synthesis of L-histidine. On the other hands, we consider that there are compounds from biochar promoting the bio-synthesis of L-histidine. However, it is difficult to find out the compounds through experiments due to the composition complexity of biochar. So, we hypothesize that the organic compounds in biochar could interact with receptor protein controlling L-histidine. If the organic compounds that acted as ligands was connected to the active site of receptor protein and the same mechanism of action as ligands, the organic compounds played the analogous biological function. So the autodocking is employed to select the compounds of biochar which can promote the bio-synthesis of L-histidine from theory basing on lock-and-key model of protein in order to efficiently produce L-histidine from *E. coli* in biochar and to understand the compounds from biochar promoting biosynthetic L-histidine of mechanism. The result provides another pathway for the production of L-histidine.

MATERIALS AND METHODS

Biochar Preparation and Culture Conditions

Agricultural biomass from tobacco straw was used in this study. All biomass was obtained from the Bijie tobacco company in China. The raw materials were pyrolyzed at 400°C for 30 min at a rate of ∼15°C/min. Biochar was generated at 300, 400, 500, 600, and 700°C in the preliminary experiment. However, the biochar at 400°C was derived for the treatments in this study, as this leads to the most favorable L-histidine content.

E. coli was obtained from Liaoning Biochar Engineering & Technology Research Center and cultivated in Luria-Bertani medium according to a previously reported method (Chu et al., 2020). The inducers include 2 g/L L-arabinose, 15 g/L agar powder, 5 g/L NaCl and 5 mol/L NaOH for pH 7.0. The biochar was then added to the medium at concentrations of 0% (control), 1, 3, 5, and 7% (inducers: biochar = w: w).

Biochar Characterization

The physicochemical properties of the biochar were analyzed in order to define the materials present (**Table 1**). Aqueous extracts of biochar (1:10 w:w) were prepared in MilliQ ultrapure water (Millipore, United States) for 1 h. The extract liquors were checked for pH, electrical conductivity, $N\text{-}NO_3$, and $N\text{-}NH_4$ (AA3, SEAL, Germany). The nutrient contents of biochar (including K, Na, Mg, Ca, Cu, Fe, Zn, B, and P) were tested using an atomic absorption spectrometer (AA6880, Shimadzu, Japan). An element analyzer (VARIO MACRO CUBE, Elementder, Germany) was employed to analyze the total organic carbon in the biochar.

Analysis of Organic Compounds From Biochar by GC-MS

The carbon skeleton is not absorbed by microorganisms. Small organic compounds can enter the cytomembrane, sometimes affecting microbial growth. Therefore, different polar organic solvents were employed to extract the organic compounds from biochar. Biochar (1.5 g) was homogenized with 100 mL non-polar organic solvents (heptane and hexane) or polar organic solvents (methanol, ethanol, acetonitrile, chloroform, ethyl acetate, and dichloromethane). The analysis procedure was performed according to a previous study (Yang et al., 2019). The ionization efficiency and the MS response were periodically tested by 1 $\mu L\ mL^{-1}$ IPA (1,000 $\mu L\ mL^{-1}$ in methylene) as certified reference material (Profumo et al., 2020) in order to assure the quality of related data.

Molecular Docking Analysis

The molecular structures of the organic compounds from the GC-MS results were constructed by Gaussview. Then, Gaussian 09 was used for geometric optimization in order to determine the stable structure (B3LYP functional with 6-311 + G). The HisG (ID: 1H3D) protein structure was downloaded from the Research Collaboratory for Structural Bioinformatics (RCSB) protein database. AutoDockTools (ADT) were used to prepare the ligands and 1H3D receptor and to determine the "search space." Organic compound optimization was docked with 1H3D in order to identify molecules that can promote the biosynthesis of L-histidine.

TABLE 1 | Physicochemical properties of biochar-exacted liquor.

Element	Biochar concentration			
	1%	3%	5%	7%
K	3.112	3.131	3.217	3.227
Na	3.063	3.072	3.188	3.195
Mg	0.029	0.031	0.033	0.036
Ca	0.026	0.025	0.038	0.041
Zn	0.000	0.000	0.000	0.000
P	0.002	0.002	0.003	0.003
S	0.607	0.611	0.625	0.628
$N\text{-}NO_3$	0.0002	0.0004	0.0004	0.0005
$N\text{-}NH_4$	0.0000	0.0000	0.0000	0.0000
pH	7.55	7.60	7.71	7.82
EC (μs/cm)	10.3	11.1	12.2	13.2
Total organic carbon	49.3	51.5	52.1	56.8

The element unit is g/kg.

Gene Expression Analyses

ATP phosphoribosyltransferase (HisG), which catalyzes the first step of histidine biosynthesis, is the most important enzyme regulated at the enzymatic level. Therefore, in this study, *his*G gene expression was analyzed to understand the synthesis state of L-histidine. DNA from the culture medium was isolated from 0.5 g using nucleic acid reagent (Takara accompany, Dalian, China) following the manufacturer's instructions. DNA quality and concentration were tested by gel electrophoresis and a NanoDrop spectrophotometer (NanoDrop Technologies, Wilmington, DE, United States). The *his*G primers were obtained according to a previous paper (18 S FWD: GTGCCAGCAGCCGCGGTA; 18 S RV: TGGACCGGCCAGCCAAGC; Huada Gene Technology Company, Shenzhen, China). Quantitative RT-PCR (qRT-PCR) was carried out in a 10-μL reaction vessel containing 5 μL 2.5 × RealMaster Mix, 20 × SYBR solution (Takara accompany, Dalian, China), 0.2 μL of both forward and reverse primers, and 1 μL of diluted cDNA (1:10). PCR amplification was performed using System LightCycler 480 equipment (Roche Applied Science, Germany); the qRT-PCR procedure comprised 95°C for 1 min, followed by 40 cycles of 95°C for 10 s, 55°C for 30 s, and 68°C for 1 min. Values for gene expression were calculated following the method outlined by Rieu and Powers (2009) using delta-delta Ct.

Substrate and Product Analyses

The glucose concentration was measured using an SBA-40E biological sensor (Shandong Academy of Sciences, Shandong, China). L-histidine was analyzed by UPLC (I-Class; Waters Company, United States) coupled to a UV photodiode array detector. And a Discovery C-18 column (2.1 × 50 mm, 1.7 μm; Waters Company, United States) was used in this experiment. The protocol for L-histidine was adapted from Ning et al. (2016). The sample manager FTN was maintained at 10°C. The column of temperature was heated 40°C. The 0.1% formic acid in milliQ water was used as the mobile phase at 0.6 mL/min. And then, 0.2 μL samples were run for 5 min, the UV photodiode array detector was tested at 570 nm, with a data acquisition rate of 20 point/s. An external calibration curve was built in a range between 1 and 10 ng/ml from certified reference of L-histidine (Aladdin accompany, China) though Empower 3 software.

Statistical Analysis

All numerical data were analyzed using the statistical software Spss (version 26, United States). The addition

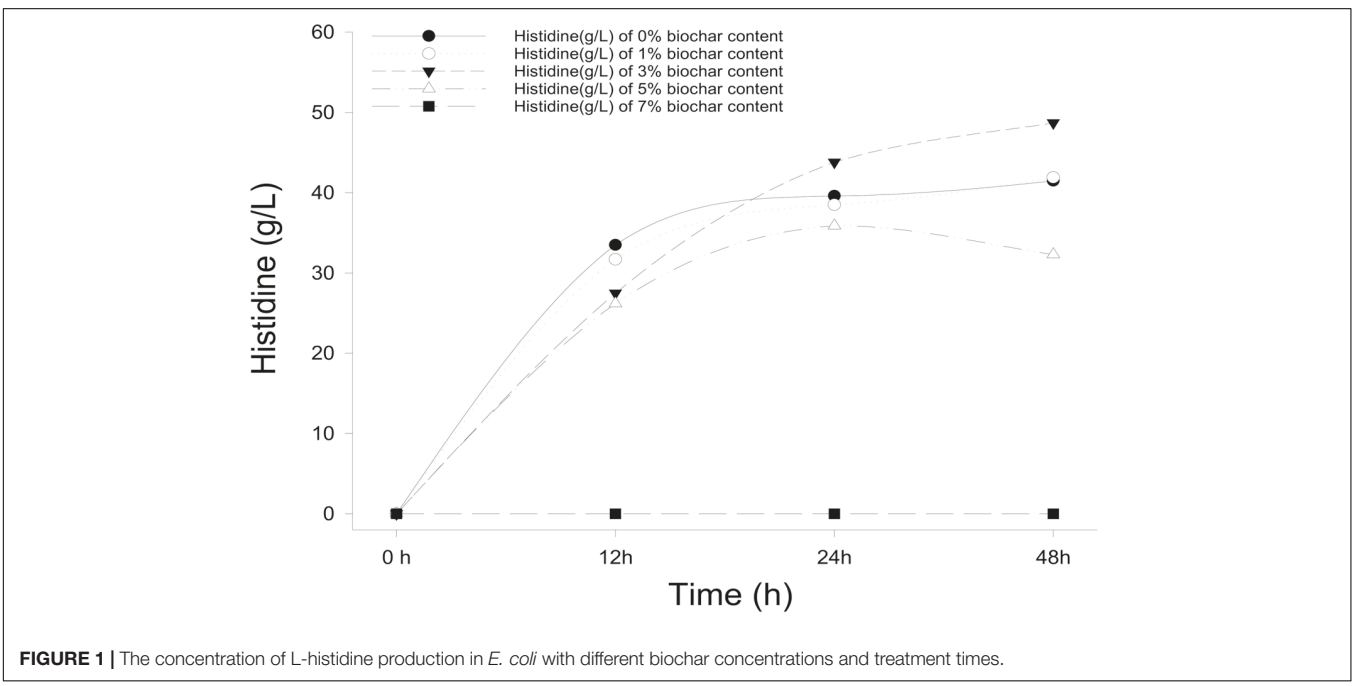

FIGURE 1 | The concentration of L-histidine production in *E. coli* with different biochar concentrations and treatment times.

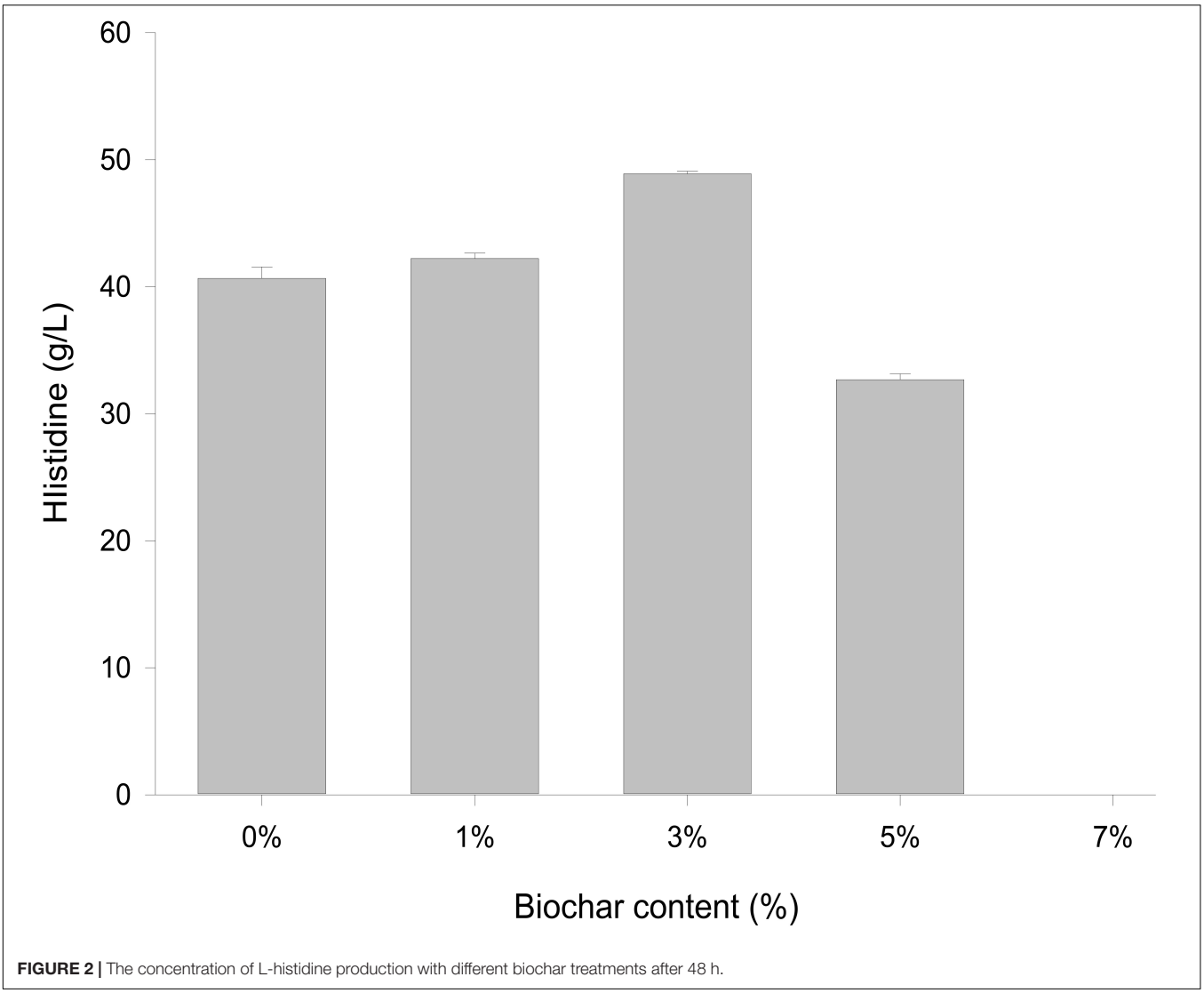

FIGURE 2 | The concentration of L-histidine production with different biochar treatments after 48 h.

of * and ** indicates that different concentrations of biochar exhibited significant differences at the $P < 0.05$ and $P < 0.01$ levels compared with those of the control, respectively. Three technical and three biological replicates were analyzed for gene expression and *E. coli* inducers.

RESULTS

Biochar Has a Positive Impact on the Production of Histidine in *E. coli*

Different concentrations of biochar (0, 1, 3, 5, and 7%) were studied in the same *E. coli* culture environment (**Figure 1**). L-histidine was promoted in all concentrations, except for the 7% biochar treatment (0 g/L L-histidine concentration). Histidine production under 3% biochar treatment, which reached about 48.7 g/L (**Figure 2**, $P < 0.05$), was significantly greater than that of the control, 1%, and 5% treatments after 48 h of culture. Variations in L-histidine production among the different biochar treatments resulted in different degrees of inhibition. With 12 h of treatment, the degree of inhibition was lower in all biochar-treatment groups compared with that of the control. Higher biochar concentrations inhibited L-histidine production in *E. coli* more strongly. However, inhibition was eliminated after 24 h with 3% biochar treatment. These results indicated that at lower concentrations, *E. coli* was adapted for the biochar environment (**Figure 1**). Over time, *E. coli* produced greater amounts of L-histidine in low concentrations of biochar (1 and 3%). However, the high biochar concentrations (5 and 7%) did not eliminate inhibition. In the 7% biochar treatment, L-histidine was completely inhibited. The results showed that 7% biochar was lethal in *E. coli.* On the other hand, many different elements and organic compounds from biochar provided nutrients for the microorganisms (**Table 1**). In addition, the microorganisms were able to live on the special structure of biochar. These factors benefited *E. coli*

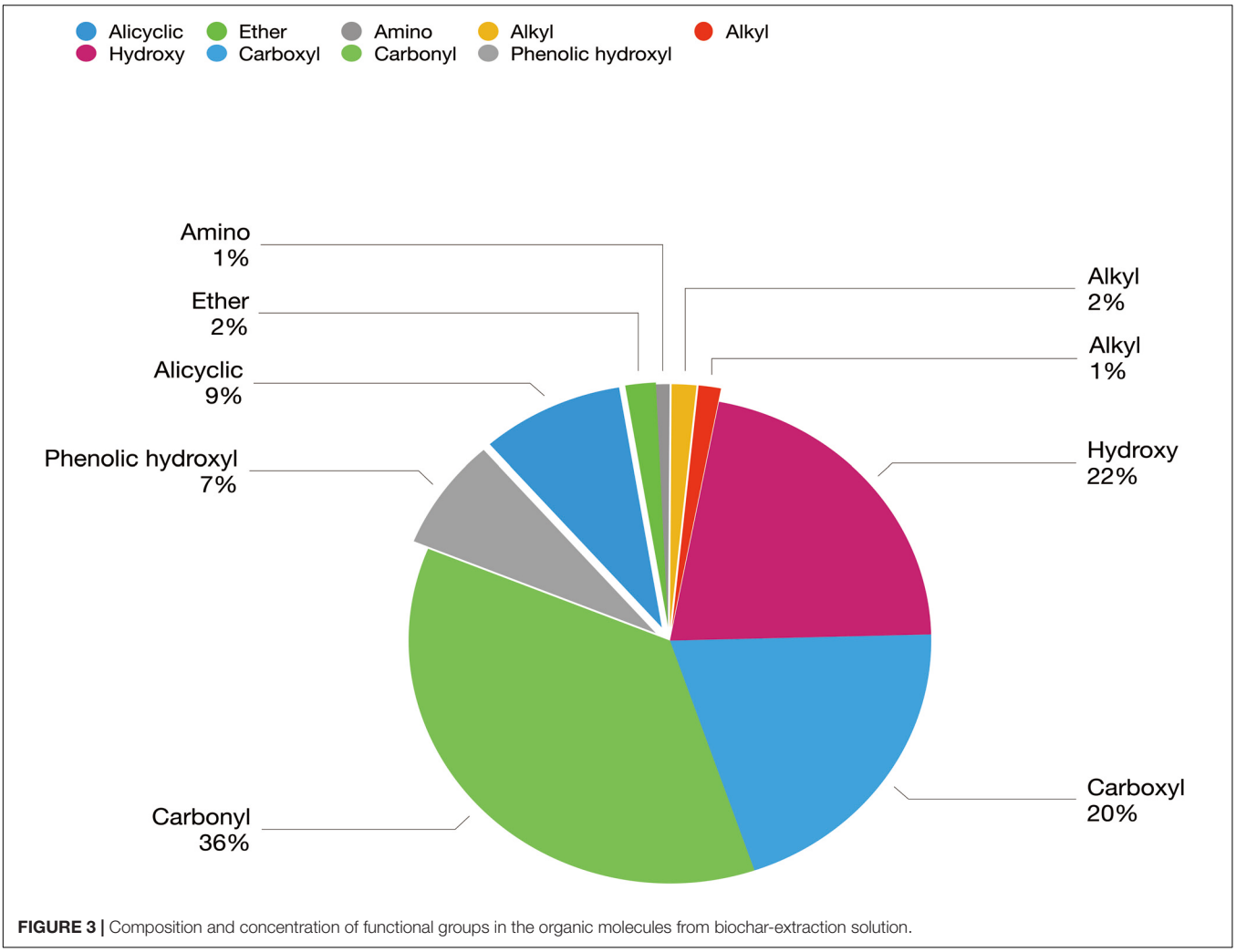

FIGURE 3 | Composition and concentration of functional groups in the organic molecules from biochar-extraction solution.

survival. The L-histidine concentration varied with different biochar concentrations.

Analysis of Organic Compounds in Biochar

The biochar comprised a carbon skeleton, inorganic elements (including N, P, and K), ash content, and organic compounds. In plants and microorganisms, the inorganic elements and organic compounds from biochar are absorbed, which affect their growth and metabolites. L-histidine is the metabolic product of *E. coli*. Therefore, in the following experiment, the influence of organic compounds was studied. There are many unknown organic compounds in biochar that are difficult to analyze. However, compound data in GC/MS was used to facilitate the identification of these unknowns. In this experiment, ion trap MS was employed to analyze the products of biochar extracts using polar and non-polar solvents. Nine different functional groups, which contribute to different biological functions, were found in the organic compounds (**Figure 3**). Cartonyl, carboxyl, and hydroxy were the main functional groups in the biochar-extraction solution (78%).

Organic Compounds Promoting Histidine Biosynthetic Gene Expression

Overexpression of a rate-limiting enzyme is one of the most common strategies to improve end-product accumulation. The HisG protein plays an important role in histidine metabolic process. The *his*G gene was analyzed to define the molecular changes resulting from different biochar treatments; its expression was suppressed in the control and each concentration of biochar treatment (**Figure 4**). There was no significant difference in the control or the 1% biochar concentration. *E. coli* treated with 3% biochar exhibited the highest expression of *his*G, and the gene was inhibited at a 7% biochar concentration. The observations of *his*G gene expression were consistent with the L-histidine product results (**Figure 2**). Thus, the analysis indicated that *his*G expression along with the L-histidine product can respond to compounds in the biochar.

Docking Analysis

We hypothesize that the biochar including organic compounds can interact with protein receptor (i.e., L-histidine biosysthesis of regulatory protein, hisG protein). The molecules of

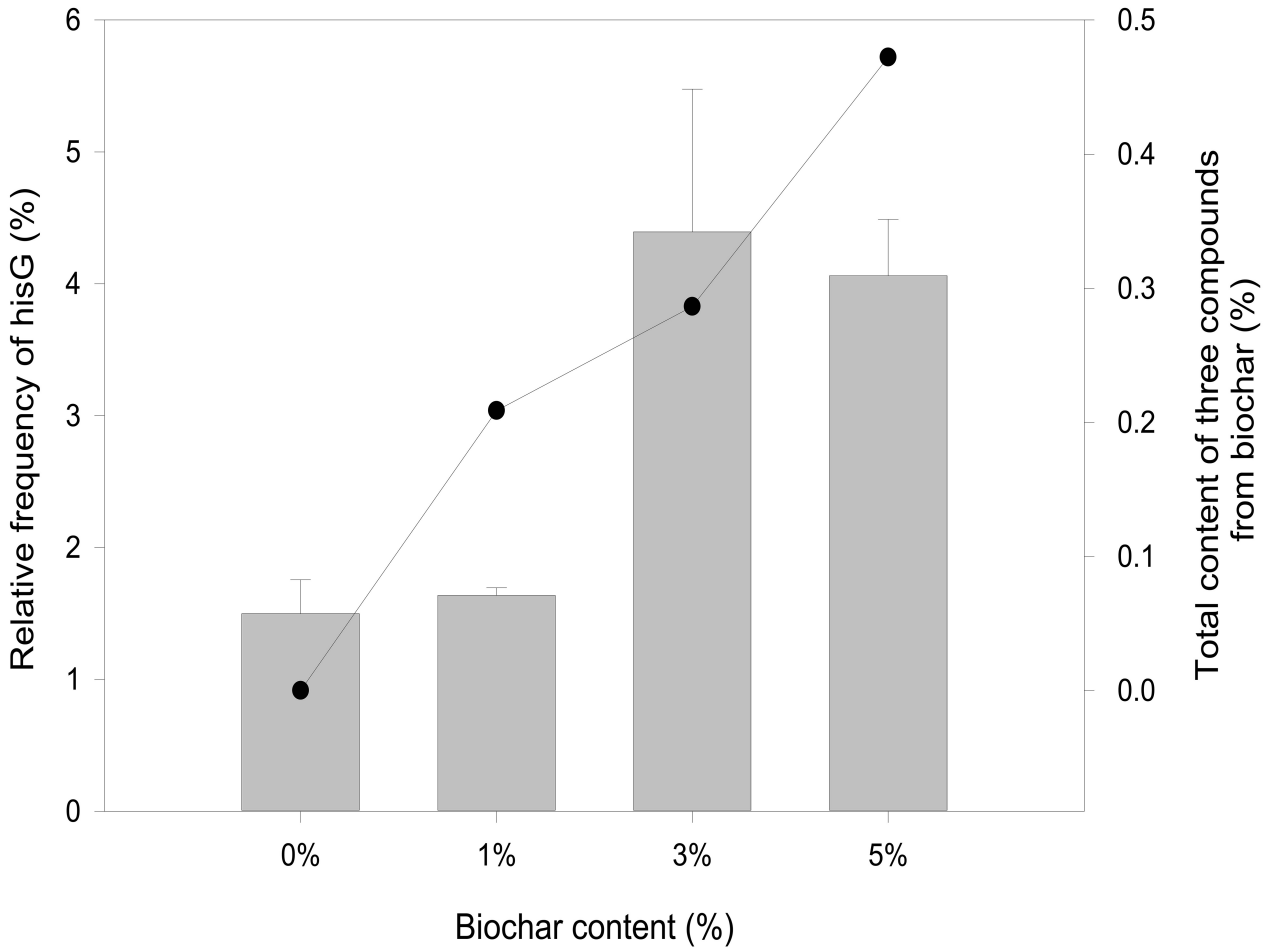

FIGURE 4 | Quantitative RT-PCR analysis of *his*G gene expression from 0, 1, 3, and 5% biochar treatment for 48 h (bar graph). The sum of eugenol, salicyl alcohol, and cyclopentane from biochar over a 48-h period.

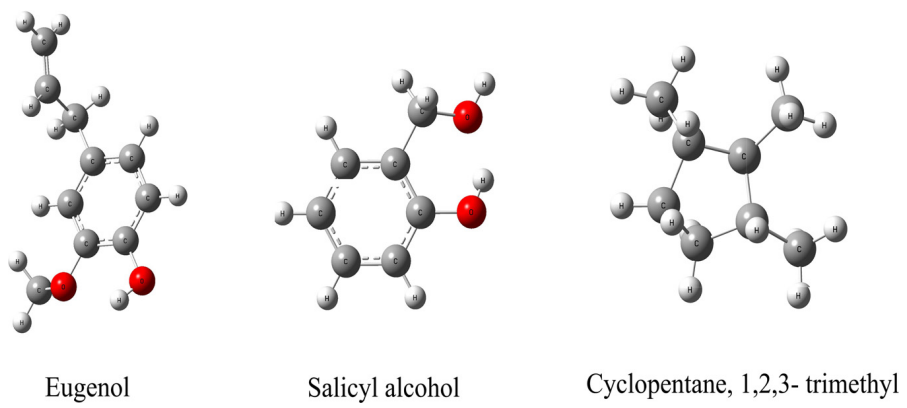

FIGURE 5 | The molecules from biochar that could interact with the HisG protein.

biological function that act as ligands are connected to hisG protein. Therefore, the hisG protein structure involved in L-histidine biosysthesis from *E. coli* was download from RCSB, the result indicated that three candidate modules (**Figure 5**) acted as ligands for target proteins (**Figure 6**). The biochar included different types of organic compounds (**Figure 3**), but there are several organic compounds including biological function. On the other hand, the three candidate

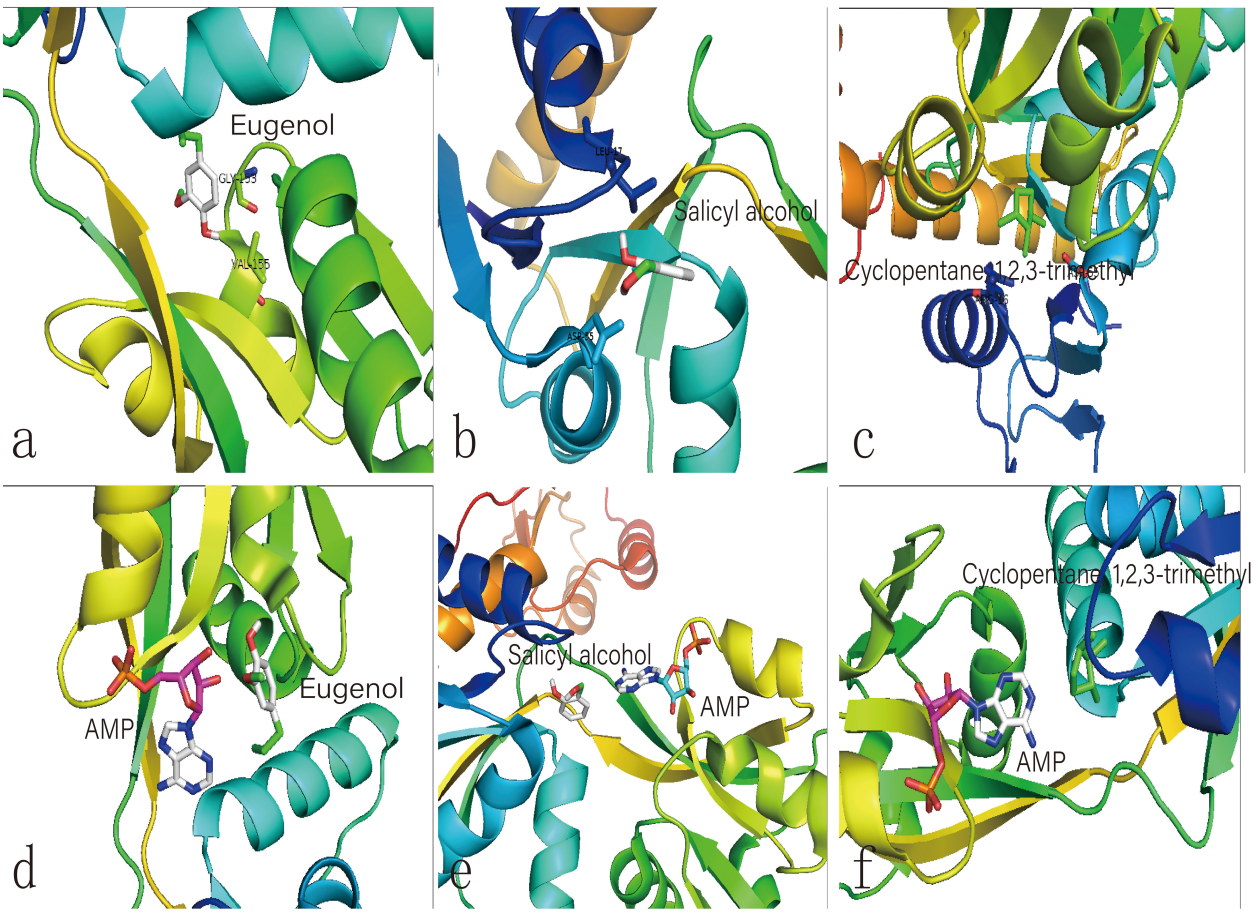

FIGURE 6 | Molecular docking analysis of HisG protein. **(a–c)** illustrate the interaction of eugenol, salicyl alcohol, and 1,2,3-trimethylcyclopentane with the activity site of the HisG protein; Comparison between AMP and eugenol **(d)**, salicyl alcohol **(e)**, and cyclopentane **(f)** in the HisG protein activity site.

molecules content is a little. So we considered that the organic compounds from biochar played a role of hormone analogs that controlled the metabolic process of microorganism. The related gene was expressed in the organic compounds stimulating (**Figure 4**).

DISCUSSION

In our study, the *his*G *gene* expression was induced by different biochar treatment, including the promotion of L-histidine biosynthesis from *E. coli*. Total L-histidine contents in 0% as well as 1, 3, and 5% treatments compared to 7% treatment in this experiment. The results indicated that the low biochar treatment was benefit for L-histidine biosynthesis. However, L-histidine biosynthesis was inhibited in the high biochar treatment. So, we considered that some organic compounds could control the L-histidine biosysthesis in the *E. coli* cell.

The metabolic process of L-histidine in *E. coli* was complex and controlled by genes, proteins, or other compounds (Martin et al., 2017). Therefore, it was difficult to understand completely (Zhao et al., 2015). Genomics, proteomics, and metabolomics are usually employed to discuss the influence of allogenic material (Lal et al., 2018). However, it was difficult to understand the interaction between allogenic material and molecules from microorganisms. When the allogenic mixture was mixed, the analysis became more difficult. And then, it was also difficult to understand whether the precise compounds from biochar could affect *his*G expression and biosysthesis by experiment method (Kulis-Horn et al., 2014). Therefore, AutoDock dockings were employed to explore molecules from biochar organic compounds (Ciemny et al., 2018). The result indicated three candidate molecules (**Figure 5**) could interact with a favorable protein site, but the combined site slightly differs. Because these three organic compounds could potentially affect the HisG protein, the relationship between *his*G *gene* expression and the concentrations of the three compounds was analyzed. The area-normalization method was employed to calculate the compound concentrations (Roy et al., 2018). The amount of different compounds in the biochar was highest under 3% biochar treatment. Therefore, the sum of the three organic compounds was reflected in the relationship between the compounds and the *his*G *gene* (r = 0.459, p = 0.003). The results indicated that the *his*G *gene* increased with the sum

of the three organic compounds from biochar (**Figure 4**), indicating that these three compounds could stimulate *his*G *gene* expression.

The same site of action was observed in the HisG protein (**Figures 6e–g**). The hydrogen bond was mainly a chemical combination between the three molecules and the activity site of HisG proteins such as AMP. In eugenol, the molecule could form a hydrogen bond with GLY153 and VAL-155 from protein residues (**Figure 6a**), salicyl alcohol was combined with LEU-17 and ASP-55 protein residues (**Figure 6b**), and 1,2,3-trimethylcyclopentane, interacted with ARG16 and ASP-55 protein residues (**Figure 6c**). The results showed that there were different acting sites with protein residues, but the acting area was the same. Therefore, it was speculated that the HisG protein was controlled by the three molecules. The results indicated that biochar could induce L-histidine biosysthesis in *E. coli*. The process of molecules interacting with HisG protein is illustrated in Cartoon1–3.

The concentrations of the three compounds, along with other organic compounds, were fairly low in the biochar. However, the molecules could induce the L-histidine biosysthesis of *E. coli* at a rate 17.3% higher than that of the control group ($r = 0.756$, $p = 0.005$). Therefore, this experiment shows that the molecules may play roles as hormone analogs, which affect plant growth, microbial structure, and the concentrations of metabolic substances (Yang et al., 2015, 2019). Therefore, organic compounds warrant consideration in the research field of biochar.

CONCLUSION

Compared with traditional genetic engineering methods to produce L-histidine, we found the L-histidine biosysthesis increased with an increasing concentration of biochar treatment (1, 3, and 5%), excepting 7% or higher concentration. According to molecular docking, three organic compounds could interact with HisG protein, involving in the response to L-histidine biosysthesis. The compounds acted as hormone analogs. It's easy to explain that the *his*G *gene* expression were positively correlated.

DATA AVAILABILITY STATEMENT

The raw data supporting the conclusions of this article will be made available by the authors, without undue reservation.

AUTHOR CONTRIBUTIONS

YE and JM: data curation, funding acquisition, writing—original draft, and writing—review and editing. JM: funding acquisition and supervision. YL: funding acquisition, methodology, and resources. SL and LS: formal analysis and methodology. CL and HC: validation and visualization. All authors contributed to the article and approved the submitted version.

FUNDING

This work was supported by the S&D Program from Bijie Tobacco Company of Guizhou Province Guizhou Tobacco Company (2018520500240066), Youth Program of National Natural Science Foundation of China (31801292), National Key R&D Program "Research and Development of Biochar-Based Fertilizer and Microbial Fertilizer" (2017YFD0200800 and 2017YFD0200802), Innovative Talents Promotion Plan of Ministry of Science and Technology (2017RA2211), LiaoNing Revitalization Talents Program (No. XLYC1802094), and the National Natural Science Foundation of China (41807101).

SUPPLEMENTARY MATERIAL

The Supplementary Material for this article can be found online at: https://www.frontiersin.org/articles/10.3389/fbioe.2020.605096/full#supplementary-material

REFERENCES

Chan, K. Y., Van Zwieten, L., Meszaros, I., Downie, A., and Joseph, S. (2007). Agronomic values of greenwaste biochar as a soil amendment. *Aust. J. Soil Res.* 45, 629–634. doi: 10.1071/SR07109

Chu, Y., Khan, M. A., Xia, M., Lei, W., Wang, F., Zhu, S., et al. (2020). Synthesis and micro-mechanistic studies of histidine modified montmorillonite for lead(II) and copper(II) adsorption from wastewater. *Chem. Eng. Res. Des.* 157, 142–152. doi: 10.1016/j.cherd.2020.02.020

Ciemny, M., Kurcinski, M., Kamel, K., Kolinski, A., Alam, N., Schueler-Furman, O., et al. (2018). Protein–peptide docking: opportunities and challenges. *Drug Discov. Today* 23, 1530–1537. doi: 10.1016/j.drudis.2018.05.006

Hong, N., Cheng, Q., Goonetilleke, A., Bandala, E. R., and Liu, A. (2020). Assessing the effect of surface hydrophobicity/hydrophilicity on pollutant leaching potential of biochar in water treatment. *J. Ind. Eng. Chem.* 89, 222–232. doi: 10.1016/j.jiec.2020.05.017

Ikeda, M. (2003). Amino acid production processes. *Adv. Biochem. Eng. Biotechnol.* 79, 1–35. doi: 10.1007/3-540-45989-8_1

Jung, S., Chun, J. Y., Yim, S. H., Lee, S. S., Cheon, C. II., Song, E., et al. (2010). Transcriptional regulation of histidine biosynthesis genes in *Corynebacterium glutamicum*. *Can. J. Microbiol.* 56, 178–187. doi: 10.1139/W09-115

Kanarek, N., Keys, H. R., Cantor, J. R., Lewis, C. A., Chan, S. H., Kunchok, T., et al. (2018). Histidine catabolism is a major determinant of methotrexate sensitivity. *Nature* 559, 632–636. doi: 10.1038/s41586-018-0316-7

Kasaoka, S., Tsuboyama-Kasaoka, N., Kawahara, Y., Inoue, S., Tsuji, M., Ezaki, O., et al. (2004). Histidine supplementation suppresses food intake and fat accumulation in rats. *Nutrition* 20, 991–996. doi: 10.1016/j.nut.2004.08.006

Kulis-Horn, R. K., Persicke, M., and Kalinowski, J. (2014). Histidine biosynthesis, its regulation and biotechnological application in *Corynebacterium glutamicum*. *Microb. Biotechnol.* 7, 5–25. doi: 10.1111/1751-7915.12055

Lal, C. V., Bhandari, V., and Ambalavanan, N. (2018). Genomics, microbiomics, proteomics, and metabolomics in bronchopulmonary dysplasia. *Semin. Perinatol.* 42, 425–431. doi: 10.1053/j.semperi.2018.09.004

Lazcano, A., Bazzicalupo, M., Alifano, P., Fani, R., Lio, P., Carlomagno, M. S., et al. (1996). Histidine biosynthetic pathway and genes: structure, regulation and evolution. *Microbiol. Rev.* 60, 44–69. doi: 10.1128/mr.60.1.44-69.1996

Lehmann, J. (2009). *Biochar for Environmental Management: Science and Technology*. Sterling, VA: Earthscan.

Martin, F. P. J., Montoliu, I., and Kussmann, M. (2017). Metabonomics of ageing – towards understanding metabolism of a long and healthy life. *Mech. Ageing Dev.* 165(Pt B), 171–179. doi: 10.1016/j.mad.2016.12.009

Maus, M. V., Fraietta, J. A., Levine, B. L., Kalos, M., Zhao, Y., and June, C. H. (2014). Adoptive immunotherapy for cancer or viruses. *Annu. Rev. Immunol.* 32, 189–225. doi: 10.1146/annurev-immunol-032713-120136

Meng, J. (2013). Biochar in China: status quo of research and trend of industrial development. *J. Shenyang Agric. Univ. Soc. Sci. Ed.* 15, 1–5.

Mitsuhashi, S. (2014). Current topics in the biotechnological production of essential amino acids, functional amino acids, and dipeptides. *Curr. Opin. Biotechnol.* 26, 38–44. doi: 10.1016/j.copbio.2013.08.020

Ning, Y., Wu, X., Zhang, C., Xu, Q., Chen, N., and Xie, X. (2016). Pathway construction and metabolic engineering for fermentative production of ectoine in *Escherichia coli*. *Metab. Eng.* 36, 10–18. doi: 10.1016/j.ymben.2016.02.013

Profumo, A., Gorroni, A., Guarnieri, S. A., Mellerio, G. G., Cucca, L., and Merli, D. (2020). GC-MS qualitative analysis of the volatile, semivolatile and volatilizable fractions of soil evidence for forensic application: a chemical fingerprinting. *Talanta* 219:121304. doi: 10.1016/j.talanta.2020.121304

Rieu, I., and Powers, S. J. (2009). Real-time quantitative RT-PCR: design, calculations, and statistics. *Plant Cell* 21, 1031–1033. doi: 10.1105/tpc.109.066001

Roy, S., kumar Jain, A., Lal, S., and Kini, J. (2018). A study about color normalization methods for histopathology images. *Micron* 114, 42–61. doi: 10.1016/j.micron.2018.07.005

Shi, Y. (2011). China's resources of biomass feedstock. *Eng. Sci.* 13, 16–23.

Shibasaki, M., Kanai, M., and Mita, T. (2008). The catalytic asymmetric strecker reaction. *Org. React.* 70, 1–119. doi: 10.1002/0471264180.or070.01

Tuttle, K. R., Milton, J. E., Packard, D. P., Shuler, L. A., and Short, R. A. (2012). Dietary amino acids and blood pressure: a cohort study of patients with cardiovascular disease. *Am. J. Kidney Dis.* 59, 803–809. doi: 10.1053/j.ajkd.2011.12.026

Yang, E., Jun, M., Haijun, H., and Wenfu, C. (2015). Chemical composition and potential bioactivity of volatile from fast pyrolysis of rice husk. *J. Anal. Appl. Pyrolysis* 112, 394–400. doi: 10.1016/j.jaap.2015.02.021

Yang, E., Meng, J., Hu, H., Cheng, D., Zhu, C., and Chen, W. (2019). Effects of organic molecules from biochar-extracted liquor on the growth of rice seedlings. *Ecotoxicol. Environ. Saf.* 170, 338–345. doi: 10.1016/j.ecoenv.2018.11.108

Yuan, J., Meng, J., Liang, X., E, Y., Yang, X., and Chen, W. (2017). Organic molecules from biochar leacheates have a positive effect on rice seedling cold tolerance. *Front. Plant Sci.* 8:1624. doi: 10.3389/fpls.2017.01624

Zhao, Y. Y., Cheng, X. L., Vaziri, N. D., Liu, S., and Lin, R. C. (2015). UPLC-based metabonomic applications for discovering biomarkers of diseases in clinical chemistry. *Clin. Biochem.* 47, 16–26. doi: 10.1016/j.clinbiochem.2014.07.019

Conflict of Interest: The authors declare that the research was conducted in the absence of any commercial or financial relationships that could be construed as a potential conflict of interest.

frontiers in Bioengineering and Biotechnology

ORIGINAL RESEARCH
published: 27 January 2021
doi: 10.3389/fbioe.2020.630476

Fermentative Production of L-2-Hydroxyglutarate by Engineered *Corynebacterium glutamicum* via Pathway Extension of L-Lysine Biosynthesis

*Carina Prell, Arthur Burgardt, Florian Meyer and Volker F. Wendisch**

Genetics of Prokaryotes, Faculty of Biology, Center for Biotechnology (CeBiTec), Bielefeld University, Bielefeld, Germany

L-2-hydroxyglutarate (L-2HG) is a trifunctional building block and highly attractive for the chemical and pharmaceutical industries. The natural L-lysine biosynthesis pathway of the amino acid producer *Corynebacterium glutamicum* was extended for the fermentative production of L-2HG. Since L-2HG is not native to the metabolism of *C. glutamicum* metabolic engineering of a genome-streamlined L-lysine overproducing strain was required to enable the conversion of L-lysine to L-2HG in a six-step synthetic pathway. To this end, L-lysine decarboxylase was cascaded with two transamination reactions, two NAD(P)-dependent oxidation reactions and the terminal 2-oxoglutarate-dependent glutarate hydroxylase. Of three sources for glutarate hydroxylase the metalloenzyme CsiD from *Pseudomonas putida* supported L-2HG production to the highest titers. Genetic experiments suggested a role of succinate exporter SucE for export of L-2HG and improving expression of its gene by chromosomal exchange of its native promoter improved L-2HG production. The availability of Fe^{2+} as cofactor of CsiD was identified as a major bottleneck in the conversion of glutarate to L-2HG. As consequence of strain engineering and media adaptation product titers of 34 ± 0 mM were obtained in a microcultivation system. The glucose-based process was stable in 2 L bioreactor cultivations and a L-2HG titer of 3.5 g L^{-1} was obtained at the higher of two tested aeration levels. Production of L-2HG from a sidestream of the starch industry as renewable substrate was demonstrated. To the best of our knowledge, this study is the first description of fermentative production of L-2HG, a monomeric precursor used in electrochromic polyamides, to cross-link polyamides or to increase their biodegradability.

Keywords: *C. glutamicum*, L-2-hydroxyglutarate, metabolic engineering, glutarate hydroxylase, wheat sidestream concentrate, bioreactor

OPEN ACCESS

Edited by:
Yi-Rui Wu,
Shantou University, China

Reviewed by:
Si Jae Park,
Ewha Womans University, South Korea
Liang Quanfeng,
Shandong University, China
Robert Bertrand,
University of California, Berkeley, United States

****Correspondence:***
Volker F. Wendisch
volker.wendisch@uni-bielefeld.de

Specialty section:
This article was submitted to Industrial Biotechnology, a section of the journal Frontiers in Bioengineering and Biotechnology

Received: *17 November 2020*
Accepted: *24 December 2020*
Published: *27 January 2021*

Citation:
Prell C, Burgardt A, Meyer F and Wendisch VF (2021) Fermentative Production of L-2-Hydroxyglutarate by Engineered Corynebacterium glutamicum via Pathway Extension of L-Lysine Biosynthesis. Front. Bioeng. Biotechnol. 8:630476. doi: 10.3389/fbioe.2020.630476

INTRODUCTION

L-2-hydroxyglutarate (L-2HG) can be obtained by hydroxylation of the C_5-dicarboxylic acid glutarate at the α-carbon position. Glutarate is known to be a demanded building block for the production of biopolymers, like aliphatic polyamide 6,5 which is mainly used in the construction industry (Navarro et al., 1997). Carbon chain length and functional groups of the monomers

are important for the performance of the biopolymer with respect to physical and chemical properties. In the case of L-2HG, the additional hydroxyl group provides greater versatility for further chemical modification with the potential to alter the properties of the resulting polymer. Furthermore, incorporation of hydroxylated monomers enhances the biodegradability of the polyamide (Varela and Orgueira, 2000). Production of L-2HG by microbial fermentation would provide the chemical industry with an environmentally friendly building block for polyamides and polyesters. The addition of functionalities on polyester backbones (hydroxyl, carboxyl, allyl, azido, and acetylene groups) facilitates covalent post-polymerization modification. In 2017, it was shown that the enantiomer D-2-hydroxyglutarate (D-2HG) can be used as a functionalized building block for a polyester after cyclization to an allyl containing lactide (Nan and Feher, 2017). Also, it was demonstrated that electrochromic polyamides with functional hydroxyl groups for homogeneous hybrid films can be produced. The repeating units of hydroxysuccinate in the polymer backbone provided reaction sites for organic-inorganic bonding resulting in homogeneous and transparent hybrid films (Pan et al., 2018).

In medicine, L-2HG is used as a diagnostic biomarker for the characterization of various cancer types (Shim et al., 2014). Under oxygen limitation, L-2HG accumulates as metabolic intermediate in healthy as well as in malignant animal cells (Shim et al., 2014; Oldham et al., 2015; Shelar et al., 2018) facilitating a physiological adaption to hypoxic stress. The accumulation of L-2HG is triggered by increasing concentrations of 2-oxoglutarate (2-OG), which is caused by tricarboxylic acid cycle dysfunction and increased mitochondrial reducing potential. As consequence, the increased cellular L-2HG concentrations lead to inhibition of the electron transport and glycolysis compensating the effects of mitochondrial reductive stress induced by hypoxia (Oldham et al., 2015). The stereospecific reduction of 2-oxoglutarate to L-2HG is catalyzed by lactate dehydrogenase (LDH) and malate dehydrogenase (MDH) under hypoxic stress conditions (Intlekofer et al., 2017). In contrast, the formation of its enantiomer D-2-hydroxyglutarate (D-2HG) is catalyzed by a mutated version of isocitrate dehydrogenase 1 or 2 (IDH1/2) contributing to the pathogenesis of cancer, whereas L-2HG biosynthesis does neither involve IDH1 nor IDH2. Albeit both enantiomers of 2-hydroxyglutarate display an inhibitory effect on 2-oxoglutarate-dependent enzymes involved in diverse biologic processes (Chowdhury et al., 2011; Xu et al., 2011), their stereospecific biosynthesis differs. Thus, bio-based routes enable stereospecific synthesis of either D-2HG or L-2HG, which is preferred over chemically synthesized racemic D,L-2HG. Beyond the occurrence as a product of cellular redox stress, L-2HG also plays a role in plants and eukaryotic cells as part of the mitochondrial metabolic repair mechanism (Hüdig et al., 2015). A side reaction of MDH yields small concentrations of L-2HG by reduction of 2-oxoglutarate. The mitochondrial FAD-containing oxidase L-2-hydroxyglutarate dehydrogenase (L2HGDH, EC 1.1.5.13) oxidizes L-2HG and the electrons produced in the reaction are transferred to the mitochondrial electron transport chain through the electron transfer protein (ETF) (Wanders et al., 1997; Rzem et al., 2004). An enzyme homologous to L2HGDH was also described in the model organism *Escherichia coli* (Knorr et al., 2018).

In bacteria, L-2HG mainly accumulates under carbon starvation conditions (Marschall et al., 1998; Metzner et al., 2004; Knorr et al., 2018). It is also an intermediate of the L-lysine degradation pathway in *Pseudomonadaceae* (Zhang et al., 2018; Thompson et al., 2019). Glutarate is the direct precursor of L-2HG. Hydroxylation of glutarate to L-2HG is catalyzed by a highly regio- and stereospecific Fe(II)/2-oxoglutarate-dependent dioxygenase CsiD (EC 1.14.11.64, also named glutarate hydroxylase) (Hibi and Ogawa, 2014). The co-product succinate is metabolized via the TCA-cycle. Since L-2-hydroxyglutarate oxidase (LghO) regenerates 2-oxoglutarate by oxidation of L-2HG (Knorr et al., 2018; Herr et al., 2019), the combined activities of CsiD and LghO convert the C5-dicarboxylic acid glutarate to the C4-dicarboxylic acid succinate. Thus, the absence of LghO is required for overproduction of L-2HG from glutarate.

Glutarate can be derived from L-lysine by four pathways that converge to 5AVA, which is converted to glutarate by GABA/5AVA aminotransferase (GabT) and the succinate/glutarate semialdehyde dehydrogenase (GabD). The first pathway from L-lysine to 5AVA employs L-lysine-α-oxidase (RaiP) from *Scomber japonicus* that catalyzes oxidative desamination of L-lysine using molecular oxygen followed by spontaneous decarboxylation (Cheng et al., 2020). The second pathway to 5AVA combines oxidative decarboxylation by L-lysine monooxygenase using molecular oxygen followed by desamidation by γ-aminovaleramidase from *P. putida* (Adkins et al., 2013). The third pathway is based on L-lysine decarboxylase from *E. coli*, putrescine oxidase PuO from *Rhodococcus qingshengii* and the γ-aminobutyraldehyde dehydrogenase from *E. coli* that catalyze decarboxylation, oxidative deamination using molecular oxygen and NAD-dependent oxidation (Haupka et al., 2020). The fourth pathway does not require molecular oxygen as it cascades L-lysine decarboxylase, 2-oxoglurate-dependent putrescine/cadaverine transaminase PatA, and NAD-dependent γ- aminobutyraldehyde dehydrogenase PatD from *E. coli* (Jorge et al., 2017). The pathway combinations for LdcC-PuO-PatD-GabT-GabD and LdcC-PatA-PatD-GabT-GabD couple conversion of lysine to glutarate in one or two transaminase reactions, respectively, that generate glutamate from 2-oxoglutarate. This coupling enabled flux enforcement, i.e., growth requires production of glutarate, which was achieved by deletion of *gdh*, the gene for the major ammonium assimilating enzyme L-glutamic acid dehydrogenase (Pérez-García et al., 2018; Haupka et al., 2020).

Since biosynthesis of L-2HG from glutarate requires molecular oxygen, glutarate biosynthesis from L-lysine by a pathway independent of molecular oxygen was extended by glutarate hydroxylase. The pathways RaiP-GabT-GabD, DavA-DavB-GabT-GabD, and LdcC-PuO-PatD-GabT-GabD involve oxygenases (RaiP, DavA, and PuO, respectively), whereas the pathway LdcC-PatA-PatD-GabT-GabD does not contain an enzyme using molecular oxygen as substrate (Jorge et al., 2017). To construct the six-step cascade LdcC-PatA-PatD-GabT-GabD-CsiD (**Figure 1**), CsiD enzymes from *E. coli* MG1655,

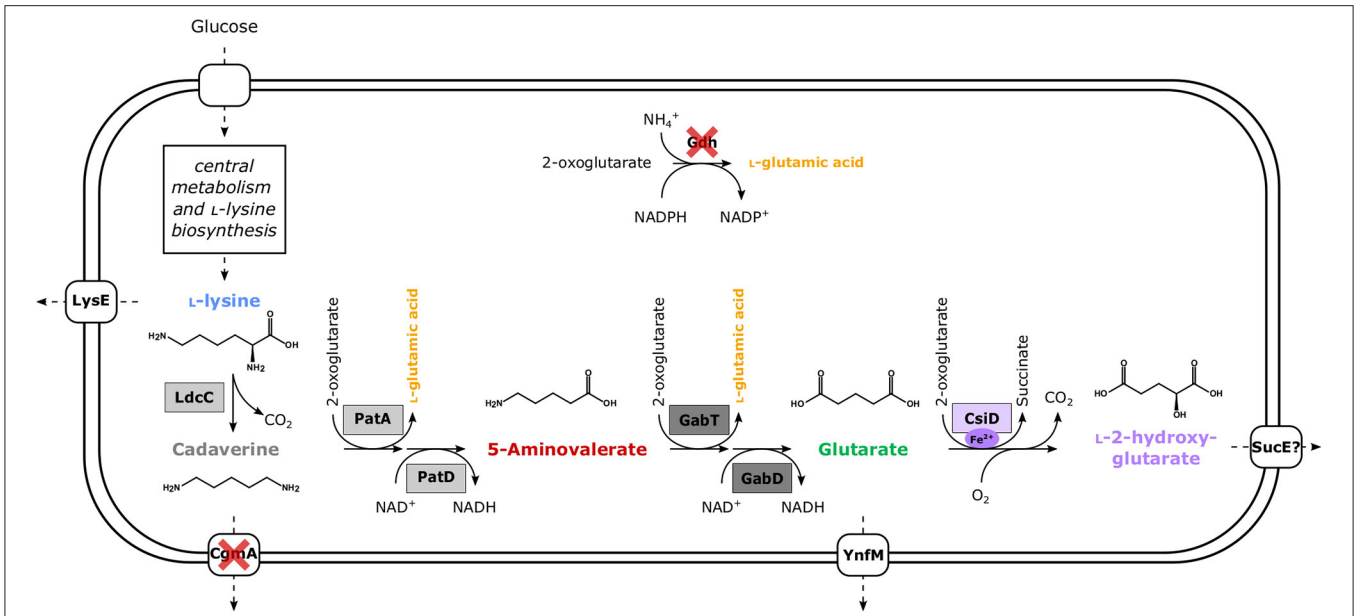

FIGURE 1 | Schematic overview of metabolically engineered *C. glutamicum* overproducing L-2HG. Enzyme names are shown next to the reaction represented by the arrows. Dashed arrows represent several reaction steps. Heterologous enzymes are boxed, while gene deletions for enzymes are indicated by red crosses. Dark gray boxes depict enzymes encoded in *P. stutzeri* (*gabT*, GABA/5AVA amino transferase; *gabD*, succinate/glutarate-semialdehyde dehydrogenase) and light gray boxes those from *E. coli* (*ldcC*, L-lysine decarboxylase; *patA*, putrescine transaminase; *patD*, γ-aminobutyraldehyde dehydrogenase). In the case of glutarate hydroxylase (EC 1.14.1.64) CsiD enzymes (violet box) were sourced from either *E. coli* (HEGluA), *P. putida* (HPGluA), or *Halobacillus sp*. (HBGluA).

P. putida KT2440 and *Halobacillus sp.* BA-2008 were tested since inspection of the genome sequence of *C. glutamicum* did not indicate that a CsiD homolog is encoded. The absence of LhgO from the *C. glutamicum* genome was considered beneficial since it indicated that L-2HG may not be degraded. This and the fact that we previously established efficient glutarate production employing the LdcC-PatA-PatD-GabT-GabD pathway provided an ideal starting point to establish fermentative production of L-2HG from renewable resources. This concept may be transferred to fermentative production of the stereoisomer D-2HG by extending the glutarate pathway with enzymes for conversion of glutarate to D-2HG.

MATERIALS AND METHODS

Microorganisms and Cultivation Conditions

E. coli DH5α strain was used as a host for cloning (Hanahan, 1985), S17-1 for transconjugation (Schäfer et al., 1994). Both strains were grown in lysogeny broth (LB) at 37 °C and supplemented with antibiotics (50 μg mL^{-1} kanamycin, 100 μg mL^{-1} spectinomycin, 10 μg mL^{-1} tetracycline) when appropriate. *C. glutamicum* ATCC 13032 derived strains were cultivated in brain heart infusion with 0.5 M sorbitol (BHIS), or CGXII minimal medium (Eggeling and Bott, 2004) supplemented with 1 mM IPTG when appropriate. All bacterial strains and plasmids are listed in **Tables 1**, **2**. For standard growth experiments in CGXII medium with *C. glutamicum*, overnight cultures in 10 mL BHIS were harvested and washed twice in TN-buffer (50 mM Tris-HCl, 50 mM NaCl, pH 6.3) before inoculation to an OD_{600} of 1 and supplementation with 40 g L^{-1} glucose as a sole carbon source. The cultivations in the BioLector microfermentation system (m2p-labs, Baesweiler, Germany) were performed in 3.2 mL FlowerPlates at 1,100 rpm with a filling volume of 1,000 μL.

To test for the utilization of L-2HG as carbon source, 12 mM L-2HG and 10 mM glucose were added, respectively, and the wildtype was inoculated to an initial OD_{600} of 0.5. For optimization of the iron concentration in CGXII minimal medium the respective concentrations of iron-(II)-sulfate (0–3 mM) were supplemented. To test the inhibitory effect of glutarate on L-2HG production, 20 or 40 mM of glutarate (pH 7.0) was added to CGXII medium, respectively.

For L-2HG production from wheat sidestream concentrate (WSC; obtained from Jäckering, Hamm, Germany) overnight cultures in 10 mL BHIS were harvested and washed twice in TN-buffer (50 mM Tris-HCl, 50 mM NaCl, pH 6.3) before inoculation to an OD_{600} of 1. The medium consisted of 246 g L^{-1} WSC, 20 g L^{-1} ammonium sulfate as nitrogen source, 42 g L^{-1} MOPS as buffer and 2 mM iron-(II)-sulfate (added as CsiD is an iron-containing enzyme). Growth in 10 mL Duetz microcultivation plates (Kuhner Shaker GmbH, Herzogenrath, Germany) was performed with different sandwich covers and culture volumes to alter the oxygen supply. Under "low oxygen" cultivation, cells were grown in 3 mL at 220 rpm in an Ecotron ET25-TA-RC (Infors HT, Einsbach, Germany) and plate sandwich covers for low evaporation (1.2 mm hole diameter) were used. For "high oxygen" supply the culture

TABLE 1 | Bacterial strains used in this study.

Strain	Relevant characteristics	References
E. coli		
DH5α	Δ*lac*U169 (ϕ80*lacZ* ΔM15), *sup*E44, *hsd*R17, *rec*A1, *end*A1, *gyr*A96, *thi*-1, *rel*A1	Hanahan, 1985
S17-1	*recA*, *pro*, *hsdR*, RP4- 2Tc::Mu Km::Tn7 integrated into the chromosome	Simon et al., 1983
C. glutamicum		
WT	*C. glutamicum* ATCC13032	ATCC
GRLys1 (DM1933ΔCGP123)	*C. glutamicum* ATCC13032 with modifications: Δ*pck*, *pyc*^{P458S}, *hom*^{V59A}, 2 copies of *lysC*^{T311I}, 2 copies of *asd*, 2 copies of *dapA*, 2 copies of *dapB*, 2 copies of *ddh*, 2 copies of *lysA*, 2 copies of *lysE*, in-frame deletion of prophages CGP1 (cg1507-cg1524), CGP2 (cg1746-cg1752) and CGP3 (cg1890-cg2071)	Unthan et al., 2015
GSLA2G	In-frame deletions of *sugR, ldhA, snaA* and *cgmA, gdh* in GRLys1	Pérez-García et al., 2018
GluA	GSLA2G(pVWEx1-*ldcC*) (pEKEx3-*patDA*) (pEC-XT99A-*gabTD**)	Pérez-García et al., 2018
GluAΔ*sucE*	GSLA2GΔ*sucE* (pVWEx1-*ldcC*) (pEKEx3-*patDA*) (pEC-XT99A-*gabTD**)	This study
GluA2	GSLA2GΔP$_{sucE}$::P$_{tuf}$ (pVWEx1-*ldcC*)(pEKEx3-*patDA*)(pEC-XT99A-*gabTD**)	This study
HEGluA	GSLA2G(pVWEx1-*ldcC-csiD*^{Ec}) (pEKEx3-*patDA*) (pEC-XT99A-*gabTD**)	This study
HBGluA	GSLA2G (pVWEx1-*ldcC-csiD*^{Hb}) (pEKEx3-*patDA*) (pEC-XT99A-*gabTD**)	This study
HPGluA	GSLA2G (pVWEx1-*ldcC-csiD*^{Pp})(pEKEx3-*patDA*)(pEC-XT99A-*gabTD**)	This study
HPGluAΔ*sucE*	GSLA2GΔ*sucE* (pVWEx1-*ldcC-csiD*^{Pp}) (pEKEx3-*patDA*) (pEC-XT99A-*gabTD**)	This study
HPGluA2	GSLA2GΔP$_{sucE}$::P$_{tuf}$ (pVWEx1-*ldcC-csiD*^{Pp}) (pEKEx3-*patDA*) (pEC-XT99A-*gabTD**)	This study

TABLE 2 | Plasmids used in this study.

Plasmid	Relevant characteristics	References
pK19*mobsacB*	Kan^{R}, mobilizable *E. coli* vector mutagenesis (*oriV*, *sacB*)	Schäfer et al., 1994
pK19*mobsacB*-Δ*sucE*	pK19*mobsacB* with a deletion construct *sucE*	This study
pK19*mobsacB*-ΔP$_{sucE}$::P$_{tuf}$	pK19*mobsacB* with a promoter exchange of *sucE* with the strong *tuf*-promoter and an optimized RBS	This study
pVWEx1	Kan^{R}, *C. glutamicum/E. coli* shuttle vector (P$_{tac}$, *lacI*^{q})	Peters-Wendisch et al., 2001
pVWEx1-*ldcC*	pVWEx1 expressing *ldcC* from *E.coli* MG1655	Pérez-García et al., 2018
pVWEx1-*ldcC-csiD*^{Ec}	pVWEx1 expressing *ldcC* and *csiD* from *E.coli* MG1655	This study
pVWEx1-*ldcC-csiD*^{Hb}	pVWEx1 expressing *ldcC* from *E.coli* MG1655 and *csiD* from *Halobacillus sp.* BA-2008	This study
pVWEx1-*ldcC-csiD*^{Pp}	pVWEx1 expressing *ldcC* from *E.coli* MG1655 and *csiD* from *Pseudomonas putida* KT2440	This study
pEC-XT99A	Tet^{R}, *C. glutamicum/E. coli* shuttle vector (P$_{trc}$, *lacI*^{q}, pGA1, *oriV*$_{Cg}$)	Kirchner and Tauch, 2003
pEC-XT99A-*gabTD**	pEC-XT99A expressing *gabT* and *gabD*^{P134L} from *P. stutzerii* ATCC17588	This study
pEKEx3	Spec^{R}, *C. glutamicum/E. coli* shuttle vector (P$_{tac}$ *lacI*^{q} pBL1, *oriV*$_{Ec}$)	Stansen et al., 2005
pEKEx3-*patDA*	pEKEx3, expressing *patD* and *patA* from *E. coli* MG1655	Pérez-García et al., 2018

Km^{R}: kanamycin resistance.
Spec^{R}: spectomycin resistance.
Tet^{R}: tetracycline resistance.

TABLE 3 | Oligonucleotides used as primers in this study.

Primer	Sequence (5′-3′)	Description
ldcC-fw	CCTGCAGGTCGACTCTAGAGG ATTCCGAAAGGAGGCCCTTCAG ATGAACATCATTGCCATTATGGG	Construction of pVWEx1-*ldcC-csiD*
ldcC-csiD^{Ec}-rv	CCTTTTGTATTCTTGTATTGGCG TTTTTATCCCGCCATTTTTAGG	
csiD^{Ec}-fw	CCTAAAAATGGCGGGATAA *AAACGCCAATACAAGAAT ACAAAAGGAGGTAATTTT* ATGAATGCACTGACCGCCG	Construction of pVWEx1-*ldcC-csiD^{Ec}*
csiD^{Ec}-rv	*GAATTCGAGCTCGGTACCCGGGGAT* CTTACTGATGCGTCTGGTAGT	
ldcC-csiD^{Pp}-rv	GTCCTGTTAACAGGACTAATTAT AATTATCCCGCCATTTTTAGG	
csiD^{Pp}-fw	CCTAAAAATGGCGGGATAA *TTATAATTAGTCCTGTTAACAG GACATCAAAGGAGGTTTTTTT* ATGAACGCCTTTACGCAG	Construction of pVWEx1-*ldcC-csiD^{Pp}*
csiD^{Pp}-rv	GAATTCGAGCTCGGTACCCGGGGATC TTATTGACCGCGCTGGTAC	
ldcC-csiD^{Hb}-rv	*TTCCTTTAAGTTATACTTTCGTTAA* TTATCCCGCCATTTTTAGG	
csiD^{Hb}-fw	CCTAAAAATGGCGGGATAA *TTAACGAAAGTATA ACTTAAAGGAACCACGTATTT* ATGTGCGCAGTAGAAATG	Construction of pVWEx1-*ldcC-csiD^{Hb}*
csiD^{Hb}-rv	*GAATTCGAGCTCGGTACCCGGGGATC* CTATTGAAGGAATCGTCC	
ldcC-seq1	TGAACGATGTAGTGCCAGTC	
ldcC-seq2	GCAATGGGATTATTGCGTGG	Sequencing of pVWEx1-*ldcC-csiD*
ldcC-seq3	CAGGCAGAATCGAAGTGA	
csiD^{Ec}-seq	CCGATTACGTGCTGATG	Sequencing of pVWEx1-*ldcC-csiD^{Ec}*
csiD^{Pp}-seq	GATCTGGTTCACGAAC	Sequencing of pVWEx1-*ldcC-csiD^{Pp}*
csiD^{Hb}-seq	GTAGGTTCCATCAGTG	Sequencing of pVWEx1-*ldcC-csiD^{Hb}*
PSucEA	*GCATGCCTGCAGGTCGACTCTAGA* GGCGTGACGTGTACAAGCGCG	
PSucEB	TACGCGCCTACTGACACGCTAAAA CTTAAGCCTCGCCCTTGCGTTC	Construction of pK19*mobsacB_* ΔP_{sucE}::P_{tuf}
P_{tuf}-fw	GGCTGAACGCAAGGGCGAGGCTTAA GTTTTAGCGTGTCAGTAGGC	
P_{tuf}-rv	AAGGAAGCTCAT *AAAAATACCTCCCCCAGTGTTCGTG CCGTCGCCCCGGCGACGAGTTTA* GTTACTGAATCCTAAGGGCA	
PSucEC	CGGCACGAACACTGGGGGAGGTATTTTT **A**TGAGCTTCCTTGTAGAAAATC	
PSucED	*AATTCGAGCTCGGTACCCGGGGATC* GAATAACGATGAGCACACCG	

(Continued)

TABLE 3 | Continued

Primer	Sequence (5′-3′)	Description
PSucEE	GACTCGCTCACAAATGTGG	Verification of Promoter exchange ΔP_{sucE}::P_{tuf}
PSucEF	GAATTGCTCACCGTCTCG	
SucEA	*GCATGCCTGCAGGTCGACTCTAGAG* GTGGCACCTGGTGTTCCAG	
SucEB	TTTGGGCGGCCAGGATCTTTGCGAT TTCTACAAGGAAGCTCAC	Construction of pK19*mobsacB_ ΔsucE*
SucEC	GAATGGGTGAGCTTCCTTGTAGAA ATCGCAAAGATCCTGGC	
SucED	*AATTCGAGCTCGGTACCCGGGGATC* CGAATGGATTGGTCAGGG	
SucEE	CTGCTGGTTGGGCTGTGG	Verification *sucE* deletion
SucEF	GTTAATCATGAGGCGTCG	Verification *sucE* deletion

Overlaps to the vector are underlined, the ribosome binding site is indicated in italic and amino acid exchanges are shown in bold.

volume was decreased to 2 mL and standard plate sandwich covers (2.5 mm hole diameter) were used. Growth was monitored by determination of the OD_{600} with a V-1200 Spectrophotometer (VWR, Radnor, PA, USA).

Molecular Biology Methods

Genomic DNA of *C. glutamicum, E. coli* and *P. putida* were isolated as described previously (Eikmanns et al., 1994). The gene *csiD* from *Halobacillus sp.* BA-2008 was codon-harmonized (Haupka, 2020) and synthesized with an optimized ribosomal binding site by Synbio Technologies (South Brunswick Township, New Jersey, United States of America). The standard molecular methods including plasmid isolation, molecular cloning and transformation of *E. coli* by heat shock and of *C. glutamicum* by electroporation with plasmid DNA were performed as described before (Eggeling and Bott, 2004). DNA sequences were amplified with the ALLin HiFi DNA Polymerase (HighQu, Kraichtal, Germany) using plasmid or genomic DNA as template. The oligonucleotides used in this study are listed in **Table 3**. The gene *ldcC* was amplified from the vector pVWEx1-*ldcC* (Pérez-García et al., 2018), whereas the different *csiD* genes were amplified from genomic DNA of the respective organisms and assembled together into BamHI-digested pVWEx1 by Gibson Assembly, using the respective primers. The constructed plasmids were transferred into *C. glutamicum* by transformation. For deletion, plasmid pK19*mobsacB* (Schäfer et al., 1994), digested with BamHI was assembled with amplified DNA fragments flanking the gene *sucE* (cg2425) using Gibson Assembly and was transferred into *E. coli* S17-1 to follow a protocol for gene deletion routinely applied (Eggeling and Bott, 2004). For replacement of the native promoter by the stronger *tuf*-promoter, the *tuf*-promoter and the flanking regions of the promoter of *sucE* were amplified from

genomic DNA of *C. glutamicum* and assembled with the digested plasmid pK19*mobsacB*. For higher expression rates the start codon of *sucE* was changed from GTG to ATG and an optimized ribosome binding site (RBS) was included (Salis, 2011).

Coupled *in vitro* Activity of GabT and GabD

The apparent activities of GABA transaminase GabT and succinate semialdehyde oxidoreductase GabD were assayed in combination by monitoring NADPH formation after the addition of 2-oxoglutarate. The preparation of the crude extract was carried out as previously described (Pérez-García et al., 2018). The 1 mL assay mix contained 150 mM phosphate buffer (pH 9.0), L-2HG (2, 4, 8, 12 mM) or NaCl as control, 0.1 mM pyridoxal-5′-phosphate, 1 mM $NADP^+$, 20 mM 5AVA, and 0.5 mg mL^{-1} crude extract. The reaction was started by the addition of 15 mM 2-oxoglutatarate. Protein concentrations were determined with the Bradford assay kit (Bio-Rad Laboratories, Hercules, CA, United States) using BSA (bovine serum albumin) as standard. The formation of NADPH was monitored photometrically at 340 nm and 30°C for 3 min using a Shimadzu UV-1202 spectrophotometer (Shimadzu, Duisburg, Germany).

Quantification of Amino Acids, Diamines, and Carboxylic Acids

The quantification of extracellular amino acids and their derivatives, carbohydrates and carboxylic acids in the cultivation medium was performed with a high-performance liquid chromatography system (1200 series, Agilent Technologies Deutschland GmbH, Böblingen, Germany). After centrifugation of 1 mL of cell cultures at 14,000 rpm for 10 min the supernatant was stored at −20°C prior to analysis. Analysis of L-lysine, 5AVA and the diamine cadaverine was performed by an automatic pre-column derivatization with *ortho*-phthaldialdehyde (OPA) and separated on a reversed phase HPLC using pre- and main column (LiChrospher 100 RP8 EC-5µ, 125 × 4.6 mm, CS Chromatographie Service GmbH) with L-asparagine as internal standard (Schneider and Wendisch, 2010). Detection of the fluorescent derivatives was carried out with a fluorescence detector with an excitation wavelength of 230 nm and an emission wavelength of 450 nm. Glutarate and L-2HG and glucose concentrations were measured with an amino exchange column (Aminex, 300 × 8 mm, 10 µm particle size, 25 Å pore diameter, CS Chromatographie Service GmbH) under isocratic conditions as described previously with a flow of 0.8 mL min^{-1} (Schneider et al., 2011). The substances were detected with a refractive index detector (RID G1362A, 1200 series, Agilent Technologies) and a diode array detector (DAD G1315B, 1200 series, Agilent Technologies) at 210 nm.

Fermentative Production

A baffled bioreactor with total a volume of 3.6 L was used (KLF, Bioengineering AG, Switzerland). Three six-bladed Rushton turbines were placed on the stirrer axis with a distance from the bottom of the reactor of 6, 12, and 18 cm. The aspect ratio of the reactor was 2.6:1.0 and the stirrer to reactor diameter ratio was 0.39. Automatic control of the stirrer speed between 400 and 1500 rpm kept the relative dissolved oxygen saturation at 30%. A constant airflow of 1 or 2 NL min^{-1} was maintained from the bottom through a sparger, corresponding to an aeration of 0.5 and 1 vvm, respectively.

The pH was kept constant at 7.0 ± 0.1 by automatic addition of phosphoric acid [10% (*v/v*)] and potassium hydroxide (4 M). The temperature was maintained at 30°C. To prevent foaming 0.6 mL L^{-1} of the antifoam agent AF204 (Sigma Aldrich, Darmstadt, Germany) was added and a mechanical foam breaker was present to serve as an additional foam control. The fermentation was performed with a head space overpressure of 0.2 bar. The initial working volume of 2 L was inoculated to an OD_{600} of 1.5 from a shake flask pre-culture in CGXII minimal medium supplemented with 40 g L^{-1} glucose, 1 mM IPTG and 2 mM $FeSO_4$. Samples were collected by an autosampler and cooled down to 4°C until further use. The feed consisted only of 600 g L^{-1} glucose ($\rho = 1.21$ kg m^{-3}) and was started 4 h after the cells reached the late stationary phase, indicated by the pO_2 rising above 80% again after the initial growth phase. The glucose feed was applied for 5 min with a flow of 1.2 mL min^{-1} when the pO_2 surpassed 60%. Further feed was only added, when the pO2 decreased to 30% after the addition of the feed solution to prevent oversaturation with glucose.

RESULTS

Establishing *de novo* Biosynthesis of L-2HG by *C. glutamicum*

As *C. glutamicum* can utilize some organic acids (Wendisch et al., 2016), the response of *C. glutamicum* WT to L-2HG was determined. When L-2HG was added to mineral salts medium as sole carbon source instead of glucose, no growth of *C. glutamicum* was observed. Moreover, when L-2HG plus glucose were assayed, *C. glutamicum* WT utilized glucose, but did not degrade L-2HG as revealed by HPLC analysis of the culture supernatants (data not shown). Thus, L-2HG does neither serve as sole nor as combined carbon source for *C. glutamicum*, which can be considered as a suitable host for production of L-2HG.

L-2HG is not a known metabolite of *C. glutamicum*, but it has been engineered for overproduction of glutarate (Pérez-García et al., 2018). Inspection of the genome of *C. glutamicum* did not indicate the presence of a gene coding for an enzyme hydroxylating glutarate. In some bacteria like *E. coli* (Marschall et al., 1998; Knorr et al., 2018; Herr et al., 2019), *P. putida*, and *Halobacillus sp.* (Thompson et al., 2019), glutarate hydroxylase, also known as glutarate dioxygenase (EC 1.14.11.64), uses molecular oxygen to hydroxylate glutarate to L-2HG with concomitant decarboxylation of 2-oxoglutarate to succinate. Thus, the respective *csiD* genes from *E. coli* MG1655, *P. putida* KT2440 and *Halobacillus sp.* BA-2008 were overexpressed in synthetic operons with *ldcC* from *E. coli*. The resulting pVWEx1-plasmids were used to transform *C. glutamicum* GSLA2G (pEKEx3_*patDA*) (pEC-XT99A_*gabTD**). The resulting strains were named HEGluA, HPGluA, and HBGluA, respectively. In production experiments, the three strains produced and secreted L-2HG. After 96 h *C. glutamicum* strain HEGluA accumulated 14 ± 0 mM L-2HG, strain HBGluA 7 ± 1 mM L-2HG, and

strain HPGluA 22 ± 2 mM L- 2HG (**Figure 2**). The strains showed comparable maximal growth rates of 0.13 ± 0.00 h^{-1}, but strain HPGluA showed a lag-phase of 24 h. Taken together, a proof-of-principle for production of L-2HG by *C. glutamicum* was demonstrated.

Role of the Succinate Exporter SucE in Export of Glutarate and L-2HG

SucE is known to play a role in the export of the dicarboxylic acid succinate out of the *C. glutamicum* cell (Huhn et al., 2011). Since L-2HG and glutarate are also dicarboxylic acids, the role of SucE in the export of L-2HG and glutarate was studied. To this end, the *sucE* gene was either overexpressed by replacing the native promoter with the stronger *tuf*-promoter or deleted. The glutarate producing strain GluA2 that overexpressed *sucE* produced significantly more glutarate than the control strain GluA (44 ± 0 vs. 48 ± 2 mM; **Figure 3A**). Similarly, upon overexpression of *sucE,* production of L-2HG was slightly elevated (24 ± 0 mM for HPGluA2 vs. 22 ± 2 mM for HPGluA; **Figure 3A**) as well as production of the by-product glutarate (26 ± 0 mM for HPGluA2 vs. 20 ± 3 mM for HPGluA; **Figure 3A**). Thus, overexpression of *sucE* was beneficial for production of glutarate as well as L-2HG.

Deletion of *sucE* in glutarate producer GluA did not negatively affect glutarate production, however, growth was slowed (0.12 ± 0.00 h^{-1} for GluA vs. 0.07 ± 0.00 h^{-1} for GluAΔ*sucE*; **Figure 3B**). Thus, SucE is not the main export system for glutarate and at least one other export system is able to compensate for the lack of SucE regarding glutarate export. Importantly, deletion of *sucE* reduced production of L-2HG more than 10-fold (2 ± 0 mM for HPGluAΔ*sucE* vs. 26 ± 1 mM for HPGluA; **Figure 3B**), while the growth rate was not significantly impacted (0.09 ± 0.00 h^{-1} for HPGluA vs. 0.08 ± 0.01 h^{-1} for HPGluAΔ*sucE*). The findings that *sucE* overexpression positively affected L-2HG production and that deletion of *sucE* dramatically reduced L-2HG production suggested that SucE may be active as export system for L-2HG.

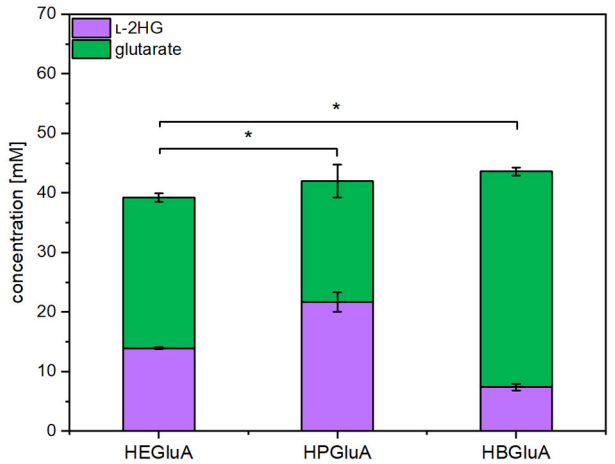

FIGURE 2 | Product titers of L-2HG and its precursor glutarate obtained with strains overproducing different glutarate hydroxylases. *C. glutamicum* strains HEGluA, HPGluA, and HBGluA expressing *csiD* from *E. coli* MG1655, *P. putida* KT2440, and *Halobacillus sp.* BA-2008, respectively, were grown in 40 g L^{-1} glucose CGXII minimal medium supplemented with 1 mM IPTG in the microcultivation device BioLector. Values and error bars represent means and standard deviations from 3 replicate cultivations with supernatants analyzed after 96 h. Statistical significance was assessed by Student's paired *t*-testing (*$p < 0.05$, n.s, not significant).

Enhanced Conversion of Glutarate to L-2HG by Increased Iron Concentrations

As the glutarate hydroxylase CsiD is an Fe^{2+}-dependent metalloenzyme (Herr et al., 2019; Thompson et al., 2019), the concentration of iron (II) in the media was varied and the effect on production of L-2HG determined. Concentrations of 0.5 to 3 mM $FeSO_4$ were added on top of the standard concentration (0.037 mM) in CGXII minimal medium

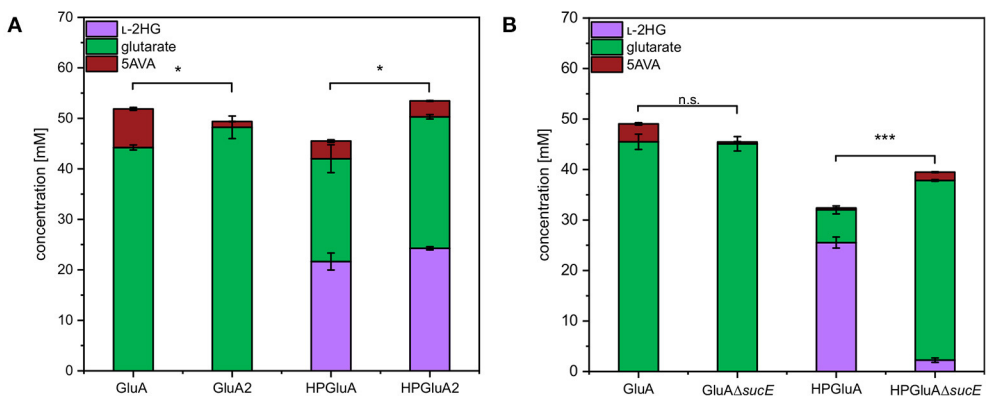

FIGURE 3 | Influence of overexpression and deletion of *sucE* on production of L-2HG, glutarate and 5AVA. **(A)** Strains GluA2 and HPGluA2 differed from strains GluA and HPGluA by overexpression of *sucE*. **(B)** Strains GluAΔ*sucE* and HPGluAΔ*sucE* were derived from strains GluA and HPGluA, respectively, by deletion of *sucE*. Strains were grown in the BioLector using 40 g L^{-1} glucose minimal medium supplemented with 1 mM IPTG and supernatants were analyzed after 120 h. Values and error bars represent mean and standard deviation values ($n = 3$ cultivations). Statistical significance was assessed in Student's paired *t*-test (***$p < 0.001$, *$p < 0.05$, n.s. not significant).

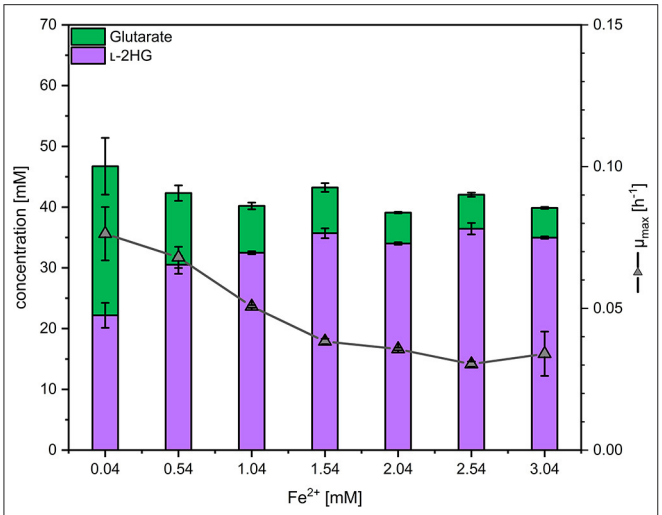

FIGURE 4 | Influence of the iron concentration on the maximal growth rate and production of L-2HG and glutarate. *C. glutamicum* HPGluA2 was grown in the BioLector with 40 g L^{-1} glucose minimal medium supplemented with 1 mM IPTG and the indicated iron concentrations. Supernatants were analyzed after 96 h. Values and error bars represent means and standard deviations ($n = 3$ cultivations).

(Eggeling and Bott, 2004). Three trends were observed: with increasing iron concentrations the growth rate and the formation of glutarate as by-product were reduced, while production of L-2HG was significantly increased (**Figure 4**). At an iron concentration of 2.04 mM, 5 ± 0 mM glutarate and 34 ± 0 mM L-2HG accumulated in the supernatant (**Figure 4**), thus, about 87% of glutarate were converted to L-2HG, while at the standard iron concentration L-2HG and glutarate accumulated to about equimolar concentrations. The growth inhibitory effect of elevated iron concentrations may be due to increased production of L-2HG and/or other effects elicited by higher iron concentrations. Thus, 2.04 mM was choosen as the optimal iron concentration for further experiments to find the best compromise between L-2HG titer and volumetric productivity.

Inhibitory Effects on Key Enzymes in L-2HG Pathway

The finding that at higher iron concentrations less glutarate and more L-2HG accumulated, while the combined concentration of glutarate plus L-2HG was highest at the lowest iron concentration indicated bottlenecks. These may arise due to inhibition of glutarate hydroxylase CsiD by its product L-2HG (Knorr et al., 2018) and/or due to inhibition of enzymes of glutarate biosynthesis. The transaminases PatA from *E. coli* and GabT from *P. stutzerii* are crucial for glutarate biosynthesis (Pérez-García et al., 2018) and some transaminases are known to be inhibited by L-2HG, which blocks binding of the substrate 2-oxoglutarate (McBrayer et al., 2018). To approach this problem, enzyme activity assays were performed with crude extracts of *C. glutamicum* GluA. A combined activity assay of GABA transaminase GabT and succinate semialdehyde dehydrogenase

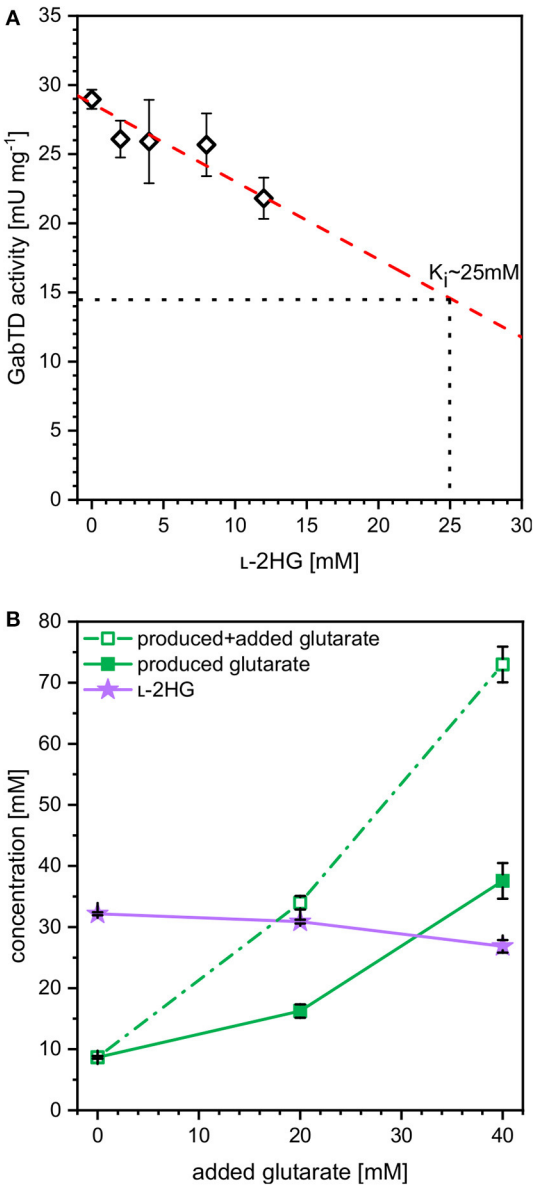

FIGURE 5 | Influence of L-2HG on the combined *in vitro* enzyme activities of GABA transaminase GabT and succinate semialdehyde dehydrogenase GabD **(A)** and influence of extracellularly added glutarate on production of L-2HG **(B)**. **(A)** Crude extracts of GluA were assayed for combined *in vitro* enzyme activities of GABA transaminase GabT and succinate semialdehyde dehydrogenase GabD in the presence of increasing concentrations of L-2HG. **(B)** Strain HPGluA2 was cultivated in the BioLector with 40 g L^{-1} glucose minimal medium supplemented with 1 mM IPTG, 2 mM iron (II)-sulfate and increasing concentrations of glutarate (0, 20, 40 mM). Supernatant concentrations of L-2HG (filled violet triangles), glutarate (open green squares) as well as the net glutarate concentrations produced in addition to the added glutarate concentration (closed green squares) were determined after 96 h and are given as means and standard deviations of three independent cultivations.

GabD was performed as described previously (Pérez-García et al., 2018). In the presence of increasing concentrations of L-2HG (0–12 mM) the combined GabT and GabD activity was

reduced. By extrapolation, it was determined that 25 mM L-2HG resulted in half-maximal GabTD activity (**Figure 5A**). Thus, L-2HG negatively affects production of its precursor glutarate.

In order to determine if increased glutarate concentrations are beneficial for production of L-2HG, production of L-2HG was determined in the absence or presence of extracellularly added glutarate (0, 20, or 40 mM). Notably, externally added glutarate slightly reduced production of L-2HG, whereas glutarate accumulation was increased (**Figure 5B**). When 0, 20, or 40 mM glutarate were added to the medium before inoculation, additional glutarate was produced: 9, 16, and 38 mM, respectively (**Figure 5B**). Thus, extracellular glutarate addition exerts a positive effect on glutarate production. The slight reduction of L-2HG production upon addition of extracellular glutarate may be due to substrate inhibition of glutarate hydroxylase CsiD.

L-2HG Production at Bioreactor Scale

In order to test if L-2HG production by strain HPGluA2 is stable at larger volumes, 2 L scale bioreactor fermentations were performed. Two aeration rates were tested: 0.5 and 1 vvm (**Figure 6**). Under both conditions cells grew with similar growth rates (0.5 vvm: 0.07 h^{-1}, 1 vvm: 0.08 h^{-1}) and displayed a similar entry into the stationary phase after 56 h. Oscillations in rDOS was due to overregulation of the stirrer, an often observed disadvantage of PID controllers, especially, when combined with the rDOS probes that are highly sensitive to fluctuations. However, almost 2-fold more biomass was formed at the higher aeration rate (0.5 vvm: 6.3 g L^{-1}, 1 vvm: 9.9 g L^{-1}). Accumulation of the precursor glutarate was growth-coupled and ceased upon entry into the stationary phase (titers of around 10 mM at 0.5 vvm and 13 mM at 1 vvm), whereas production of L-2HG was delayed and started after 30 h. While L-2HG production at an aeration rate of 0.5 vvm reached the highest titer of 16 mM at 120 h (**Figure 6A**), L-2HG production at an aeration rate of 1 vvm stopped at a titer of 6 mM shortly after glucose was fully depleted (**Figure 6B**). Thus, the latter fermentation was switched to feeding mode to supply the culture with more carbon source. As consequence, the strain grew to a 2-fold higher biomass concentration of 16.3 g L^{-1} and produced fourfold more L-2HG reaching a titer of 24 mM (**Figure 6B**).

Comparing the different cultivations in batch mode (**Table 4**) it becomes obvious that the L-2HG product yield showed an inverse relationship with the aeration rate, as its production was highest in the not actively aerated microcultivation system. Although HPGluA2 grew 2-fold slower in the microcultivation system, the volumetric productivity was higher than in the bioreactors (**Table 4**). By contrast, growth proceeded to the highest biomass concentration and the highest biomass yield was observed when aeration was highest (**Table 4**).

L-2HG Production From Wheat Sidestream Concentrate

Sustainable processes based on renewable feedstock are sought after. Therefore, it was tested if L-2HG can be produced from

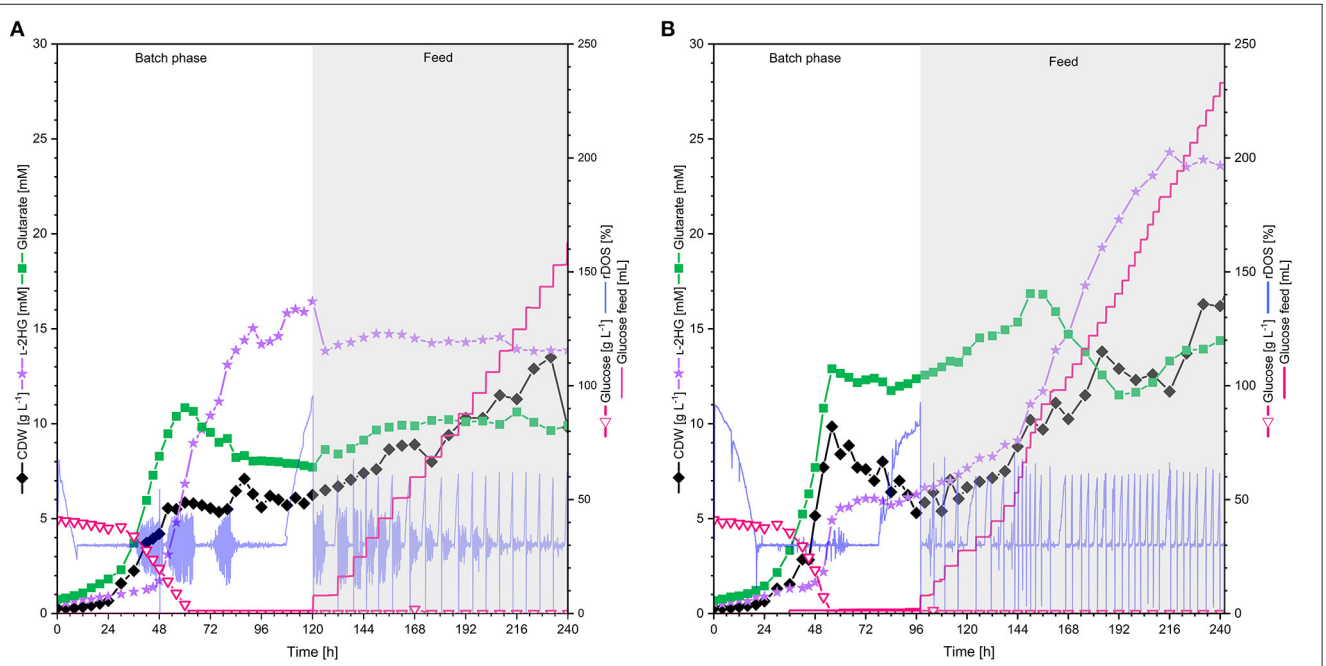

FIGURE 6 | L-2HG production by *C. glutamicum* HPGluA2 in fed-batch fermentation with **(A)** 0.5 vvm and **(B)** 1 vvm aeration rate. HPGluA2 was cultivated in CGXII minimal medium in fed-batch mode over 240 h, containing 40 g L^{-1} glucose and feeding 600 g L^{-1} glucose solution. L-2HG concentration is indicated in violet stars (mM), biomass concentration (CDW) is shown in black diamands (g L^{-1}), glucose concentration (g L^{-1}) is plotted as pink hollow triangles, and glutarate concentration (mM) in green squares, 600 g L^{-1} glucose feed (mL) is plotted as pink line and the relative dissolved oxygen saturation (rDOS) is indicated in light blue (%). Cultivation was performed at 30°C and pH 7.0 regulated with 10% (*v/v*) H_3PO_4 and 4 M KOH. An overpressure of 0.2 bar was applied. 0.6 mL L^{-1} of antifoam agent AF204 (Sigma Aldrich, Taufkirchen, Germany) was added to the medium manually before inoculation.

TABLE 4 | Comparison of L-2HG process parameters during different cultivation strategies.

System	Mode/Phase	Aeration rate [vvm]	μ_{max} [h^{-1}]	CDW [g L^{-1}]	Titer [g L^{-1}]	$Y_{X/S}$ [g g^{-1}]	$Y_{P/S}$ [g g^{-1}]	VP [g L^{-1} h^{-1}]
Micro-Cultivation	Batch	–	0.04	4.3	5.0	0.11	0.13	0.05
Bioreactor	Batch	0.5	0.07	6.3	2.4	0.16	0.06	0.02
	Batch	1	0.08	9.9	0.9	0.25	0.02	0.01
	Fed-batch	1	0.07	16.3	3.5	0.09	0.02	0.01

μ_{max}, *maximal growth rate; CDW, cell dry weight;* $Y_{X/S}$, *biomass yield;* $Y_{P/S}$, *product yield; VP, volumetric productivity.*

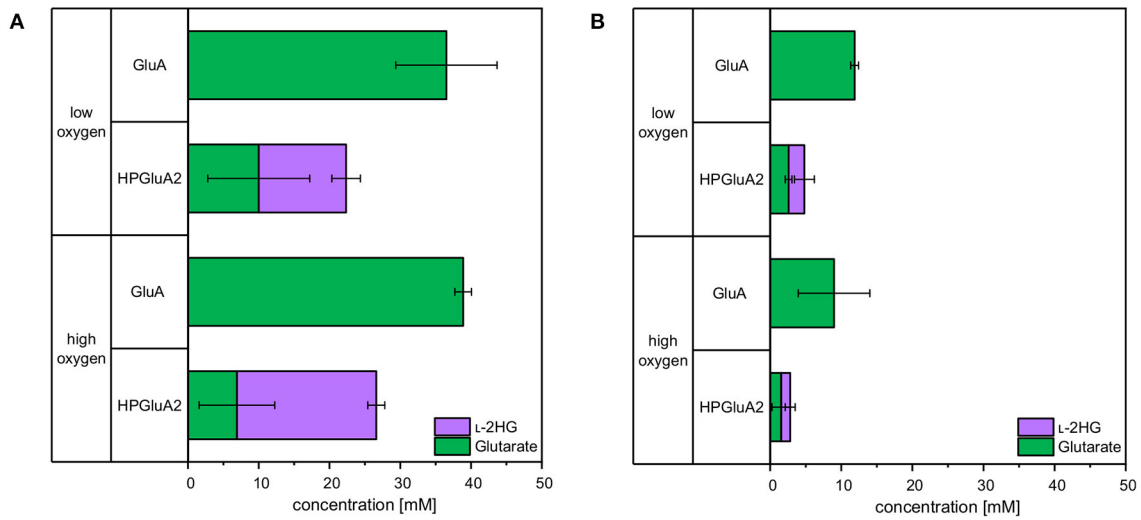

FIGURE 7 | Comparison of glutarate and L-2HG production based on glucose **(A)** or wheat sidestream concentrate **(B)**. *C. glutamicum* glutarate producer GluA and L-2HG producer HPGluA2 were grown in the Duetz microcultivation plates with low or high oxygen supply using covers of different air permeability and different volumes (3 and 2 mL). Strains were cultivated in CGXII minimal medium with 40 g L^{-1} glucose or with a mixture containing 246 g L^{-1} WSC, 20 g L^{-1} ammonium sulfate and 42 g L^{-1} MOPS. Both media were supplemented with 1 mM IPTG and 2 mM $FeSO_4$. Supernatants were analyzed after 96 h. Values and error bars represent means and standard deviations of 3 cultivations.

a sidestream of industrial starch production (wheat sidestream concentrate; WSC). WSC contains hardly any starch, but various sugars like glucose, fructose, sucrose, raffinose, xylose and arabinose (D'Appolonia and Rayas-Duarte, 1994). Production of glutarate from WSC was also analyzed. To this end, *C. glutamicum* strains GluA and HPGluA2 were cultivated for 96 h either in CGXII medium with glucose or in WSC medium. Aeration was altered by different cultivation volumes and by using either "low oxygen" or "high oxygen" Duetz plates. For HPGluA2 both media were supplemented with 2 mM $FeSO_4$. Glucose-based glutarate production by strain GluA was comparable for both aeration schemes (37 ± 7 and 39 ± 1 mM; **Figure 7**), whereas it was lower in WSC medium (12 ± 1 and 9 ± 5 mM of glutarate under high and low oxygen supply, respectively; **Figure 7**). HPLC analysis of WSC using a refractive index detector did not allow to identify all peaks, but we could show that around 12 mM glucose and 6 mM maltose were utilized (data not shown) and 3 ±0 mM glutarate and 2 ± 1 mM L-2HG accumulated under low oxygen conditions. No significant differences with respect to L-2HG production by strain HPGluA2 with different oxygen supply were observed (**Figure 7**). Albeit leading to lower titers, production of L-2HG to concentrations around 2 mM were achieved. Thus, L-2HG production from the renewable feedstock wheat sidestream concentrate was demonstrated.

DISCUSSION

In this study, production of the sought after compound L-2HG by the industrial workhorse *C. glutamicum* was demonstrated after extension of lysine biosynthesis in a six-step cascade employing the metalloenzyme CsiD from *P. putida* as final step. The glucose-based process was stable in 2 L bioreactor cultivations and a L-2HG titer of 3.5 g L^{-1} was obtained in fed-batch fermentation. Moreover, L-2HG production based on the renewable feedstock wheat sidestream concentrate was demonstrated.

L-2HG production was achieved by glutarate hydroxylase extending lysine biosynthesis in a six-step cascade, in which only the last committed step catalyzed by oxygen-dependent glutarate hydroxylase requires oxygen. Glutarate hydroxylases belong to the large family of non-heme Fe(II)- and 2-oxoglutarate-dependendent oxygenases, which are essential for diverse biological functions. These enzymes form an Fe(IV)-oxo intermediate to initiate oxidative transformations and can be assigned to four major types of reactions: hydroxylation, halogenation, ring formation and desaturation (Hausinger, 2004). The glutarate hydroxylases which have been studied in this research belong to the enzymes catalyzing a hydroxylation reaction at an unactivated carbon center by incorporation of molecular oxygen (Guengerich, 2015; Martinez and Hausinger, 2015). The CsiD enzymes from *E. coli* MG1655 and *P. putida* KT2440 have been recently characterized in different studies displaying their high specificities toward the native substrate glutarate with K_M-values around 0.65 mM in *E. coli* (Knorr et al., 2018) and around 0.15 mM for *P. putida* (Zhang et al., 2018). The K_M-values of around 0.1 mM for the co-substrate 2-oxoglutarate are comparable for both enzymes. The higher affinity of glutarate hydroxylase from *P. putida* for glutarate is reflected by the better conversion of glutarate to L-2HG observed in this study. Even though no K_M value for the glutarate hydroxylase from *Halobacillus sp.* BA-2008 has been determined yet, it was demonstrated that it converts 5 mM glutarate to L-2HG with comparable efficiency to the other tested hydroxylases with 2-oxoglutarate as co-substrate (Thompson et al., 2019). Although the capability of CsiD from *Halobacillus sp.* BA-2008 to produce L-2HG from glutarate was demonstrated in *C. glutamicum*, the efficiency of the codon harmonized version of CsiD was inferior compared to the enzymes derived from other organisms.

It could be demonstrated that L-2HG inhibits the combined GabTD activity with an inhibitory constant of about 25 mM (**Figure 5A**). Due to its structural similarity to 2-OG, L-2HG potentially inhibits transamination reactions (McBrayer et al., 2018) by competitive inhibition (Intlekofer et al., 2015). Here, possibly competitive inhibition of 2-OG dependent transaminase GabT by L-2HG may have limited L-2HG product titers. Potentially, this may be overcome by enzyme engineering of the 2-OG binding pocket of GabT for better differentiation of this substrate from L-2HG. We have chosen enzymes GabT and GabD from *P. stutzeri* as they performed better than those from *C. glutamicum, P. putida* and *P. syringae* regarding glutarate production (Pérez-García et al., 2018). Since we did not compare GabT and GabD enzymes from various sources for inhibition of their activities by L-2HG, identifying feedback resistant enzymes/variants of the GabT and GabD enzymes in future work may help to increase L-2HG production. On the other hand, glutarate hydroxylase CsiD is subject to weak product inhibition (Knorr et al., 2018). Therefore, CsiD from other sources or variants may be selected that exhibit no or reduced product inhibition in order to improve L-2HG production.

Moreover, a weak substrate inhibition on L-2HG production by glutarate could also be identified (**Figure 5B**). CsiD from *E. coli* was recently characterized and the reaction mechanism was described (Knorr et al., 2018; Herr et al., 2019). Since the substrate analogon *N*-oxalylglycine (NOG), a 2-OG mimic, inhibited CsiD (Knorr et al., 2018), this feedback inhibition may limit L-2HG production. However, since we did not assay feedback inhibition of various glutarate hydroxylases by L-2HG, future work to improve L-2HG production should involve the identification of feedback resistant CsiD enzymes/variants.

Surprisingly, extracellular addition of glutarate boosted glutarate production. This is unlikely due to effects on enzyme activities. *C. glutamicum* possesses chromosomal copies of *gabT* and *gabD* (Pérez-García et al., 2018; Haupka et al., 2020). The PucR-like regulator GabR that requires GABA as coactivator activates transcription of the *gabTDP* operon (Zhu et al., 2020). Possibly, glutarate mimics GABA as coactivator of GabR activating the endogenous *gabTDP* operon and increasing GabT and GabD enzyme levels in addition to plasmid-borne expression of *gabT* and *gabD* from *P. stutzeri.*

Cultivation schemes with higher oxygen supply reduced L-2HG production, but improved growth to high biomass concentrations. Glutarate hydroxylases are 2-OG-dependent enzymes and these metalloenzymes specifically require Fe^{2+} as cofactor for their function (Mitchell et al., 2017; Dunham et al., 2018). Previously, it has been shown that increased iron concentrations improve enzyme activity (Fukumori and Hausinger, 1993). Increased Fe^{2+} concentrations improved L-2HG product titers, but slowed growth significantly. This might be due to iron effects such as toxicity mainly due to the formation of hydroxyl radicals as oxidative stress response (Braun, 1997; Touati, 2000; Eid et al., 2017) and/or due to inhibition of 2-OG-dependent dioxygenases and methylases, which play an essential role in DNA/RNA repair (van den Born et al., 2009), by L-2HG (Low et al., 2001; Ledesma-García et al., 2016). Provision of oxygen and iron to the *C. glutamicum* cell are interlinked. Molecular oxygen is required for 2-OG-dependent dioxygenases such as CsiD to form the Fe(IV)-oxo intermediate, but with too much oxygen decoupling occurs via "non-productive reactions" resulting in inactive Fe(III)-containing enzymes (Hausinger, 2004) as observed with AlkB (Henshaw et al., 2004) and TfdA (Liu et al., 2001). Secondly, an "uncoupled turnover" of the co-substrate 2-OG may occur by decomposition of 2-OG to carbon dioxide and succinate. These "uncoupled reactions" might contribute to the lower titers of L-2HG obtained in 2 L scale fermentative production with the highest oxygen supply. The addition of ascorbic acid is a promising option since ascorbate improved hydroxylase activity (Fukumori and Hausinger, 1993). Alternatively, production of L-2HG may be improved by concomitant overproduction of either glutathione (Liu et al., 2019) or ascorbate in *C. glutamicum*.

Our results suggested that export of L-2HG involves SucE (**Figure 3**). Surprisingly, glutarate export does not depend solely on SucE. Overexpression of *sucE* increased succinate production (Zhu et al., 2014) similar to increased production of glutarate and L-2HG observed here. Deletion of *sucE* revealed that SucE is the main export system for L-2HG, but not for glutarate. Production of L-2HG may benefit from re-uptake of glutarate secreted to the culture medium as by-product. However, the uptake system for glutarate is unknown. MctC is involved in the uptake of pyruvate,

propionate, and acetate, but it is not clear if it accepts glutarate (Jolkver et al., 2009).

Glutarate was observed as significant by-product. Unlike L-2HG, which likely is exported by SucE (s. above), glutarate is exported by YnfM (Fukui et al., 2019). Overexpression of *ynfM* improved production of glutarate, succinate, and 2-OG (Fukui et al., 2019; Han et al., 2020). Thus, deletion of *ynfM* is a suitable strategy to abolish export of glutarate as by-product of L-2HG production.

Alternative feedstocks are important to achieve sustainable biotechnological processes. In this respect, sidestreams are highly relevant. Glycerol is a sidestream of the biodiesel process and glycerol accumulates as stoichiometric by-product. *C. glutamicum* has been engineered to produce amino acids from pure and technical grade glycerol (Rittmann et al., 2008; Meiswinkel et al., 2013b). Access to nitrogenous sidestreams from the fishery industry such as glucosamine or *N*-acetyl-glucosamine is important if the target product is containing nitrogen atoms (Matano et al., 2014, 2016). For products lacking nitrogen atoms, access to lignocellulosics is pivotal (Gopinath et al., 2011; Buschke et al., 2013; Meiswinkel et al., 2013a; Hadiati et al., 2014; Matsuura et al., 2019). The focus of this study was a sidestream of industrial starch production. Although production was lower compared to glucose (30% for glutarate, 15% for L-2HG), media composition was easy and required only a buffer, a nitrogen source for growth and iron for glutarate hydroxylase. We envision improved production of L-2HG from wheat sidestream concentrate once access to sugars other than the native substrates glucose, fructose, maltose, and sucrose is achieved, e.g., to raffinose, xylose and arabinose, that are present in this feedstock (D'Appolonia and Rayas-Duarte, 1994). Strategies for access to the lignocellulosic pentoses xylose and arabinose have been established (Kawaguchi et al., 2008; Gopinath et al., 2011; Schneider et al., 2011; Meiswinkel et al., 2013a; Imao et al., 2017) and may prove useful for improved production of L-2HG from the alternative feedstock wheat sidestream concentrate. In this respect, provision of iron and/or iron chelators may prove essential as shown here for CsiD function.

The approach described here may be followed for production of the stereoisomer D-2HG. To this end, the glutarate pathway described here has to be extended with enzymes for conversion of glutarate to D-2HG. These enzymes may be sourced from lysine degrading bacteria as D-2HG occurs as intermediate in some of these pathways, e.g., in *E. coli* (Zhao and Winkler, 1996) and different *Pseudomonaceace* (Zhang et al., 2017; Guo et al., 2018; Thompson et al., 2019). Future work will reveal if this approach is suitable for fermentative production of D-2HG.

DATA AVAILABILITY STATEMENT

The original contributions presented in the study are included in the article/supplementary material, further inquiries can be directed to the corresponding author/s.

AUTHOR'S NOTE

VFW wishes to dedicate this article in memoriam of scientific and personal friend Michael M. Goodin, Professor of Plant Pathology, University of Kentucky, Lexington, KY.

AUTHOR CONTRIBUTIONS

CP and VFW conceived and designed the experiments. CP constructed plasmids and strains, cultivated, and analyzed *C. glutamicum* strains and prepared a draft of the manuscript. CP and FM performed bioreactor experiments and evaluated data. AB conducted the growth experiment on wheat sidestream concentrate. CP, AB, FM, and VFW finalized the manuscript. VFW acquired funding and coordinated the study. All authors read and approved the final version of the manuscript.

FUNDING

This research was funded in part by the European Regional Development Fund (ERDF) and the Ministry of Economic Affairs, Innovation, Digitalization, and Energy of the State of North Rhine-Westphalia and CP, AB, and VFW acknowledge support by grant Cluster Industrial Biotechnology (CLIB) Kompetenzzentrum Biotechnologie (CKB) (34.EFRE-0300095/1703FI04) and FM and VFW by grant Bicomer (EFRE-0400184). Support for the Article Processing Charge by the Deutsche Forschungsgemeinschaft and the Open Access Publication Fund of Bielefeld University is acknowledged. The funding bodies had no role in the design of the study or the collection, analysis, or interpretation of data or in writing the manuscript.

ACKNOWLEDGMENTS

We thank Dr. T. Roick and M. Andreae from Jäckering Mühlen- und Nährmittelwerke GmbH, Hamm, Germany, for providing wheat sidestream concentrate. Moreover, we thank Dr. Joe Risse and Dipl.-Ing. Thomas Schäffer from Fermentation Technology, Technical Faculty & CeBiTec, University of Bielefeld, for technical assistance and kind advice. We additionally thank Anastasia Kerbs for scientific discussion.

REFERENCES

Adkins, J., Jordan, J., and Nielsen, D. R. (2013). Engineering *Escherichia coli* for renewable production of the 5-carbon polyamide building-blocks 5-aminovalerate and glutarate. *Biotechnol. Bioeng.* 110, 1726–1734. doi: 10.1002/bit.24828

Braun, V. (1997). Avoidance of iron toxicity through regulation of bacterial iron transport. *Biol. Chem.* 378, 779–786.

Buschke, N., Becker, J., Schäfer, R., Kiefer, P., Biedendieck, R., and Wittmann, C. (2013). Systems metabolic engineering of xylose-utilizing *Corynebacterium glutamicum* for production of 1,5-diaminopentane. *Biotechnol. J.* 8, 557–570. doi: 10.1002/biot.201200367

Cheng, J., Luo, Q., Duan, H., Peng, H., Zhang, Y., Hu, J., et al. Efficient whole-cell catalysis for 5-aminovalerate production from L-lysine by using engineered *Escherichia coli* with ethanol pretreatment. *Sci Rep.* (2020) 10, 990. doi: 10.1038/s41598-020-57752-x

Chowdhury, R., Yeoh, K. K., Tian, Y., Hillringhaus, L., Bagg, E. A., Rose, N. R., et al. (2011). The oncometabolite 2-hydroxyglutarate inhibits histone lysine demethylases. *EMBO Rep.* 12, 463–469. doi: 10.1038/embor.2011.43

D'Appolonia, B. L., and Rayas-Duarte, P. (1994). "Wheat carbohydrates: structure and functionality," in *Wheat: Production, Properties and Quality*, eds W. Bushuk, and V. F. Rasper (Boston, MA: Springer), 107–127. doi: 10.1007/978-1-4615-2672-8_8

Dunham, N. P., Chang, W., Mitchell, A. J., Martinie, R. J., Zhang, B., Bergman, J. A., et al. (2018). Two distinct mechanisms for C–C desaturation by iron(II)- and 2-(Oxo)glutarate-dependent oxygenases: importance of α-heteroatom assistance. *J. Am. Chem. Soc.* 140, 7116–7126. doi: 10.1021/jacs.8b01933

Eggeling, L., and Bott, M. (2004). Handbook of *Corynebacterium glutamicum, 1st Edn.* Bota Raton, FL: CRC Press; LLC.

Eid, R., Arab, N. T. T., and Greenwood, M. T. (2017). Iron mediated toxicity and programmed cell death: a review and a re-examination of existing paradigms. *Biochim. Biophys. Acta Mol. Cell Res.* 1864, 399–430. doi: 10.1016/j.bbamcr.2016.12.002

Eikmanns, B. J., Thum-Schmitz, N., Eggeling, L., Lüdtke, K. U., and Sahm, H. (1994). Nucleotide sequence, expression and transcriptional analysis of the *Corynebacterium glutamicum gltA* gene encoding citrate synthase. *Microbiology* 140, 1817–1828. doi: 10.1099/13500872-140-8-1817

Fukui, K., Nanatani, K., Nakayama, M., Hara, Y., Tokura, M., and Abe, K. (2019). *Corynebacterium glutamicum* CgynfM encodes a dicarboxylate transporter applicable to succinate production. *J. Biosci. Bioeng.* 127, 465–471. doi: 10.1016/j.jbiosc.2018.10.004

Fukumori, F., and Hausinger, R. P. (1993). Purification and characterization of 2,4-dichlorophenoxyacetate/alpha-ketoglutarate dioxygenase. *J. Biol. Chem.* 268, 24311–24317.

Gopinath, V., Meiswinkel, T. M., Wendisch, V. F., and Nampoothiri, K. M. (2011). Amino acid production from rice straw and wheat bran hydrolysates by recombinant pentose-utilizing *Corynebacterium glutamicum*. *Appl. Microbiol. Biotechnol.* 92, 985–996. doi: 10.1007/s00253-011-3478-x

Guengerich, F. P. (2015). Introduction: metals in biology: α-ketoglutarate/iron-dependent dioxygenases. *J. Biol. Chem.* 290, 20700–20701. doi: 10.1074/jbc.R115.675652

Guo, X., Zhang, M., Cao, M., Zhang, W., Kang, Z., Xu, P., et al. (2018). d-2-Hydroxyglutarate dehydrogenase plays a dual role in L-serine biosynthesis and d-malate utilization in the bacterium *Pseudomonas stutzeri*. *J. Biol. Chem.* 293, 15513–15523. doi: 10.1074/jbc.RA118.003897

Hadiati, A., Krahn, I., Lindner, S. N., and Wendisch, V. F. (2014). Engineering of *Corynebacterium glutamicum* for growth and production of L-ornithine, L-lysine, and lycopene from hexuronic acids. *Bioresour. Bioprocess.* 1:25. doi: 10.1186/s40643-014-0025-5

Han, T., Kim, G. B., and Lee, S. Y. (2020). Glutaric acid production by systems metabolic engineering of an L-lysine–overproducing *Corynebacterium glutamicum*. *Proc. Natl. Sci. U.S.A.*117, 30328–30334. doi: 10.1073/pnas.2017483117

Hanahan, D. (1985). Techniques for transformation of *E. coli*. *DNA Cloning A Practical Approach* 1, 109–135.

Haupka, C. (2020). *Chaupka/Codon_Harmonization: Release v1.2.0.* doi: 10.5281/zenodo.4062177

Haupka, C., Delépine, B., Irla, M., Heux, S., and Wendisch, V. F. (2020). Flux enforcement for fermentative production of 5-aminovalerate and glutarate by *Corynebacterium glutamicum*. *Catalysts* 10:1065. doi: 10.3390/catal10091065

Hausinger, R. P. (2004). Fe(II)/α-ketoglutarate-dependent hydroxylases and related enzymes. *Crit. Rev. Biochem. Mol. Biol.* 39, 21–68. doi: 10.1080/10409230490440541

Henshaw, T. F., Feig, M., and Hausinger, R. P. (2004). Aberrant activity of the DNA repair enzyme AlkB. *J. Inorg. Biochem.* 98, 856–861. doi: 10.1016/j.jinorgbio.2003.10.021

Herr, C. Q., Macomber, L., Kalliri, E., and Hausinger, R. P. (2019). Glutarate L-2-hydroxylase (CsiD/GlaH) is an archetype Fe(II)/2-oxoglutarate-dependent dioxygenase. *Adv. Protein Chem. Struct. Biol.* 117, 63–90. doi: 10.1016/bs.apcsb.2019.05.001

Hibi, M., and Ogawa, J. (2014). Characteristics and biotechnology applications of aliphatic amino acid hydroxylases belonging to the Fe(II)/α-ketoglutarate-dependent dioxygenase superfamily. *Appl. Microbiol. Biotechnol.* 98, 3869–3876. doi: 10.1007/s00253-014-5620-z

Hüdig, M., Maier, A., Scherrers, I., Seidel, L., Jansen, E. E. W., Mettler-Altmann, T., et al. (2015). Plants possess a cyclic mitochondrial metabolic pathway similar to the mammalian metabolic repair mechanism involving malate dehydrogenase and L-2-hydroxyglutarate dehydrogenase. *Plant Cell Physiol.* 56, 1820–1830. doi: 10.1093/pcp/pcv108

Huhn, S., Jolkver, E., Krämer, R., and Marin, K. (2011). Identification of the membrane protein SucE and its role in succinate transport in *Corynebacterium glutamicum*. *Appl. Microbiol. Biotechnol.* 89, 327–335. doi: 10.1007/s00253-010-2855-1

Imao, K., Konishi, R., Kishida, M., Hirata, Y., Segawa, S., Adachi, N., et al. (2017). 1,5-Diaminopentane production from xylooligosaccharides using metabolically engineered *Corynebacterium glutamicum* displaying beta-xylosidase on the cell surface. *Bioresour. Technol.* 245, 1684–1691. doi: 10.1016/j.biortech.2017.05.135

Intlekofer, A. M., Dematteo, R. G., Venneti, S., Finley, L. W. S., Lu, C., Judkins, A. R., et al. (2015). Hypoxia induces production of L-2-hydroxyglutarate. *Cell Metab.* 22, 304–311. doi: 10.1016/j.cmet.2015.06.023

Intlekofer, A. M., Wang, B., Liu, H., Shah, H., Carmona-Fontaine, C., Rustenburg, A. S., et al. (2017). L-2-Hydroxyglutarate production arises from noncanonical enzyme function at acidic pH. *Nat. Chem. Biol.* 13, 494–500. doi: 10.1038/nchembio.2307

Jolkver, E., Emer, D., Ballan, S., Krämer, R., Eikmanns, B. J., and Marin, K. (2009). Identification and characterization of a bacterial transport system for the uptake of pyruvate, propionate, and acetate in *Corynebacterium glutamicum*. *J. Bacteriol. Res.* 191, 940–948. doi: 10.1128/JB.01155-08

Jorge, J. M. P., Pérez-García, F., and Wendisch, V. F. (2017). A new metabolic route for the fermentative production of 5-aminovalerate from glucose and alternative carbon sources. *Bioresour. Technol.* 245, 1701–1709. doi: 10.1016/j.biortech.2017.04.108

Kawaguchi, H., Sasaki, M., Vertès, A. A., Inui, M., and Yukawa, H. (2008). Engineering of an L-arabinose metabolic pathway in *Corynebacterium glutamicum*. *Appl. Microbiol. Biotechnol.* 77, 1053–1062. doi: 10.1007/s00253-007-1244-x

Kirchner, O., and Tauch, A. (2003). Tools for genetic engineering in the amino acid-producing bacterium *Corynebacterium glutamicum*. *J. Biotechnol.* 104, 287–299. doi: 10.1016/S0168-1656(03)00148-2

Knorr, S., Sinn, M., Galetskiy, D., Williams, R. M., Wang, C., Müller, N., et al. (2018). Widespread bacterial lysine degradation proceeding via glutarate and L-2-hydroxyglutarate. *Nat. Commun.* 9:5071. doi: 10.1038/s41467-018-07563-6

Ledesma-García, L., Sánchez-Azqueta, A., Medina, M., Reyes-Ramírez, F., and Santero, E. (2016). Redox proteins of hydroxylating bacterial dioxygenases establish a regulatory cascade that prevents gratuitous induction of tetralin biodegradation genes. *Sci. Rep.* 6:23848. doi: 10.1038/srep23848

Liu, A., Ho, R. Y. N., Que, L., Ryle, M. J., Phinney, B. S., and Hausinger, R. P. (2001). Alternative reactivity of an α-ketoglutarate-dependent iron(II) oxygenase: enzyme self-hydroxylation. *J. Am. Chem. Soc.* 123, 5126–5127. doi: 10.1021/ja005879x

Liu, W., Zhu, X., Lian, J., Huang, L., and Xu, Z. (2019). Efficient production of glutathione with multi-pathway engineering in *Corynebacterium glutamicum*. *J. Ind. Microbiol. Biotechnol.* 46, 1685–1695. doi: 10.1007/s10295-019-02220-3

Low, D. A., Weyand, N. J., and Mahan, M. J. (2001). Roles of DNA adenine methylation in regulating bacterial gene expression and virulence. *Infect. Immun.* 69, 7197–7204. doi: 10.1128/IAI.69.12.7197-7204.2001

Marschall, C., Labrousse, V., Kreimer, M., Weichart, D., Kolb, A., and Hengge-Aronis, R. (1998). Molecular analysis of the regulation of *csiD*, a carbon starvation-inducible gene in *Escherichia coli* that is exclusively dependent on σS and requires activation by cAMP-CRP. *J. Mol. Biol.* 276, 339–353. doi: 10.1006/jmbi.1997.1533

Martinez, S., and Hausinger, R. P. (2015). Catalytic mechanisms of Fe(II)- and 2-oxoglutarate-dependent oxygenases. *J. Biol. Chem.* 290, 20702–20711. doi: 10.1074/jbc.R115.648691

Matano, C., Kolkenbrock, S., Hamer, S. N., Sgobba, E., Moerschbacher, B. M., and Wendisch, V. F. (2016). *Corynebacterium glutamicum* possesses β-N-acetylglucosaminidase. *BMC Microbiol.* 16:177. doi: 10.1186/s12866-016-0795-3

Matano, C., Uhde, A., Youn, J.-W., Maeda, T., Clermont, L., Marin, K., et al. (2014). Engineering of *Corynebacterium glutamicum* for growth and L-lysine and lycopene production from N-acetyl-glucosamine. *Appl. Microbiol. Biotechnol.* 98, 5633–5643. doi: 10.1007/s00253-014-5676-9

Matsuura, R., Kishida, M., Konishi, R., Hirata, Y., Adachi, N., Segawa, S., et al. (2019). Metabolic engineering to improve 1,5-diaminopentane production from cellobiose using β-glucosidase-secreting *Corynebacterium glutamicum*. *Biotechnol. Bioeng.* 116, 2640–2651. doi: 10.1002/bit.27082

McBrayer, S. K., Mayers, J. R., DiNatale, G. J., Shi, D. D., Khanal, J., Chakraborty, A. A., et al. (2018). Transaminase inhibition by 2-hydroxyglutarate impairs

glutamate biosynthesis and redox homeostasis in glioma. *Cell* 175, 101–116.e25. doi: 10.1016/j.cell.2018.08.038

Meiswinkel, T. M., Gopinath, V., Lindner, S. N., Nampoothiri, K. M., and Wendisch, V. F. (2013a). Accelerated pentose utilization by *Corynebacterium glutamicum* for accelerated production of lysine, glutamate, ornithine and putrescine. *Microb. Biotechnol.* 6, 131–140. doi: 10.1111/1751-7915.12001

Meiswinkel, T. M., Rittmann, D., Lindner, S. N., and Wendisch, V. F. (2013b). Crude glycerol-based production of amino acids and putrescine by *Corynebacterium glutamicum*. *Bioresour. Technol.* 145, 254–258. doi: 10.1016/j.biortech.2013.02.053

Metzner, M., Germer, J., and Hengge, R. (2004). Multiple stress signal integration in the regulation of the complex σS-dependent *csiD-ygaF-gabDTP* operon in *Escherichia coli*. *Mol. Microbiol.* 51, 799–811. doi: 10.1046/j.1365-2958.2003.03867.x

Mitchell, A. J., Dunham, N. P., Martinie, R. J., Bergman, J. A., Pollock, C. J., Hu, K., et al. (2017). Visualizing the reaction cycle in an iron(II)- and 2-(oxo)-glutarate-dependent hydroxylase. *J. Am. Chem. Soc.* 139, 13830–13836. doi: 10.1021/jacs.7b07374

Nan, A., and Feher, I. C. (2017). A new polyester based on allyl α-hydroxy glutarate as shell for magnetite nanoparticles. *AIP Conf. Proc.* 1917:040003. doi: 10.1063/1.5018285

Navarro, E., Subirana, J. A., and Puiggali, J. (1997). The structure of nylon 12,5 is characterized by two hydrogen bond directions as are other polyamides derived from glutaric acid. *Polymer* 38, 3429–3432. doi: 10.1016/S0032-3861(97)00017-7

Oldham, W. M., Clish, C. B., Yang, Y., and Loscalzo, J. (2015). Hypoxia-mediated increases in L-2-hydroxyglutarate coordinate the metabolic response to reductive stress. *Cell Metab.* 22, 291–303. doi: 10.1016/j.cmet.2015.06.021

Pan, B.-C., Chen, W.-H., Lee, T.-M., and Liou, G.-S. (2018). Synthesis and characterization of novel electrochromic devices derived from redox-active polyamide–TiO2 hybrids. *J. Mater. Chem. C* 6, 12422–12428. doi: 10.1039/C8TC04469D

Pérez-García, F., Jorge, J. M. P., Dreyszas, A., Risse, J. M., and Wendisch, V. F. (2018). Efficient production of the dicarboxylic acid glutarate by *Corynebacterium glutamicum* via a novel synthetic pathway. *Front. Microbiol.* 9:2589. doi: 10.3389/fmicb.2018.02589

Peters-Wendisch, P., Schiel, B., Wendisch, V. F., Katsoulidis, E., Möckel, B., Sahm, H., et al. (2001). Pyruvate carboxylase is a major bottleneck for glutamate and lysine production by *Corynebacterium glutamicum*. *J. Mol. Microbiol. Biotechnol.* 3, 295–300. Available online at: https://www.caister.com/backlist/jmmb/v/v3/v3n2/22.pdf

Rittmann, D., Lindner, S. N., and Wendisch, V. F. (2008). Engineering of a glycerol utilization pathway for amino acid production by *Corynebacterium glutamicum*. *Appl. Environ. Microbiol.* 74, 6216–6222. doi: 10.1128/AEM.00963-08

Rzem, R., Veiga-da-Cunha, M., Noel, G., Goffette, S., Nassogne, M.-C., Tabarki, B., et al. (2004). A gene encoding a putative FAD-dependent L-2-hydroxyglutarate dehydrogenase is mutated in L-2-hydroxyglutaric aciduria. *Proc. Natl. Acad. Sci. U.S.A.* 101, 16849–16854. doi: 10.1073/pnas.0404840101

Salis, H. M. (2011). "Chapter two - the ribosome binding site calculator," in *Methods in Enzymology* Synthetic *Biology, Part B*, ed C. Voigt (Cambridge, MA: Academic Press), 19–42. doi: 10.1016/B978-0-12-385120-8.00002-4

Schäfer, A., Tauch, A., Jäger, W., Kalinowski, J., Thierbach, G., and Pühler, A. (1994). Small mobilizable multi-purpose cloning vectors derived from the *Escherichia coli* plasmids pK18 and pK19: selection of defined deletions in the chromosome of *Corynebacterium glutamicum*. *Gene* 145, 69–73. doi: 10.1016/0378-1119(94)90324-7

Schneider, J., Niermann, K., and Wendisch, V. F. (2011). Production of the amino acids L-glutamate, L-glutamate, L-lysine, L-ornithine and L-arginine from arabinose by recombinant *Corynebacterium glutamicum*. *J. Biotechnol.* 154, 191–198. doi: 10.1016/j.jbiotec.2010.07.009

Schneider, J., and Wendisch, V. F. (2010). Putrescine production by engineered *Corynebacterium glutamicum*. *Appl. Microbiol. Biotechnol.* 88, 859–868. doi: 10.1007/s00253-010-2778-x

Shelar, S., Shim, E.-H., Brinkley, G. J., Kundu, A., Carobbio, F., Poston, T., et al. (2018). Biochemical and epigenetic insights into L-2-hydroxyglutarate, a potential therapeutic target in renal cancer. *Clin. Cancer Res.* 24, 6433–6446. doi: 10.1158/1078-0432.CCR-18-1727

Shim, E.-H., Livi, C. B., Rakheja, D., Tan, J., Benson, D., Parekh, V., et al. (2014). L-2-Hydroxyglutarate: an epigenetic modifier and putative oncometabolite in renal cancer. *Cancer Discov.* 4, 1290–1298. doi: 10.1158/2159-8290.CD-13-0696

Simon, R., Priefer, U., and Pühler, A. (1983). A broad host range mobilization system for *in vivo* genetic engineering: transposon mutagenesis in gram negative bacteria. *Bio/Technology* 1, 784–791. doi: 10.1038/nbt1183-784

Stansen, C., Uy, D., Delaunay, S., Eggeling, L., Goergen, J. L., and Wendisch, V. F. (2005). Characterization of a *Corynebacterium glutamicum* lactate utilization operon induced during temperature-triggered glutamate production. *Appl. Environ. Microbiol.* 71, 5920–5928. doi: 10.1128/AEM.71.10.5920-5928.2005

Thompson, M. G., Blake-Hedges, J. M., Cruz-Morales, P., Barajas, J. F., Curran, S. C., Eiben, C. B., et al. (2019). Massively parallel fitness profiling reveals multiple novel enzymes in *Pseudomonas putida* lysine metabolism. *mBio* 10:e02577–18. doi: 10.1128/mBio.02577-18

Touati, D. (2000). Iron and oxidative stress in bacteria. *Arch. Biochem. Biophys.* 373, 1–6. doi: 10.1006/abbi.1999.1518

Unthan, S., Baumgart, M., Radek, A., Herbst, M., Siebert, D., Brühl, N., et al. (2015). Chassis organism from Corynebacterium glutamicum-a top-down approach to identify and delete irrelevant gene clusters. *Biotechnol. J.* 10, 290–301. doi: 10.1002/biot.201400041

van den Born, E., Bekkelund, A., Moen, M. N., Omelchenko, M. V., Klungland, A., and Falnes, P. Ø. (2009). Bioinformatics and functional analysis define four distinct groups of AlkB DNA-dioxygenases in bacteria. *Nucleic. Acids Res.* 37, 7124–7136. doi: 10.1093/nar/gkp774

Varela, O., and Orgueira, H. A. (2000). "Synthesis of chiral polyamides from carbohydrate-derived monomers," in *Advances in Carbohydrate Chemistry and Biochemistry*, ed D. Horton (Cambridge, MA: Academic Press), 137–174. doi: 10.1016/S0065-2318(00)55005-7

Wanders, R. J. A., Vilarinho, L., Hartung, H. P., Hoffmann, G. F., Mooijer, P. A. W., Jansen, G. A., et al. (1997). L-2-hydroxyglutaric aciduria: normal L-2-hydroxyglutarate dehydrogenase activity in liver from two new patients. *J. Inherit. Metab. Dis.* 20, 725–726. doi: 10.1023/A:1005355316599

Wendisch, V. F., Brito, L. F., Gil Lopez, M., Hennig, G., Pfeifenschneider, J., Sgobba, E., et al. (2016). The flexible feedstock concept in industrial biotechnology: metabolic engineering of *Escherichia coli, Corynebacterium glutamicum, Pseudomonas, Bacillus* and yeast strains for access to alternative carbon sources. *J. Biotechnol.* 234, 139–157. doi: 10.1016/j.jbiotec.2016.07.022

Xu, W., Yang, H., Liu, Y., Yang, Y., Wang, P., Kim, S.-H., et al. (2011). Oncometabolite 2-hydroxyglutarate is a competitive inhibitor of α-ketoglutarate-dependent dioxygenases. *Cancer Cell* 19, 17–30. doi: 10.1016/j.ccr.2010.12.014

Zhang, M., Gao, C., Guo, X., Guo, S., Kang, Z., Xiao, D., et al. (2018). Increased glutarate production by blocking the glutaryl-CoA dehydrogenation pathway and a catabolic pathway involving L-2-hydroxyglutarate. *Nat. Commun.* 9:2114. doi: 10.1038/s41467-018-04513-0

Zhang, W., Zhang, M., Gao, C., Zhang, Y., Ge, Y., Guo, S., et al. (2017). Coupling between d-3-phosphoglycerate dehydrogenase and d-2-hydroxyglutarate dehydrogenase drives bacterial L-serine synthesis. *Proc. Natl. Acad. Sci. U.S.A.* 114, E7574–E7582. doi: 10.1073/pnas.1619034114

Zhao, G., and Winkler, M. E. (1996). A novel alpha-ketoglutarate reductase activity of the *serA*-encoded 3-phosphoglycerate dehydrogenase of *Escherichia coli* K-12 and its possible implications for human 2-hydroxyglutaric aciduria. *J. Bacteriol.* 178, 232–239. doi: 10.1128/JB.178.1.232-239.1996

Zhu, L., Mack, C., Wirtz, A., Kranz, A., Polen, T., Baumgart, M., et al. (2020). Regulation of γ-aminobutyrate (GABA) utilization in *Corynebacterium glutamicum* by the PucR-type transcriptional regulator GabR and by alternative nitrogen and carbon sources. *Front. Microbiol.* 11:544045. doi: 10.3389/fmicb.2020.544045

Zhu, N., Xia, H., Yang, J., Zhao, X., and Chen, T. (2014). Improved succinate production in *Corynebacterium glutamicum* by engineering glyoxylate pathway and succinate export system. *Biotechnol. Lett.* 36, 553–560. doi: 10.1007/s10529-013-1376-2

Conflict of Interest: The authors declare that the research was conducted in the absence of any commercial or financial relationships that could be construed as a potential conflict of interest.

frontiers in Bioengineering and Biotechnology

REVIEW
published: 03 February 2021
doi: 10.3389/fbioe.2021.624503

Advances in the Microbial Synthesis of 5-Hydroxytryptophan

Xin-Xin Liu[1], *Bin Zhang*[2] *and Lian-Zhong Ai*[1]*

[1] *Shanghai Engineering Research Center of Food Microbiology, School of Medical Instrument and Food Engineering, University of Shanghai for Science and Technology, Shanghai, China,* [2] *College of Bioscience and Bioengineering, Jiangxi Agricultural University, Nanchang, China*

5-Hydroxytryptophan (5-HTP) plays an important role in the regulation of emotion, behavior, sleep, pain, body temperature, and other physiological functions. It is used in the treatment of depression, insomnia, migraine, and other diseases. Due to a lack of effective biosynthesis methods, 5-HTP is mainly obtained by natural extraction, which has been unable to meet the needs of the market. Through the directed evolution of enzymes and the introduction of substrate supply pathways, 5-HTP biosynthesis and yield increase have been realized. This review provides examples that illustrate the production mode of 5-HTP and the latest progress in microbial synthesis.

Keywords: 5-hydroxytryptophan, tryptophan hydroxylase, L-trp, biosynthesis, tetrahydrobiopterin

OPEN ACCESS

Edited by:
Yi-Rui Wu,
Shantou University, China

Reviewed by:
Zhongyang Qiu,
Huaiyin Normal University, China
K. Madhavan Nampoothiri,
National Institute for Interdisciplinary Science and Technology (CSIR), India

***Correspondence:**
Lian-Zhong Ai
ailianzhong1@126.com

Specialty section:
This article was submitted to Industrial Biotechnology, a section of the journal Frontiers in Bioengineering and Biotechnology

Received: *31 October 2020*
Accepted: *04 January 2021*
Published: *03 February 2021*

Citation:
Liu X-X, Zhang B and Ai L-Z (2021) Advances in the Microbial Synthesis of 5-Hydroxytryptophan. Front. Bioeng. Biotechnol. 9:624503. doi: 10.3389/fbioe.2021.624503

INTRODUCTION

5-Hydroxytryptophan (5-HTP) is a natural amino acid (AA) that does not participate in protein synthesis. It is derived from tryptophan (trp), and the hydrogen atoms at the 5′-position on the benzene ring of trp are replaced by hydroxyl groups. 5-HTP appears as a fine white powder that is insoluble in water, but is soluble in alcohol. In mammals, 5-HTP is the precursor of the neurotransmitter serotonin and the amine hormone melatonin. It has been successfully used in the treatment of depression, insomnia, migraines, and other diseases due to its regulatory effects on sleep, pain, appetite, and other physiological functions (**Figure 1**) (Birdsall, 1998). 5-HTP is widely used for psychotropic drugs and weight loss in developed countries. Health-care drugs with 5-HTP as the main ingredient are used in 20 countries. To date, 44 preparation types have been developed worldwide mainly in the form of capsules with 100–150 mg content, as well as in the form of tablets, powders, and sustained-release agents (JunDe et al., 2014). According to the 2014 Thomson Reuters market research report, the annual global sales of 5-HTP were $7.5 million, an increase of 50% over the same period the previous year, with an annual consumption of 1.6 tons.

At present, 5-HTP is mainly extracted from natural products, specifically from the seeds of the African plant *Griffonia Simplicifolia*, but this method of extraction is unable to meet the market demand due to high cost and a lack of raw materials. Chemical synthesis does not depend on natural products. However, it is not currently possible to synthesize 5-HTP economically and effectively due to the tedious steps involved and harsh conditions required. With the development of biotechnology in bioinformatics, genetics, metabolic engineering, biochemistry, protein engineering, and so on, new strategies are available for the use of microorganisms to synthesize 5-HTP. The production of 5-HTP by the microbial method has the advantages of short production cycle, continuous production and mild reaction conditions. Among the organisms used for this method, *Escherichia coli* is a model strain of prokaryotes with clear genetic information and well-established fermentation conditions, making it particularly well-suited for use as a host cell for the study of 5-HTP biosynthesis.

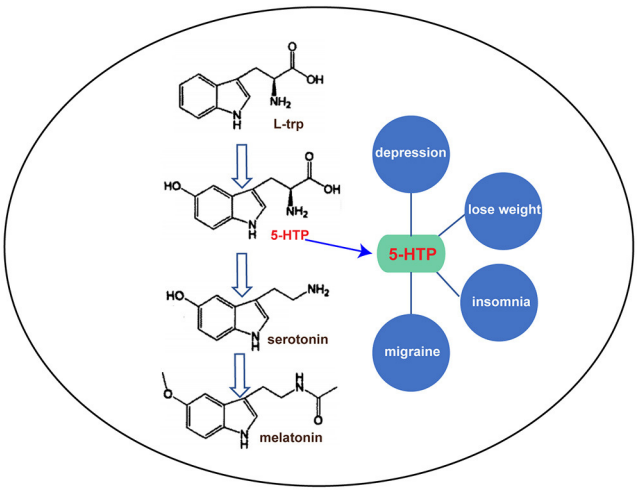

FIGURE 1 | The 5-HTP metabolic pathway and its function.

PHYSIOLOGICAL FUNCTION OF 5-HTP

As shown in **Figure 1**, 5-HTP has been widely studied for its important role in the treatment of depression and for weight loss. Depression is a common mental disorder with high levels of disability and stress. More than 350 million people worldwide suffer from depression, and ∼1 million people commit suicide due to depression every year (World Health Organization, 2017). It has become the second most important disease worldwide, posing a serious burden on human beings. Dysfunction of serotonin in the brain is thought to be a major cause of depression. 5-HTP is a natural and safe antidepressant because it can increase serotonin levels in the brain. In a clinical trial of 107 patients with depression, 69% of symptoms improved through the daily intake of 50–300 mg of 5-HTP. The response rate to this drug was significantly faster than that of ordinary drugs (Sano, 1972). In addition, the content of 5-hydroxyindoleacetic acid (a serotonin-decomposition product) in the cerebrospinal fluid of the patients significantly increased after 5-HTP intake, indicating that 5-HTP was successfully converted to serotonin after entering the central nervous system (Takahashi et al., 1975).

Dieting leads to a sharp decrease in serotonin levels in the serum and brain, and a decrease in serotonin leads to gluttonous gluttony. 5-HTP can prevent dieting induced decrease in serotonin in patients with obesity, thus reducing appetite and assisting with weight loss (Ceci et al., 1989; Cangiano et al., 1991, 1992). In addition, 5-HTP can also improve the symptoms of fibromyalgia, including pain, morning stiffness, anxiety, and fatigue (Caruso et al., 1990; Sarzi Puttini and Caruso, 1992; Nicolodi and Sicuteri, 1996). Chronic headaches are caused by reduced serotonin levels in the body. 5-HTP has successfully been used to prevent various types of chronic headaches, including migraines, tension headaches, and adolescent headaches (Bono et al., 1982; Longo et al., 1984; Benedittis and Massei, 1985; Titus et al., 1986; De Giorgis et al., 1987; Maissen and Ludin, 1991; Nicolodi and Sicuteri, 1996). In addition, 5-HTP can increase the rapid eye movement sleep period to improve sleep quality for the treatment of insomnia.

PRODUCTION OF 5-HTP

The anabolic-metabolic engineering design for 5-HTP has gained considerable attention and has been widely studied because of its important physiological functions and huge market demand. At present, the main methods for producing 5-HTP are natural product extraction, chemical synthesis, and microbial fermentation. Among these methods, natural product extraction remains the primary method for the commercial production of 5-HTP. While microbial synthesis and catalysis provide a fast and environmentally friendly alternative to produce natural compounds of medical value.

Natural Extraction of 5-HTP

5-HTP is widely present in the seeds of legumes, with the seeds of African plant *Griffonia Simplicifolia* haing the highest content. The leaves and seeds of the Ghanaian tree have been used as medicine in Africa since ancient times to treat wounds, kidney disease, and for enemas. The paste made from its bark is also used to treat skin diseases, in which the main active ingredient is 5-HTP. Lemaire and Adosraku extracted 5-HTP using the alcohol method, and found that it constituted 20.83% of the fresh weight of the seeds (Lemaire and Adosraku, 2010). After optimization of the extraction temperature, the content of 5-HTP in the extract increased from 6.37 to 8.98% and the purity reached 92% (Addotey, 2009). Using ultrafiltration membrane separation technology, the 5-HTP transfer rate was found to be 83.5%, and purity reached 90.5% (Qin et al., 2014). In addition, high-purity 5-HTP was also obtained from flower beans by ultrasonic method (Duan et al., 2017).

However, the natural source of 5-HTP is relatively singular. There is a shortage of raw materials and costs are continually increasing with the increase of exploitation. The increasing market demand is impossible to meet through natural extraction alone. Therefore, there has recently been an increasing number of studies regarding the production of 5-HTP via chemical synthesis and biological fermentation.

Chemical Synthesis of 5-HTP

5-HTP is synthesized by Michael addition reaction using 5-bromoindole 3-bromo-2-hydroxyimino-propionate as the substrate. The addition reaction connects the side chain of 2-hydroxyimino-propionate to the 3-position of the indole. Subsequently, the reduction reaction, hydrolysis reaction, and resolution steps are introduced to obtain 5-HTP (Fuchun et al., 2013). In an invention patent, Raney-Ni and ZnO were added to an autoclave as catalysts. Trp, glycolic acid, and hydrochloric acid were reacted in the autoclave for 0.25–6 h, then filtered and dried to obtain poly-hydroxy-trp drying substance. The dried substance was then reacted with trp, sodium hydroxide, and deionized water. The 5-HTP crystals were finally obtained after filtration, chromatography and cooling crystallization (Rihe, 2010). Wenhui and colleagues first demonstrated the methyl (ethyl) esterification of L-trp to form tryptophan methyl

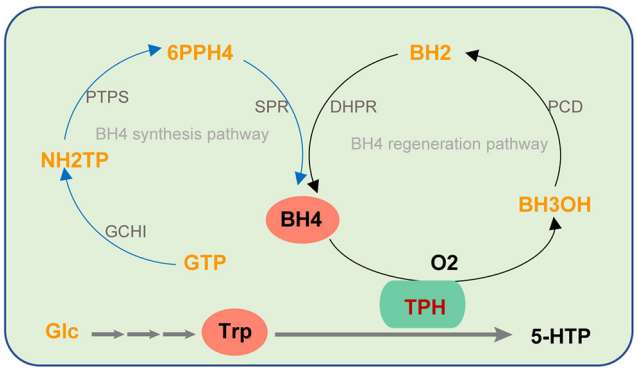

FIGURE 2 | The biosynthesis pathway of 5-HTP catalyzed by TPH using BH_4 as a cofactor. The blue line represents the BH_4 synthesis pathway. The black line represents BH_4 regeneration pathway.

(ethyl) ester hydrochloride. 5-HTP was obtained after desalting, acetylation, redox, deacetylation, and other reactions. After cooling and crystallization, 5-HTP crystals were obtained. The purity of the product was 99.2% and the overall yield was 45% (Wenhui et al., 2013).

The chemical method for the synthesis of 5-HTP is tedious, harsh, and costly. It uses a variety of organic reagents, resulting in serious environmental pollution. Therefore, this method is not suitable for the large-scale production of 5-HTP.

Biosynthesis of 5-HTP

5-HTP production by biological methods is favored due to its advantages, such as a short production cycle, continuous production, and mild reaction conditions. *In vivo*, 5-HTP is obtained by L-trp hydroxylation catalyzed by trp hydroxylase (TPH) using L-trp as a substrate (**Figure 2**). TPH is a monooxygenase that uses trp and oxygen as substrates, and tetrahydrobiopterin (BH_4) and Fe^{2+} are required as cofactors in its catalytic process (Kappock and Caradonna, 1996; Fitzpatrick, 1999; Olsson et al., 2010; Roberts and Fitzpatrick, 2013).

METABOLIC ENGINEERING STRATEGY FOR 5-HTP SYNTHESIS

In vivo, 5-HTP is produced from L-trp and the reaction is catalyzed by TPH, which uses L-trp and O_2 as substrates and requires BH_4 and Fe^{2+} as cofactors. The activity of TPH, the supply of L-trp, and the synthesis and regeneration of BH_4 are three key factors that restrict restricting 5-HTP synthesis.

L-Tryptophan Hydroxylase (TPH)

TPH, phenylalanine hydroxylase (PAH), and tyrosine Hydroxylase (TH) are pterin-dependent aromatic AA hydroxylases (AAAHs) (Windahl et al., 2008; Olsson et al., 2010). Moreover, these three hydroxylases have substrate interconnectedness, and each hydroxylase can catalyze the hydroxylation of these three aromatic AAs (Olsson et al., 2010; Roberts and Fitzpatrick, 2013). There are two subtypes of TPH in mammals: TPHI and TPH2 (Walther et al., 2003). TPH1 was discovered first and studied in depth. In adults, TPH1 is mainly expressed in non-nerve cells (Murphy et al., 2008). Walther et al. found that the brains of mice could still produce serotonin normally after knocking out the TPH1 gene. Further studies found another TPH, TPH2, in the brains of mice (Walther et al., 2003). TPH1 and TPH2 have 71% AA sequence homology. TPH2 is mainly responsible for the synthesis of serotonin in the central nervous system, including the frontal area, thalamus, hippocampus, amygdala, and hypothalamus, whereas TPH1 is mainly expressed in the pineal gland and the gut and is responsible for the synthesis of serotonin in other parts of the body, such as the heart, lungs, and kidneys (Walther and Bader, 2003; Walther et al., 2003; Patel et al., 2004; Zhang et al., 2004; Sakowski et al., 2006).

First, TPH was heterologous expressed in *E. coli*, and its structure, enzymatic properties, and catalytic mechanism were studied. Windahl et al. (2008) studied the active center structure of chicken TPH1. The Fe^{2+} coordination structure was found to belong to the heme-independent general Fe^{2+} coordination structure. The Fe^{2+} coordination is a distorted trigonal bipyramidal coordination with His273, His278, Glu318, and an imidazole ligand. The substrate trp binds to the hydrophobic pocket of the active center. This hydrophobic pocket is composed of Tyr236, Thr266, Pro267, Glu268, Pro269, His273, Phe314, Phe319, and Lie367 (Windahl et al., 2008). McKinney et al. (2004) expressed human TPH in *E. coli* and *yeast* expression system. They found that the soluble expression of TPH could be enhanced by fusion expression with maltose-binding protein. The fusion expressed TPH's enzyme activity and affinity with L-trp was significantly improved. Moran et al. (1998) expressed rabbit-derived TPH in *E. coli*. It was found that the soluble expression was significantly increased after removing 101 AAs at the N-terminal and 28 AAs at the C-terminal. Interestingly, this mutated TPH exists in the form of a monomer rather than a tetramer. Kino et al. (2009) found that Leu101 and Trp180 from the active center of *Pseudomonas aeruginosa* PAH exerted effects on substrate specificity and hydroxylase activity. The enzyme catalytic rate constant, $K_{cat,}$ increased 5.2 times after mutation at these two sites (Kino et al., 2009).

Synthesis and Regeneration of BH_4

One difficulty in using *E. coli* to produce 5-HTP is that it does not synthesize the coenzyme $BH_{4,}$ which is essential for TPH. *E. coli* can synthesize analogs of BH_4, tetrahydromonapterin (MH_4) (Ikemoto et al., 2002). PAH of *Pseudomonas aeruginosa* can use MH_4 as a coenzyme to hydroxylate L-phenylalanine to L-tyrosine. Zhang et al. (2016) expressed mutant PAH or TPH in *Saccharomyces cerevisiae* to catalyze the production of 5-HTP from L-trp. The activities of PAH and TPH in the hydroxylation of trp with MH_4 and BH_4 as cofactors were compared. The results showed that the hydroxylation activity of TPH using BH_4 as a cofactor was 17 times higher than that of PAH using MH_4 (Zhang et al., 2016).

With an in-depth understanding of the biosynthetic pathway of BH_4, Yamamoto et al. (2003) synthesized BH_4 through the heterologous expression in *E. coli*. The synthetic pathway of

TABLE 1 | Overview of 5-HTP production by microorganism.

Strains	Modulations	Titer (g/L)	Cultivation	References
E. coli	Overexpression of mutant PAH,	0.1762	Shake flask; Supplementation of BH_4 and 5 mM L-trp	Kino et al., 2009; Hara and Kino, 2013
E. coli	Overexpression of mutant PAH; Insertion of BH_4 regeneration pathway; Insertion of glucose dehydrogenase from *Bacillus subtilis*	0.55	Shake flask; Supplementation of 5 mM L-Trp	Hara and Kino, 2013
E. coli	Mutation of PAH from *Xanthomonas campestris*; Co-expression of MH_4 regeneration pathway and L-trp synthesis pathway	0.1529	Shake flask; Supplementation of glucose	Lin et al., 2014
E. coli	Mutation of the PAH from Xanthomonas campestris; Co-expression of MH_4 regeneration and the L-trp synthesis pathway; Transformation into an L-trp high-yield strain	0.962	Fed-batch	Mora-Villalobos and Zeng, 2018
E. coli	Mutation of phenylalanine-4-hydroxylases (P4Hs); Deletion of the *pheA, tyrA*, and *tnaA* genes	1.1–1.2	Shake flask; Supplementation of 2 g/L L-Trp	Lin et al., 2014
E. coli	Mutation of AAAH; Insertion of the human BH_4 regeneration pathway; Disruption of tryptophanase	0.55	Supplementation of 1 g/L L-Trp	Mora-Villalobos and Zeng, 2017
E. coli	Expression of a truncated human TPH2; Reconstitution of the BH_4 synthesis and regeneration pathway; Modulation of the plasmid copy number and promoter strength; Modulation of different modules' expression levels	1.3	Shake flask; Glycerol as carbon source	Wang et al., 2018
E. coli	Same as the previous line	5.1	Fed-batch; Glycerol as carbon source	Wang et al., 2018
E. coli	Expression of a truncated human TPH2; Reconstitution of the BH_4 synthesis and regeneration pathway; Modulation of the plasmid copy number and promoter strength; Modulation of the relative expression levels among different modules; Designing promoter strength to increase tryptophan production	1.61	Shake flask; Glycerol as carbon source	Xu et al., 2020

BH_4 is shown in **Figure 2**. The production capacity of GTP (the precursor of BH_4) was increased by mutation breeding (Perkins et al., 1999). By optimizing the activity of GCHI (the enzyme that catalyzes the first step of BH_4 biosynthesis) from different sources, 4 g/L BH_4 was obtained under fed-batch fermentation (Yamamoto et al., 2003).

Kino et al. (2009) first expressed the mutagenic TPH in *E. coli* and synthesized 0.8 mM of 5-HTP by adding BH_4 as a substrate. Subsequently, the BH_4 regeneration pathway and glucose dehydrogenase from *Bacillus subtilis* were introduced to increase the utilization rate of BH_4. The yield of 5-HTP increased to 2.5 mM under these conditions (**Table 1**) (Kino et al., 2009; Hara and Kino, 2013). Knight et al. (2013) introduced the mammalian BH_4 synthesis pathway and regeneration pathway into *E. coli* and co-expressed it with rabbit-derived TPH1. When L-trp was used as the substrate, the yield of 5-HTP reached 198 mg/L (Knight et al., 2013). Although 5-HTP synthesis was achieved by introducing the synthesis and regeneration pathway of BH_4, the yield of 5-HTP was low and additional L-trp was needed, indicating that it is not a suitable method for mass production.

Optimization of trp Supply

5-HTP yield can be increased by increasing TPH activity and introducing BH_4 synthesis and regeneration pathways. Mora-Villalobos and Zeng (2017) mutated the aromatic amino acid hydroxylase of Cu*priavidus taiwanensis* and obtained the trp preference mutant enzyme C_tAAAH-W192F. The mutated enzyme was co-expressed with the BH_4 regeneration pathway in *E. coli*. Additionally, 5 mM trp could be transformed into 2.5 mM of 5-HTP by shaking flask culture for 24 h. After converting this pathway into L-trp producing bacteria, the synthesis of 5-HTP from glucose was realized. The flask yield was 100 mg/L in 60 h, and the batch fermentation yield was 962 mg/L (Mora-Villalobos and Zeng, 2018).

Wang et al. (2018) introduced human TPH into *E. coli* BL21, and co-expressed it with the synthetic and regenerative pathways of human BH_4. The engineered bacteria hydroxylated 2 g/L trp to produce 1.24 g/L 5-HTP. The authors further introduced the trp synthesis pathway into the recombinant *E. coli* to realize the biosynthesis of 5-HTP. After the optimization of culture conditions, the yield of 5-HTP was further increased by 13 times to 314.8 mg/L. After module optimization, which included: (a)enzymatic modification to improve the hydroxylation activity of TPH, (b)reduction of the copy number of the trp synthesis gene, and (c) regulation of the promoter strength of genes involved in BH_4 synthesis and regeneration, the yield of 5-HTP in the modified recombinant strain HTPL01-LMT was 1.29 g/L, 3.1-fold increase (Wang et al., 2018). To improve the stability of this system, the authors further integrated the L-trp biosynthesis pathway into *E. coli* genome and designed the promoter strength of the enzyme-coding gene, which catalyzes the first step of L-trp biosynthesis. To regulate the production of 5-HTP, they also regulated the copy number of the L-TPH coding gene plasmid. After these optimization steps, the amount of 5-HTP of shake flask fermentation increased to 1.61 g/ml, which was 24% higher than that of the original strain (**Table 1**) (Xu et al., 2020).

PROSPECTS

This review assesses the synthesis and research progress of 5-HTP. Compared with natural product extraction and chemical synthesis, biosynthesis has the advantages of a short cycle, continuous production and mild reaction conditions; thus, it has garnered considerable research attention. In the biosynthesis process, three aspects of optimization have been implemented to increase the output of 5-HTP; (a) improving the hydroxylation activity of the TPH enzyme by directed evolution, (b) introducing BH_4 synthesis and the regeneration pathway, (c) introducing the trp synthesis pathway. To date, the yield of shake flask culture has reached 1.61 g /L.

Although 5-HTP production has increased 10-fold, remains insufficient for large-scale commercial production. The metabolic network is a complex system, and the efficiency of the target metabolic pathway is often affected by other metabolic pathways. Therefore, strain evolution and breeding for global metabolism may effectively improve the yield of the target product. Besides, high-density cell culture is another strategy for increasing the yield. Combined with the optimization of fermentation conditions and the improvement of cell culture density, the yield of 5-HTP could be further improved.

AUTHOR CONTRIBUTIONS

X-XL wrote the manuscript. BZ and L-ZA revised the Metabolic engineering strategy for 5-HTP synthesis section. All the authors contributed to the literature collection and data analysis, and approved it for publication.

FUNDING

This work was sponsored by the Shanghai Sailing Program (20YF1433500); the National Key R&D Program of China [Grant No. 2018YFC1604305]; the Shanghai Agriculture Applied Technology Development Program, China [Grant No. 2019-02-08-00-07-F01152]; the Natural Science Foundation of China [Grant No. 31871757]. Shanghai Technical Standard Program, China [18DZ2200200]; Shanghai Engineering Research Center of food microbiology program [19DZ22 81100].

ACKNOWLEDGMENTS

We would like to thank Editage (www.editage.cn) for English language editing.

REFERENCES

Addotey, J. (2009). Local production of 5-HTP from the seeds of *Griffonia simplicifolia*. *World J. Pharm. Pharm*. 5.

Benedittis, G. D., and Massei, R. (1985). Serotonin precursors in chronic primary headache. A double-blind cross-over study with L-5-hydroxytryptophan vs. placebo. *J. Neurosurg. Sci.* 29, 239–248.

Birdsall, T. C. (1998). 5-Hydroxytryptophan: a clinically-effective serotonin precursor. *Altern. Med. Rev*. 3, 271–280.

Bono, G., Criscuoli, M., Martignoni, E., Salmon, S., and Nappi, G. (1982). Serotonin precursors in migraine prophylaxis. *Adv. Neurol*. 33:357.

Cangiano, C., Ceci, F., Cairella, M., Cascino, A., Ben, M. D., Laviano, A., et al. (1991). *Effects of 5-Hydroxytryptophan on Eating Behavior and Adherence to Dietary Prescriptions in Obese Adult Subjects*. New York, NY: Springer. doi: 10.1007/978-1-4684-5952-4_73

Cangiano, C., Ceci, F., Cascino, A., Del Ben, M., Laviano, A., Muscaritoli, M., et al. (1992). Eating behavior and adherence to dietary prescriptions in obese adult subjects treated with 5-hydroxytryptophan. *Am. J. Clin. Nutr*. 56, 863–867. doi: 10.1093/ajcn/56.5.863

Caruso, I., Sarzi Puttini, P., Cazzola, M., and Azzolini, V. (1990). Double-blind study of 5-hydroxytryptophan versus placebo in the treatment of primary fibromyalgia syndrome. *J. Int. Med. Res.* 18, 201–209. doi: 10.1177/030006059001800304

Ceci, F., Cangiano, C., Cairella, M., Cascino, A., Del Ben, M., Muscaritoli, M., et al. (1989). The effects of oral 5-hydroxytryptophan administration on feeding behavior in obese adult female subjects. *J. Neural Transm*. 76, 109–117. doi: 10.1007/BF01578751

De Giorgis, G., Miletto, R., Iannuccelli, M., Camuffo, M., and Scerni, S. (1987). Headache in association with sleep disorders in children: a psychodiagnostic evaluation and controlled clinical study–L-5-HTP versus placebo. *Drugs Exp. Clin. Res* 13:425.

Duan, G., Mingbo, G., Qiao, C., Xiaochen, W., and Yining, L. (2017). Ultrasonic extraction of 5-hydroxytryptophan from adzuki bean. *Guangzhou Chem. Indus.* 45, 52–54.

Fitzpatrick, P. F. (1999). Tetrahydropterin-dependent amino acid hydroxylases. *Annu. Rev. Biochem*. 68, 355–381. doi: 10.1146/annurev.biochem.68.1.355

Fuchun, G., Can, L., and Yan, X. (2013). *A New Simple Method for Synthesis of L-5-hydroxytryptophan, CN*. Patent CN103554005A.

Hara, R., and Kino, K. (2013). Enhanced synthesis of 5-hydroxy-l-tryptophan through tetrahydropterin regeneration. *AMB Express* 3:70. doi: 10.1186/2191-0855-3-70

Ikemoto, K., Sugimoto, T., Murata, S., Tazawa, M., Nomura, T., Ichinose, H., et al. (2002). (6R)-5,6,7,8-tetrahydro-L-monapterin from *Escherichia coli*, a novel natural unconjugated tetrahydropterin. *Biol. Chem*. 383, 325–330. doi: 10.1515/BC.2002.035

JunDe, L., Shaohua, L., and Mi, T. (2014). Research progress of 5-hydroxytryptophan. *Fine Specialized Chem.* 22, 36–39.

Kappock, T. J., and Caradonna, J. P. (1996). Pterin-dependent amino acid hydroxylases. *Chem. Rev*. 96, 2659–2756. doi: 10.1021/cr9402034

Kino, K., Hara, R., and Nozawa, A. (2009). Enhancement of L-tryptophan 5-hydroxylation activity by structure-based modification of L-phenylalanine 4-hydroxylase from Chromobacterium violaceum. *J. Biosci. Bioeng*. 108, 184–189. doi: 10.1016/j.jbiosc.2009.04.002

Knight, E. M., Zhu, J., Förster, J., and Hao, L. (2013). Microorganisms for the production of 5-hydroxytryptophan. *Nippon Hinyokika Gakkai Zasshi the Japanese J. Urol*. 56, 317–330. doi: 10.1093/mnras/stt2484

Lemaire, P. A., and Adosraku, R. K. (2010). An HPLC method for the direct assay of the serotonin precursor, 5-hydroxytrophan, in seeds of *Griffonia simplicifolia*. *Phytochem. Anal*. 13, 333–337. doi: 10.1002/pca.659

Lin, Y., Sun, X., Yuan, Q., and Yan, Y. (2014). Engineering bacterial phenylalanine 4-hydroxylase for microbial synthesis of human neurotransmitter precursor 5-hydroxytryptophan. *ACS Synth. Biol.* 3, 497–505. doi: 10.1021/sb5002505

Longo, G., Rudoi, I., Iannuccelli, M., Strinati, R., and Panizon, F. (1984). Treatment of essential headache in developmental age with L-5-HTP (cross over double-blind study versus placebo). *Pediatr. Med. Chir*. 6, 241–245.

Maissen, C. P., and Ludin, H. P. (1991). Comparison of the effect of 5-hydroxytryptophan and propranolol in the interval treatment of migraine. *Schwzerische Medizinische Wochenschrift* 121, 1585–1590.

McKinney, J., Knappskog, P. M., Pereira, J., Ekern, T., Toska, K., Kuitert, B. B., et al. (2004). Expression and purification of human tryptophan hydroxylase from *Escherichia coli* and *Pichia pastoris*. *Protein Expr. Purif*. 33, 185–194. doi: 10.1016/j.pep.2003.09.014

Moran, G. R., Daubner, S. C., and Fitzpatrick, P. F. (1998). Expression and characterization of the catalytic core of tryptophan hydroxylase. *J. Biol. Chem.* 273, 12259–12266. doi: 10.1074/jbc.273.20.12259

Mora-Villalobos, J.-A., and Zeng, A. P. (2017). Protein and pathway engineering for the biosynthesis of 5-hydroxytryptophan in *Escherichia coli*. *Eng. Life Sci.* 17, 892–899. doi: 10.1002/elsc.201700064

Mora-Villalobos, J. A., and Zeng, A. P. (2018). Synthetic pathways and processes for effective production of 5-hydroxytryptophan and serotonin from glucose in *Escherichia coli*. *J. Biol. Eng.* 12:3. doi: 10.1186/s13036-018-0094-7

Murphy, K. L., Zhang, X., Gainetdinov, R. R., Beaulieu, J. M., and Caron, M. G. (2008). A regulatory domain in the n terminus of tryptophan hydroxylase 2 controls enzyme expression. *J. Biol. Chem.* 283, 13216–13224. doi: 10.1074/jbc.M706749200

Nicolodi, M., and Sicuteri, F. (1996). Fibromyalgia and migraine, two faces of the same mechanism. Serotonin as the common clue for pathogenesis and therapy. *Adv. Exp. Med. Biol.* 398, 373–379. doi: 10.1007/978-1-4613-0381-7_58

Olsson, E., Teigen, K., Martinez, A., and Jensen, V. R. (2010). The aromatic amino acid hydroxylase mechanism: a perspective from computational chemistry. *Adv. Inorg. Chem.* 62, 437–500. doi: 10.1016/S0898-8838(10)62011-9

Patel, P. D., Pontrello, C., and Burke, S. (2004). Robust and tissue-specific expression of TPH2 versus TPH1 in rat raphe and pineal gland. *Biol. Psychiatry* 55, 428–433. doi: 10.1016/j.biopsych.2003.09.002

Perkins, J. B., Sloma, A., Hermann, T., Theriault, K., Zachgo, E., Erdenberger, T., et al. (1999). Genetic engineering of Bacillus subtilis for the commercial production of riboflavin. *J. Indus. Microbiol. Biotechnol.* 22, 8–18. doi: 10.1038/sj.jim.2900587

Qin, Z., Xuesong, H., Ling, Q., and Yanjie, K. (2014). Study on separation and purification of 5-hydroxytryptophan from Ghanaian seeds by ultrafiltration membrane. *Res. Dev. Nat. Products* 26, 2033–2036.

Rihe, S. (2010). *Synthesis of L-5-Hydroxytryptophan*. Patent CN101323586B.

Roberts, K. M., and Fitzpatrick, P. F. (2013). Mechanisms of tryptophan and tyrosine hydroxylase. *IUBMB Life* 65, 350–357. doi: 10.1002/iub.1144

Sakowski, S. A., Geddes, T. J., Thomas, D. M., Levi, E., Hatfield, J. S., and Kuhn, D. M. (2006). Differential tissue distribution of tryptophan hydroxylase isoforms 1 and 2 as revealed with monospecific antibodies. *Brain Res.* 1085, 11–18. doi: 10.1016/j.brainres.2006.02.047

Sano, I. (1972). L-5-hydroxytryptophan(L-5-HTP) therapy in endogenous depression. *Munch. Med. Wochenschr.* 114, 1713–1716. doi: 10.1111/j.1440-1819.1972.tb01107.x

Sarzi Puttini, P., and Caruso, I. (1992). Primary fibromyalgia syndrome and 5-hydroxy-L-tryptophan: a 90-day open study. *J. Int. Med. Res.* 20, 182–189. doi: 10.1177/030006059202000210

Takahashi, S., Kondo, H., and Kato, N. (1975). Effect of l-5-hydroxytryptophan on brain monoamine metabolism and evaluation of its clinical effect in depressed patients. *J. Psychiatr. Res.* 12, 177–187. doi: 10.1016/0022-3956(75)90025-4

Titus, F., Dávalos, A., Alom, J., and Codina, A. (1986). 5-Hydroxytryptophan versus methysergide in the prophylaxis of migraine. Randomized clinical trial. *Eur. Neurol.* 25, 327–329. doi: 10.1159/000116030

Walther, D. J., and Bader, M. (2003). A unique central tryptophan hydroxylase isoform. *Biochem. Pharmacol.* 66, 1673–1680. doi: 10.1016/S0006-2952(03)00556-2

Walther, D. J., Peter, J. U., Bashammakh, S., Hörtnagl, H., Voits, M., Fink, H., et al. (2003). Synthesis of serotonin by a second tryptophan hydroxylase isoform. *Science* 299:76. doi: 10.1126/science.1078197

Wang, H., Liu, W., Shi, F., Huang, L., Lian, J., Qu, L., et al. (2018). Metabolic pathway engineering for high-level production of 5-hydroxytryptophan in *Escherichia coli*. *Metab. Eng.* 48, 279–287. doi: 10.1016/j.ymben.2018.06.007

Wenhui, H., Xing, T., Xiaobing, L., and Jiajin, Y. (2013). *A Method for Preparing L-5-Hydroxytryptophan*. Patent CN201110272240.3.

Windahl, M. S., Petersen, C. R., Christensen, H. E., and Harris, P. (2008). Crystal structure of tryptophan hydroxylase with bound amino acid substrate. *Biochemistry* 47, 12087–12094. doi: 10.1021/bi8015263

World Health Organization (2017). *Depression and Other Common Mental Disorders: Global Health Estimates*. Geneva: World Health Organization.

Xu, D., Fang, M., Wang, H., Huang, L., Xu, Q., and Xu, Z. (2020). Enhanced production of 5-hydroxytryptophan through the regulation of L-tryptophan biosynthetic pathway. *Appl. Microbiol. Biotechnol.* 104, 2481–2488. doi: 10.1007/s00253-020-10371-y

Yamamoto, K., Kataoka, E., Miyamoto, N., Furukawa, K., Ohsuye, K., and Yabuta, M. (2003). Genetic engineering of *Escherichia coli* for production of tetrahydrobiopterin. *Metab. Eng.* 5, 246–254. doi: 10.1016/S1096-7176(03)00046-6

Zhang, J., Wu, C., Sheng, J., and Feng, X. (2016). Molecular basis of 5-hydroxytryptophan synthesis in *Saccharomyces cerevisiae*. *Mol. Biosyst.* 12, 1432–1435. doi: 10.1039/C5MB00888C

Zhang, X., Beaulieu, J. M., Sotnikova, T. D., Gainetdinov, R. R., and Caron, M. G. (2004). Tryptophan hydroxylase-2 controls brain serotonin synthesis. *Science* 305:217. doi: 10.1126/science.1097540

Conflict of Interest: The authors declare that the research was conducted in the absence of any commercial or financial relationships that could be construed as a potential conflict of interest.

frontiers in Bioengineering and Biotechnology

ORIGINAL RESEARCH
published: 09 February 2021
doi: 10.3389/fbioe.2021.633028

A High-Efficiency Artificial Synthetic Pathway for 5-Aminovalerate Production From Biobased L-Lysine in *Escherichia coli*

Jie Cheng[1], Wenying Tu[1], Zhou Luo[1], Xinghua Gou[1], Qiang Li[1], Dan Wang[2]* and Jingwen Zhou[3]**

[1] Key Laboratory of Meat Processing of Sichuan Province, Key Laboratory of Coarse Cereal Processing, Ministry of Agriculture and Rural Affairs, College of Food and Biological Engineering, Chengdu University, Chengdu, China, [2] Department of Chemical Engineering, School of Chemistry and Chemical Engineering, Chongqing University, Chongqing, China, [3] National Engineering Laboratory for Cereal Fermentation Technology, Jiangnan University, Wuxi, China

OPEN ACCESS

Edited by:
K. Madhavan Nampoothiri, National Institute for Interdisciplinary Science and Technology (CSIR), India

Reviewed by:
Volker F. Wendisch, Bielefeld University, Germany
Yanning Zheng, Institute of Microbiology, Chinese Academy of Sciences, China

***Correspondence:**
Jie Cheng
jcheng@cqu.edu.cn
Dan Wang
dwang@cqu.edu.cn
Jingwen Zhou
zhoujw1982@jiangnan.edu.cn

Specialty section:
This article was submitted to Industrial Biotechnology, a section of the journal Frontiers in Bioengineering and Biotechnology

Received: 24 November 2020
Accepted: 20 January 2021
Published: 09 February 2021

Citation:
Cheng J, Tu W, Luo Z, Gou X, Li Q, Wang D and Zhou J (2021) A High-Efficiency Artificial Synthetic Pathway for 5-Aminovalerate Production From Biobased L-Lysine in Escherichia coli. Front. Bioeng. Biotechnol. 9:633028. doi: 10.3389/fbioe.2021.633028

Bioproduction of 5-aminovalerate (5AVA) from renewable feedstock can support a sustainable biorefinery process to produce bioplastics, such as nylon 5 and nylon 56. In order to achieve the biobased production of 5AVA, a 2-keto-6-aminocaproate-mediated synthetic pathway was established. Combination of L-Lysine α-oxidase from *Scomber japonicus*, α-ketoacid decarboxylase from *Lactococcus lactis* and aldehyde dehydrogenase from *Escherichia coli* could achieve the biosynthesis of 5AVA from biobased L-Lysine in *E. coli*. The H_2O_2 produced by L-Lysine α-oxidase was decomposed by the expression of catalase KatE. Finally, 52.24 g/L of 5AVA were obtained through fed-batch biotransformation. Moreover, homology modeling, molecular docking and molecular dynamic simulation analyses were used to identify mutation sites and propose a possible trait-improvement strategy: the expanded catalytic channel of mutant and more hydrogen bonds formed might be beneficial for the substrates stretch. In summary, we have developed a promising artificial pathway for efficient 5AVA synthesis.

Keywords: 5-aminovalerate, L-Lysine HCl, artificial pathway, molecular dynamic simulation, molecular docking

INTRODUCTION

Increasing concerns over global water pollution, climate change, public health, and petroleum shortages have attracted considerable attention to sustainable development as promising green alternatives to traditional petrochemical-derived chemicals renewable feedstock (Tsuge et al., 2016). Recently a variety of valuable chemicals such as 6-aminocaproate (Cheng et al., 2019), fructose (Yang et al., 2016), mandelic acid (Youn et al., 2020), vitamin B_{12} (Fang et al., 2018), naringenin (Gao et al., 2020b), *p*-coumaric acid (Gao et al., 2020a), breviscapine (Liu et al., 2018), 4-hydroxybenzoic acid (Klenk et al., 2020), curcuminoids (Rodrigues et al., 2020) and hydroxytyrosol (Zeng et al., 2020) have been produced in microorganisms. As a kind of green alternative to petrochemical products, microbial bioplastics are composed of monomers containing appropriate functional groups, which have become the focus of metabolic engineering research. These compounds include amino acids such as methionine (Kromer et al., 2006) and leucine

(Zhang et al., 2008), organic acids such as adipic acid (Zhao et al., 2018a) and glutarate (Zhao et al., 2018b), diamines such as 1,3-diaminopropane (Chae et al., 2015) and diaminopentane (Kind et al., 2010; Rui et al., 2020), as well as diols like 1,3-propanediol (Nakamura and Whited, 2003) and 1,2-propanediol (Niimi et al., 2011). It is worth mentioning that two straight-chain amino acids—5-aminovalerate (5AVA) and 4-aminobutyrate—are promising platform compounds for the synthesis of polyimides, serving as raw materials for disposable goods, clothes and automobile parts like nylon 5 (Adkins et al., 2013) and nylon 4 (Park et al., 2013a) because of its high temperature and organic solvent resistance.

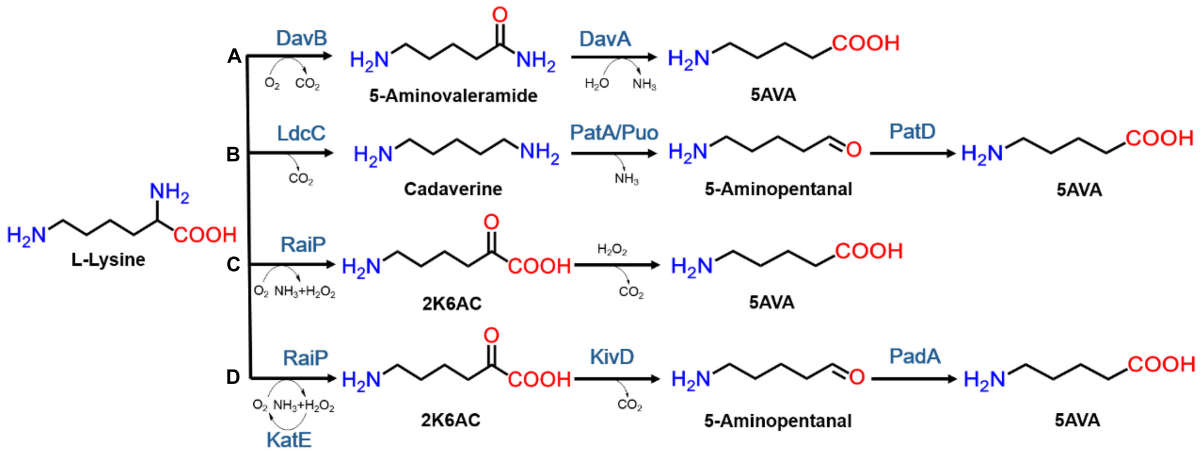

FIGURE 1 | The biosynthesis routes of 5AVA from L-Lysine in microorganisms. The enzymes included in those routes are: **(A)** lysine 2-monooxygenase (DavB), δ-aminovaleramidase (DavA); **(B)** L-Lysine decarboxylase (LdcC), putrescine transaminase (PatA), monooxygenase putrescine oxidase (Puo), and γ-aminobutyraldehyde dehydrogenase (PatD); **(C)** L-Lysine α-oxidase (RaiP); **(D)** L-Lysine α-oxidase (RaiP), α-ketoacid decarboxylase (KivD), catalyze (KatE), and aldehyde dehydrogenase (PadA).

TABLE 1 | The production of 5-AVA in different synthetic pathway.

Synthetic pathway	Host strain	Strategy	Description	5AVA titer (g/L)	Yield (g/g)	Substrate/ feedstock	References
A	*E. coli*	Whole-cell biotransformation	Expression of DavB and DavA in *E. coli*	240.70	0.70	L-Lysine	Wang et al., 2016
A	*E. coli*	Enzymatic catalysis	Overexpression of DavB, DavA, PP2911 from *P. putida* and LysP from *E. coli*	63.20	0.62	L-Lysine	Li et al., 2016
A	*C. glutamicum*	Fed-batch fermentation	Expression of codon-optimized *davA* and *davB*, promoter engineering	33.10	0.10	Glucose	Shin et al., 2016
A	*C. glutamicum*	Fed-batch fermentation	Pretreatment, hydrolysis, purification and concentration of the *Miscanthus* hydrolyzate solution	12.51	0.10	*Miscanthus* hydrolyzate	Joo et al., 2017
B	*C. glutamicum*	Fermentation	N-acetylcadaverine and glutarate in a genome-streamlined L-Lysine producing strain expressing ldcC, patA, and patD from *E. coli*	5.10	0.13	Glucose and alternative carbon sources	Jorge et al., 2017
B	*C. glutamicum*	Fermentation	*C. glutamicum* GSLA2ΔgabTDP with overexpression of LdcC, Puo, and PatD	3.70	0.09	Glucose	Haupka et al., 2020
C	*E. coli*	Whole-cell biotransformation	Overexpression of RaiP from *S. japonicus* and addition of 4% ethanol and 10 mM H_2O_2	29.12	0.44	L-Lysine HCl	Cheng et al., 2018b
D	*E. coli*	Whole-cell biotransformation	Combination of native RaiP, KivD, PadA, KatE, and LysP, without addition of ethanol and H_2O_2	52.24	0.38	L-Lysine HCl	This study

5AVA, 5-Aminovalerate; DavB, Lysine 2-monooxygenase; DavA, δ-Aminovaleramidase; RaiP, Lysine α-oxidase; LdcC, Lysine decarboxylase; PatA, Putrescine transaminase; PatD, γ-Aminobutyraldehyde dehydrogenase; PP2911, 4-Aminobutyrate; LysP, Lysine permease; Puo, Monooxygenase putrescine oxidase; KivD, Ketoacid decarboxylase; KatE, Catalase; PadA, Aldehyde dehydrogenase.

Due to the high demand in the animal feed industry, the production of L-Lysine (L-lys) is saturated today and may even be in oversupply (Vassilev et al., 2018). As one of the most important bulk chemicals, 5AVA has become the precursor for the synthesis of δ-valerolactam (Zhang et al., 2017), glutarate (Rohles et al., 2016; Hong et al., 2018), nylon 5 (Adkins et al., 2013), 5-hydroxyvalerate (Liu et al., 2014) and 1,5-pentanediol (Park et al., 2014). 5AVA is currently produced from petroleum feedstocks with aerobic oxidation of piperidine catalyzed by ceria-supported nanogold (Dairo et al., 2016). However, this chemical synthesis method not only requires higher temperature, but results in greater pollution (Dairo et al., 2016), so it is necessary to discover alternative approaches to produce 5AVA. Recently, with the rapid development of biotechnology, the synthesis of 5AVA by means of metabolic engineering and synthetic biology has attracted more and more attention (Hong et al., 2018).

In nature, 5AVA synthesis is closely related to L-lys catabolism in *Pseudomonas putida* (Ying et al., 2017). As seen in **Figure 1A**, 5AVA was produced through the overexpression of L-lys 2-monooxygenase (DavB) and 5AVA amidohydrolase (DavA) (Joo et al., 2017). According to Park's report (Park et al., 2013b), 3.6 g/L of 5AVA was succsessfully produced in WL3110/DavA-DavB, but the titer was relatively low. 33.1 g/L of 5AVA was produced under a novel artificial H_{36} promoter in *Corynebacterium glutamicum* (Shin et al., 2016). Interestingly, L-lys specific permease (LysP) has been shown to increase 5AVA titer to 63.2 g/L (**Table 1**; Li et al., 2016). As seen from **Figure 1B**, 5AVA has been successfully produced from L-lys via cadaverine-mediated and 5-aminopentanal-mediated pathway (Jorge et al., 2017). With the expression of L-lys α-oxidase (RaiP) from *Scomber japonicus* (*S. japonicus*), 29.12 g/L of 5AVA could be successfully formed from L-lys hydrochloride (L-lys HCl) via 2-keto-6-aminocaproate (2K6AC) as intermediate as seen in **Figure 1C** (Cheng et al., 2018b). However, the addition of ethanol and H_2O_2 were unsafe and uneconomical (Cheng et al., 2018b). 13.4 g/L 5AVA could be successfully obtained with RaiP immobilized on a solid support (Pukin et al., 2010). In addition, 5AVA could be effectively separated by macroporous adsorption resin AK-1 from bioconversion liquid with the purity of 99.3% (Xu et al., 2019).

The promiscuous α-ketoacid decarboxylase (KivD) has been demonstrated in the decarboxylation of α-ketoacids (Atsumi et al., 2008; Chen et al., 2017). In its native pathway, KivD catalyzes a wide variety of α-ketoacids into aldehydes (Xiong et al., 2012; Jambunathan and Zhang, 2014; Wang et al., 2017). Compared with the substrates of wild-type KivD, are mainly smaller substrates, such as 2-ketoisovalerate and α-ketoadipate (Zhang et al., 2008; Wang et al., 2017), KivD mutants are relatively longer, such as 2-keto-4-methylhexanoate and 2-keto-3-methylvalerate (Zhang et al., 2008). Overexpression of KivD from *Lactococcus lactis* (*L. lactis*) and alcohol dehydrogenase 2 (ADH2) in *Escherichia coli*, 1-propanol could be successfully produced from 2-ketobutyrate with a final titer of 2 g/L (Shen and Liao, 2008).

In this study, 5AVA was synthesized using 2-keto-6-aminocaproate as intermediate, which is related to the involvement of three key enzymes—RaiP, KivD, and aldehyde dehydrogenase (PadA)—as seen in **Figure 1D**. Compared with the wild type, the two mutants of KivD in residues F381 and M461 showed higher substrate recognition and catalytic efficiency. Moreover, the overexpression of KatE and LysP, contributes to the removal of H_2O_2 and the transport of L-lys, thereby increasing the production of 5AVA, respectively. As can be expected, this artificial pathway has a potential prospect in industrial application, which enhances the value of L-lys and produces 5AVA efficiently in engineered *E. coli*.

MATERIALS AND METHODS

Strains and Plasmids

The strains and plasmids involved in this work are listed in **Table 2**. The nucleotide sequences of genes *raiP* from

TABLE 2 | Strains and plasmids used in this study.

Strains or plasmids	Description	Sources
Strains		
DH5α	Wild type	Novagen
BL21(DE3)	Wild type	Novagen
ML03	*E. coli* BL21(DE3) Δ*cadA*	Cheng et al., 2018a
CJ00	*E. coli* BL21(DE3) harboring plasmid pET21a	Cheng et al., 2018b
CJ01	*E. coli* BL21(DE3) harboring plasmid pCJ01	Cheng et al., 2018b
CJ02	*E. coli* ML03 harboring plasmid pCJ01	Cheng et al., 2018b
CJ05	*E. coli* BL21(DE3) harboring plasmid pETaRPK	This study
CJ06	*E. coli* ML03 harboring plasmid pETaRPK	This study
CJ07	*E. coli* ML03 harboring plasmid pETaRPK$^{\#}$	This study
CJ08	*E. coli* ML03 harboring plasmid pETaRPK$^{\#}$ and pZAkatE	This study
CJ09	*E. coli* ML03 harboring plasmid pETaRPK$^{\#}$ and pZAKL	This study
Plasmids		
pZA22	Empty plasmid used as control, Kan^R	Cheng et al., 2019
pCJ01	pET21a-*raiP*, pET21a carries a L-Lysine α-oxidase gene (*raiP*) from *S. japonicus* with *Nde*I and *Bam*HI restrictions, Amp^R	Cheng et al., 2018b
pETaRPK	pET21a-*raiP-kivD-padA*, pET21a carries a L-Lysine α-oxidase gene (*raiP*) from *S. japonicus*, a α-ketoacid decarboxylase gene (*kivD*) from *L. lactis* and a aldehyde dehydrogenase gene (*padA*) from *E. coli*, Amp^R	This study
pETaRPK$^{\#}$	pET21a-*raiP-kivD*$^{\#}$*-padA*, pET21a carries a L-Lysine α-oxidase gene (*raiP*) from *S. japonicus*, a α-ketoacid decarboxylase mutant (F381A/V461A) gene from *L. lactis* and a aldehyde dehydrogenase gene (*padA*) from *E. coli*, Amp^R	This study
pZAkatE	pZA22-*katE*, pZA22 carries a catalase gene (*katE*) from *E. coli*, Kan^R	This study
pZAKL	pZA22-*katE-lysP*, pZA22 carries a catalase gene (*katE*) from *E. coli* and a lysine permease gene (*lysP*) from *E. coli*, Kan^R	This study

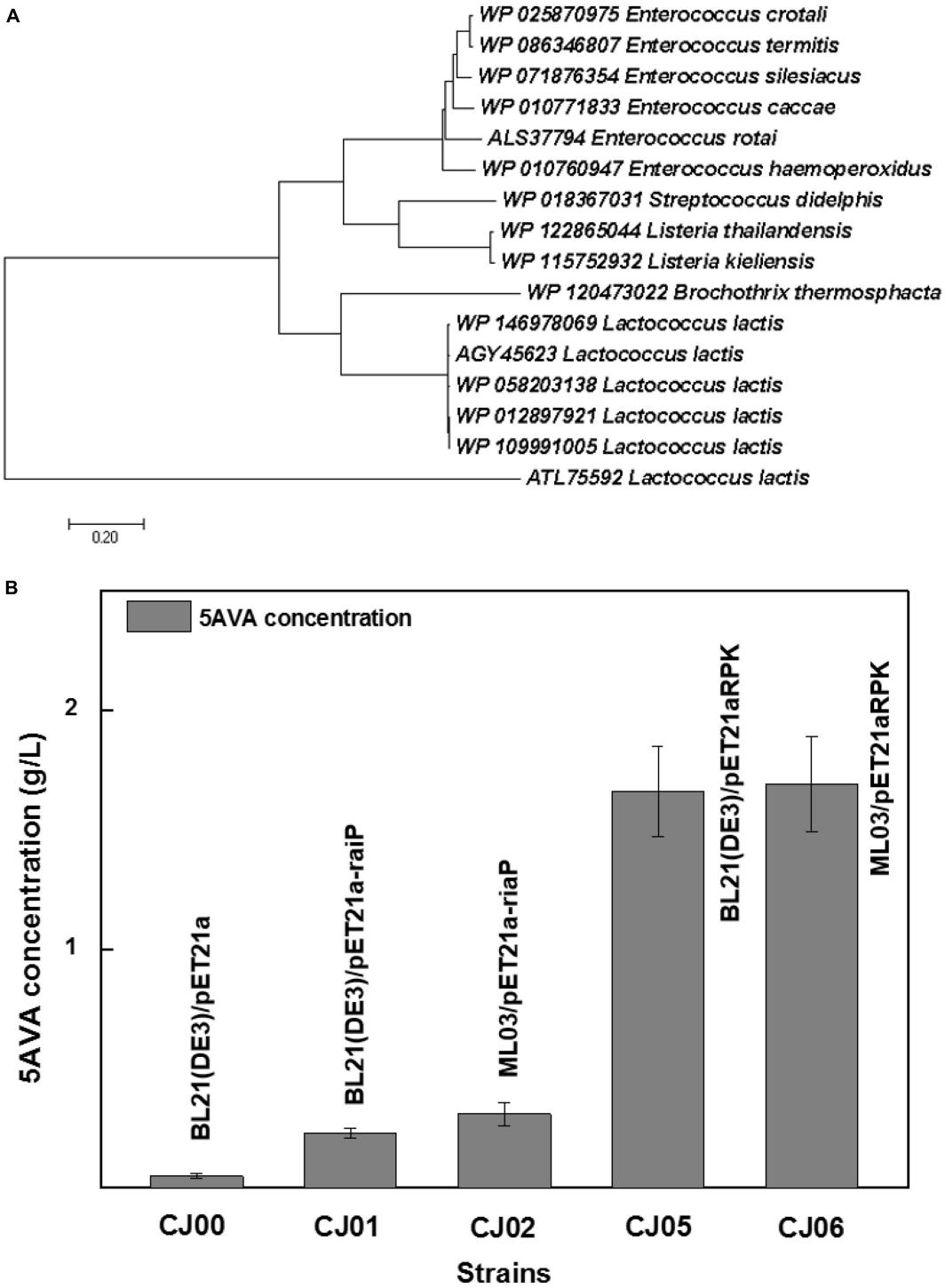

FIGURE 2 | Function identification of α-ketoacid decarboxylase subfamily. **(A)** The phylogenetic relationship of α-ketoacid decarboxylase subfamily. WP 012897921 *Lactococcus lactis* was the α-ketoacid decarboxylase used in this study. All α-ketoacid decarboxylase genes were downloaded from NCBI by blastp against the nr database. The genes were from the species, *L. lactis*, *Enterococcus crotali*, *Enterococcus termitis*, *Enterococcus Silesiacus*, *Enterococcus Caccae*, *Enterococcus rotai*, *Enterococcus haemoperoxidus*, *Streptococcus didelphis*, *Listeria thailandensis*, *Listeria kieliensis*, and *Brochothrix thermosphacta*. The maximum-likelihood tree was constructed by MEGA (Li et al., 2019a,b). **(B)** An artificial pathway confirmed for the biosynthesis of 5AVA. 6.5 g/L of L-Lysine HCl was as substrate. All experiments were performed a minimum of three independent sets. All error bars represent standard deviations with $n \geq 3$ independent reactions.

S. japonicus, *kivD* from *L. lactis* and *padA* from *E. coli* are available in the GenBank database with the accession numbers of MG423617 (Cheng et al., 2018a), AIS03677.1 (McCulloch et al., 2014) and NP_415903.4 (Riley et al., 2006), respectively. In order to establish the synthetic pathway, the *raiP*, *padA*, and *kivD* genes were inserted into pET21a, and then the plasmid pET21a-*raiP-padA-kivD* was generated, which was also named as pETaRPK. Primers for saturation mutation of KivD are listed in **Supplementary Table 1**. *kivD* was replaced by *kivD*$^{\#}$ (*kivD* with F381A/V461A mutations) to form the engineered pET21a-*raiP-padA-kivD*$^{\#}$, also named as pETaRPK$^{\#}$. The lysine permease gene *lysP* from *E. coli* (GenBank accession No. WP_000253273.1) was amplified from plasmid pLMAIP-04 (Cheng et al., 2018a), and the catalase gene *katE* (GenBank accession No. AAT48137.1) from *E. coli* MG1655. In order to remove H_2O_2, accelerate transportation of L-lys and reduce energy consumption, the *katE*, and *lysP* genes were firstly constructed in another single operon with the transcriptional order of *katE-lysP*, and then the engineered pZA22-*katE-lysP* was produced, also named as pZAKL. In addition, *E. coli* BL21 (DE3) with knocked out *cadA* was transformed with the plasmid pCJ01, pETaRPK, pETaRPK$^{\#}$, pETakatE, or pETaKL to obtain the strains CJ02, CJ06, CJ07, CJ08, or CJ09, respectively.

Cultivation Medium and Conditions

The *E. coli* strains harboring the corresponding plasmids were streaked onto Luria-Bertani (LB) agar plates with appropriate antibiotics at 37°C for overnight. Engineering strains used for shake flask fermentation were cultured in the medium containing 5 g/L yeast extract, 10 g/L tryptone, 15 g/L glucose, 0.1 g/L $FeCl_3$, 2.1 g/L citric acid·H_2O, 2.5 g/L $(NH_4)_2SO_4$, 0.5 g/L $K_2PO_4{\cdot}3H_2O$, 1.0 mM $MgSO_4$, 3 g/L KH_2PO_4, and 0.5 mM thiamine diphosphate (ThDP) with appropriate antibiotics. After the OD_{600} of the strains reached 0.5, 0.5 mM of isopropyl β-D-thiogalactoside (IPTG) and 6.5 g/L of L-lys HCl were added.

Fed-batch biotransformation of engineering strains were conducted in a 5.0 L fermenter. The composition of the medium was described in our previous report as follows: glucose, 55 g/L; $MgSO_4{\cdot}7H_2O$, 1.6 g/L; $FeSO_4{\cdot}7H_2O$, 0.00756 g/L; $(NH_4)_2SO_4$, 1.6 g/L; citric acid, 2 g/L; $K_2HPO_4{\cdot}3H_2O$, 7.5 g/L; Na_2SO_4, 0.02 g/L; $ZnSO_4$, 0.0064 g/L; $Cu_2SO_4{\cdot}5H_2O$, 0.0006 g/L; $CoCl_2{\cdot}6H_2O$, 0.004 g/L (Cheng et al., 2018a). The pH was controlled at 6.7–6.9 by the automatic addition of $NH_3{\cdot}H_2O$, and the temperature was set at 30°C. Antifoam 289 was gradually added to prevent the formation of foam during biotransformation. The initial concentration of L-lys HCl was 40 g/L. The concentration of glucose and L-lys were maintained around 15 and 20 g/L during the whole fermentation process, respectively.

Protein Expression and Purification

The media for protein expression was supplemented by 0.5 mM ThDP in LB at 37°C. At an OD_{600} of 0.5, 0.5 mM of IPTG was added and then cultured at 20°C for 16 h, cells were washed with potassium phosphate buffer (KPB, 50 mM, pH 8.0) and disrupted by sonication in an ice bath of 50 mM KPB. The enzymes were purified with AKTA Purifier 10 using a Ni-NTA column (Cheng et al., 2019). The concentration of protein was measured by

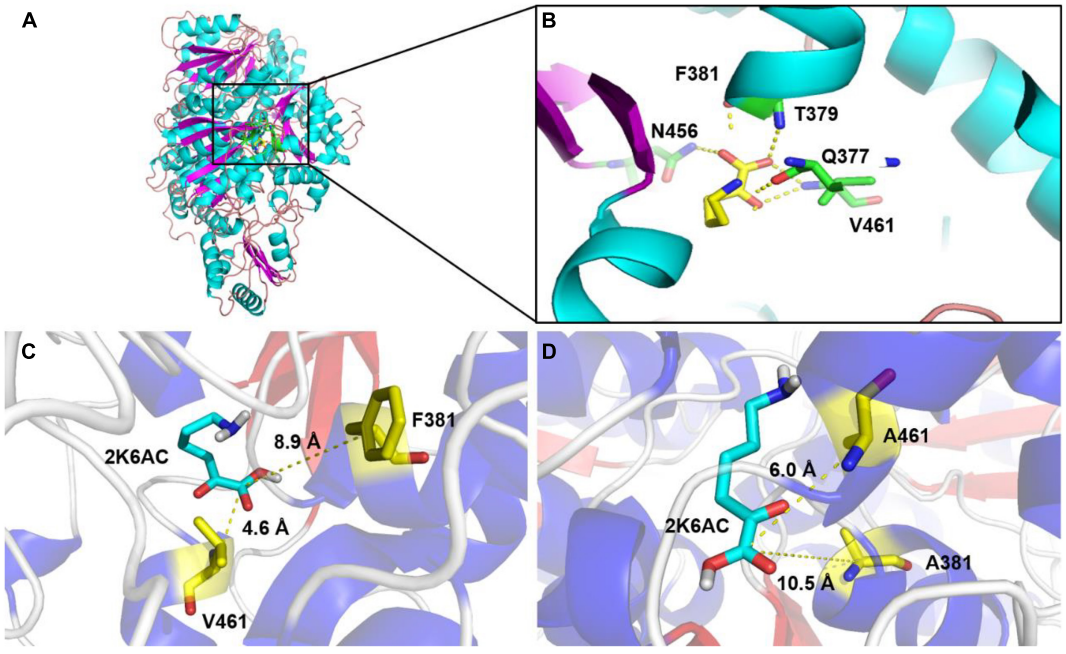

FIGURE 3 | Homology modeling and structure comparison between KivD and KivD$^{\#}$(F381A/V461A). **(A)** Overall architecture of the KivD system; **(B)** Interactions of the ligand 2K6AC with their surroundings in KivD system; Binding pocket of *L. lactis* KivD (PDB: 2VBF) **(C)** and KivD$^{\#}$(F381A/V461A) **(D)** complexed with its substrate 2K6AC. The active pocket of KivD which is constituted by a number of hydrophobic residues, including F381, T379, and V461. KivD, α-ketoacid decarboxylase.

SpectraMax M2^e at 280 nm. The detections of 5AVA and L-lys were reported in our previous work (Cheng et al., 2018b).

Enzyme Assay

The oxidation activity of RaiP was measured according to the concentration of hydrogen peroxide (Cheng et al., 2018b). The decarboxylation activity of KivD and KivD mutations (KivD*) were determined at 30°C, using a coupled enzymatic assay (Wang et al., 2017). The reaction mixture contained 1.0 mM NAD^+, 1.1 μM PadA, 1.1 μM RaiP, 0.85 μM KivD, or KivD* and different concentrations of L-lys in assay buffer (50 mM KPB, pH 8.0, 1 mM $MgSO_4$, 1.0 mM TCEP, 0.5 mM ThDP). The reactions began with the addition of the substrate L-lys, and the formation of NADH was monitored at 340 nm with the extinction coefficient of 6.22 mM^{-1} cm^{-1}.

Homology Modeling, Substrate Docking, and Molecular Dynamic Simulation

The theoretical structure of native KivD and mutant KivD$^\#$ (KivD with F381A/V461A mutations) (PDB: 2VBF), both were generated by SWISS-MODEL online Server[1]. The 3D structural comparison between KivD and KivD$^\#$ was revealed using PyMOL 2.2. The ligand 2K6AC was docked into the pocket of KivD or KivD$^\#$ using AutoDock 4.2.6 package, where the lowest energy conformation in the largest cluster was considered to be the approximately natural complex model (Xie et al., 2019; Tahara et al., 2020). Molecular dynamic (MD) simulation was used to simulate the relationship between structure and function of biomacromolecules in solution in this study (Wu et al., 2020). Two comparative MD simulations at 300 K were executed for KivD and KivD-2K6AC systems with AMBER 18 package (Zuo et al., 2017; Wu et al., 2020).

[1]https://swissmodel.expasy.org/

RESULTS AND DISCUSSION

Construction of an Artificial Synthetic Route for the Biosynthesis of 5AVA in *E. coli*

Figure 1D showed a heterogeneous artificial route for the bioconversion of L-lys to 5AVA. The designed artificial biosynthetic pathway of 5AVA consists of three steps: (1) deamination of L-lys to form intermediate 2K6AC via RaiP; (2) decarboxylation of 2K6AC to produce 5-aminopentanal via KivD; (3) oxidation of 5-aminopentanal to 5AVA via PadA. Firstly, a plasmid pETaRPK was constructed and introduced into

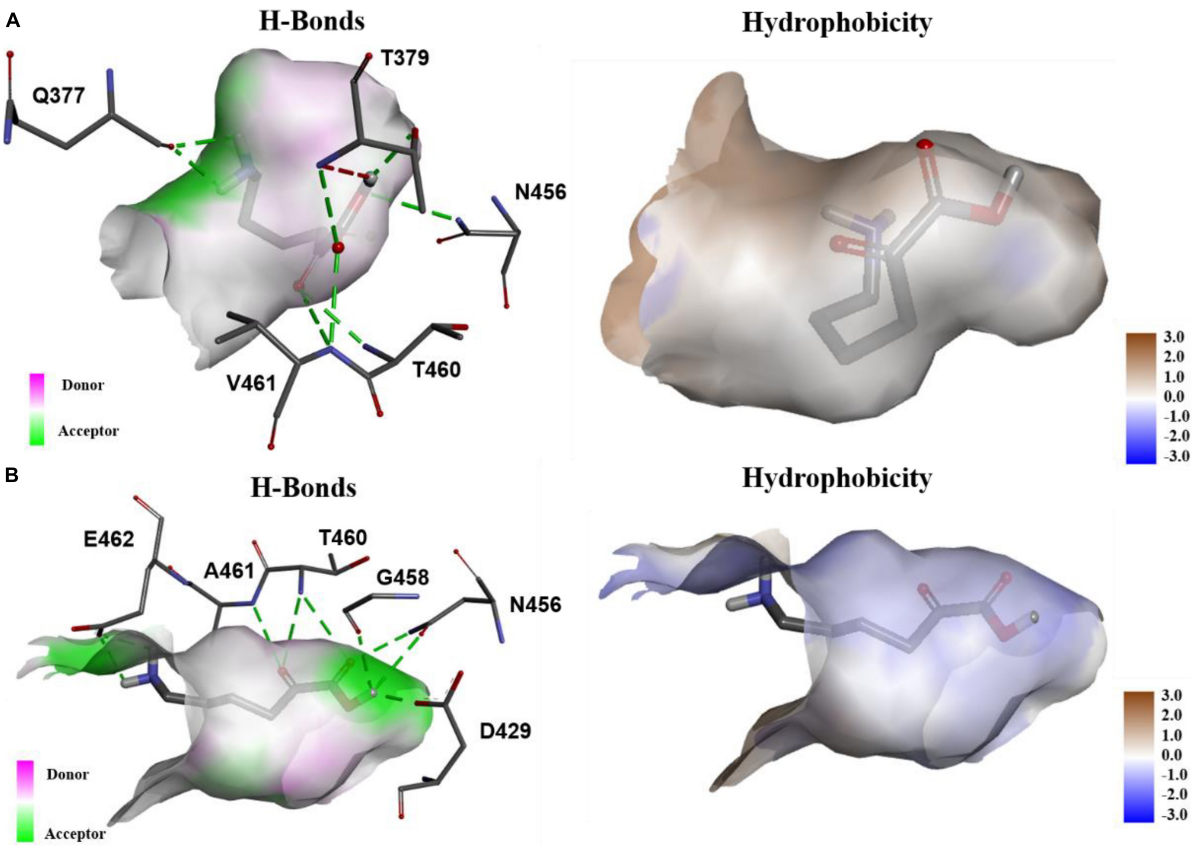

FIGURE 4 | The analysis of hydrogen bonds and hydrophobicity. **(A)** The hydrogen bonds formed of KivD and 2K6AC, and the hydrophobicity of the active pocket in KivD; **(B)** The hydrogen bonds formed of KivD$^\#$(F381A/V461A) and 2K6AC, and the hydrophobicity of the active pocket in KivD$^\#$(F381A/V461A).

E. coli ML03 to obtain the strain CJ05, with the co-expression of RaiP, KivD, and PadA under a T7 promoter. To reduce the degradation of L-lys to cadaverine, the lysine decarboxylase gene *cadA* was knocked out to obtain the strain CJ06. The maximum-likelihood tree was displayed in **Figure 2A**. Notably, 5AVA could be produced in strains CJ01, CJ02, CJ05, and CJ06. As shown in **Figure 2B**, the control strain CJ00 only produced 0.06 g/L 5AVA from 6.5 g/L L-lys HCl with the consumption of 0.01 g/g L-lys. For engineered strain CJ01, a titer of 0.23 g/L 5AVA was acquired. Moreover, the strain CJ05 produced 1.66 g/L of 5AVA

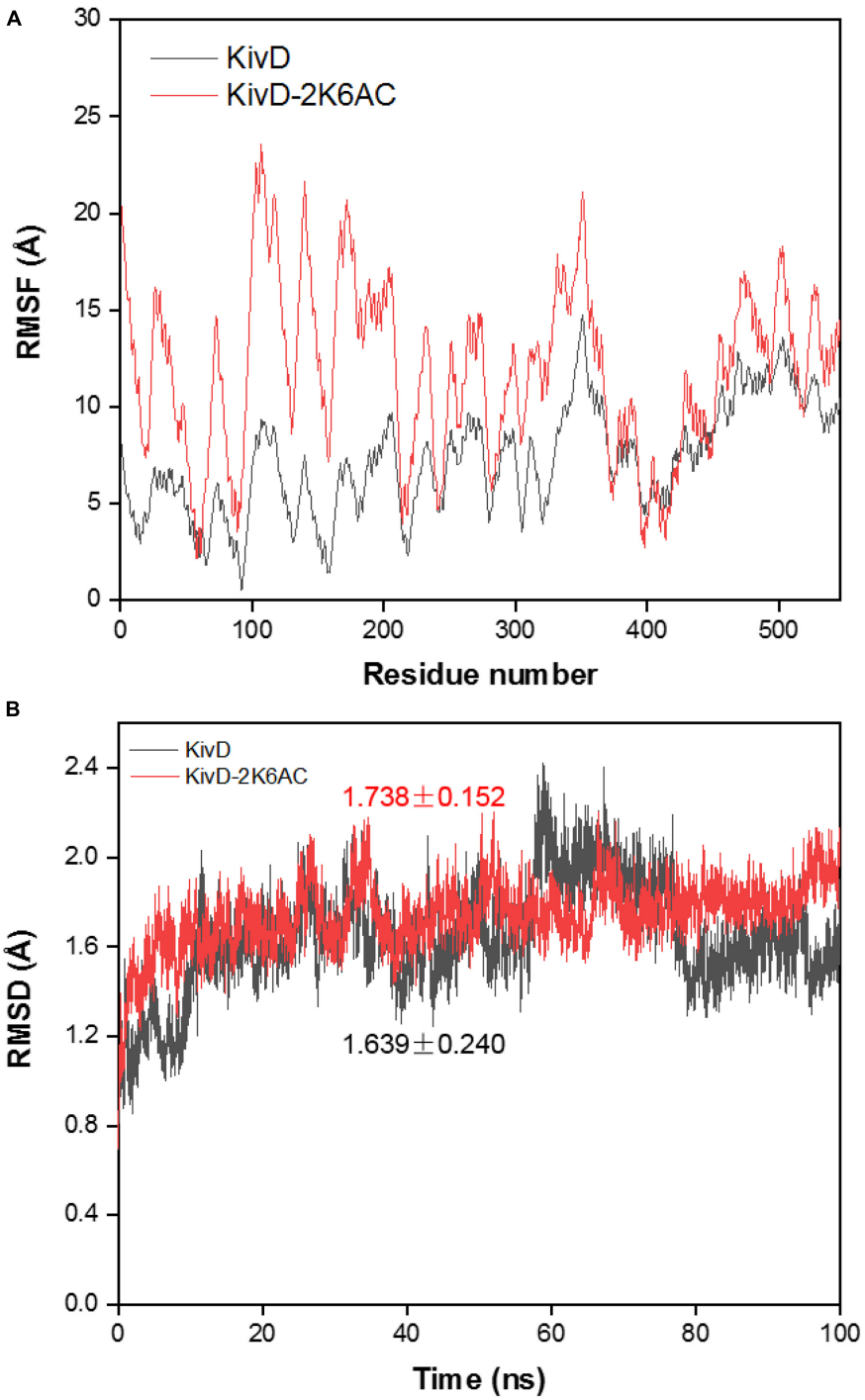

FIGURE 5 | Molecular dynamic simulation of KivD and KivD-2K6AC. **(A)** RMSD of the C_α atoms in the KivD and KivD-2K6AC versus simulation time. **(B)** RMSF distribution of the C_α atom in the KivD and KivD-2K6AC. RMSD, Root mean squared deviation; RMSF, Root mean squared fluctuation.

by this artificial pathway (see **Figure 1D**), with a yield increase of 774% compared to the single gene pathway (see **Figure 1C**). These results demonstrate the feasibility of this proposed artificial 5AVA pathway.

Molecular Docking and MD Simulation of KivD and KivD#

In order to explore the mechanism of the 5AVA increase in mutants, molecular docking and MD simulation were discussed (Xiang et al., 2019). The structures of KivD and KivD# both are mainly composed of 23 α-helices and 17 β-strands, containing a large activity pocket. Compared with that of KivD, the structure of KivD# remains almost unchanged. Nevertheless based on homology modeling analysis, the catalytic channel of mutant KivD# was enlarged. According to bioinformatics and crystal structure information (PDB: 2VBF) (Berthold et al., 2007), residues F381 and V461 are the two key residues for KivD catalysis (see **Figure 3**). Modeling and molecular docking of KivD with ligand 2K6AC further highlight the residues involved in substrate recognition. As shown in **Figure 3**, the substrate docking results indicated that the distances of ligand 2K6AC with F381A, V461A active sites both became farther. The docking results of KivD and 2K6AC showed that 2K6AC formed eight hydrogen bonds with the side chain Q377, T379, N456, T460, and V461. 2K6AC formed nine hydrogen bonds with the side chain D429, N456, G458, T460, A461, and E462 of KivD# (**Figure 4**). At the same time, the surface hydrophobicity of the catalytic pocket in mutated protein KivD# has also changed (**Figure 4**). We speculated that the increase in catalytic activity of KivD# may be due to the expansion of catalytic channel and the formation of more hydrogen bonds, the expansion that is likely to result in a change in the conformation of the small molecule 2K6AC which was beneficial to stretch. Through the MD simulations, the results of the root mean squared deviation (RMSD) showed that the RMSD of the KivD system and the complex system KivD-2K6AC were basically maintained at 1.639 ± 0.240 Å and 1.738 ± 0.152 Å (see **Figure 5B**), which indicated that the MD simulation process was reliable (Zuo et al., 2017). As seen in **Figure 5A**, there are four fragments of the KivD with lower root mean squared fluctuation (RMSF) values, that is G58-L69, T212-N223, T379-F388, and D457-H466. These four fragments are located near ThDP, which may be related to the activity of KivD (Zuo et al., 2017; Liu et al., 2019).

KivD mutations (F381A/V461, F381L/V461, F381/V461A, F381/V461L, and F381A/V461A) displayed enhanced activities in **Table 3**. The KivD F381A/V461A (KivD#) showed the greatest activity shown in **Table 3**. KivD# displays a K_m value of 2.52 mM, a K_{cat} value of 562.16 s^{-1} and a K_{cat}/K_m value of 223.08 $mM^{-1}s^{-1}$ with 2K6AC used as the substrate shown in **Table 3**.

TABLE 3 | Kinetic parameters of α-ketoacid decarboxylase KivD mutants (KivD*) on 2-keto-6-aminocaproate (2K6AC).

Enzyme	V_{max} (mM min^{-1})	K_m (mM)	V_{max}/K_m (h^{-1})
KivD (F381/V461)	22.69 ± 3.28	6.67 ± 0.26	204.08
KivD*(F381L/V461)	22.56 ± 3.12	5.45 ± 0.22	248.36
KivD*(F381A/V461)	27.25 ± 2.87	3.75 ± 0.18	436.02
KivD*(F381/V461L)	22.63 ± 2.48	6.10 ± 0.23	222.55
KivD*(F381/V461A)	25.88 ± 3.00	3.99 ± 0.15	389.24
KivD*(F381A/V461A)	28.67 ± 3.69	2.52 ± 0.11	682.64

Data are presented as means ± STDV calculated from three replicate biotransformation experiments. The KivD activity toward 2K6AC was performed on 50 mM KPB (pH 8.0), 1 mM $MgSO_4$, 1.0 mM TCEP, 0.5 mM ThDP, 1.0 mM NAD^+, 1.1 μM PadA, 1.1 μM RaiP, 0.85 μM KivD, or KivD* and different concentrations of* L-*lys.*

Overexpression of Catalase KcatE and Lysine Permease LysP Favoring the Increase of 5AVA Production

There are four strategies used in this study to increase the production of 5AVA. Firstly, lysine decarboxylase gene *cadA* was knocked out and L-lys HCl was selected as the industrial substrate for enhancing the utilization of L-lys (Cheng et al., 2018a,b, 2020). Thirdly, H_2O_2 could inhibit cell growth, thus affecting the production of goal production (Niu et al., 2014). In Liu's experiments, through the expression of catalase, the content of H_2O_2 was significantly reduced, and the output of α-ketoglutarate was greatly increased (Liu et al., 2017). In this study, the co-expression of *katE*, *raiP*, *kivD#*, and *padA* in strain CJ08 yielded 1.88 g/L of 5AVA without addition of catalase, there was no significant difference compared to strain CJ07 (**Table 4**). In fact, the H_2O_2 generated by RaiP in this work was instantly eliminated by KatE. The data in rows 5 and 7 of **Table 4** showed that the overexpression of *katE* did not significantly increase the OD_{600} and the production of 5AVA during shake flask fermentation. On the contrary, it decreased the OD_{600}, possibly because the increase in gene expression caused an increase in cell burden (Camara et al., 2017). However, in the fermentation tank, H_2O_2 could significantly inhibit cell growth, resulting in limited production of 5AVA (Cheng et al., 2018b, 2020). In addition, a lysine transporter gene *lysP* was overexpressed and inserted into the plasmid pZAkatE to form a new plasmid pZAKL. As shown in **Table 4**, strain CJ09 produced 1.93 g/L of 5AVA.

Fed-Batch Biotransformation for 5AVA Production

Figure 6 showed the results of the fed-batch biotransformation in *E. coli* strain CJ09. Recombinant *E. coli* strain CJ09 grew quickly throughout the biotransformation, reaching the highest cell concentration of an OD_{600} of 142 in 18 h. After the addition of L-lys HCl, 5AVA was accumulated to 48.3 g/L between 18 and 36 h. With the fermentation time increasing to 48 h, 52.24 g/L of 5AVA was successfully acquired. The productivity and yield of 5AVA were 1.09 g/L/h and 0.65 g/g L-lys, respectively. The control strain CJ02 just produced 9.16 g/L 5AVA with a yield of 0.11 g/g L-lys. Interestingly, the expression of KatE in strain CJ08 had no effect on the production of 5AVA in shake flask (**Table 4**), but it could significantly improve the production of 5AVA to 45.92 g/L in fermentation tank compared to strain CJ07 with a titer of 16.48 g/L. This is because H_2O_2 can significantly inhibit the growth of strain CJ07, resulting in OD_{600} of only 40.

TABLE 4 | 5AVA synthesis by engineered strains in 250 mL flasks.

Strains	Time (h)	Cell density (OD_{600})	Glucose consumed (g/L)	5AVA production (g/L)	Statistic analysis[a]	5AVA yield (g/g)[b]
CJ06	12	5.24 ± 0.38	7.22 ± 0.33	0.85 ± 0.04	–	0.19 ± 0.03
	24	8.15 ± 0.52	11.36 ± 0.46	1.69 ± 0.03	–	0.35 ± 0.03
CJ07	12	5.19 ± 0.41	7.09 ± 0.25	0.96 ± 0.02	*	0.25 ± 0.01
	24	8.08 ± 0.55	11.25 ± 0.48	1.85 ± 0.02	*	0.39 ± 0.03
CJ08	12	5.14 ± 0.36	7.02 ± 0.28	0.94 ± 0.01	ns	0.25 ± 0.02
	24	7.91 ± 0.46	11.17 ± 0.41	1.88 ± 0.02	ns	0.40 ± 0.03
CJ09	12	5.08 ± 0.33	6.88 ± 0.18	1.01 ± 0.03	*	0.23 ± 0.01
	24	7.85 ± 0.42	11.11 ± 0.39	1.93 ± 0.01	*	0.41 ± 0.02

Data are presented as means ± STDV calculated from three replicate biotransformation experiments. Statistics were performed by the two-tailed student t-test.
**P < 0.05; ns, not significant.*
[a]*Statistic analysis of the 5AVA production were performed with every two separated lines.*
[b]*The yield of 5AVA was calculated based on* L-lys *consumption. 6.5 g/L* L-lys HCl*, 15 g/L glucose, 0.5 mM IPTG, 1.0 mM $MgSO_4$ and 0.5 mM ThDP were added.*

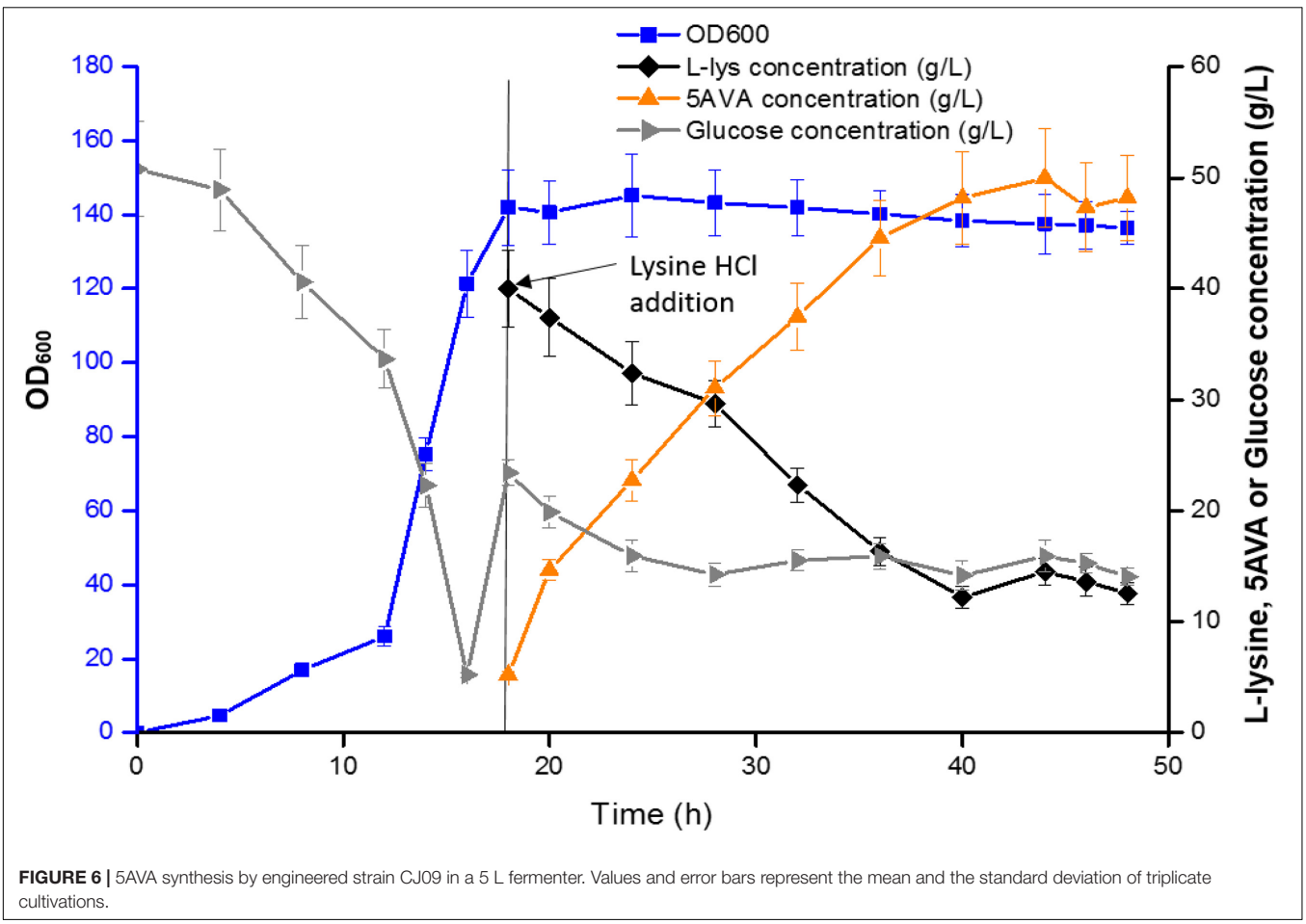

FIGURE 6 | 5AVA synthesis by engineered strain CJ09 in a 5 L fermenter. Values and error bars represent the mean and the standard deviation of triplicate cultivations.

The above results advocated that the synthetic route developed in this work can effectively produce 5AVA.

Compared with a previous whole cell transformation, the titer of 5AVA based on this synthesis pathway increased by about 79.4% from 29.12 to 52.24 g/L as seen in **Table 1**; the inhibition of cell growth and enzyme activity by H_2O_2 both resulted in the lower yields of 5AVA (Cheng et al., 2018b). Compared with another new synthesis pathway for the fermentative production of 5AVA, in which the titer was only 5.1 g/L (seen in **Table 1**; Jorge et al., 2017), and the titer was greatly increased in this study. Compared with another whole-cell catalysis work, this synthetic pathway increased the titer of 5AVA by about 3.20% from 50.62 to 52.24 g/L (Cheng et al., 2020). Importantly, the industrial production of 5AVA without the addition of ethanol and H_2O_2 was more safe and economical in this study. In terms of reaction mechanism, the new 5AVA synthesis strategy proposed in this work mainly includes three steps: (1) the accumulation of intermediate 6A2KCA by RaiP; (2) the decarboxylation of

6A2KCA to 5-aminopentanal by KivD; (3) the oxidization of 5-aminopentanal to 5AVA by PadA.

CONCLUSION

From renewable feedstocks, an artificial pathway in *E. coli* was proposed and optimized to produce 5AVA in this study. Since the inhibition of enzyme activity and cell growth by H_2O_2 is the main limiting factor in the production of 5AVA, catalase KatE was overexpressed to decompose H_2O_2 to achieve high yield of 5AVA. Finally, an engineered strain CJ09 with RaiP, KivD, PadA, KatE, and LysP overexpression successfully produced 5AVA from biobased L-lys HCl at a final titer of 52.24 g/L. The renewable substrate and simple culture conditions were adopted in this work, while possessing higher yield and less environmental pollution. The improvement of substrate utilization and H_2O_2 decomposition efficiency contributes to the increase in the yield of 5AVA, which has the potential to become a common strategy for the sustainable production of other chemicals.

DATA AVAILABILITY STATEMENT

The original contributions presented in the study are included in the article/**Supplementary Material**, further inquiries can be directed to the corresponding authors.

AUTHOR CONTRIBUTIONS

JC and WT performed the experiments, analyzed the data, and drafted the manuscript. ZL, QL, and XG analyzed the data. JC and DW conceived and coordinated the study. JC, DW, and JZ finalized the manuscript. All authors contributed to the article and approved the submitted version.

FUNDING

This work was supported by the Open Funding Project of the Key Laboratory of Meat Processing of Sichuan Province (20-R-06), the Open Funding Project of Key Laboratory of Coarse Cereal Processing, Ministry of Agriculture and Rural Affairs (2020CC010), the National Key Research and Development Program of China (2018YFC1602101), the National Natural Science Foundation of China (21978027), and the Project of Chongqing Key Laboratory of Environmental Materials and Restoration Technology (CEK1803).

SUPPLEMENTARY MATERIAL

The Supplementary Material for this article can be found online at: https://www.frontiersin.org/articles/10.3389/fbioe.2021.633028/full#supplementary-material

REFERENCES

Adkins, J., Jordan, J., and Nielsen, D. R. (2013). Engineering *Escherichia coli* for renewable production of the 5-carbon polyamide building-blocks 5-aminovalerate and glutarate. *Biotechnol. Bioeng.* 110, 1726–1734. doi: 10.1002/bit.24828

Atsumi, S., Hanai, T., and Liao, J. C. (2008). Non-fermentative pathways for synthesis of branched-chain higher alcohols as biofuels. *Nature* 451, 86–89. doi: 10.1038/nature06450

Berthold, C. L., Gocke, D., Wood, M. D., Leeper, F. J., Pohl, M., and Schneider, G. (2007). Structure of the branched-chain keto acid decarboxylase (KdcA) from *Lactococcus lactis* provides insights into the structural basis for the chemoselective and enantioselective carboligation reaction. *Acta Crystallogr. D. Biol. Crystallogr.* 63(Pt 12), 1217–1224. doi: 10.1107/s0907444907050433

Camara, E., Landes, N., Albiol, J., Gasser, B., Mattanovich, D., and Ferrer, P. (2017). Increased dosage of AOX1 promoter-regulated expression cassettes leads to transcription attenuation of the methanol metabolism in Pichia pastoris. *Sci. Rep.* 7:44302.

Chae, T. U., Kim, W. J., Choi, S., Park, S. J., and Lee, S. Y. (2015). Metabolic engineering of *Escherichia coli* for the production of 1,3-diaminopropane, a three carbon diamine. *Sci. Rep.* 5:13040.

Chen, G. S., Siao, S. W., and Shen, C. R. (2017). Saturated mutagenesis of ketoisovalerate decarboxylase V461 enabled specific synthesis of 1-pentanol via the ketoacid elongation cycle. *Sci. Rep.* 7:11284.

Cheng, J., Hu, G., Xu, Y., Torrens-Spence, M. P., Zhou, X., Wang, D., et al. (2019). Production of nonnatural straight-chain amino acid 6-aminocaproate via an artificial iterative carbon-chain-extension cycle. *Metab. Eng.* 55, 23–32. doi: 10.1016/j.ymben.2019.06.009

Cheng, J., Huang, Y., Mi, L., Chen, W., Wang, D., and Wang, Q. (2018a). An economically and environmentally acceptable synthesis of chiral drug intermediate L-pipecolic acid from biomass-derived lysine via artificially engineered microbes. *J. Ind. Microbiol. Biot.* 45, 405–415. doi: 10.1007/s10295-018-2044-2

Cheng, J., Luo, Q., Duan, H., Peng, H., Zhang, Y., Hu, J., et al. (2020). Efficient whole-cell catalysis for 5-aminovalerate production from L-lysine by using engineered *Escherichia coli* with ethanol pretreatment. *Sci. Rep.* 10:990.

Cheng, J., Zhang, Y., Huang, M., Chen, P., Zhou, X., Wang, D., et al. (2018b). Enhanced 5-aminovalerate production in *Escherichia coli* from L-lysine with ethanol and hydrogen peroxide addition. *J. Chem. Technol. Biot.* 93, 3492–3501. doi: 10.1002/jctb.5708

Dairo, T. O., Nelson, N. C., Slowing, I. I., Angelici, R. J., and Woo, L. K. (2016). Aerobic oxidation of cyclic amines to lactams catalyzed by ceria-supported nanogold. *Catal Lett.* 146, 2278–2291. doi: 10.1007/s10562-016-1834-2

Fang, H., Li, D., Kang, J., Jiang, P., Sun, J., and Zhang, D. (2018). Metabolic engineering of *Escherichia coli* for de novo biosynthesis of vitamin B12. *Nat. Commun.* 9:4917.

Gao, S., Lyu, Y., Zeng, W., Du, G., Zhou, J., and Chen, J. (2020a). Efficient biosynthesis of (2S)-Naringenin from p-Coumaric Acid in *Saccharomyces cerevisiae*. *J. Agric. Food Chem.* 68, 1015–1021. doi: 10.1021/acs.jafc.9b05218

Gao, S., Zhou, H., Zhou, J., and Chen, J. (2020b). Promoter-library-based pathway optimization for efficient (2S)-naringenin production from p-Coumaric acid in *Saccharomyces cerevisiae*. *J. Agric. Food Chem.* 68, 6884–6891. doi: 10.1021/acs.jafc.0c01130

Haupka, C., Delépine, B., Irla, M., Heux, S., and Wendisch, V. F. (2020). Flux enforcement for fermentative production of 5-aminovalerate and glutarate by *Corynebacterium glutamicum*. *Catalysts* 10:1065. doi: 10.3390/catal10091065

Hong, Y. G., Moon, Y. M., Hong, J. W., No, S. Y., Choi, T. R., Jung, H. R., et al. (2018). Production of glutaric acid from 5-aminovaleric acid using *Escherichia coli* whole cell bio-catalyst overexpressing GabTD from Bacillus subtilis. *Enzyme Microb. Technol.* 118, 57–65. doi: 10.1016/j.enzmictec.2018.07.002

Jambunathan, P., and Zhang, K. (2014). Novel pathways and products from 2-keto acids. *Curr. Opin. Biotechnol.* 29, 1–7. doi: 10.1016/j.copbio.2014.01.008

Joo, J. C., Oh, Y. H., Yu, J. H., Hyun, S. M., Khang, T. U., Kang, K. H., et al. (2017). Production of 5-aminovaleric acid in recombinant *Corynebacterium glutamicum* strains from a Miscanthus hydrolysate solution prepared by a

newly developed Miscanthus hydrolysis process. *Bioresour. Technol.* 245(Pt B), 1692–1700. doi: 10.1016/j.biortech.2017.05.131

Jorge, J. M. P., Perez-Garcia, F., and Wendisch, V. F. (2017). A new metabolic route for the fermentative production of 5-aminovalerate from glucose and alternative carbon sources. *Bioresour. Technol.* 245(Pt B), 1701–1709. doi: 10.1016/j.biortech.2017.04.108

Kind, S., Jeong, W. K., Schroder, H., and Wittmann, C. (2010). Systems-wide metabolic pathway engineering in *Corynebacterium glutamicum* for bio-based production of diaminopentane. *Metab. Eng.* 12, 341–351. doi: 10.1016/j.ymben.2010.03.005

Klenk, J. M., Ertl, J., Rapp, L., Fischer, M.-P., and Hauer, B. (2020). Expression and characterization of the benzoic acid hydroxylase CYP199A25 from Arthrobacter sp. *Mol. Catal.* 484:110739. doi: 10.1016/j.mcat.2019.110739

Kromer, J. O., Wittmann, C., Schroder, H., and Heinzle, E. (2006). Metabolic pathway analysis for rational design of L-methionine production by *Escherichia coli* and *Corynebacterium glutamicum*. *Metab. Eng.* 8, 353–369. doi: 10.1016/j.ymben.2006.02.001

Li, Q., Ren, Y., Shi, X., Peng, L., Zhao, J., Song, Y., et al. (2019a). Comparative mitochondrial genome analysis of two ectomycorrhizal fungi (Rhizopogon) reveals dynamic changes of intron and phylogenetic relationships of the subphylum agaricomycotina. *Int. J. Mol. Sci.* 20:1567.

Li, Q., Wang, Q., Jin, X., Chen, Z., Xiong, C., Li, P., et al. (2019b). Characterization and comparison of the mitochondrial genomes from two *Lyophyllum fungal* species and insights into phylogeny of Agaricomycetes. *Int. J. Biol. Macromol.* 121, 364–372. doi: 10.1016/j.ijbiomac.2018.10.037

Li, Z., Xu, J., Jiang, T., Ge, Y., Liu, P., Zhang, M., et al. (2016). Overexpression of transport proteins improves the production of 5-aminovalerate from L-lysine in *Escherichia coli*. *Sci. Rep.* 6:30884.

Liu, B. B., Qu, G., Li, J. K., Fan, W. C., Ma, J. A., Xu, Y., et al. (2019). Conformational dynamics-guided loop engineering of an alcohol dehydrogenase: capture, turnover and enantioselective transformation of difficult-to-reduce ketones. *Adv. Synth. Catal.* 361, 3182–3190. doi: 10.1002/adsc.201900249

Liu, P., Zhang, H., Lv, M., Hu, M., Li, Z., Gao, C., et al. (2014). Enzymatic production of 5-aminovalerate from L-lysine using L-lysine monooxygenase and 5-aminovaleramide amidohydrolase. *Sci. Rep.* 4:5657.

Liu, Q., Ma, X., Cheng, H., Xu, N., Liu, J., and Ma, Y. (2017). Co-expression of L-glutamate oxidase and catalase in *Escherichia coli* to produce alpha-ketoglutaric acid by whole-cell biocatalyst. *Biotechnol. Lett.* 39, 913–919. doi: 10.1007/s10529-017-2314-5

Liu, X., Cheng, J., Zhang, G., Ding, W., Duan, L., Yang, J., et al. (2018). Engineering yeast for the production of breviscapine by genomic analysis and synthetic biology approaches. *Nat. Commun.* 9:448.

McCulloch, J. A., de Oliveira, V. M., de Almeida Pina, A. V., Pérez-Chaparro, P. J., de Almeida, L. M., de Vasconcelos, J. M., et al. (2014). Complete genome sequence of Lactococcus lactis strain AI06, an endophyte of the amazonian açaí palm. *Genome Announc.* 2, e1225–e1214.

Nakamura, C. E., and Whited, G. M. (2003). Metabolic engineering for the microbial production of 1,3-propanediol. *Curr. Opin. Biotechnol.* 14, 454–459. doi: 10.1016/j.copbio.2003.08.005

Niimi, S., Suzuki, N., Inui, M., and Yukawa, H. (2011). Metabolic engineering of 1,2-propanediol pathways in *Corynebacterium glutamicum*. *Appl. Microbiol. Biotechnol.* 90, 1721–1729. doi: 10.1007/s00253-011-3190-x

Niu, P., Dong, X., Wang, Y., and Liu, L. (2014). Enzymatic production of alpha-ketoglutaric acid from l-glutamic acid via l-glutamate oxidase. *J. Biotechnol.* 179, 56–62. doi: 10.1016/j.jbiotec.2014.03.021

Park, S. J., Kim, E. Y., Noh, W., Oh, Y. H., Kim, H. Y., Song, B. K., et al. (2013a). Synthesis of nylon 4 from gamma-aminobutyrate (GABA) produced by recombinant *Escherichia coli*. *Bioprocess Biosyst. Eng.* 36, 885–892. doi: 10.1007/s00449-012-0821-2

Park, S. J., Kim, E. Y., Noh, W., Park, H. M., Oh, Y. H., Lee, S. H., et al. (2013b). Metabolic engineering of *Escherichia coli* for the production of 5-aminovalerate and glutarate as C5 platform chemicals. *Metab. Eng.* 16, 42–47. doi: 10.1016/j.ymben.2012.11.011

Park, S. J., Oh, Y. H., Noh, W., Kim, H. Y., Shin, J. H., Lee, E. G., et al. (2014). High-level conversion of L-lysine into 5-aminovalerate that can be used for nylon 6,5 synthesis. *Biotechnol. J.* 9, 1322–1328. doi: 10.1002/biot.201400156

Pukin, A. V., Boeriu, C. G., Scott, E. L., Sanders, J. P. M., and Franssen, M. C. R. (2010). An efficient enzymatic synthesis of 5-aminovaleric acid. *J. Mol. Catal. B Enzym* 65, 58–62. doi: 10.1016/j.molcatb.2009.12.006

Riley, M., Abe, T., Arnaud, M. B., Berlyn, M. K., Blattner, F. R., Chaudhuri, R. R., et al. (2006). *Escherichia coli* K-12: a cooperatively developed annotation snapshot–2005. *Nucleic Acids Res.* 34, 1–9. doi: 10.1093/nar/gkj405

Rodrigues, J. L., Gomes, D., and Rodrigues, L. R. (2020). A combinatorial approach to optimize the production of curcuminoids from tyrosine in *Escherichia coli*. *Front. Bioeng. Biotechnol.* 8:59.

Rohles, C. M., Giesselmann, G., Kohlstedt, M., Wittmann, C., and Becker, J. (2016). Systems metabolic engineering of *Corynebacterium glutamicum* for the production of the carbon-5 platform chemicals 5-aminovalerate and glutarate. *Microb. Cell Fact.* 15:154.

Rui, J., You, S., Zheng, Y., Wang, C., Gao, Y., Zhang, W., et al. (2020). High-efficiency and low-cost production of cadaverine from a permeabilized-cell bioconversion by a Lysine-induced engineered *Escherichia coli*. *Bioresour. Technol.* 302:122844. doi: 10.1016/j.biortech.2020.122844

Shen, C. R., and Liao, J. C. (2008). Metabolic engineering of *Escherichia coli* for 1-butanol and 1-propanol production via the keto-acid pathways. *Metab. Eng.* 10, 312–320. doi: 10.1016/j.ymben.2008.08.001

Shin, J. H., Park, S. H., Oh, Y. H., Choi, J. W., Lee, M. H., Cho, J. S., et al. (2016). Metabolic engineering of *Corynebacterium glutamicum* for enhanced production of 5-aminovaleric acid. *Microb. Cell Fact.* 15:174.

Tahara, T., Watanabe, A., Yutani, M., Yamano, Y., Sagara, M., Nagai, S., et al. (2020). STAT3 inhibitory activity of naphthoquinones isolated from *Tabebuia avellanedae*. *Bioorg. Med. Chem.* 28:115347. doi: 10.1016/j.bmc.2020.115347

Tsuge, Y., Kawaguchi, H., Sasaki, K., and Kondo, A. (2016). Engineering cell factories for producing building block chemicals for bio-polymer synthesis. *Microb. Cell Fact.* 15:19.

Vassilev, I., Giesselmann, G., Schwechheimer, S. K., Wittmann, C., Virdis, B., and Kromer, J. O. (2018). Anodic electro-fermentation: anaerobic production of L-Lysine by recombinant *Corynebacterium glutamicum*. *Biotechnol. Bioeng.* 115, 1499–1508. doi: 10.1002/bit.26562

Wang, J., Wu, Y. F., Sun, X. X., Yuan, Q. P., and Yan, Y. J. (2017). De novo biosynthesis of glutarate via alpha-keto acid carbon chain extension and decarboxylation pathway in *Escherichia coli*. *ACS Synth. Biol.* 6, 1922–1930. doi: 10.1021/acssynbio.7b00136

Wang, X., Cai, P., Chen, K., and Ouyang, P. (2016). Efficient production of 5-aminovalerate from L-lysine by engineered *Escherichia coli* whole-cell biocatalysts. *J. Mol. Catal. B Enzym* 134, 115–121. doi: 10.1016/j.molcatb.2016.10.008

Wu, Z., Peng, L., Hu, Y., Xie, T., Yan, H., Wan, H., et al. (2020). BP[dG]-induced distortions to DNA polymerase and DNA duplex: a detailed mechanism of BP adducts blocking replication. *Food Chem. Toxicol.* 140:111325. doi: 10.1016/j.fct.2020.111325

Xiang, L., Lu, Y., Wang, H., Wang, M., and Zhang, G. (2019). Improving the specific activity and pH stability of xylanase XynHBN188A by directed evolution. *Bioresour. Bioprocess.* 6:25.

Xie, T., Wu, Z., Gu, J., Guo, R., Yan, X., Duan, H., et al. (2019). The global motion affecting electron transfer in *Plasmodium falciparum* type II NADH dehydrogenases: a novel non-competitive mechanism for quinoline ketone derivative inhibitors. *Phys. Chem. Chem. Phys.* 21, 18105–18118. doi: 10.1039/c9cp02645b

Xiong, M., Deng, J., Woodruff, A. P., Zhu, M., Zhou, J., Park, S. W., et al. (2012). A bio-catalytic approach to aliphatic ketones. *Sci. Rep.* 2:311.

Xu, S., Lu, X., Li, M., Wang, J., Li, H., He, X., et al. (2019). Separation of 5-aminovalerate from its bioconversion liquid by macroporous adsorption resin: mechanism and dynamic separation. *J. Chem. Technol. Biot.* 95, 686–693. doi: 10.1002/jctb.6249

Yang, J., Zhu, Y., Men, Y., Sun, S., Zeng, Y., Zhang, Y., et al. (2016). Pathway construction in *Corynebacterium glutamicum* and strain engineering to produce rare sugars from glycerol. *J. Agric. Food Chem.* 64, 9497–9505. doi: 10.1021/acs.jafc.6b03423

Ying, H., Tao, S., Wang, J., Ma, W., Chen, K., Wang, X., et al. (2017). Expanding metabolic pathway for de novo biosynthesis of the chiral pharmaceutical intermediate L-pipecolic acid in *Escherichia coli*. *Microb. Cell Fact.* 16:52.

Youn, J.-W., Albermann, C., and Sprenger, G. A. (2020). In vivo cascade catalysis of aromatic amino acids to the respective mandelic acids

using recombinant *E. coli* cells expressing hydroxymandelate synthase (HMS) from *Amycolatopsis mediterranei*. *Mol. Catal.* 483:110713. doi: 10.1016/j.mcat.2019.110713

Zeng, B., Lai, Y., Liu, L., Cheng, J., Zhang, Y., and Yuan, J. (2020). Engineering *Escherichia coli* for high-yielding hydroxytyrosol synthesis from biobased L-tyrosine. *J. Agric. Food Chem.* 68, 7691–7696. doi: 10.1021/acs.jafc.0c03065

Zhang, J., Barajas, J. F., Burdu, M., Wang, G., Baidoo, E. E., and Keasling, J. D. (2017). Application of an Acyl-CoA ligase from Streptomyces aizunensis for Lactam biosynthesis. *ACS Synth. Biol.* 6, 884–890. doi: 10.1021/acssynbio.6b00372

Zhang, K., Sawaya, M. R., Eisenberg, D. S., and Liao, J. C. (2008). Expanding metabolism for biosynthesis of nonnatural alcohols. *Proc. Natl. Acad. Sci. U.S.A.* 105, 20653–20658. doi: 10.1073/pnas.0807157106

Zhao, M., Huang, D., Zhang, X., Koffas, M. A. G., Zhou, J., and Deng, Y. (2018a). Metabolic engineering of *Escherichia coli* for producing adipic acid through the reverse adipate-degradation pathway. *Metab. Eng.* 47, 254–262. doi: 10.1016/j.ymben.2018.04.002

Zhao, M., Li, G., and Deng, Y. (2018b). Engineering *Escherichia coli* for glutarate production as the C5 platform backbone. *Appl. Environ. Microbiol.* 84, e814–e818.

Zuo, K., Liang, L., Du, W., Sun, X., Liu, W., Gou, X., et al. (2017). 3D-QSAR, molecular docking and molecular dynamics simulation of *Pseudomonas aeruginosa* LpxC inhibitors. *Int. J. Mol. Sci.* 18:761. doi: 10.3390/ijms18050761

Conflict of Interest: The authors declare that the research was conducted in the absence of any commercial or financial relationships that could be construed as a potential conflict of interest.

frontiers in Bioengineering and Biotechnology

ORIGINAL RESEARCH
published: 29 March 2021
doi: 10.3389/fbioe.2021.635509

Production of Biopolyamide Precursors 5-Amino Valeric Acid and Putrescine From Rice Straw Hydrolysate by Engineered *Corynebacterium glutamicum*

*Keerthi Sasikumar[1,2], Silvin Hannibal[3], Volker F. Wendisch[3] and K. Madhavan Nampoothiri[1,2]**

[1] Microbial Processes and Technology Division (MPTD), CSIR-National Institute for Interdisciplinary Science and Technology, Thiruvananthapuram, India, [2] Academy of Scientific and Innovative Research (AcSIR), Ghaziabad, India, [3] Genetics of Prokaryotes, Faculty of Biology & CeBiTec, Bielefeld University, Bielefeld, Germany

OPEN ACCESS

Edited by:
Evangelos Topakas,
National Technical University of Athens, Greece

Reviewed by:
Gerd M. Seibold,
Technical University of Denmark, Denmark
Fengjie Cui,
Jiangsu University, China

***Correspondence:**
K. Madhavan Nampoothiri
madhavan@niist.res.in;
madhavan85@hotmail.com

Specialty section:
This article was submitted to Industrial Biotechnology, a section of the journal Frontiers in Bioengineering and Biotechnology

Received: 30 November 2020
Accepted: 09 March 2021
Published: 29 March 2021

Citation:
Sasikumar K, Hannibal S, Wendisch VF and Nampoothiri KM (2021) Production of Biopolyamide Precursors 5-Amino Valeric Acid and Putrescine From Rice Straw Hydrolysate by Engineered Corynebacterium glutamicum. Front. Bioeng. Biotechnol. 9:635509. doi: 10.3389/fbioe.2021.635509

The non-proteinogenic amino acid 5-amino valeric acid (5-AVA) and the diamine putrescine are potential building blocks in the bio-polyamide industry. The production of 5-AVA and putrescine using engineered *Corynebacterium glutamicum* by the co-consumption of biomass-derived sugars is an attractive strategy and an alternative to their petrochemical synthesis. In our previous work, 5-AVA production from pure xylose by C. *glutamicum* was shown by heterologously expressing *xylA* from *Xanthomonas campestris* and *xylB* from *C. glutamicum*. Apart from this AVA Xyl culture, the heterologous expression of $xylA_{Xc}$ and $xylB_{Cg}$ was also carried out in a putrescine producing *C. glutamicum* to engineer a PUT Xyl strain. Even though, the pure glucose (40 g L^{-1}) gave the maximum product yield by both the strains, the utilization of varying combinations of pure xylose and glucose by AVA Xyl and PUT Xyl in CGXII synthetic medium was initially validated. A blend of 25 g L^{-1} of glucose and 15 g L^{-1} of xylose in CGXII medium yielded 109 ± 2 mg L^{-1} putrescine and 874 ± 1 mg L^{-1} 5-AVA after 72 h of fermentation. Subsequently, to demonstrate the utilization of biomass-derived sugars, the alkali (NaOH) pretreated-enzyme hydrolyzed rice straw containing a mixture of glucose (23.7 g L^{-1}) and xylose (13.6 g L^{-1}) was fermented by PUT Xyl and AVA Xyl to yield 91 ± 3 mg L^{-1} putrescine and 260 ± 2 mg L^{-1} 5-AVA, respectively, after 72 h of fermentation. To the best of our knowledge, this is the first proof of concept report on the production of 5-AVA and putrescine using rice straw hydrolysate (RSH) as the raw material.

Keywords: 5-amino valeric acid, *Corynebacterium glutamicum*, polyamides, putrescine, rice straw hydrolysate

INTRODUCTION

The severe global environmental impact of the polyamide industries demands an alternative process to their current synthesis from the petrochemical routes. As the demand for these commercially relevant conventional plastics increases tremendously day by day, a new green approach for their sustainable production from renewable sources, with biodegradability and biocompatibility owes a competitive advantage and could be the most significant replacement for the current scenario.

Polyamides are homopolymers of terminal amino acids or co-polymers of diacids and diamines. The non-ribosomal amino acid 5-AVA is a glutaric acid derivative, an important precursor and an attractive building block for the synthesis of the polyamides. Apart from considering the importance of this five-carbon non-proteinogenic amino acid, as a potential monomer for the synthesis of nylon 5 and nylon 65 (Pukin et al., 2010; Adkins et al., 2013), their biotechnological production also gains considerable interest. A global high-performance polyamide market size report (Grand View Research Inc, 2020) projects a Compound annual growth rate (CAGR) of 7.1% for the high-performance polyamides from 2020 to 2027 as their consumption is highly increased for the production of insulation materials, industrial brushes and medical, healthcare products. 5-AVA is naturally produced as an intermediate by *Pseudomonas putida* in the degradation of L-lysine by AMV pathway (Liu et al., 2014), whereas, in *Pseudomonas aeruginosa* 5-AVA is produced by the transamination and oxidation of cadaverine, which in turn is produced by the decarboxylation of lysine (Jae et al., 2013). Successful metabolic engineering approaches have been established in *E. coli* and *Corynebacterium* strains for the production of 5-AVA from glucose, by the expression of L-lysine monoxygenase (DavB) and 5-amino valeramide amidohydrolase (DavA) genes of *Pseudomonas putida* (Cho et al., 2016). The four-carbon diamine—putrescine called 1,4-diaminobutane is a low molecular weight nitrogenous base and an essential monomer used in the chemical industry for the synthesis of effective bioplastic nylon-4,6 with a high melting point and exceptional chemical resistance. A metabolically engineered *E. coli* K12 W3110 was reported to produce putrescine from glucose minimal medium (Qian et al., 2009). The requirement for putrescine is estimated to be about 10,000 tons per year in Europe and this demand is expected to drastically increase in the coming years. Schneider et al. (2012) have reported a stable putrescine production from glucose with *C. glutamicum* by modifying the OTC activity and by expressing ornithine decarboxylase gene *speC* from *E. coli*.

The soil-dwelling Gram-positive bacterium *Corynebacterium glutamicum* has a very well-developed genetic toolbox and has been extensively explored by metabolic engineering, for decades for the effectual industrial production of amino acids such as lysine. Many value-added compounds like the *N*-methylated amino acids, sarcosine (Mindt et al., 2019), 7-choro tryptophan (Veldmann et al., 2019) and several intermediate precursors of amino acids, for example, 2-oxovalerate (Krause et al., 2010) and pyruvate (Wieschalka et al., 2012) have been successfully produced by the recombinant *C. glutamicum* strains. Several researchers across the globe have been studying the possibilities of ethanol production from the agro-residues for decades as these commodities are cheaply available in large quantities (Duff and Murray, 1996; Binod et al., 2010; Oberoi et al., 2010, 2012; Sarkar et al., 2012). The major agro-residual biomass includes rice straw, wheat straw, corn straw, cottonseed hair, seaweed, paper, pineapple leaf, banana stem, jatropha waste, and sugarcane bagasse (Kim and Dale, 2004).

Rice straw is one of the most abundant and underutilized agricultural wastes, rich in the structural carbohydrates—cellulose (32–47 %) and hemicellulose (19–27 %), densely packed in lignin (5–24 %) (Mosier et al., 2005; Kawaguchi et al., 2006). Cellulose is composed of repeating units of cellobiose and hemicellulose consists of several sugars like D-glucose, D-mannose, D-galactose, D-xylose, arabinose, and rhamnose. The depolymerization of rice straw into fermentable sugars turns it into a preferable primary carbon source for the microbial biocatalysts and biotransformation to commercially significant high-performance compounds making it an alternative to the pure sugar monomers like glucose, which have competing uses in the food industries (Jorge et al., 2016). The pretreatment of rice straw results in the formation of several compounds like furfural, hydroxyl methyl furfural, and 4-hydroxybenzaldehyde which inhibit the growth of many bacteria but *C. glutamicum* has been shown to withstand the pretreatment derived inhibitors (Gopinath et al., 2011). The wild type *C. glutamicum* ATCC 31831 utilize arabinose (Sasaki et al., 2009), whereas *C. glutamicum* ATCC 13032 consumes the pentose ribose (Wendisch, 2003; Rey et al., 2005) but cannot utilize xylose (Kawaguchi et al., 2006). *C. glutamicum* has been successfully engineered to consume xylose for growth and production. The scarcity of pentose utilizing microorganisms is a drawback for the successful industrial application of bioprocesses for the synthesis of economically important platform chemicals from lignocellulosic biomass. This study dealt with the exploitation of rice straw, a locally available surplus lignocellulosic biomass, as an alternative renewable raw material for the production of high-value products such as 5-AVA and putrescine by the simultaneous utilization of glucose and xylose, the abundant pentose sugar in biomass by employing the metabolically engineered *C. glutamicum* strains.

MATERIALS AND METHODS

Bacterial Strains and Culture Conditions

Bacterial strains and plasmids used in this work are listed in **Table 1**. *Escherichia coli* DH5α containing the pECXT99A-$xylA_{Xc}xylB_{Cg}$ plasmid (Jorge et al., 2017b) was used for extracting plasmid DNA. *E. coli* and *C. glutamicum* cells were cultivated in lysogeny broth (LB) medium (10 g L^{-1} of tryptone, 5 g L^{-1} yeast extract, and 10 g L^{-1} sodium chloride) or brain-heart-infusion (BHI) broth in 100 mL baffled flasks at 120 rpm at 37°C or 30°C, respectively. Kanamycin (25 μg mL^{-1}), tetracycline (5 μg mL^{-1}), spectinomycin (100 μg mL^{-1}), and 1 mM isopropyl β-D-1-thiogalactopyranoside (IPTG) were added when necessary. The pre-cultures of *C. glutamicum* AVA Xyl and PUT Xyl were grown in brain-heart-infusion (BHI) broth and incubated at 30°C and 200 rpm. For fermentation experiments, *C. glutamicum* strains were grown in CGXII basal medium with desired sugar concentrations and antibiotics, incubated at 30°C, in a rotary shaker (200 rpm). For all the fermentation experiments, the seed cultures were inoculated from fresh BHI agar plates containing appropriate antibiotics and a final concentration of 1 mM isopropyl-β–D-thiogalactopyranoside (IPTG) was added at the time of inoculation. The bacterial strains

TABLE 1 | Strains and plasmids used in this study.

Strains and plasmids	Characteristics	References
Strains		
C. glutamicum NA6	Putrescine producer strain; *C. glutamicum* ATCC13032 $odhA^{TTG}odhI^{T15A}$ Δ*argF* Δ*argR*Δ*snaA*, carrying IPTG-inducible pVWEx1-*speC-gapA-pyc-*$arg^{BA49V/M54V}$*-*$argF_{21}$	Nguyen et al., 2015
C. glutamicum PUT Xyl	Putrescine producer strain growing on xylose; *C. glutamicum* NA6 derivative, carrying IPTG-inducible plasmid pECXT99A-$xylA_{Xc}xylB_{Cg}$	This work
C. glutamicum AVA Xyl	5-Aminovalerate producer strain growing on xylose; *C. glutamicum* 5AVA3 (pECXT99A-$xylA_{Xc}xylB_{Cg}$) = GRLys1 Δ*sugR*Δ*ldhA*Δ*snaA*Δ*cgmA*Δ*gabTDP* derivative carrying IPTG-inducible plasmids pVWEx1-*ldcC*, pEKEx3-*patDA*, and pECXT99A-$xylA_{Xc}xylB_{Cg}$	Jorge et al., 2017b
E. coli DH5α (pECXT99A-$xylA_{Xc}xylB_{Cg}$)	*E. coli* DH5α strain carrying IPTG-inducible plasmid pECXT99A-$xylA_{Xc}xylB_{Cg}$	Jorge et al., 2017b
Plasmids		
pECXT99A-$xylA_{Xc}xylB_{Cg}$	pECXT99A-derived (Kirchner and Tauch, 2003), IPTG-inducible vector for the simultaneous overexpression of *xylA* from *Xanthomonas campestris SCC1758 and xylB from C. glutamicum ATCC13032*	Jorge et al., 2017b

were preserved in 40% glycerol at 80°C for long-term storage and maintained BHI agar plates supplemented with necessary antibiotics and preserved at 4°C for the short term.

Genetic Manipulations

C. glutamicum competent cells were prepared as described by Jorge et al. (2017a). Competent cells were transformed by electroporation (Eggeling and Bott, 2005) at 25 μF, 200 Ω, and 2.5 kV using plasmid DNA extracted from *E. coli* DH5α cells. Plasmid DNA extraction was performed with a GeneJET^{TM} Plasmid Miniprep Kit (Thermo Fisher Scientific, MA, United States) following the manufacturer's information.

Molecular Design and Genetic Engineering of *C. glutamicum* PUT Xyl and AVA Xyl

The *C. glutamicum* ATCC13032 derived strain NA6 (Nguyen et al., 2015) used for the construction of xylose-utilizing Put Xyl (see **Figure 1A**) carries several modifications for putrescine production, including modifications for the improvement of 2-oxoglutarate supply (overexpression of *gapA* and *pyc*, and reduced 2-oxoglutarate dehydrogenase activity due to $odhA^{TTG}$ and $odhI^{T15A}$), for the de-repression of the arginine biosynthesis by chromosomal deletion of *argR*, for the overexpression of a feedback-resistant N-acetyl glutamate kinase ($argB^{A49V/M54V}$), as well as for the prevention of by-product formation by the chromosomal deletions of *argF* and *snaA*. To avoid costly arginine supplementation due to the resulting arginine auxotrophy, a plasmid addiction system was created by inserting the $argF_{21}$ gene variant (Schneider et al., 2012), which encodes an ornithine transcarbamoylase with reduced activity, into the pVWEx1-derived (Peters-Wendisch et al., 2001) expression vector (Nguyen et al., 2015).

C. glutamicum, harboring xylulose kinase *xylB* but lacking xylose isomerase *xylA* for the first conversion step of the xylose isomerase pathway, is not capable of metabolizing xylose naturally. In this work, the NA6 strain (Nguyen et al., 2015) was transformed with the ITPG-inducible pECXT99A-$xylA_{Xc}xylB_{Cg}$ vector (Jorge et al., 2017b) for the overexpression of the xylose isomerase pathway, containing *xylA* from *Xanthomonas campestris* SCC1758 and *xylB* from *C. glutamicum* ATCC13032.

The corresponding 5-aminovalerate producer strain 5-AVA3 (pECXT99A-$xylA_{Xc}xylB_{Cg}$) already constructed in the previous work of Jorge et al. (2017b) was renamed to AVA Xyl (see **Figure 1B**) in this study. 5-AVA3 is a derivative of the genome-reduced lysine producer strain GRLys1 (Unthan et al., 2015), which lacks three genomic prophage regions and the phosphoenolpyruvate carboxykinase gene *pck*. Introduction of point mutations into the genes *lysC*, *pyc*, and *hom*, and chromosomal duplication of the lysine pathway genes *lysC*, *asd*, *dapA*, *dapB*, *ddh*, *lysA*, and *lysE* resulted in an effective lysine producer strain. For the construction of the production strain 5-AVA3 (Jorge et al., 2017b) deleted the transcriptional regulator of the sugar metabolism *sugR* to improve the glucose uptake, *ldhA*, *snaA*, *cgmA*, and *gabTDP* to prevent the side-product formation of lactate, N-acetyl cadaverine, cadaverine, as well as glutarate, and introduced the expression vectors pVWEx1-*ldcC* and pEKEx3-*patDA* to establish 5-AVA formation from lysine.

Supplementary Figure 1 shows the agarose gel of PCR fragments to verify the transformation of *C. glutamicum* NA6 with pECXT99A-$xylA_{Xc}B_{Cg}$ vector (expected fragment size: 3,312 bp) and **Supplementary Table 1** shows the pECXT99A primers used.

Quantification of Sugars and Amines in the Fermented Broth

The sugars and amines in the fermentation broth were analyzed by RP-HPLC. The quantification of sugars was performed on a Shimadzu UFLC system LC-20AT Prominance Liquid Chromatograph equipped with a Refractive Index Detector (Shimadzu RID-10A), an autosampler (SIL 20AC HT) and a Column oven (CTO-20ACV) operated at 80°C. Shimadzu Lab Solutions data management software was used. The monomeric sugars (xylose and glucose) were resolved using Rezex RPM Pb^{+} cation exchange monosaccharide column (300 × 7.5 mm, Phenomenex) with Milli Q water (Millipore) at a 0.60 mL/min isocratic flow rate and a 10 μL sample injection volume. Putrescine and 5-AVA were quantified using a Shimadzu UFLC system equipped with a fluorescence detector (RF 20A) at excitation and emission wavelengths of 348 and 450 nm, respectively. The samples were filtered through 0.22 μm filter membranes (PALL Lifesciences), buffered at a pH 10 using borate buffer (Agilent) and pre-derivatized with o-phthaldialdehyde

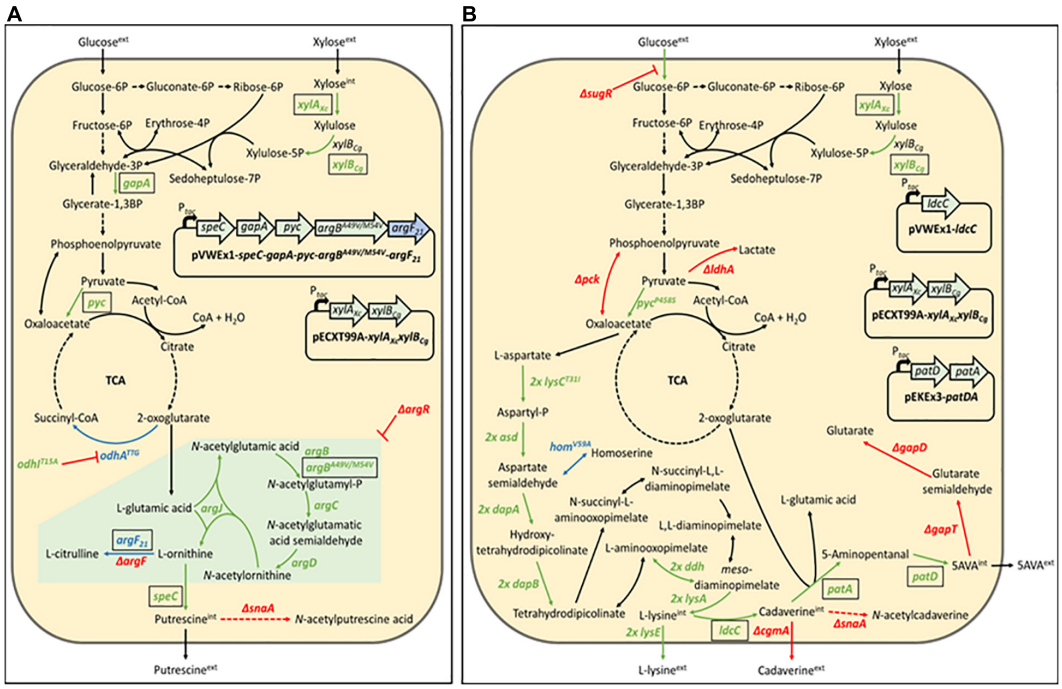

FIGURE 1 | Schematic representation of the putrescine production route in *Corynebacterium glutamicum* PUT Xyl **(A)** and the 5-aminovalerate production route in *C. glutamicum* AVA Xyl **(B)**. Gene names of key enzymes are given next to the corresponding reaction (pointed arrows). Black-boxed gene names indicate plasmid-borne expression, unboxed gene names indicate genomic expression. Reaction routes involving more than one gene are depicted by dashed arrows. Repression is represented by blunt arrows. Upregulated reactions are shown in green, downregulated reactions are shown in blue, and deleted reactions are shown in red. The green-boxed arginine pathway in **(A)** indicate upregulation by deletion of the repressor of the arginine biosynthesis ***ArgR***. ***argB*$^{A449V/M54V}$**, feedback-resistant N-acetyl glutamate kinase; ***argF***, ornithine transcarbamoylase; ***argF*$_{21}$**, ornithine transcarbamoylase with reduced activity; ***argR***, repressor of the arginine biosynthesis; ***asd*** (2 copies), aspartate-semialdehyde dehydrogenase; ***cgmA***, cyclic beta-1,2-glucan modification protein; ***dapA*** (2 copies), 4-hydroxy-tetrahydrodipicolinate synthase; ***dapB*** (2 copies), 4-hydroxy-tetrahydrodipicolinate reductase; ***ddh*** (2 copies), meso-diaminopimelate D-dehydrogenase; ***gabD***, succinate-semialdehyde dehydrogenase; ***gabT***, 4-aminobutyrate aminotransferase; ***gapA***, Glyceraldehyde-3-phosphate dehydrogenase A; ***hom*^{V59A}**, reduced activity homoserine dehydrogenase; ***ldcC***, constitutive lysine decarboxylase; ***ldhA***, D-lactate dehydrogenase; ***lysA*** (2 copies), diaminopimelate decarboxylase; ***lysC*^{T311I}** (2 copies), high activity aspartokinase; ***lysE*** (2 copies), lysine exporter; ***odhA*^{TTG}**, reduced activity 2-oxoglutarate dehydrogenase; ***odhI*^{T15A}**, high activity oxoglutarate dehydrogenase inhibitor; ***patA***, putrescine aminotransferase; ***patD***, gamma-aminobutyraldehyde dehydrogenase; ***pck***, phosphoenolpyruvate carboxykinase; ***P*$_{tac}$**, IPTG-inducible tac promoter; ***pyc***, pyruvate carboxylase; ***pyc*^{P458S}**, high activity pyruvate carboxylase; ***snaA***, N-acetyltransferase; ***speC***, ornithine decarboxylase; ***sugR***, central transcriptional regulator of the carbon metabolism; ***xylA*$_{Xc}$**, xylose isomerase from *Xanthomonas campestris*; ***xylB*$_{Cg}$**, xylulose kinase from *C. glutamicum*.

[OPA] (Agilent). Putrescine and 5-AVA were resolved with Zorbax Eclipse AAA column (Agilent) using 40 mM sodium phosphate buffer (Agilent) and acetonitrile methanol-water in the ratio (45:45:10) in a gradient elution program.

Authentication of Putrescine Production From Xylose by Engineered *C. glutamicum* PUT Xyl

Even though the 5-aminovalerate production from xylose by *C. glutamicum* AVA Xyl was already shown by Jorge et al. (2017b), the putrescine production from xylose by *C. glutamicum* PUT Xyl has to be confirmed. Therefore, a growth and production study using CGXII minimal medium was conducted and subsequent putrescine measurement via HPLC analysis was performed. Since a previous growth experiment showed a slow growth of PUT Xyl ($\mu = 0.05 \pm 0.003$) on xylose (data not shown), a control supplemented with minimum glucose of 0.5 g L^{-1} for supporting the initial growth rate was chosen. Growth was observed by measuring OD_{600}, and samples for HPLC analysis were taken after 6, 24, and 72 h of cultivation.

Simultaneous Utilization of Glucose and Xylose by the Engineered *C. glutamicum* Strains in CGXII Minimal Medium by Batch Fermentation

For the production experiments, CGXII medium was formulated with different combinations of glucose and xylose making the total sugar concentration 40 g L^{-1} and a pH of 7. Overnight cultures of the *C. glutamicum* strains in BHI medium were harvested by centrifugation at 5,000 rpm for 10 min, washed in minimal medium without sugar and inoculated to the CGXII minimal medium with an initial optical density at 600 nm (OD_{600}) of 1.0. The growth of the cells was monitored by measuring the absorbance at 600 nm in a spectrophotometer (Tecan plate reader infinite 200 Pro, Switzerland). Samples were

withdrawn at the desired interval of time and checked for sugar consumption and product formation as per standard protocols.

Preparation of Rice Straw Hydrolysate (RSH)

Rice straw procured from the local markets was used for the study. Dried rice straw milled into a particle size of ≤ 1 mm was subjected to alkali pretreatment with a solid loading of 20 % (w/w) and NaOH loading of 2 % (w/v), at 121 °C for 1 h. The pretreated biomass slurry was allowed to cool at room temperature, neutralized with 10 N H_2SO_4, wet sieved and air-dried before enzymatic hydrolysis. Later, the wet sieved neutralized biomass was saccharified with commercial cellulase (Zytex India Limited, Mumbai) with an enzyme load of 20 FPUs/g of the substrate and a biomass loading of 10 % (w/w), at 50 °C, 180 rpm for 48 h. A pH of 4.8 was maintained using citrate buffer (0.5 M). The liquid fraction called the RSH was separated from the whole slurries by centrifugation and filter-sterilized using 0.22 (47 mm) μm filter membranes (Millipore, Massachusetts, United States) prior to fermentation.

Utilization of RSH as a Sole Carbon Source by AVA Xyl and PUT Xyl

To study the potential of utilizing low-value sugars in the agro-residual wastes by the *Corynebacterium* biocatalysts, shake flask batch fermentations were carried out at 30 °C and 200 rpm. The production medium with RSH was formulated with 20 g L^{-1} $(NH_4)_2SO_4$, 5 g L^{-1} Urea, 1 g L^{-1} K_2HPO_4, 1 g L^{-1} KH_2PO_4, 0.25 g L^{-1} $MgSO_4$. $7H_2O$, 42 g L^{-1} MOPS, 0.02 mg L^{-1} biotin, 10 mg L^{-1} $CaCl_2$ and necessary trace elements in RSH, adjusted to pH 7 using 10 N NaOH. Overnight grown seed cultures in the BHI medium were inoculated to RSH based production medium (100 mL) to attain an initial OD of 1.0 and incubated at 30 °C, in a rotary shaker (200 rpm). The growth pattern of both strains was determined by a spectrophotometer. The sugar utilization and the production of the two recombinant strains were estimated by HPLC.

All the experiments were performed in triplicates and all the data were expressed as the mean ± standard deviation of three independent replicates.

RESULTS AND DISCUSSION

Validation of Biosynthesis of Putrescine by the Recombinant Strain PUT Xyl in CGXII Medium

Unlike AVA Xyl, which was studied earlier for 5-AVA biosynthesis, as indicated in the methodology, initially we checked the xylose utilization potentiality of the new construct PUT Xyl for proof of the concept. As shown in **Figure 2B**, a lower putrescine production of 26.66 ± 1.40 mg L^{-1} and a growth rate of 0.040 ± 0.002 h^{-1} was observed after 72 h, in the shake flask which initially contained 40 g L^{-1} of xylose alone as the carbon source. The growth was picked up to 0.137 ± 0.008 h^{-1} (**Figure 2A**) when a minimal amount of glucose (5 g L^{-1}) was supplemented initially along with xylose (35 g L^{-1}) and the putrescine production titer increased to 97.88 ± 2.07 mg L^{-1}.

Production of Putrescine and 5-AVA by PUT Xyl and AVA Xyl in CGXII Minimal Medium With the Simultaneous Utilization of Glucose and Xylose

A detailed study was conducted with varying concentrations of glucose (5–40 g L^{-1}) and xylose (5–40 g L^{-1}), to analyze the efficacy of both AVA Xyl and PUT Xyl strains in co-utilizing pure glucose and xylose initially making a total sugar of 40 g L^{-1} in CGXII minimal medium. After 72 h of fermentation, 96.74 ± 5.66 mg L^{-1} putrescine was obtained with a growth rate of 0.145 ± 0.100 h^{-1}, when the PUT Xyl strain fermented an equal amount of glucose (20 g L^{-1}) and xylose (20 g L^{-1}). The same 1:1 combination of sugars yielded 602.74 ± 2.15 mg L^{-1} 5-AVA after 72 h and a growth rate of 0.187 ± 0.002 h^{-1}

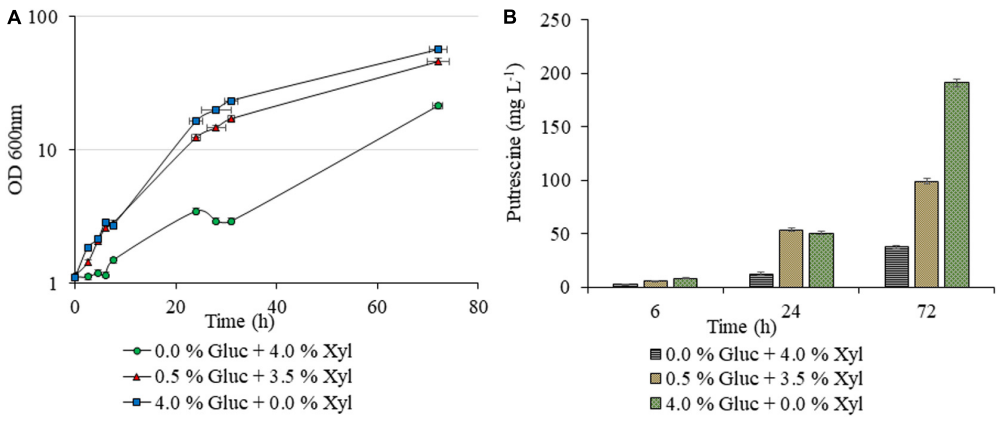

FIGURE 2 | Putrescine production of *C. glutamicum* PUT Xyl. Growth curves of *C. glutamicum* PUT Xyl cultivated in shake flasks of 20 mL CGXII minimal medium supplemented with different compositions of glucose (Gluc) and xylose (Xyl) **(A)**, and putrescine concentrations measured after 0, 6, 24, and 72 h of cultivation **(B)**. Measurements are given as means from triplicates of independent cultivations with standard deviation.

when AVA Xyl strain was used. The utilization of xylose by the two recombinant strains, even in the presence of glucose shows their efficacy to co-metabolize the xylose and glucose present in the fermentation medium. The xylose consumption was evidently facilitated once the glucose pool reached a depletion. This metabolic shift from glucose to xylose suggests that the xylose machinery including the overexpressed *xylA xylB* genes is also active even in the presence of glucose. When the medium contained 25 g L^{-1} glucose and 15 g L^{-1} xylose, the entire glucose and 64.28 ± 0.13% (**Figure 3A**) of xylose was consumed by PUT Xyl, which is about 9.29 ± 0.04 g L^{-1}, at a rate of 0.152 ± 0.004 g L^{-1} h^{-1} (**Figure 3B**) to produce 109.43 ± 2.11 mg L^{-1} of putrescine (**Figure 3C**) after 72 h and grew faster (μ = 0.148 ± 0.060 h^{-1}). The percentage of xylose utilized by the AVA Xyl strain is shown in **Figure 4A**. Almost 9.10 ± 0.05 g L^{-1} of xylose was uptaken by AVA Xyl at a rate of 0.198 ± 0.012 g L^{-1} h^{-1} (**Figure 4B**), along with the whole glucose, grew at a rate of 0.188 ± 0.005 h^{-1} and gave an AVA titer of 874.43 ± 0.98 mg L^{-1} (**Figure 4C**) after 72 h. The increase in the initial glucose concentration in the medium resulted in a slight decline of the xylose uptake which may be due to the repression offered by glucose.

A slight decrease in the production, of putrescine (92.93 ± 2.83 mg L^{-1}) and 5-AVA (553.93 ± 4.67 mg L^{-1}) as well as in the growth of PUT Xyl and AVA Xyl was observed with a combination of 15 g L^{-1} glucose and 25 g L^{-1} xylose. As mentioned in section "Validation of Biosynthesis of Putrescine by the Recombinant Strain PUT Xyl in CGXII Medium," the least putrescine (26.66 ± 1.40 mg L−1) and also 5-AVA production (52.66 ± 0.09 mg L^{-1}) was observed when xylose (40 g L^{-1}) alone was the only sugar source. Though the highest amounts of putrescine of about 195.71 ± 0.69 mg L^{-1} and 5-AVA of 1508.71 ± 3.21 mg L^{-1} were obtained in the shake flask with 40 g L^{-1} glucose, significant productions were observed when glucose is partially replaced with different ratios of xylose. The comparable production titer of the respective compounds when a mixture of glucose and xylose was used, revealed that both the recombinant strains were capable of co utilizing them to produce respective products, the putrescine and 5-AVA.

Exploitation of the Fermentable Sugars in the RSH for the Production of Putrescine and 5-AVA

The efficacy of PUT Xyl and AVA Xyl strains to ferment the saccharified sugars in the lignocellulosic hydrolysate was evaluated after validating the proof of concept in the CGXII synthetic medium. The RSH after 48 h of hydrolysis contained glucose (23.76 g L^{-1}) and xylose (12.65 g L^{-1}) (**Figure 5A**) and the formulated RSH based production medium had a total sugar (mainly glucose and xylose) of 3.64 %. The sugar utilization, growth and production by PUT Xyl and AVA Xyl in the RSH based medium containing (23.7 g L^{-1} glucose + 12.6 g L^{-1} xylose) was comparable to that in the CGXII medium, with the most proximate sugar concentration (25 g L^{-1} glucose and 15 g L^{-1} xylose). However, engineered *C. glutamicum* strains when cultivated in the RSH based medium had a longer lag phase. After 24 h, the PUT Xyl strain attained a growth rate of

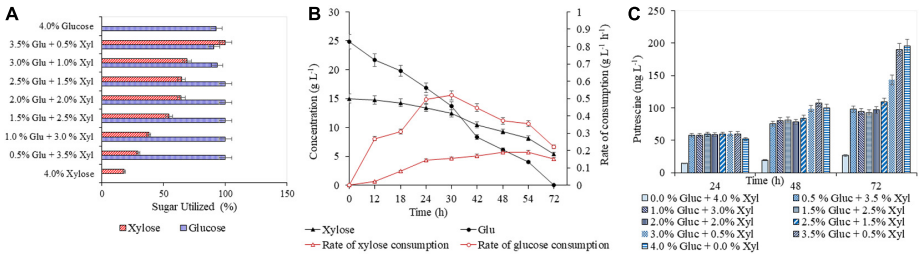

FIGURE 3 | Production of putrescine in CGXII synthetic medium with different blends of glucose and xylose. The percentage utilization of glucose and xylose by PUT Xyl is shown in **(A)**. The glucose and xylose consumption rate of PUT Xyl is shown in **(B)**. The time profile of the putrescine production is shown in **(C)**. Measurements are given as means from triplicates of independent cultivations with standard deviation.

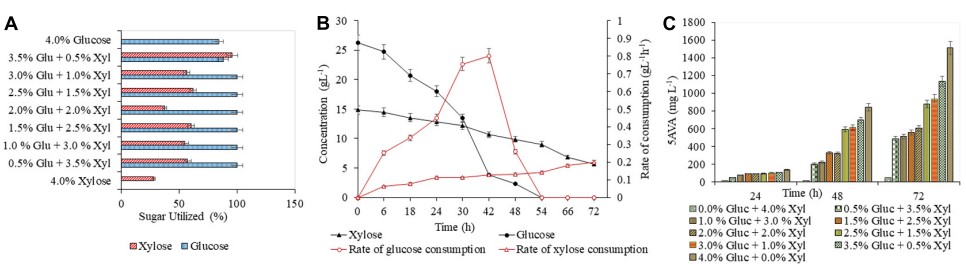

FIGURE 4 | Production of 5-AVA in CGXII medium with different blends of glucose and xylose. The utilization of glucose and xylose by PUT Xyl is shown in **(A)**. The glucose and xylose consumption rate of AVA Xyl is shown in **(B)**. The time profile of the 5-AVA production is shown in **(C)**. Measurements are given as means from triplicates of independent cultivations with standard deviation.

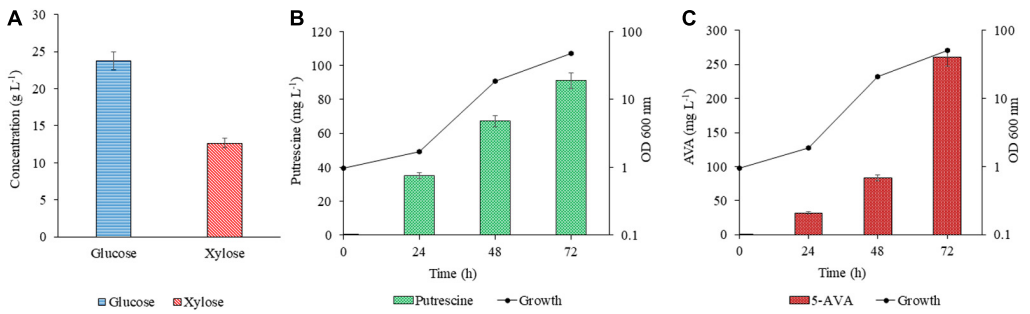

FIGURE 5 | Concentration of glucose and xylose in RSH **(A)**. Production of putrescine **(B)** and 5 AVA **(C)** from RSH. Hydrolysate contained 2.37 g L^{-1} glucose + 12.6 g L^{-1} xylose. The downward diagonal column represents the production and the line graph with marker shows the absorbance at OD 600 nm. Measurements are given as means from triplicates of independent cultivations with standard deviation.

$0.013 \pm 0.004\ h^{-1}$, whereas the AVA Xyl strain had a growth rate of $0.003 \pm 0.001\ h^{-1}$. Thereafter, the growth was picked up to $0.130 \pm 0.028\ h^{-1}$ and $0.140 \pm 0.031\ h^{-1}$ by PUT Xyl and AVA Xyl, respectively, and the xylose and glucose in the RSH were fermented to yield 91.00 ± 2.58 mg L^{-1} putrescine (**Figure 5B**) and 260.33 ± 2.47 mg L^{-1} 5-AVA (**Figure 5C**) after 72 h.

Polyamide (PA), commonly known as nylon, is a polymer with a myriad of pharmaceutical and industrial applications and is currently synthesized by petrochemical routes. Chemically, the polymer backbone is composed of repetitive units of diamines and dicarboxylic acids that contain different numbers of carbon atoms, imparting a variety of material properties. Globally, the demand for polyamides has fairly increased and is expected to grow at a CAGR of 7.1 % in a forecast period of 2020–2027. The petroleum-based fossil fuels remarkably contribute to 60 % of one-fifth of the CO_2 emission because nearly 82 % of the global energy needs are met by non-renewable energy sources such as petroleum, coal and natural gas (Gupta and Verma, 2015).

Biomass has been considered to be the only sustainable source of organic carbon on earth and the net-zero carbon emission makes it the best analogy to petroleum for the production of value-added chemicals (Sharma et al., 2019). Howbeit we have employed the plasmid-based expression, a genome-based expression for the amplification of the *xylA* and *xylB,* genes are preferred over the plasmid-based expression system to avert its instability problems for industrial-scale applications. In the current study, we have focused on the bacterial synthesis of a diamine and a dicarboxylic acid by exploiting the low-value sugars in the lignocellulosic biomass—rice straw, using the engineered *C. glutamicum* strains capable of consuming xylose and glucose. This was established by genetically modifying the metabolic pathways in *C. glutamicum* and make it a self-sufficient host for the utilization of the C5 sugar xylose, a fair amount of which is gone underutilized in the form of agro-residues. Since the wild type *C. glutamicum* deficient of the xylose isomerase activity is unable to utilize xylose neither in aerobic nor in oxygen-deprived conditions (Kawaguchi et al., 2006) here in this study, we have further modified the NA6 strain, previously reported by Nguyen et al. (2015), for xylose utilization and its biotransformation to putrescine. Meiswinkel et al. (2013) studied the growth of *C. glutamicum* strains harboring different *xylA* and *xylB* genes from *B. subtilis, E. coli, M. smegmatis*, and *X. campestris* and reported that the recombinant strains with heterologous expression of the endogenous *xylB* gene from *C. glutamicum* in addition to the *xylA* gene from *X. campestris* improved xylose utilization and grew well ($\mu = 0.199 \pm 0.009\ h^{-1}$) in CGXII medium with xylose as the sole carbon source. The toxicity of putrescine to any microorganisms (Incorvia, 2015) was believed to be a hindrance for the active exploration of bacterial putrescine production (Qian et al., 2009) but *C. glutamicum* can tolerate higher concentrations (44 g L^{-1}) of putrescine (Schneider and Wendisch, 2010; Jorge et al., 2017a). An *E. coli* strain XQ52 harboring p15SpeC was reported to produce 21.7 g L^{-1} in 32 h, by the consumption of glucose via fed-batch fermentation (Noh et al., 2017). In our study, the putrescine titer obtained using the engineered *C. glutamicum* strain PUT Xyl was 109.43 ± 2.11 mg L^{-1} in the shake flasks with CGXII containing 25 g L^{-1} glucose and 15 g L^{-1} xylose.

The collection of raw material, its availability throughout the seasons, transportation and storage are the major difficulties in any study related to the agro residual biomass. The digestibility of cellulose present in lignocellulosic biomass is hindered by many physicochemical, structural, and compositional factors are one of the major concerns. The biomass needs to be treated so that the cellulose in the plant fibers is exposed. The goal of the pretreatment process is to break down the lignin structure and disrupt the crystalline structure of cellulose so that the enzymes can easily access and hydrolyze the cellulose. The alkali pretreatment decreases the lignin by about 47 % and increases the glucan by about 50 % (Oberoi et al., 2012). The enzymatic hydrolysis of the alkali pretreated rice straw had a fair glucose (23.7 g L^{-1}) and xylose (12.6 g L^{-1}) composition, which were fermented to value-added chemicals such as 5-AVA (260.33 ± 2.47 mg L^{-1}) and putrescine (91.00 ± 2.58 mg L^{-1}) by AVA Xyl and PUT Xyl. The recombinant *C. glutamicum* strains overexpressing the transformed *xylA*, *xylB* genes were proved efficient to uptake the fermentable sugars from RSH based medium and biosynthesize the compounds of interest. The recombinant *C. glutamicum* strains co-utilize the xylose along

with glucose present in the lignocellulosic hydrolysates but the presence of pre-treatment derived inhibitors like furfural and/or hydroxyl methyl furfural attributes to the slower growth and production when hydrolysate based media is used (Gopinath et al., 2011). In this study, we have observed the utilization of both glucose and xylose by the modified *C. glutamicum* strains in the CGXII medium and as well as in the RSH based medium. A higher titer of 5-AVA (39.93 g L^{-1}) than from the glucose fermentation was obtained in Miscanthus hydrolysate solution by fed-batch fermentation employing the recombinant *C. glutamicum* KCTC 1857 expressing the *davBA* genes (Joo et al., 2017). Industrial sugar beet thick juice was reported as a suitable carbon source for *Corynebacterium* and produced putrescine with a volumetric productivity of 0.28 ± 0.01 g L^{-1} h^{-1} (Meiswinkel et al., 2014). In our study, *C. glutamicum* PUT Xyl produced putrescine from the rice straw hydrolysate-based medium with a volumetric productivity of 1.26 ± 0.31 mg L^{-1} h^{-1}. A study by Nguyen and Lee (2019), represented the bioconversion of methane to putrescine using an engineered *Methylomicrobium alcaliphilum* 20ZE4-pACO strain with a putrescine titer of 98.08 mg L^{-1}. A lower growth rate was observed in RSH based medium when compared to the most proximate sugar concentration of that in the CGXII minimal medium for both the strains, which may be due to the hindrances offered by the pre-treatment derived inhibitors (Gopinath et al., 2011).

CONCLUSION

The ability for the simultaneous utilization of glucose and the pentose sugar xylose by the two engineered *C. glutamicum* strains AVA Xyl and PUT Xyl to produce 5-AVA and putrescine opened up a new avenue to utilize them for the production of such value-added products from renewable sources such as lignocellulosic biomass which generally goes as a surplus waste product in the agricultural sector. The tolerance of *C. glutamicum* to grow in pretreated biomass hydrolysate is yet another added advantage of this wonderful industrial strain making them an excellent biocatalyst in biorefineries for improving the techno-economic feasibility of the entire processes. As of now, we could demonstrate the production of value-added wide spectrum products such as lysine, xylitol, xylonic acid, etc., from biomass using carefully drafted and engineered *C. glutamicum* strains. Here we have demonstrated a green bioprocess for the production of two highly demanded building blocks of the polyamide industry such as 5AVA and putrescine from a renewable raw material like rice straw. Process strategies employing synthetic, mutually dependent consortia (Sgobba et al., 2018) or dynamically controlled co-cultivation of two recombinant *C. glutamicum* strains (Pérez-Garcia et al., 2021) may be used for further optimization. Successful upscaling of the process can be a breakthrough in white biotechnology for the production of bioplastics.

DATA AVAILABILITY STATEMENT

The raw data supporting the conclusions of this article will be made available by the authors, without undue reservation.

AUTHOR CONTRIBUTIONS

KN and VW acquired funding and designed the study. KS carried out the biomass pretreatment, shake flask fermentation, and production data analysis. SH and VW constructed the production strains as part of the Indo German collaboration work. SH wrote the manuscript portions pertaining to the strain construction details. KS and KN designed and drafted the final manuscript. VW did the critical reading. All authors read and approved the final manuscript.

FUNDING

This study was supported by the grant from the Indo-German DBT BMBF project BIOCON.

ACKNOWLEDGMENTS

We would like to thank the DBT, New Delhi and BMBF, Germany for financial support.

SUPPLEMENTARY MATERIAL

The Supplementary Material for this article can be found online at: https://www.frontiersin.org/articles/10.3389/fbioe.2021.635509/full#supplementary-material

REFERENCES

Adkins, J., Jordan, J., and Nielsen, D. R. (2013). Engineering *Escherichia coli* for renewable production of the 5-carbon polyamide building-blocks 5-aminovalerate and glutarate. *Biotechnol. Bioeng.* 110, 1726–1734. doi: 10.1002/bit.24828

Binod, P., Sindhu, R., Singhania, R. R., Vikram, S., Devi, L., Nagalakshmi, S., et al. (2010). Bioethanol production from rice straw: an overview. *Bioresour. Technol.* 101, 4767–4774. doi: 10.1016/j.biortech.2009.10.079

Cho, J. S., Jeong, K. J., Choi, J. W., Park, S. H., Joo, J. C., Park, S. J., et al. (2016). Metabolic engineering of *Corynebacterium glutamicum* for enhanced production of 5-aminovaleric acid. *Microb. Cell Fact.* 15, 1–13.

Duff, S. J. B., and Murray, W. D. (1996). Bioconversion of forest products industry waste cellulosics to fuel ethanol: a review. *Bioresour. Technol.* 55, 1–33. doi: 10.1016/0960-8524(95)00122-0

Eggeling, L., and Bott, M. (eds). (2005). *Handbook of Corynebacterium glutamicum*, 1st Edn, FL, United States: CRC Press. doi: 10.1201/9781420039696

Gopinath, V., Meiswinkel, T. M., Wendisch, V. F., and Nampoothiri, K. M. (2011). Amino acid production from rice straw and wheat bran hydrolysates by recombinant pentose-utilizing *Corynebacterium glutamicum*. *Appl. Microbiol. Biotechnol.* 92, 985–996. doi: 10.1007/s00253-011-3478-x

Grand View Research Inc (2020). *High Performance Polyamides Market Size, Share & Trends Analysis Report By Type (PA 6T, Polyarylamide, PA 12, PA 9T, PA 11, PA 46, Polyphthalamides), By End-use Industry, By Region, And Segment Forecasts, 2020 - 2027*. GVR-4-68038-813-8, R. id.

Gupta, A., and Verma, J. P. (2015). Sustainable bio-ethanol production from agro-residues: a review. *Renew. Sustain. Energy Rev.* 41, 550–567. doi: 10.1016/j.rser.2014.08.032

Incorvia, C. (2015). (**??**) *United States Patent*, Vol. 2. 3131–3135.

Jae, S., Young, E., Noh, W., Min, H., Hoon, Y., Hwan, S., et al. (2013). Metabolic engineering of *Escherichia coli* for the production of 5-aminovalerate and glutarate as C5 platform chemicals. *Metab. Eng.* 16, 42–47. doi: 10.1016/j.ymben.2012.11.011

Joo, J. C., Oh, Y. H., Yu, J. H., Hyun, S. M., Khang, T. U., Kang, K. H., et al. (2017). Production of 5-aminovaleric acid in recombinant *Corynebacterium glutamicum* strains from a Miscanthus hydrolysate solution prepared by a newly developed Miscanthus hydrolysis process. *Bioresour. Technol.* 245, 1692–1700. doi: 10.1016/j.biortech.2017.05.131

Jorge, J. M. P., Leggewie, C., and Wendisch, V. F. (2016). A new metabolic route for the production of gamma-aminobutyric acid by *Corynebacterium glutamicum* from glucose. *Amino Acids* 48, 2519–2531. doi: 10.1007/s00726-016-2272-6

Jorge, J. M. P., Nguyen, A. Q. D., Pérez-García, F., Kind, S., and Wendisch, V. F. (2017a). Improved fermentative production of gamma-aminobutyric acid via the putrescine route: systems metabolic engineering for production from glucose, amino sugars, and xylose. *Biotechnol. Bioeng.* 114, 862–873. doi: 10.1002/bit.26211

Jorge, J. M. P., Pérez-García, F., and Wendisch, V. F. (2017b). A new metabolic route for the fermentative production of 5-aminovalerate from glucose and alternative carbon sources. *Bioresour. Technol.* 245, 1701–1709. doi: 10.1016/j.biortech.2017.04.108

Kawaguchi, H., Sasaki, M., Vertès, A. A., Inui, M., and Yukawa, H. (2006). Engineering of a xylose metabolic pathway in *Corynebacterium glutamicum*. *Appl. Microbiol. Biotechnol.* 77, 1053–1062. doi: 10.1007/s00253-007-1244-x

Kim, S., and Dale, B. E. (2004). Global potential bioethanol production from wasted crops and crop residues. *Biomass Bioenergy* 26, 361–375. doi: 10.1016/j.biombioe.2003.08.002

Kirchner, O., and Tauch, A. (2003). Tools for genetic engineering in the amino acid-producing bacterium *Corynebacterium glutamicum*. *J. Biotechnol.* 104, 287–299. doi: 10.1016/S0168-1656(03)00148-2

Krause, F. S., Blombach, B., and Eikmanns, B. J. (2010). Metabolic engineering of *Corynebacterium glutamicum* for 2-Ketoisovalerate production. *Appl. Environ. Microbiol.* 76, 8053–8061. doi: 10.1128/AEM.01710-10

Liu, P., Zhang, H., Lv, M., Hu, M., Li, Z., Gao, C., et al. (2014). Enzymatic production of 5-aminovalerate from L-lysine using L-lysine monooxygenase and 5-aminovaleramide amidohydrolase. *Sci. Rep.* 4:5657. doi: 10.1038/srep05657

Meiswinkel, T., Lindner, S., and Wendisch, V. F. (2014). Thick juice-based production of amino acids and putrescine by *Corynebacterium glutamicum*. *J. Biotechnol. Biomater.* 4:167. doi: 10.4172/2155-952x.1000167

Meiswinkel, T. M., Gopinath, V., Lindner, S. N., Nampoothiri, K. M., and Wendisch, V. F. (2013). Accelerated pentose utilization by *Corynebacterium glutamicum* for accelerated production of lysine, glutamate, ornithine and putrescine. *Microb. Biotechnol.* 6, 131–140. doi: 10.1111/1751-7915.12001

Mindt, M., Hannibal, S., Heuser, M., Risse, J. M., Sasikumar, K., Nampoothiri, M., et al. (2019). Fermentative production of N-alkylated glycine derivatives by recombinant *Corynebacterium glutamicum* using a mutant of imine reductase DpkA from *Pseudomonas putida*. *Front. Bioeng. Biotechnol.* 7:232. doi: 10.3389/fbioe.2019.00232

Mosier, N., Wyman, C., Dale, B., Elander, R., Lee, Y. Y., Holtzapple, M., et al. (2005). Features of promising technologies for pretreatment of lignocellulosic biomass. *Bioresour. Technol.* 96, 673–686. doi: 10.1016/j.biortech.2004.06.025

Nguyen, A. Q. D., Schneider, J., Reddy, G. K., and Wendisch, V. F. (2015). Fermentative production of the diamine Putrescine: system metabolic engineering of *Corynebacterium glutamicum*. *Metabolites* 5, 211–231. doi: 10.3390/metabo5020211

Nguyen, L. T., and Lee, E. Y. (2019). Biological conversion of methane to putrescine using genome-scale model-guided metabolic engineering of a methanotrophic bacterium *Methylomicrobium alcaliphilum* 20Z. *Biotechnol. Biofuels* 12, 1–12. doi: 10.1186/s13068-019-1490-z

Noh, M., Yoo, S. M., Kim, W. J., and Lee, S. Y. (2017). Gene expression knockdown by modulating synthetic small RNA Expression in *Escherichia coli*. *Cell Syst.* 5, 418–426.e4. doi: 10.1016/j.cels.2017.08.016

Oberoi, H. S., Babbar, N., Sandhu, S. K., Dhaliwal, S. S., Kaur, U., Chadha, B. S., et al. (2012). Ethanol production from alkali-treated rice straw via simultaneous saccharification and fermentation using newly isolated thermotolerant *Pichia kudriavzevii* HOP-1. *J. Ind. Microbiol. Biotechnol.* 39, 557–566. doi: 10.1007/s10295-011-1060-2

Oberoi, H. S., Vadlani, P. V., Brijwani, K., Bhargav, V. K., and Patil, R. T. (2010). Enhanced ethanol production via fermentation of rice straw with hydrolysate-adapted *Candida tropicalis* ATCC 13803. *Process Biochem.* 45, 1299–1306. doi: 10.1016/j.procbio.2010.04.017

Pérez-Garcia, F., Burgardt, A., Kallman, D. R., Wendisch, V. F., and Bar, N. (2021). Dynamic co-cultivation process of *Corynebacterium glutamicum* strains for the fermentative production of riboflavin. *Fermentation* 7:11. doi: 10.3390/fermentation7010011

Peters-Wendisch, P. G., Schiel, B., Wendisch, V. F., Katsoulidis, E., Möckel, B., Sahm, H., et al. (2001). Pyruvate carboxylase is a major bottleneck for glutamate and lysine production by *Corynebacterium glutamicum*. *J. Mol. Microbiol. Biotechnol.* 3, 295–300.

Pukin, A. V., Boeriu, C. G., Scott, E. L., Sanders, J. P. M., and Franssen, M. C. R. (2010). An efficient enzymatic synthesis of 5-aminovaleric acid. *J. Mol. Catal. B Enzym.* 65, 58–62. doi: 10.1016/j.molcatb.2009.12.006

Qian, Z. G., Xia, X. X., and Lee, S. Y. (2009). Metabolic engineering of *Escherichia coli* for the production of putrescine: a four carbon diamine. *Biotechnol. Bioeng.* 104, 651–662. doi: 10.1002/bit.22502

Rey, D. A., Nentwich, S. S., Koch, D. J., Rückert, C., Pühler, A., Tauch, A., et al. (2005). The McbR repressor modulated by the effector substance S-adenosylhomocysteine controls directly the transcription of a regulon involved in sulphur metabolism of *Corynebacterium glutamicum* ATCC 13032. *Mol. Microbiol.* 56, 871–887. doi: 10.1111/j.1365-2958.2005.04586.x

Sarkar, N., Ghosh, S. K., Bannerjee, S., and Aikat, K. (2012). Bioethanol production from agricultural wastes: an overview. *Renew. Energy* 37, 19–27.

Sasaki, M., Jojima, T., Kawaguchi, H., Inui, M., and Yukawa, H. (2009). Engineering of pentose transport in *Corynebacterium glutamicum* to improve simultaneous utilization of mixed sugars. *Appl. Microbiol. Biotechnol.* 85, 105–115. doi: 10.1007/s00253-009-2065-x

Schneider, J., Eberhardt, D., and Wendisch, V. F. (2012). Improving putrescine production by *Corynebacterium glutamicum* by fine-tuning ornithine transcarbamoylase activity using a plasmid addiction system. *Appl. Microbiol. Biotechnol.* 95, 169–178. doi: 10.1007/s00253-012-3956-9

Schneider, J., and Wendisch, V. F. (2010). Putrescine production by engineered *Corynebacterium glutamicum*. *Appl. Microbiol. Biotechnol.* 88, 859–868.

Sgobba, E., Stumpf, A. K., Vortmann, M., Jagmann, N., Dirks-hofmeister, M., Moerschbacher, B., et al. (2018). Synthetic *Escherichia coli-Corynebacterium glutamicum* consortia for l-lysine production from starch and sucrose. *Bioresour. Technol.* 260, 302–310. doi: 10.1016/j.biortech.2018.03.113

Sharma, M., Singh, J., Baskar, C., and Kumar, A. (2019). A comprehensive review of renewable energy production from biomass-derived bio-oil. *Biotechnologia* 100, 179–194. doi: 10.5114/bta.2019.85323

Unthan, S., Baumgart, M., Radek, A., Herbst, M., Siebert, D., Brühl, N., et al. (2015). Chassis organism from *Corynebacterium glutamicum* - a top-down approach to identify and delete irrelevant gene clusters. *Biotechnol. J.* 10, 290–301. doi: 10.1002/biot.201400041

Veldmann, K. H., Minges, H., Sewald, N., Lee, J. H., and Wendisch, V. F. (2019). Metabolic engineering of *Corynebacterium glutamicum* for the fermentative production of halogenated tryptophan. *J. Biotechnol.* 291, 7–16. doi: 10.1016/j.jbiotec.2018.12.008

Wendisch, V. F. (2003). Genome-wide expression analysis in *Corynebacterium glutamicum* using DNA microarrays. *J. Biotechnol.* 104, 273–285. doi: 10.1016/S0168-1656(03)00147-0

Wieschalka, S., Blombach, B., and Eikmanns, B. J. (2012). Engineering *Corynebacterium glutamicum* for the production of pyruvate. *Appl. Microbiol. Biotechnol.* 94, 449–459. doi: 10.1007/s00253-011-3843-9

Conflict of Interest: The authors declare that the research was conducted in the absence of any commercial or financial relationships that could be construed as a potential conflict of interest.

frontiers in Bioengineering and Biotechnology

ORIGINAL RESEARCH
published: 16 April 2021
doi: 10.3389/fbioe.2021.671321

L-Carnitine Production Through Biosensor-Guided Construction of the *Neurospora crassa* Biosynthesis Pathway in *Escherichia coli*

*Pierre Kugler[1], Marika Trumm[1], Marcel Frese[2] and Volker F. Wendisch[1]**

[1] Genetics of Prokaryotes, Faculty of Biology and CeBiTec, Bielefeld University, Bielefeld, Germany, [2] Department of Chemistry, Organic and Bioorganic Chemistry (OCIII), Bielefeld University, Bielefeld, Germany

L-Carnitine is a bioactive compound derived from L-lysine and *S*-adenosyl-L-methionine, which is closely associated with the transport of long-chain fatty acids in the intermediary metabolism of eukaryotes and sought after in the pharmaceutical, food, and feed industries. The L-carnitine biosynthesis pathway has not been observed in prokaryotes, and the use of eukaryotic microorganisms as natural L-carnitine producers lacks economic viability due to complex cultivation and low titers. While biotransformation processes based on petrochemical achiral precursors have been described for bacterial hosts, fermentative *de novo* synthesis has not been established although it holds the potential for a sustainable and economical one-pot process using renewable feedstocks. This study describes the metabolic engineering of *Escherichia coli* for L-carnitine production. L-carnitine biosynthesis enzymes from the fungus *Neurospora crassa* that were functionally active in *E. coli* were identified and applied individually or in cascades to assemble and optimize a four-step L-carnitine biosynthesis pathway in this host. Pathway performance was monitored by a transcription factor-based L-carnitine biosensor. The engineered *E. coli* strain produced L-carnitine from supplemented L-N^{ε}-trimethyllysine in a whole cell biotransformation, resulting in 15.9 μM carnitine found in the supernatant. Notably, this strain also produced 1.7 μM L-carnitine *de novo* from glycerol and ammonium as carbon and nitrogen sources through endogenous N^{ε}-trimethyllysine. This work provides a proof of concept for the *de novo* L-carnitine production in *E. coli*, which does not depend on petrochemical synthesis of achiral precursors, but makes use of renewable feedstocks instead. To the best of our knowledge, this is the first description of L-carnitine *de novo* synthesis using an engineered bacterium.

Keywords: carnitine, biosynthesis, biosensor, metabolic engineering, biosynthetic cascade, trimethyllysine

OPEN ACCESS

Edited by:
Yi-Rui Wu,
Shantou University, China

Reviewed by:
Xiaoyuan Wang,
Jiangnan University, China
Kequan Chen,
Nanjing Tech University, China

****Correspondence:***
Volker F. Wendisch
volker.wendisch@uni-bielefeld.de

Specialty section:
This article was submitted to Industrial Biotechnology, a section of the journal Frontiers in Bioengineering and Biotechnology

Received: *23 February 2021*
Accepted: *26 March 2021*
Published: *16 April 2021*

Citation:
Kugler P, Trumm M, Frese M and Wendisch VF (2021) L-Carnitine Production Through Biosensor-Guided Construction of the Neurospora crassa Biosynthesis Pathway in Escherichia coli. Front. Bioeng. Biotechnol. 9:671321. doi: 10.3389/fbioe.2021.671321

INTRODUCTION

L-Carnitine [(*R*)-3-hydroxy-4-trimethylaminobutyrate] is an essential compound in the intermediary metabolism of eukaryotes, which is involved in the transport of activated long-chain fatty acids and products of peroxisomal β-oxidation into the mitochondria for subsequent completion of β-oxidation (Vaz and Wanders, 2002). Only the L-isomer is physiologically

functional in fatty acid transport (Reuter and Evans, 2012), while the other is linked to inhibitory or other toxic effects in different organisms (Rebouche, 1977, 1983; Gross et al., 1986; Li J.M. et al., 2019). In humans, 75% of the L-carnitine requirement is covered by the diet, while the remaining 25% are synthesized endogenously (Longo et al., 2016). Carnitine deficiency can lead to a wide range of symptoms that weaken the body (Magoulas and El-Hattab, 2012; Longo et al., 2016). Carnitine can be used as dietary supplement for the treatment of this deficiency (Flanagan et al., 2010; El-Hattab and Scaglia, 2015), but also as feed additive to improve livestock performance (Rehman et al., 2017; Ringseis et al., 2018a,b; Li L. et al., 2019), and as L-carnitine or acyl-L-carnitine esters in further pharmaceutical applications (DiNicolantonio et al., 2013; Chen et al., 2014; Song et al., 2017; Parvanova et al., 2018; Veronese et al., 2018). It is also marketed as food additive and dietary supplement for improving athletic performance and weight management as positive effects on physical performance and weight loss under conditions with disorders have been observed (Fielding et al., 2018), while an improvement in healthy individuals or athletes is debated (Gnoni et al., 2020). The carnitine market of US$ ∼170 million in 2018 is expected to grow by 4.8% annually (Grand View Research, 2019; The Insight Partners, 2020).

Racemic D,L-carnitine can be produced chemically from cheap epichlorohydrin and trimethylamine (Kabat et al., 1997), but to obtain enantiomerically pure L-carnitine, either chiral resolution or stereospecific synthesis is required. These approaches are not environmentally friendly, due to the number of reactions, and the need to use chiral starting materials or chiral auxiliaries (Meyer and Robins, 2005; Bernal et al., 2007). Achiral precursors such as crotonobetaine (dehydrated D,L-carnitine), γ-butyrobetaine, and 3-dehydrocarnitine are converted in highly regio- and enantioselective biotransformations under mild conditions (Bernal et al., 2016). These processes use *Pseudomonas* sp., *Proteus* sp., or *Escherichia coli* (Naidu et al., 2000) and are characterized by a significant reduction in environmental impact, e.g., 89% less waste to be incinerated, 82% less waste water, and 76% less salts (Meyer and Robins, 2005). Fermentative processes hold the potential for *de novo* biosynthesis from renewable feedstocks and to abandon the petrochemical synthesis of precursors. The use of eukaryotic microorganisms as natural L-carnitine producers suffers from low titers and demanding cultivation conditions with complex media (Wargo and Meadows, 2015; Bernal et al., 2016). Metabolic engineering of established bacterial producers such as *E. coli* holds the potential to establish *de novo* L-carnitine production in fermentative one-pot processes.

Biosynthesis of L-carnitine in the filamentous fungus *Neurospora crassa* initiates with L-N^{ε}-trimethyllysine (TML) (Horne and Broquist, 1973; Kaufman and Broquist, 1977; Vaz and Wanders, 2002). In eukaryotes, TML is the product of lysosomal or proteasomal degradation of proteins such as calmodulin, myosin, actin, cytochrome c, and histones, which contain *N*-methylated lysine residues from post-translational modification (Strijbis et al., 2010). TML is converted to L-carnitine in four enzymatic steps (**Figure 1**), starting with the hydroxylation in β-position by the TML hydroxylase (TMLH; EC 1.14.11.8) to yield (2*S*,3*S*)-3-hydroxy-TML (HTML) (Sachan and Hoppel, 1980; Vaz et al., 2001; Al Temimi et al., 2016; Reddy et al., 2017). In the next step, HTML is cleaved into glycine and 4-trimethylaminobutyraldehyde (TMABA) by HTML aldolase (HTMLA; EC 4.1.2. "X"). Instead of an aldolase with strict HTML specificity, serine hydroxymethyltransferases (SHMT) (Hulse et al., 1978; Henderson et al., 1982) and threonine aldolases (Strijbis et al., 2009; Franken et al., 2015) show side activities as HTMLA. In the third step, the NAD^+-dependent TMABA dehydrogenase (TMABADH; EC 1.2.1.47) oxidizes TMABA to γ-butyrobetaine (γ-BB) as shown for *Pseudomonas* sp. 13CM (Hassan et al., 2008; Bari et al., 2013). Finally, stereoselective hydroxylation of γ-BB by γ-BB hydroxylase (γ-BBH; EC 1.14.11.1) yields L-carnitine. γ-BBH was not only found in mammals (Lindstedt, 1967; Lindstedt and Lindstedt, 1970), but also in the bacterium *Pseudomonas* sp. AK 1 (Lindstedt et al., 1967, 1970), where it is involved in utilization of γ-BB as the sole source of carbon and nitrogen for growth.

Transfer of the L-carnitine biosynthetic pathway from *N. crassa* to *Saccharomyces cerevisiae* suffered from low conversion of TML to L-carnitine (Franken et al., 2015). In a similar approach using different genes, production of L-carnitine from L-lysine in an *E. coli* whole cell biotransformation was described in a patent application (Kang et al., 2013). Discrepancies between these studies suggest that the *N. crassa* genes coding for γ-BBH gene and TMABADH have not been unequivocally identified (Kang et al., 2013; Franken et al., 2015), while genes encoding enzymes with TMLH and HTMLA activities are known.

In this study, the enzymes of the L-carnitine biosynthetic pathway from *N. crassa* and their corresponding genes were identified and functionally expressed in *E. coli*. This organism was chosen as production host because its natural interactions with L-carnitine are already well understood: It uses L-carnitine as compatible solute under hyperosmotic stress conditions and as terminal electron acceptor in anaerobic respiration yielding γ-BB (Seim et al., 1980; Wargo and Meadows, 2015). Uptake of L-carnitine is mediated by ATP-dependent ABC transport system ProU and to a lesser extent by ProP, a major facilitator superfamily (MFS) proton-metabolite symporter accepting proline, glycine betaine, stachydrine, pipecolic acid, ectoine, taurine, and L-carnitine (Verheul et al., 1998). Anaerobic respiration of L-carnitine involves the enzymes encoded in the divergent operons *caiTABCDE* and *fixABCX* (Jung and Kleber, 1991; Eichler et al., 1994; Preusser et al., 1999; Elssner et al., 2001; Jung et al., 2002; Bernal et al., 2007; Bracher et al., 2019; Kugler et al., 2020) that have been used in biotransformation processes of crotonobetaine or D-carnitine to L-carnitine (Castellar et al., 1998, 2001; Obón et al., 1999; Sevilla et al., 2005a,b; Bernal et al., 2007; Arense et al., 2013). We have recently developed a genetically encoded biosensor that responds in a dose-dependent manner to external L-carnitine in a concentration range of 0.1–100 μM by expression of the fluorescent reporter mVenus (Kugler et al., 2020). Its use to screen and score enzymes of L-carnitine biosynthesis in *E. coli* has been exemplarily shown for betaine:CoA ligases (Kugler et al., 2020). Here, this biosensor was applied to establish the L-carnitine biosynthetic pathway in

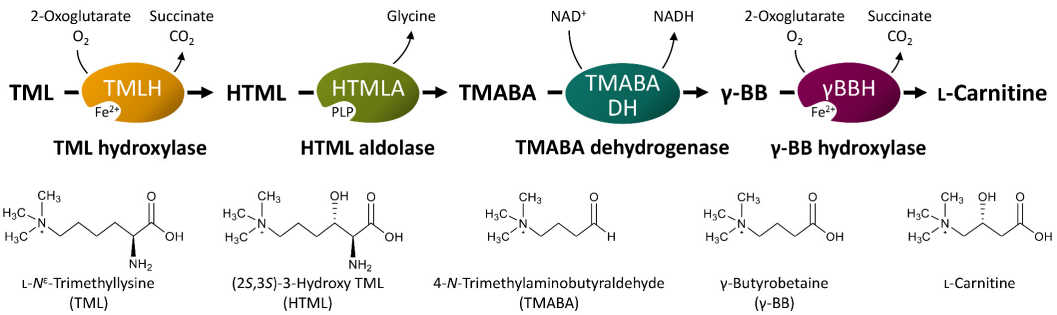

FIGURE 1 | Schematic illustration of L-carnitine synthesis from the precursor TML. PLP, pyridoxal 5′-phosphate; NAD^+, nicotinamide adenine dinucleotide (oxidized form); NADH, nicotinamide adenine dinucleotide (reduced form). Other abbreviated substances are written in full in the bottom of the figure. Modified from Strijbis et al. (2010).

E. coli. Besides one-pot biotransformation of TML to L-carnitine, L-carnitine could be produced without TML addition. To the best of our knowledge, this is the first fermentative *de novo* process for L-carnitine production.

MATERIALS AND METHODS

Bacterial Strains, Recombinant DNA Work, Media, and Growth Conditions

A complete list of the bacterial strains and plasmids is given in **Supplementary Table 2**. *E. coli* DH5α was used as a cloning host, for plasmid propagation, and as the expression host for the TMABADH enzyme assay and SDS-PAGE. For cloning purposes, cells were grown in lysogeny broth (LB) medium (10 g L^{-1} tryptone, 5 g L^{-1} yeast extract, and 10 g L^{-1} sodium chloride) at 37°C on a shaking incubator (shaking frequency: 180 min^{-1}, eccentricity: 25 mm). All media were supplemented with antibiotics where appropriate for selection: kanamycin (50 μg mL^{-1}), tetracycline (10 μg mL^{-1}), and chloramphenicol (25 μg mL^{-1}).

For each tested enzyme of the carnitine biosynthetic pathway from *N. crassa*, a synthetic gene was designed based on the amino acid sequence. The codon usage in these genes was optimized based on codon usage tables[1] (Nakamura, 2000) in a codon harmonization tool (Haupka, 2020). The DNA material of these artificial genes was ordered as gene synthesis from BioCat GmbH (Heidelberg, Germany). Artificial optimized 5′ untranslated regions (5′ UTRs) including the ribosome binding sites (RBS) were generated for each gene and vector combination with the online RBS calculator of the Salis Laboratory of Penn State University[2] and were introduced *via* the oligonucleotides during cloning.

The standard molecular genetic techniques were performed as described in detail elsewhere (Green et al., 2012). Genes were amplified by PCR using the respective primers given in **Supplementary Table 3**. The oligonucleotides were supplied by Metabion GmbH (Planegg/Steinkirchen, Germany), and the PCR kit containing ALLin HiFi DNA Polymerase was purchased from highQu GmbH (Kraichtal, Germany) and used according to the manufacturer's instructions. Plasmids were digested using restriction enzymes supplied by Thermo Fisher Scientific Inc. (Waltham, MA, United States) which were used according to the manufacturer's protocols. Insertion of the amplified PCR products was done with Gibson assembly (Gibson et al., 2009). New vectors were confirmed by insert sequencing. The cloning of the vectors is described in detail in the **Supplementary Material**.

Biosensor Experiments

The biosensor experiments were conducted as described earlier (Kugler et al., 2020). In short, M9 minimal medium with 24 g L^{-1} glycerol as the carbon source and supplemented antibiotics as stated above and 0.1 mM Isopropyl-β-D-thiogalactopyranosid (IPTG) was used for the cultivation at 37°C in 48-well microtiter FlowerPlates with the Biolector cultivation system (m2p-laboratories GmbH, Baesweiler, Germany) (Funke et al., 2009; Kensy et al., 2009). The medium was inoculated to an optical density at 600 nm (OD_{600}) of 0.1 from precultures that were made in the M9 medium supplemented with 1% (v/v) LB medium. The formation of biomass was recorded as well as the fluorescence of the yellow fluorescent protein mVenus NB. The fluorescence signal was divided by the biomass signal to obtain the normalized fluorescence signal. The maximum normalized fluorescence signal observed during the whole cultivation was used for the evaluation. Unless stated otherwise, the maximum normalized fluorescence was detected between the middle and end of the exponential growth phase of the culture and for the controls (i.e., empty vector or supplemented water) in the stationary phase.

Assay of TMABA Dehydrogenase Activity in *E. coli* Crude Extracts

Escherichia coli DH5α was used as host for the expression of the potential TMABA dehydrogenases. The enzymes were expressed from the pECXT99A-derived vectors containing the genes TMABADH.1S, TMABADH.1, or TMABADH.2. The cultivation was performed in 500 mL baffled shake flasks with 50 mL LB medium supplemented with antibiotics as stated above on a shaking incubator (37°C, shaking frequency: 180 min^{-1}, eccentricity: 25 mm) with a starting OD_{600} of 0.1. At an OD_{600}

[1]www.kazusa.or.jp/codon/
[2]https://salislab.net/software/

of 0.6–0.7, expression was induced with 1 mM IPTG and the culture was continued up to an OD_{600} of ∼3.0 where the cells were harvested at the end of the exponential growth phase by centrifugation (10 min, 3,220 × *g*, 4°C). The supernatant was discarded, and the cell pellets were stored at −80°C until further use.

Frozen cell pellets were thawed on ice, resuspended in 1.8 mL lysis buffer [50 mM potassium phosphate buffer, 1 mM dithiothreitol (DTT); pH 7.5], and sonicated for 3 min on ice water (UP200S, Hielscher Ultrasonics GmbH, Teltow, Germany; amplitude 60%, cycle 0.5 s). The cell debris was removed by centrifugation (45 min, 28,000 × *g*, 4°C), and the extracts were stored on ice until use in the enzyme assay and for determination of protein concentration with Bradford Reagent (Sigma-Aldrich, St. Louis, MO, United States), using bovine serum albumin as the standard.

TMABA dehydrogenase activity was determined as described before (Bari et al., 2013) with slight modifications. The reaction was followed by measuring the formation of 1 mol NADH per consumed mol of TMABA photometrically at 340 nm (ε_{NADH} = 6,220 M^{-1} cm^{-1}, d = 1 cm, 30°C). The reaction mixture of 1 mL consisted of 150 mM glycine-NaOH buffer (pH 9.5), 2 mM NAD^+, 0.4 mM TMABA iodide, and 250 μL crude extract. The basal absorption change was followed for 3 min and then the reaction was initialized by the addition of TMABA. Where necessary, the crude extract was diluted with the lysis buffer to achieve a rate of absorption change during the measurement in the range of 0.03–0.15 per min.

Protein Gel Analysis

The crude extracts from the TMABA dehydrogenase activity assay were further analyzed by sodium dodecyl sulfate polyacrylamide gel electrophoresis (SDS-PAGE) as described elsewhere (Green et al., 2012) using the Mini-PROTEAN Tetra Cell #1658000EDU System from Bio-Rad Laboratories Inc. (Hercules, CA, United States). The amount of protein used per sample was 12 μg, and the PageRuler Prestained Protein Ladder 10–180 kDa (Thermo Fisher Scientific Inc., Waltham, MA, United States) was used as molecular weight marker.

Carnitine Production Experiment With Recombinant *E. coli* Expressing the Carnitine Biosynthetic Pathway From *N. crassa*

The cultivation was done in 100 mL baffled shake flasks with 10 mL modified M9 medium with 30 g L^{-1} glycerol as carbon source and with antibiotics as described above. Nitrogen is the limiting factor for biomass formation in the composition of the M9 medium, which is why NH_4Cl was supplemented in this experiment to double the concentration to 2 g L^{-1} to reach a higher biomass in this cultivation. The cultures were inoculated to an OD_{600} of 0.1 from precultures that were made in standard M9 medium supplemented with 1% (v/v) LB medium and placed in a shaking incubator (37°C, 180 min^{-1} shaking frequency, 25 mm eccentricity). At an OD_{600} of 0.5–0.6, expression was induced with 0.1 mM IPTG and the substrate TML was added at a concentration of 1 mM. Cultivation was continued for 48 h, and then a 2 mL sample was drawn from which the cell pellet and supernatant were obtained by centrifugation (10 min, 12,000 × *g*, 4°C). After washing the cells with saline (9 g L^{-1} NaCl), the cells were pelleted again by centrifugation (10 min, 12,000 × *g*, 4°C) and then all samples were frozen at −20°C until analysis *via* LC-MS.

LC-MS Measurement

The supernatant samples were thawed on ice and then centrifuged (10 min, 12,000 × *g*, 4°C) to separate possible precipitates from freezing. Subsequently, the undiluted samples were analyzed by LC-MS. The cell pellets were resuspended in 800 μL of ice-cold 80% (v/v) methanol, mixed with 0.35 g of 0.2 mm zirconia-silica beads (BioSpec Products Inc., Bartlesville, OK, United States) in 1.5 mL microtubes, and cooled on ice. The suspensions were placed in the Digital Disruptor Genie Cell Disruptor (Scientific Industries Inc., Bohemia, NY, United States), and the cells were disrupted for 3 min at full speed. Next, cell debris and beads were separated by centrifugation (10 min, 12,000 × *g*, 4°C). The methanol was evaporated from 600 μL of the resulting supernatant in a vacuum concentrator (Eppendorf AG, Hamburg, Germany) for 4 h at 45°C. The residue was re-dissolved in 120 μL water and analyzed by LC-MS. For the LC-MS measurement, an Agilent 6220 TOF-MS with a Dual ESI-source and a 1200 HPLC system (Agilent Technologies, Inc., Santa Clara, CA, United States) with a Hypersil Gold C18 column (1.9 μm, 50 × 2.1 mm; Thermo Fisher Scientific Inc., Waltham, MA, United States) was used. Solvent A consisted of 94.9% (v/v) water, 5% (v/v) acetonitrile, and 0.1% (v/v) formic acid, and solvent B was composed of 5% (v/v) water, 94.9% (v/v) acetonitrile, and 0.1% (v/v) formic acid. A gradient was started at 0% B when 5 μL sample was injected and increased to 98% B over 11 min, went back to 0% B in 0.5 min, which was held for 3.5 min to a total run time of 15 min. The flow rate was 300 μL min^{-1}, and column oven temperature was at 40°C. The extended dynamic range mode was used with a Dual-ESI source, operating with a spray voltage of 2.5 kV. The data were analyzed with MassHunter Workstation Software Version B.07.00 (Agilent Technologies, Inc., Santa Clara, CA, United States). Carnitine was identified in an accurate mass measurement from its mass to charge ratio (*m/z*) of 162.11267 (deviation <5 ppm to calculated *m/z* of 162.11247). The mass spectrum of L-carnitine is shown in **Supplementary Figure 2**. The quantitative analysis was performed using a set of L-carnitine standard samples with the concentrations (in μM): 0, 1.56, 3.13 6.25, 12.5, 25, and 50. From the resulting total ion count (TIC), a regression line was calculated (R^2 = 0.998), which was used as the calibration curve. Intracellular carnitine concentrations were calculated from the carnitine concentration determined for the cell pellet extract and the total cell volume of the cell pellet, which was calculated from the final OD_{600} of the 2 mL samples at 48 h fermentation and the OD specific total cell volume for starved *E. coli* cells in the stationary phase of 3.3 μL mL^{-1} $OD_{600}{}^{-1}$ (Volkmer and Heinemann, 2011).

Analytical Quantification of Glycerol in the Carnitine Production Experiment

Samples were drawn at 24 h and 48 h cultivation time. The supernatant was collected by centrifugation (10 min, 12,000 × *g*, 4°C) and frozen at −20°C until analysis *via* HPLC. For analysis, the samples were thawed on ice and then centrifuged (10 min, 12,000 × *g*, 4°C) to separate possible precipitates from freezing. Subsequently, the undiluted samples were analyzed on an HPLC system (1200 series, Agilent Technologies Deutschland GmbH, Böblingen, Germany) with an organic acid resin column (300 mm × 8 mm) and the corresponding pre-column (40 mm × 8 mm) (Chromatographie-Service GmbH, Langerwehe, Germany) heated to 60°C. The mobile phase was 5 mM sulfuric acid in water (Milli-Q grade) with an isocratic flow rate of 0.8 mL min^{-1}. A refractive index detector was used for molecule detection. A calibration curve (R^2 = 0.999) was generated from glycerol standards with the concentrations (in g L^{-1}): 1, 2, 4, 8, 16, and 32.

Reagents

Unless specified, all chemical standard reagents were purchased in the highest grade available from Sigma-Aldrich (St. Louis, MO, United States) and Carl Roth GmbH + Co., KG (Karlsruhe, Germany). L-N^{ε} -trimethyllysine was purchased from Glentham Life Sciences Ltd. (Corsham, United Kingdom), and L-carnitine and γ-butyrobetaine were ordered at Sigma-Aldrich (St. Louis, MO, United States). The TMABA iodide was prepared from 4-aminobutyraldehyde diethyl acetal (Acros Organics B.V.B.A, Fair Lawn, NJ, United States) as described in the **Supplementary Material.**

RESULTS

Selection and Cloning of the L-Carnitine Biosynthetic Pathway Genes From *Neurospora crassa*

The selection of the potential enzymes for the L-carnitine biosynthetic pathway in this study was based on two sets of *N. crassa* genes that were previously considered for a transfer of the pathway to heterologous hosts (Kang et al., 2013; Franken et al., 2015). An overview of the enzymes and their respective genes used in this study is given for each step in **Supplementary Table 1**. Both sets share the enzymes for the first two steps (TMLH and HTMLA). The TMLH has been previously cloned and confirmed in *S. cerevisiae* (Swiegers et al., 2002), and for the HTMLA, the gene of the *N. crassa* SHMT was selected, as it additionally possesses aldolase activity (Kruschwitz et al., 1993; Franken et al., 2015). In case of the TMABADH, a third variant (TMABADH.1) was tested here in addition to the versions TMABADH.1S (Kang et al., 2013) and TMABADH.2 (Franken et al., 2015). Both TMABADH.1S and TMABADH.1 are based on the ORF NCU00378; however, TMABADH.1 (549 AA; RefSeq: XP_957264.2) is longer than TMABADH.1S (495 AA; XP_957264.1), which results from a reannotation extending the ORF to a start codon 153 bp upstream. For γ-BBH, two different enzymes termed γBBH.1 (Kang et al., 2013) and γBBH.2 (Franken et al., 2015) were selected from the literature and chosen for this study.

A codon-harmonized gene and corresponding optimized 5′ UTRs including the RBS were designed for each variant using a codon harmonization tool (Haupka, 2020) and codon usage tables[3] (Nakamura, 2000), and the online RBS calculator of the Salis Laboratory of Penn State University (see text footnote 1).

Screening for Functional γ-Butyrobetaine Hydroxylases

For the screening of the γ-butyrobetaine hydroxylases, the genes γBBH.1 and γBBH.2 (**Supplementary Table 1**) were cloned into the expression plasmid pECXT99A. To score γ-butyrobetaine hydroxylase activity, an L-carnitine biosensor strain was used, and fluorescence was measured upon extracellular addition of γ-BB. Specifically, the enzymes were tested for L-carnitine formation from γ-BB in the L-carnitine biosensor strain *E. coli* BW25113 Δ*cai-fix* (pGP2-Sensor1-*caiCD*) (see **Supplementary Table 2**), which was transformed with pECXT99A-γBBH.1, pECXT99A-γBBH.2, or pECXT99A as empty vector control. A microbioreactor cultivation was performed using the Biolector system (m2p-laboratories GmbH, Baesweiler, Germany) (Funke et al., 2009; Kensy et al., 2009) with the resulting strains in M9 minimal medium supplemented with 100 μM γ-BB or water as control and the maximum normalized mVenus fluorescence was measured (**Figure 2**). M9 minimal medium was selected for all cultivation experiments because it significantly increases the utility and sensitivity of the biosensor used (Kugler et al., 2020).

As expected, no L-carnitine biosensor fluorescence signal was measured in the empty vector control by the addition of γ-BB. While γBBH.1 showed no activity when γ-BB was supplemented, an L-carnitine biosensor fluorescence signal could be detected for γBBH.2 upon addition of γ-BB. Thus, γBBH.2 was confirmed in this screening as functionally active γ-butyrobetaine hydroxylase and used for further work on the L-carnitine biosynthetic pathway.

Screening for Functional TMABA Dehydrogenases

An *in vitro* photometric enzyme assay based on cell extracts was chosen for screening TMABA dehydrogenase activity, as it is easily feasible due to the co-conversion of NAD^+ to NADH in the TMABADH reaction (**Figure 3**). A screening with the biosensor as for the γ-BBH was not chosen because external supplementation of aldehydes can have toxic effects on the cells due to their high reactivity and it is uncertain that the aldehyde is taken up by the cells (Kunjapur and Prather, 2015). *E. coli* DH5α was transformed with pECXT99A-based plasmids harboring the dehydrogenases TMABADH.1S, TMABDH.1, or TMABADH.2 (**Supplementary Table 1**) and with pECXT99A as the empty vector control. Cell extracts were prepared from the induced strains and examined in an enzyme assay in which the reaction was photometrically monitored by measuring the formation of NADH (**Figure 3**).

[3]www.kazusa.or.jp/codon/

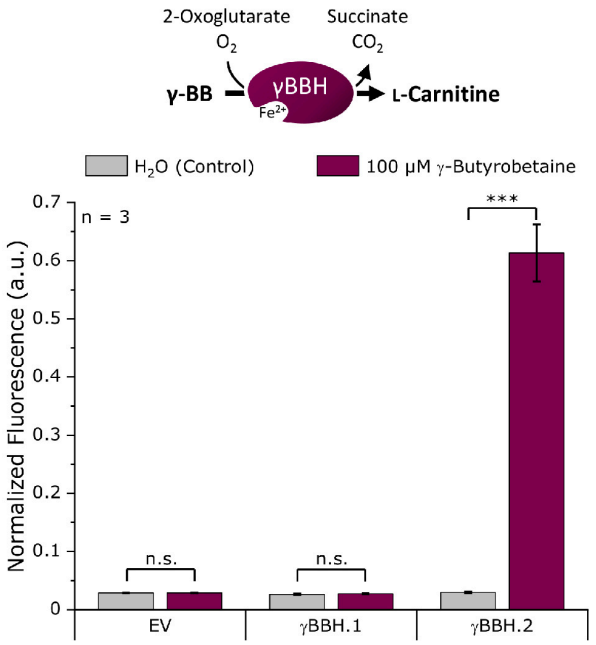

FIGURE 2 | Biosensor screening of potential γ-butyrobetaine hydroxylases from *N. crassa*. The artificial genes γBBH.1 and γBBH.2 derived from the ORFs NCU02196 and NCU12046, respectively, were cloned into pECXT99A and tested in the L-carnitine biosensor strain *E. coli* Δ*cai-fix* (pGP2-Sensor1-*caiCD*). The empty vector (EV) of pECXT99A was used as a control. The maximum normalized fluorescence signal observed during the cultivation process with 100 µM γ-butyrobetaine or water as the control is shown. Error bars indicate the standard deviation of the mean of three replicates. Three asterisks (***) indicate a p-value ≤ 0.001 in a student's t-test; n.s., not significant.

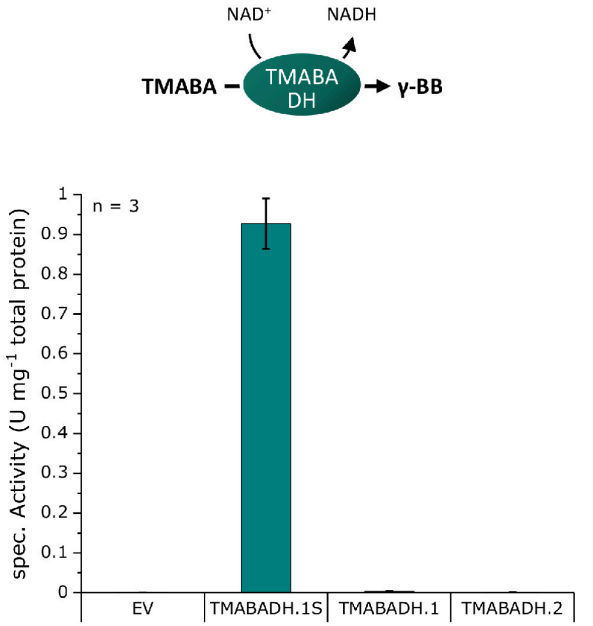

FIGURE 3 | TMABADH activities in crude extracts of *E. coli* DH5α transformed with pECXT99A derivatives expressing potential TMABADH from *N. crassa*. TMABADH.1S and TMABADH.1 were derived from NCU00378, and TMABADH.2 was derived from NCU03415. pECXT99A was used as the empty vector control (EV). Means of three replicates are shown. Error bars were calculated by error analysis from the standard deviations of the enzyme assays and Bradford measurements.

As expected, no activity could be detected in the empty vector control, and neither TMABADH.1 nor TMABADH.2 showed activity. By contrast, TMABA dehydrogenase activity was revealed for TMABADH.1S (**Figure 3**). Since TMABADH.1 and TMABADH.1S share a great similarity on the amino acid level, it was speculated whether the expression of TMABADH.1 was affected by the N-terminal modification compared to TMABADH.1S. To investigate this, an SDS-PAGE was performed from the same cell extracts. Indeed, protein abundance of TMABADH.1 was significantly lower as compared to TMABADH.1S and TMABADH.2 (**Supplementary Figure 1**). Since TMABADH.1S could be expressed well and showed about 0.9 U mg^{-1} activity, it was selected for further work on the carnitine biosynthetic pathway.

Assembly of the L-Carnitine Biosynthetic Pathway

After efficient enzymes for the last and penultimate step of the L-carnitine biosynthetic pathway had been identified, enzymes for the first two steps were selected: TML hydroxylase and an HTML aldolase (**Supplementary Table 1**). With the biosensor as a read-out tool for L-carnitine formation, the pathway was gradually assembled in the biosensor strain and the formation of L-carnitine from externally supplemented TML was studied. Additionally, this experimental setup was used to investigate the TMABADH variants *in vivo* in combination with the other pathway enzymes. The L-carnitine biosensor strain *E. coli* BW25113 Δ*cai-fix* (pGP2-Sensor1-*caiCD*) was transformed with different plasmid combinations to assemble the full pathway. The TMABADH variants were included to validate the results from the *in vitro* assay in an *in vivo* biolector cultivation experiment. M9 minimal medium supplemented with 100 µM TML or water as control was used and the maximum normalized mVenus fluorescence was measured (**Figure 4**). Individual expression of γBBH.2 or TMLH (combinations A and B, respectively) did not result in an L-carnitine biosensor signal upon addition of TML as precursor. Cascading of all four enzymes *in vivo* gave a strong L-carnitine biosensor signal (combination H) indicating that the pathway operated as anticipated.

Surprisingly, cascades with TMLH, but lacking one or more (active) enzymes (combination C, D, E, F, and G) also showed L-carnitine biosensor signal output, albeit it was significantly lower than that of the complete cascade (combination H). This suggests that enzymes present in the *E. coli* host strain are active in the conversion of HTML to γ-BB. However, currently their identities remain unknown. For further work on the pathway, the cascade TML hydroxylase/HTML aldolase/TMABADH.1S/γBBH.2 (combination H) was chosen.

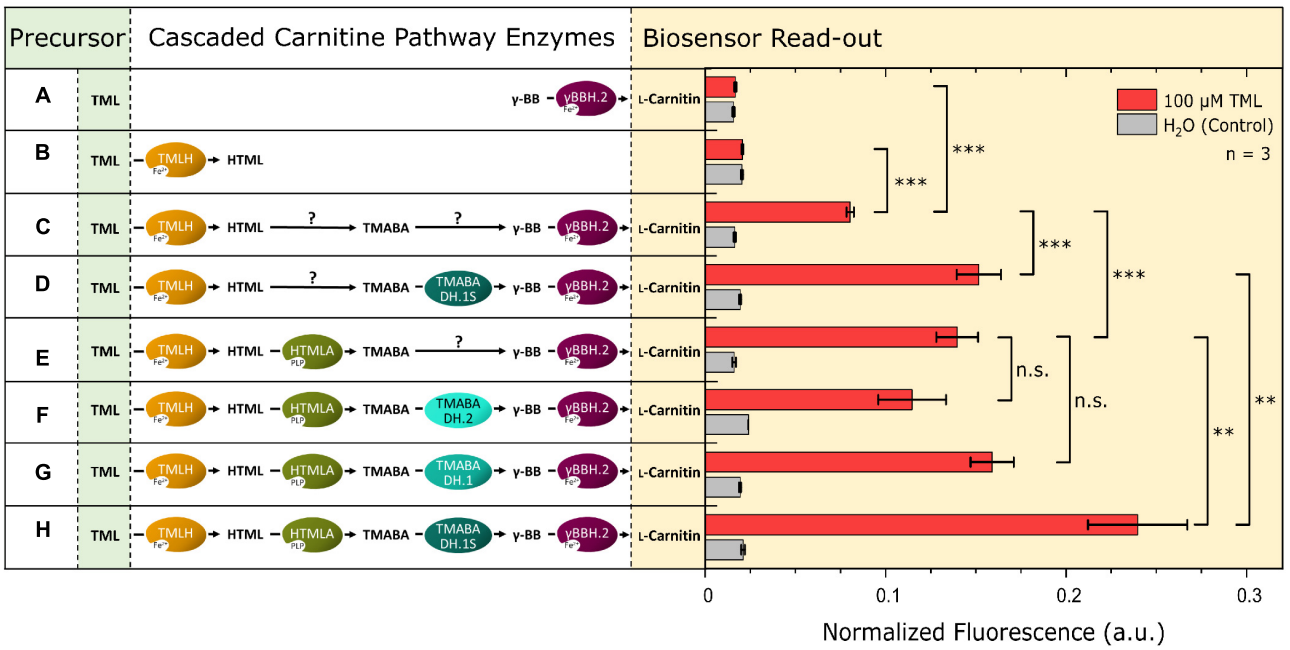

FIGURE 4 | Assembly of the four steps of the L-carnitine biosynthetic pathway of *N. crassa* in *E. coli*. The expression of a gene encoding a cascaded enzyme is depicted by an oval on the left side. Arrows marked with a "?" indicate that the reaction may proceed *via* endogenous enzymes although no dedicated gene was overexpressed. Plasmid pPLib3 was used for the individual expression of TMLH (pPLib3-TMLH; Combinations B, C, and D) and together with HTMLA as synthetic operon (pPLib3-TMLH-HTMLA; Combinations E, F, G, and H) and as empty vector control (pPLib3; Combination A). pECXT99A was used to express γBBH.2 individually (pECXT99A-γBBH.2; Combinations A, C, and E) or in a synthetic operon with one of the TMABADH variants (pPLib3-TMABADH.1S-γBBH.2; Combinations D and H, pPLib3-TMABADH.1-γBBH.2; Combination G, or pPLib3-TMABADH.2-γBBH.2; Combination F) and as empty vector control (Combination B). The shown enzyme combinations were tested in the L-carnitine biosensor strain *E. coli* Δ*cai-fix* (pGP2-Sensor1-*caiCD*). The maximum normalized fluorescence signal observed during the cultivation process with 100 µM TML (red columns) or water (gray columns) as the control is shown. Error bars indicate the standard deviation of the mean of three replicates. Three asterisks (***) indicate a *p*-value ≤ 0.001 in a student's *t*-test, **p-value ≤ 0.01, and n.s., not significant.

Improving the L-Carnitine Biosynthesis Pathway for *de novo* Production by *E. coli*

After having selected the enzymes for the L-carnitine biosynthetic pathway, expression of the four genes was optimized by combining the individual genes in a single plasmid as a synthetic operon. The plasmid pTrc99A was used as backbone and the previously identified genes for the pathway (TMLH, HTMLA, TMABADH.1S, and γBBH.2; **Figure 4**, combination H) were cloned with optimized 5′UTRs in a single synthetic operon. The gene order was the same as that of the reaction steps, and the constructed plasmid for conversion of TML to L-carnitine was called pTrc99A-TML2Car. The plasmid was transformed in the L-carnitine biosensor strain *E. coli* BW25113 Δ*cai-fix* (pGP2-Sensor1-*caiCD*) and tested in parallel with pTrc99A as empty vector control in a biolector experiment. The medium was supplemented with either 100 µM TML or water as control, and the normalized mVenus fluorescence was monitored over the cultivation time (**Figure 5A**). In the strain harboring the L-carnitine biosynthetic pathway (labeled TML2Car), the supplementation of 100 µM TML resulted in a fluorescence response of the L-carnitine biosensor. The maximum signal (**Figure 5B**) was more than twofold higher than the signal previously measured for the pathway when its genes were expressed from two separate plasmids (**Figure 4**, Combination H). Interestingly, strain TML2Car showed a significantly increased biosensor signal compared to the empty vector strain even when no TML was supplemented (**Figure 5B**, H_2O control). This may indicate *de novo* L-carnitine formation from endogenous TML. In contrast to the measurement with supplemented TML, the maximum normalized fluorescence was detected in the stationary phase and not at the end of the exponential growth phase (**Figure 5A**). The origin of TML in the *E. coli* host is unknown. While interesting from a physiological point of view, it was not required for the L-carnitine biosynthetic cascade developed here.

LC-MS Analysis of L-Carnitine Production by Recombinant *E. coli* Expressing the L-Carnitine Biosynthetic Pathway from *N. crassa*

The heterologous expression of the genes for the full L-carnitine biosynthesis cascade by the plasmid pTrc99A-TML2Car revealed L-carnitine production not only from the supplemented precursor TML, but also without it, providing evidence of *de novo* L-carnitine biosynthesis (**Figure 5**). To further substantiate these results, L-carnitine formation was studied in a shake flask

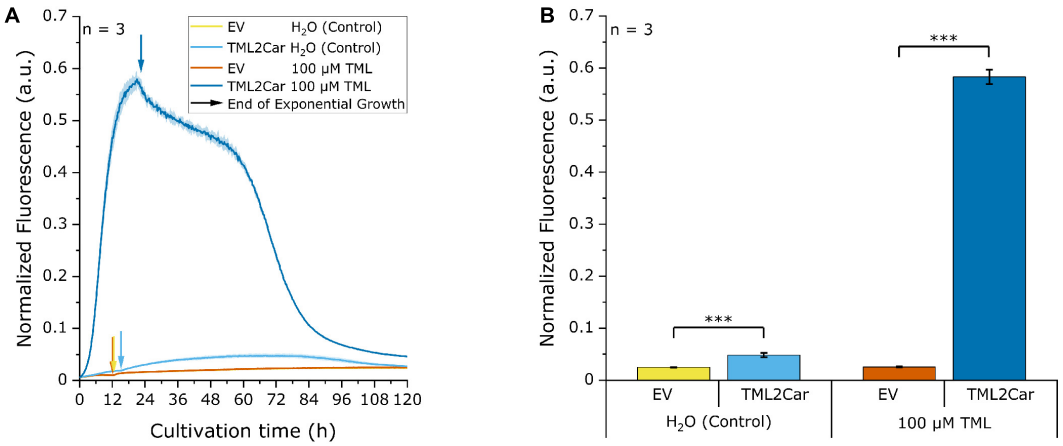

FIGURE 5 | Biosensor experiment with the synthetic L-carnitine biosynthesis pathway operon. The pathway genes were cloned in the order of the respective reaction steps into pECXT99A resulting in plasmid pECXT99A-TML2Car and tested in the L-carnitine biosensor strain *E. coli* Δ*cai-fix* (pGP2-Sensor1-*caiCD*). The empty vector (EV) of pTrc99A was used as a control. In the cultivation, either 100 μM TML was supplemented, or water was used as control. **(A)** Development of the normalized fluorescence signal over the cultivation process. The yellow (EV, H_2O) and orange lines (EV, 100 μM TML) are largely overlapping. The end of the exponential growth phase and transition to the stationary growth phase is marked with arrows for each condition. **(B)** Analogous to the previous readouts, the maximum normalized fluorescence signal for each cultivation was extracted from **(A)** and analyzed for significance of values between TML2Car and the respective EV control. Error bars indicate the standard deviation of the mean of three replicates. Three asterisks (***) indicate a *p*-value ≤ 0.001 in a student's *t*-test.

production experiment, and extracellular and intracellular L-carnitine concentrations were analyzed by LC-MS. The strains were similar to those used in the previous experiment but lacked the biosensor plasmid. *E. coli* strains BW25113 Δ*cai-fix* (pTrc99A-TML2Car) and empty vector control BW25113 Δ*cai-fix* (pTrc99A) were cultivated for 48 h in modified M9 minimal medium with increased levels of glycerol and ammonium as carbon and nitrogen sources and with and without supplementation of 1 mM TML. LB or another complex medium was not used to keep the cultivation comparable to the biosensor experiments and to avoid potential TML and carnitine sources in the medium, e.g., yeast extract. The growth and carbon source consumption were followed over the cultivation time (**Figure 6A**). The EV strain grew slightly faster with a maximum growth rate of 0.52 h^{-1} and an average final OD_{600} of 17.3, whereas the TML2Car strain grew at a rate of 0.46 h^{-1} to an average OD_{600} of 15.3 at the end of the fermentation after 48 h, with all strains converting ∼50% of the provided carbon source glycerol.

The supernatant and cells pellets were analyzed by LC-MS, and the extracellular and intracellular L-carnitine concentrations were determined (**Figure 6B**). The mass of L-carnitine (*m/z* ratio 162.11247) could be scored in the supernatants and cells of the strain expressing the L-carnitine biosynthetic pathway (labeled TML2Car), but not in the empty vector control strain. An extracellular concentration of 1.7 μM was produced without supplementation of TML. When 1 mM of the precursor was supplemented, 15.9 μM L-carnitine could be found in the supernatant (1.6% molar yield as judged by the L-carnitine and TML concentrations in the culture medium). The intracellular L-carnitine concentrations were similar to the supernatants but slightly higher.

DISCUSSION

Implementing a cascade of enzymes from *N. crassa* into *E. coli* enabled biotransformation of TML to L-carnitine as demonstrated using a genetically encoded L-carnitine biosensor and by LC-MS analysis. Moreover, the metabolically engineered *E. coli* strain enabled *de novo* production of L-carnitine from a mineral salts medium with glycerol and ammonium as carbon and nitrogen sources.

The ability of *E. coli* to synthesize sufficient TML for *de novo* production of L-carnitine came as a surprise since *E. coli* synthesizes TML to a much lesser extent than eukaryotic cells (Klagsbrun and Furano, 1975; Zhang et al., 2018). Methyltransferase PrmA methylates two lysyl residues of protein L11 from the large ribosomal subunit (Colson et al., 1979; Vanet et al., 1994) and free TML accumulates upon degradation of methylated protein L11 similar to TML release in eukaryotes (Vaz and Wanders, 2002). Our observation of accumulation of L-carnitine in the stationary phase is consistent with release of TML by protein degradation, which primarily occurs in this growth phase. Alternatively, it is possible that PrmA methylates free lysine to free TML as a side reaction as demonstrated for the RuBisCo large subunit *N*-methyltransferase (RBCMT) from *Pisum sativum* (Trievel et al., 2003).

Endogenous enzymes of *E. coli* complemented the four-step pathway when only TMLH and γ-BBH were provided (**Figure 4**; Combination C), thus, enzymes with (side) activities as HTML aldolase and TMABA dehydrogenase exist in *E. coli*. The low-specificity L-threonine aldolase LtaE, which cleaves several L-3-hydroxy-α-amino acids, like HTML, to glycine and a corresponding aldehyde and which may accommodate molecules larger than L-threonine in its large substrate binding pocket (di Salvo et al., 2014), may exhibit side activity as HTML

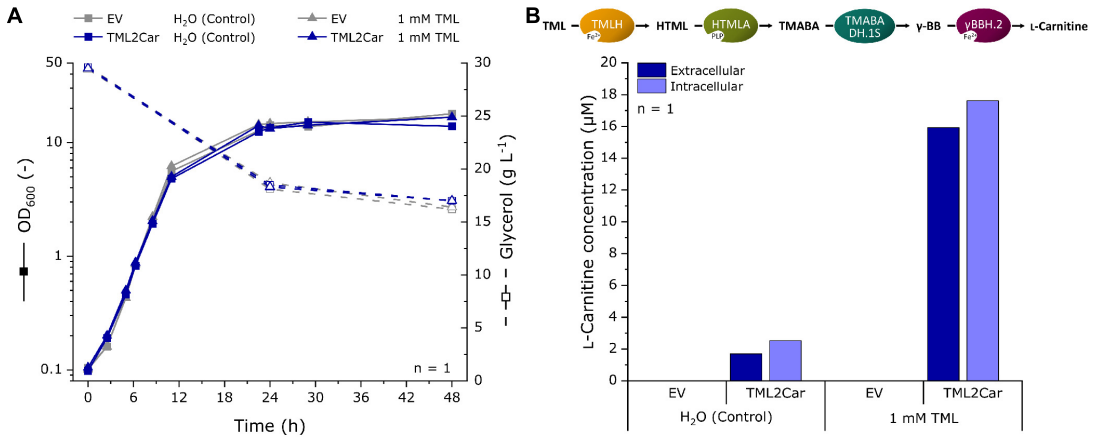

FIGURE 6 | Fermentation for L-carnitine production in modified M9 minimal medium with supplementation of 1 mM TML or water as a control using recombinant *E. coli* expressing the L-carnitine biosynthetic pathway from *N. crassa.* The pathway was expressed in *E. coli* BW25113 Δ*cai-fix* from plasmid pTrc99A-TML2Car. The empty vector (EV) pTrc99A was used as control. **(A)** Growth curve and residual glycerol concentrations of the fermentation experiment. **(B)** LC-MS analysis of the extracellular and intracellular L-carnitine concentration at the end of the cultivation after 48 h. L-carnitine was identified by its mass to charge ratio (*m/z*) of 162.11247. The detection limit was 0.5 µM. Intracellular concentrations were determined from the L-carnitine concentration in cell pellet extracts and the calculated total cell volume of the pellet.

aldolase. Alternatively, this activity may be catalyzed by *E. coli*'s SHMT GlyA, which shares 48% amino acid identity with the *N. crassa* SHMT that was used in this study (Schirch et al., 1985). In the case of TMABA dehydrogenase, numerous aldehyde dehydrogenases native to *E. coli* may possess this side activity (Sophos and Vasiliou, 2003). The most likely candidates among them may be γ-aminobutyraldehyde dehydrogenase PatD that is active with unmethylated TMABA (γ-aminobutyraldehyde) or with betaine aldehyde (Gruez et al., 2004; Samsonova et al., 2005) and PuuC, a non-specific aldehyde dehydrogenase that oxidizes all aldehydes in putrescine catabolism including γ-aminobutyraldehyde (Schneider and Reitzer, 2012). It remains to be shown if overexpression of the genes for these enzymes is beneficial for *de novo* production of L-carnitine since accumulation of intermediates in the conversion of TML to L-carnitine was not observed.

The *E. coli* strain constructed here produced 1.7 µM L-carnitine *de novo,* which is fourfold higher than by biotransformation from 100 µM supplemented TML by recombinant *S. cerevisiae* (Franken et al., 2015). However, our finding that addition of 1 mM TML to the *E. coli* strain constructed here improved L-carnitine production about 10-fold (1.7 µM as compared to around 16 µM) suggested that the supply of the precursor TML may limit *de novo* production. It remains to be shown if overexpression of endogenous *prmA* or heterologous expression of the RBCMT gene from *P. sativum* increases *de novo* production of L-carnitine by the *E. coli* strain constructed here. Alternatively, a *bona fide* L-lysine methyltransferase (K-NMT) yielding TML may be used. Such an enzyme has been reported for *N. crassa* (Borum and Broquist, 1977). The gene NCU03826 that was speculated to encode K-NMT in a patent application (Kang et al., 2013) did not result in a biosensor response that would indicate improved L-carnitine levels and the supplementation of lysine and methionine as precursors did not change this outcome (data not shown). Consistent with this finding, NCU03826 did not function as K-NMT in the *S. cerevisiae* strain (Franken et al., 2015). Thus, the gene for a *bona fide* K-NMT remains elusive.

Metabolic engineering to improve provision of the precursor metabolites L-lysine and *S*-adenosyL-methionine (SAM) may increase *de novo* production of L-carnitine by the *E. coli* strain constructed here. Strategies to overproduce L-lysine by *E. coli* are well established (Wendisch, 2020) and an *E. coli* strain overproducing L-lysine to a titer of 194 g L^{-1} from glucose and ammonium has recently been described (Ye et al., 2020). Regeneration of SAM, the major co-substrate for methyltransferases, using the renewable feedstock methanol as source of the methyl group proved very efficient in *E. coli* (Okano et al., 2020). Enzyme engineering of *E. coli* SAM synthetase to reduce product inhibition and increase catalytic activity is a complementary strategy (Wang et al., 2019).

The L-carnitine biosensor fluorescence signal suggested high conversion of L-carnitine from intracellular TML (**Figure 5B**) as values were comparable to direct L-carnitine supplementation (Kugler et al., 2020). However, only low L-carnitine concentrations were found intra- and extracellularly (**Figure 6B**), suggesting that the biosensor is sensitive to low intracellular L-carnitine levels and that the export of L-carnitine out of the *E. coli* cell may also limit biotransformation and its *de novo* production. Consistent with this hypothesis, transport limitations have also been observed for biotransformation processes converting achiral precursors such as crotonobetaine to L-carnitine using recombinant *E. coli* strains (Bernal et al., 2007). For biotransformations, this can be overcome by cell permeabilization, for example, with polyethylenimine (Cánovas et al., 2005; Bernal et al., 2007). However, strategies for production of L-carnitine *de novo* have to maintain the

cell's integrity. Deletion of the gene for Braun's lipoprotein from the outer membrane of *E. coli* improved L-carnitine production from crotonobetaine without affecting cell growth and metabolism (Bernal et al., 2007; Ni et al., 2007). To prevent re-uptake of L-carnitine secreted from the *E. coli* cell, the genes coding for L-carnitine uptake systems ProU and ProP were deleted (Verheul et al., 1998; Sevilla et al., 2005a). Engineering L-carnitine export was possible for biotransformation, but is not suitable for *de novo* production. This is due to the fact that CaiT is an antiporter catalyzing exchange of intracellular and extracellular trimethylammonium compounds such as L-carnitine, crotonobetaine, and γ-butyrobetaine, while it does not catalyze uniport of L-carnitine out of the *E. coli* cell (Jung et al., 2002). A transport system for export of L-carnitine operating in uniport mode is currently not known.

In this work, a proof of concept for the *de novo* L-carnitine production in *E. coli* was shown. The developed fermentation does not depend on petrochemical synthesis of achiral precursors, but instead makes use of renewable feedstocks. Implementation of the L-carnitine biosynthesis pathway was guided by the recently developed L-carnitine biosensor, which allowed the identification of the enzymes and their assembly into an optimized biosynthetic pathway in the form of an enzyme cascade. The biosensor additionally made it possible to identify the precursor supply and product export as current bottlenecks that need to be addressed to further advance L-carnitine *de novo* production by *E. coli*. To the best of our knowledge, this is the first description of L-carnitine *de novo* synthesis using an engineered bacterium.

DATA AVAILABILITY STATEMENT

The original contributions presented in the study are included in the article/**Supplementary Material**, further inquiries can be directed to the corresponding author/s.

AUTHOR CONTRIBUTIONS

PK designed the study. PK, MT, and MF conducted the experiments. VW provided funding. MF and VW provided resources. PK, MF, and VW drafted the manuscript. PK and VW finalized the manuscript. All authors read and approved the final version of the manuscript.

FUNDING

Support for the Article Processing Charge by the Deutsche Forschungsgemeinschaft and the Open Access Publication Fund of Bielefeld University is acknowledged. The funding bodies had no role in the design of the study or the collection, analysis, or interpretation of data or in writing the manuscript.

SUPPLEMENTARY MATERIAL

The Supplementary Material for this article can be found online at: https://www.frontiersin.org/articles/10.3389/fbioe.2021.671321/full#supplementary-material

REFERENCES

Al Temimi, A. H. K., Pieters, B. J. G. E., Reddy, Y. V., White, P. B., and Mecinović, J. (2016). Substrate scope for trimethyllysine hydroxylase catalysis. *Chem. Commun.* 52, 12849–12852. doi: 10.1039/C6CC07845A

Arense, P., Bernal, V., Charlier, D., Iborra, J., Foulquié-Moreno, M., and Cánovas, M. (2013). Metabolic engineering for high yielding L(-)-carnitine production in *Escherichia coli*. *Microb. Cell Fact.* 12:56. doi: 10.1186/1475-2859-12-56

Bari, M. d. R, Hassan, M., Akai, N., Arima, J., and Mori, N. (2013). Gene cloning and biochemical characterization of 4-N-trimethylaminobutyraldehyde dehydrogenase II from *Pseudomonas* sp. 13CM. *World J. Microbiol. Biotechnol.* 29, 683–692. doi: 10.1007/s11274-012-1224-x

Bernal, V., Arense, P., and Cánovas, M. (2016). "L-Carnitine, the vitamin B_T: uses and production by the secondary metabolism of Bacteria," in *Industrial Biotechnology of Vitamins, Biopigments, and Antioxidants*, eds E. J. Vandamme and J. L. Revuelta (Weinheim: Wiley-VCH Verlag GmbH & Co), 389–419. doi: 10.1002/9783527681754.ch14

Bernal, V., Sevilla, A., Cánovas, M., and Iborra, J. L. (2007). Production of L-carnitine by secondary metabolism of bacteria. *Microb. Cell Fact.* 6:31. doi: 10.1186/1475-2859-6-31

Borum, P. R., and Broquist, H. P. (1977). Purification of *S*-adenosylmethionine: epsilon-*N*-L-lysine methyltransferase. the first enzyme in carnitine biosynthesis. *J. Biol. Chem.* 252, 5651–5655.

Bracher, S., Hilger, D., Guérin, K., Polyhach, Y., Jeschke, G., Krafczyk, R., et al. (2019). Comparison of the functional properties of trimeric and monomeric CaiT of *Escherichia coli*. *Sci. Rep.* 9:3787. doi: 10.1038/s41598-019-40516-7

Cánovas, M., Torroglosa, T., and Iborra, J. L. (2005). Permeabilization of *Escherichia coli* cells in the biotransformation of trimethylammonium compounds into L-carnitine. *Enzyme Microb. Technol.* 37, 300–308. doi: 10.1016/j.enzmictec.2004.07.023

Castellar, M. R., Cánovas, M., Kleber, H. P., and Iborra, J. L. (1998). Biotransformation of D(+)-carnitine into L(-)-carnitine by resting cells of *Escherichia coli* O44 K74. *J. Appl. Microbiol.* 85, 883–890. doi: 10.1046/j.1365-2672.1998.00601.x

Castellar, M. R., Obón, J. M., Marán, A., Cánovas, M., and Iborra, J. L. (2001). L(-)-carnitine production using a recombinant *Escherichia coli* strain. *Enzyme Microb. Technol.* 28, 785–791. doi: 10.1016/s0141-0229(01)00332-5

Chen, Y., Abbate, M., Tang, L., Cai, G., Gong, Z., Wei, R., et al. (2014). L-Carnitine supplementation for adults with end-stage kidney disease requiring maintenance hemodialysis: a systematic review and meta-analysis. *Am. J. Clin. Nutr.* 99, 408–422. doi: 10.3945/ajcn.113.062802

Colson, C., Lhoest, J., and Urlings, C. (1979). Genetics of ribosomal protein methylation in *Escherichia coli*: III. Map position of two genes, *prmA* and *prmB*, governing methylation of proteins L11 and L3. *Molec. Gen. Genet.* 169, 245–250. doi: 10.1007/BF00382270

di Salvo, M. L., Remesh, S. G., Vivoli, M., Ghatge, M. S., Paiardini, A., D'Aguanno, S., et al. (2014). On the catalytic mechanism and stereospecificity of *Escherichia coli* L-threonine aldolase. *FEBS J.* 281, 129–145. doi: 10.1111/febs.12581

DiNicolantonio, J. J., Lavie, C. J., Fares, H., Menezes, A. R., and O'Keefe, J. H. (2013). L-carnitine in the secondary prevention of cardiovascular disease: systematic review and meta-analysis. *Mayo Clin. Proc.* 88, 544–551. doi: 10.1016/j.mayocp.2013.02.007

Eichler, K., Bourgis, F., Buchet, A., Kleber, H. P., and Mandrand-Berthelot, M. A. (1994). Molecular characterization of the *cai* operon necessary for carnitine metabolism in *Escherichia coli*. *Mol. Microbiol.* 13, 775–786. doi: 10.1111/j.1365-2958.1994.tb00470.x

El-Hattab, A. W., and Scaglia, F. (2015). Disorders of carnitine biosynthesis and transport. *Mol. Genet. Metab.* 116, 107–112. doi: 10.1016/j.ymgme.2015.09.004

Elssner, T., Engemann, C., Baumgart, K., and Kleber, H.-P. (2001). Involvement of coenzyme A esters and two new enzymes, an Enoyl-CoA hydratase and a CoA-transferase, in the hydration of crotonobetaine to L-carnitine by *Escherichia coli*. *Biochemistry* 40, 11140–11148. doi: 10.1021/bi0108812

Fielding, R., Riede, L., Lugo, J., and Bellamine, A. (2018). L-carnitine supplementation in recovery after exercise. *Nutrients* 10:349. doi: 10.3390/nu10030349

Flanagan, J. L., Simmons, P. A., Vehige, J., Willcox, M. D., and Garrett, Q. (2010). Role of carnitine in disease. *Nutr. Metab.* 7:30. doi: 10.1186/1743-7075-7-30

Franken, J., Burger, A., Swiegers, J. H., and Bauer, F. F. (2015). Reconstruction of the carnitine biosynthesis pathway from *Neurospora crassa* in the yeast *Saccharomyces cerevisiae*. *Appl. Microbiol. Biotechnol.* 99, 6377–6389. doi: 10.1007/s00253-015-6561-x

Funke, M., Diederichs, S., Kensy, F., Müller, C., and Büchs, J. (2009). The baffled microtiter plate: Increased oxygen transfer and improved online monitoring in small scale fermentations. *Biotechnol. Bioeng.* 103, 1118–1128. doi: 10.1002/bit.22341

Gibson, D. G., Young, L., Chuang, R.-Y., Venter, J. C., Hutchison, C. A., and Smith, H. O. (2009). Enzymatic assembly of DNA molecules up to several hundred kilobases. *Nat. Methods* 6, 343–345. doi: 10.1038/nmeth.1318

Gnoni, A., Longo, S., Gnoni, G. V., and Giudetti, A. M. (2020). Carnitine in human muscle bioenergetics: can carnitine supplementation improve physical exercise? *Molecules* 25:182. doi: 10.3390/molecules25010182

Grand View Research (2019). *L-Carnitine Market to Grow at a CAGR of 4.8% to reach US$ 262.6 Million from 2019 to 2027*. Available online at: https://www.theinsightpartners.com/reports/l-carnitine-marker-market (accessed July 30, 2020).

Green, M. R., Sambrook, J., and Sambrook, J. (2012). *Molecular Cloning: A Laboratory Manual. 4th Edition*. Cold Spring Harbor, NY: Cold Spring Harbor Laboratory Press.

Gross, C. J., Henderson, L. M., and Savaiano, D. A. (1986). Uptake of L-carnitine, D-carnitine and acetyl-L-carnitine by isolated guinea-pig enterocytes. *Biochim. Biophys. Acta, Mol. Cell Res.* 886, 425–433. doi: 10.1016/0167-4889(86)90178-3

Gruez, A., Roig-Zamboni, V., Grisel, S., Salomoni, A., Valencia, C., Campanacci, V., et al. (2004). Crystal structure and kinetics identify *Escherichia coli* YdcW gene product as a medium-chain aldehyde dehydrogenase. *J. Mol. Biol.* 343, 29–41. doi: 10.1016/j.jmb.2004.08.030

Hassan, M., Okada, M., Ichiyanagi, T., and Mori, N. (2008). 4-*N*-Trimethylaminobutyraldehyde dehydrogenase: purification and characterization of an enzyme from *Pseudomonas* sp. 13CM. *Biosci., Biotechnol., Biochem.* 72, 155–162. doi: 10.1271/bbb.70514

Haupka, C. (2020). *Chaupka/Codon_Harmonization: Release v1.2.0*. Zenodo. Genève, Switzerland: CERN. doi: 10.5281/ZENODO.4062177

Henderson, L. M., Nelson, P. J., and Henderson, L. (1982). Mammalian enzymes of trimethyllysine conversion to trimethylaminobutyrate. *Fed. Proc.* 41, 2843–2847.

Horne, D. W., and Broquist, H. P. (1973). Role of lysine and epsilon-*N*-trimethyllysine in carnitine biosynthesis. I. Studies in *Neurospora crassa*. *J. Biol. Chem.* 248, 2170–2175.

Hulse, J. D., Ellis, S. R., and Henderson, L. M. (1978). Carnitine biosynthesis. beta-Hydroxylation of trimethyllysine by an alpha-ketoglutarate-dependent mitochondrial dioxygenase. *J. Biol. Chem.* 253, 1654–1659.

Jung, H., and Kleber, H.-P. (1991). Metabolism of D(+)-carnitine by *Escherichia coli*. *Appl. Microbiol. Biotechnol.* 35, 393–395. doi: 10.1007/BF00172731

Jung, H., Buchholz, M., Clausen, J., Nietschke, M., Revermann, A., Schmid, R., et al. (2002). CaiT of *Escherichia coli*, a new transporter catalyzing L-carnitine/γ-butyrobetaine exchange. *J. Biol. Chem.* 277, 39251–39258. doi: 10.1074/jbc.M206319200

Kabat, M. M., Daniewski, A. R., and Burger, W. (1997). A convenient synthesis of R-(−)-carnitine from R-(−)-epichlorohydrin. *Tetrahedron* 8, 2663–2665. doi: 10.1016/S0957-4166(97)00324-8

Kang, W.-K., Park, Y.-H., Koh, E.-S., Ju, J.-Y., Lee, J.-H., Choi, H.-J., et al. (2013). *A Microorganism of Enterobacteriaceae Genus Haboring Genes Associated With L-Carnitine Biosynthesis and Method of Producing L-Carnitine Using the Microorganism*. Available online at: https://patents.google.com/patent/EP1904620B1/en (accessed September 8, 2020).

Kaufman, R. A., and Broquist, H. P. (1977). Biosynthesis of carnitine in *Neurospora crassa*. *J. Biol. Chem.* 252, 7437–7439.

Kensy, F., Zang, E., Faulhammer, C., Tan, R.-K., and Büchs, J. (2009). Validation of a high-throughput fermentation system based on online monitoring of biomass and fluorescence in continuously shaken microtiter plates. *Microb. Cell Fact.* 8:31. doi: 10.1186/1475-2859-8-31

Klagsbrun, M., and Furano, A. V. (1975). Methylated amino acids in the proteins of bacterial and mammalian cells. *Arch. Biochem. Biophys.* 169, 529–539. doi: 10.1016/0003-9861(75)90196-4

Kruschwitz, H., McDonald, D., Cossins, E., and Schirch, V. (1993). "Purification of *Neurospora crassa* cytosolic serine hydroxymethyltransferase," in *Chemistry and Biology of Pteridines and Folates Advances in Experimental Medicine and Biology*, eds J. E. Ayling, M. G. Nair, and C. M. Baugh (Boston, MA: Springer), 719–722. doi: 10.1007/978-1-4615-2960-6_149

Kugler, P., Fröhlich, D., and Wendisch, V. F. (2020). Development of a biosensor for crotonobetaine-CoA ligase screening based on the elucidation of *Escherichia coli* carnitine metabolism. *ACS Synth. Biol.* 9, 2460–2471. doi: 10.1021/acssynbio.0c00234

Kunjapur, A. M., and Prather, K. L. J. (2015). Microbial engineering for aldehyde synthesis. *Appl. Environ. Microbiol.* 81, 1892–1901. doi: 10.1128/AEM.03319-14

Li, J.-M., Li, L.-Y., Zhang, Y.-X., Jiang, Z.-Y., Limbu, S. M., Qiao, F., et al. (2019). Functional differences between L- and D-carnitine in metabolic regulation evaluated using a low-carnitine Nile tilapia model. *Br. J. Nutr.* 122, 625–638. doi: 10.1017/S000711451900148X

Li, L., Limbu, S. M., Ma, Q., Chen, L., Zhang, M., and Du, Z. (2019). The metabolic regulation of dietary L-carnitine in aquaculture nutrition: present status and future research strategies. *Rev. Aquacult.* 11, 1228–1257. doi: 10.1111/raq.12289

Lindstedt, G. (1967). Hydroxylation of γ-butyrobetaine to carnitine in rat liver*. *Biochemistry* 6, 1271–1282. doi: 10.1021/bi00857a007

Lindstedt, G., and Lindstedt, S. (1970). Cofactor requirements of gamma-butyrobetaine hydroxylase from rat liver. *J. Biol. Chem.* 245, 4178–4186.

Lindstedt, G., Lindstedt, S., and Tofft, M. (1970). Gamma-butyrobetaine hydroxylase from *Pseudomonas* sp AK 1. *Biochemistry* 9, 4336–4342. doi: 10.1021/bi00824a014

Lindstedt, G., Lindstedt, S., Midtvedt, T., and Tofft, M. (1967). The Formation and degradation of carnitine in *Pseudomonas**. *Biochemistry* 6, 1262–1270. doi: 10.1021/bi00857a006

Longo, N., Frigeni, M., and Pasquali, M. (2016). Carnitine transport and fatty acid oxidation. *Biochim. Biophys. Acta, Mol. Cell Res.* 1863, 2422–2435. doi: 10.1016/j.bbamcr.2016.01.023

Magoulas, P. L., and El-Hattab, A. W. (2012). Systemic primary carnitine deficiency: an overview of clinical manifestations, diagnosis, and management. *Orphanet J. Rare. Dis.* 7:68. doi: 10.1186/1750-1172-7-68

Meyer, H.-P., and Robins, K. T. (2005). Large scale bioprocess for the production of optically pure L-carnitine. *Monatsh. Chem.* 136, 1269–1277. doi: 10.1007/s00706-005-0330-y

Naidu, G. S. N., Lee, I. Y., Lee, E. G., Kang, G. H., and Park, Y. H. (2000). Microbial and enzymatic production of L-carnitine. *Bioprocess Eng.* 23, 627–635. doi: 10.1007/s004490000212

Nakamura, Y. (2000). Codon usage tabulated from international DNA sequence databases: status for the year 2000. *Nucleic Acids Res.* 28, 292–292. doi: 10.1093/nar/28.1.292

Ni, Y., Reye, J., and Chen, R. R. (2007). lpp deletion as a permeabilization method. *Biotechnol. Bioeng.* 97, 1347–1356. doi: 10.1002/bit.21375

Obón, J. M., Maiquez, J. R., Cánovas, M., Kleber, H.-P., and Iborra, J. L. (1999). High-density *Escherichia coli* cultures for continuous L(−)-carnitine production. *Appl. Microbiol. Biotechnol.* 51, 760–764. doi: 10.1007/s002530051459

Okano, K., Sato, Y., Inoue, S., Kawakami, S., Kitani, S., and Honda, K. (2020). Enhancement of *S*-adenosylmethionine-dependent methylation by integrating methanol metabolism with 5-Methyl-tetrahydrofolate formation in *Escherichia coli*. *Catalysts* 10:1001. doi: 10.3390/catal10091001

Parvanova, A., Trillini, M., Podestà, M. A., Iliev, I. P., Aparicio, C., Perna, A., et al. (2018). Blood Pressure and metabolic effects of Acetyl-L-carnitine in Type 2 diabetes: DIABASI randomized controlled trial. *J. Endocr. Soc.* 2, 420–436. doi: 10.1210/js.2017-00426

Preusser, A., Wagner, U., Elssner, T., and Kleber, H.-P. (1999). Crotonobetaine reductase from *Escherichia coli* consists of two proteins. *Biochim. Biophys.*

Acta, Protein Struct. Mol. Enzymol. 1431, 166–178. doi: 10.1016/S0167-4838(99)00032-1

Rebouche, C. J. (1977). Carnitine movement across muscle cell membranes. Studies in isolated rat muscle. *Biochim. Biophys. Acta, Biomembr.* 471, 145–155. doi: 10.1016/0005-2736(77)90402-3

Rebouche, C. J. (1983). Effect of dietary carnitine isomers and γ-butyrobetaine on L-carnitine biosynthesis and metabolism in the rat. *J. Nutr.* 113, 1906–1913. doi: 10.1093/jn/113.10.1906

Reddy, Y. V., Al Temimi, A. H. K., White, P. B., and Mecinoviæ, J. (2017). Evidence that trimethyllysine hydroxylase catalyzes the formation of (2*S*,3*S*)-3-hydroxy-N^{ε}-trimethyllysine. *Org. Lett.* 19, 400–403. doi: 10.1021/acs.orglett.6b03608

Rehman, Z., Naz, S., Khan, R. U., and Tahir, M. (2017). An update on potential applications of L-carnitine in poultry. *World's Poult. Sci. J.* 73, 823–830. doi: 10.1017/S0043933917000733

Reuter, S. E., and Evans, A. M. (2012). Carnitine and acylcarnitines: pharmacokinetic, pharmacological and clinical aspects. *Clin. Pharmacokinet.* 51, 553–572. doi: 10.1007/BF03261931

Ringseis, R., Keller, J., and Eder, K. (2018a). Basic mechanisms of the regulation of L-carnitine status in monogastrics and efficacy of L-carnitine as a feed additive in pigs and poultry. *J. Anim. Physiol. Anim. Nutr.* 102, 1686–1719. doi: 10.1111/jpn.12959

Ringseis, R., Keller, J., and Eder, K. (2018b). Regulation of carnitine status in ruminants and efficacy of carnitine supplementation on performance and health aspects of ruminant livestock: a review. *Arch. Anim. Nutr.* 72, 1–30. doi: 10.1080/1745039X.2017.1421340

Sachan, D. S., and Hoppel, C. L. (1980). Carnitine biosynthesis. Hydroxylation of N6-trimethyl-lysine to 3-hydroxy-N6-trimethyl-lysine. *Biochem. J.* 188, 529–534. doi: 10.1042/bj1880529

Samsonova, N. N., Smirnov, S. V., Novikova, A. E., and Ptitsyn, L. R. (2005). Identification of *Escherichia coli* K12 YdcW protein as a γ-aminobutyraldehyde dehydrogenase. *FEBS Lett.* 579, 4107–4112. doi: 10.1016/j.febslet.2005.06.038

Schirch, V., Hopkins, S., Villar, E., and Angelaccio, S. (1985). Serine hydroxymethyltransferase from *Escherichia coli*: purification and properties. *J. Bacteriol.* 163, 1–7. doi: 10.1128/JB.163.1.1-7.1985

Schneider, B. L., and Reitzer, L. (2012). Pathway and enzyme redundancy in putrescine catabolism in *Escherichia coli*. *J. Bacteriol.* 194, 4080–4088. doi: 10.1128/JB.05063-11

Seim, H., Ezold, R., Kleber, H.-P., Strack, E., and Seim, H. (1980). Stoffwechsel des L-Carnitins bei Enterobakterien. *Zeitschr. Allgem. Mikrobiol.* 20, 591–594.

Sevilla, A., Schmid, J. W., Mauch, K., Iborra, J. L., Reuss, M., and Cánovas, M. (2005a). Model of central and trimethylammonium metabolism for optimizing L-carnitine production by *E. coli*. *Metab. Eng.* 7, 401–425. doi: 10.1016/j.ymben.2005.06.005

Sevilla, A., Vera, J., Díaz, Z., Cánovas, M., Torres, N. V., and Iborra, J. L. (2005b). Design of metabolic engineering strategies for maximizing L-(-)-carnitine production by *Escherichia coli*. Integration of the metabolic and bioreactor levels. *Biotechnol. Prog.* 21, 329–337. doi: 10.1021/bp0497583

Song, X., Qu, H., Yang, Z., Rong, J., Cai, W., and Zhou, H. (2017). Efficacy and safety of L-carnitine treatment for chronic heart failure: a meta-analysis of randomized controlled trials. *BioMed Res. Int.* 2017, 1–11. doi: 10.1155/2017/6274854

Sophos, N. A., and Vasiliou, V. (2003). Aldehyde dehydrogenase gene superfamily: the 2002 update. *Chem. Biol. Interact.* 14, 5–22. doi: 10.1016/S0009-2797(02)00163-1

Strijbis, K., Van Roermund, C. W. T., Hardy, G. P., Van den Burg, J., Bloem, K., Haan, J., et al. (2009). Identification and characterization of a complete carnitine biosynthesis pathway in *Candida albicans*. *FASEB J.* 23, 2349–2359. doi: 10.1096/fj.08-127985

Strijbis, K., Vaz, F. M., and Distel, B. (2010). Enzymology of the carnitine biosynthesis pathway. *IUBMB Life* 62, 357–362. doi: 10.1002/iub.323

Swiegers, J. H., Vaz, F. M., Pretorius, I. S., Wanders, R. J. A., and Bauer, F. F. (2002). Carnitine biosynthesis in *Neurospora crassa*: identification of a cDNA coding for ε-*N*-trimethyllysine hydroxylase and its functional expression in *Saccharomyces cerevisiae*. *FEMS Microbiol. Lett.* 210, 19–23. doi: 10.1111/j.1574-6968.2002.tb11154.x

The Insight Partners (2020). *L-Carnitine Market Size, Share, Trends | Global Industry Report, 2025*. Available online at: https://www.grandviewresearch.com/industry-analysis/l-carnitine-market (accessed July 30, 2020).

Trievel, R. C., Flynn, E. M., Houtz, R. L., and Hurley, J. H. (2003). Mechanism of multiple lysine methylation by the SET domain enzyme Rubisco LSMT. *Nat. Struct. Mol. Biol.* 10, 545–552. doi: 10.1038/nsb946

Vanet, A., Plumbridge, J. A., Guérin, M.-F., and Alix, J.-H. (1994). Ribosomal protein methylation in *Escherichia coli*: the gene *prmA*, encoding the ribosomal protein L11 methyltransferase, is dispensable. *Mol. Microbiol.* 14, 947–958. doi: 10.1111/j.1365-2958.1994.tb01330.x

Vaz, F. M., and Wanders, R. J. A. (2002). Carnitine biosynthesis in mammals. *Biochem. J.* 361, 417–429. doi: 10.1042/bj3610417

Vaz, F. M., Ofman, R., Westinga, K., Back, J. W., and Wanders, R. J. A. (2001). Molecular and Biochemical characterization of Rat ε-*N*-trimethyllysine hydroxylase, the first enzyme of carnitine biosynthesis. *J. Biol. Chem.* 276, 33512–33517. doi: 10.1074/jbc.M105929200

Verheul, A., Wouters, J. A., Rombouts, F. M., and Abee, T. (1998). A possible role of ProP, ProU and CaiT in osmoprotection of *Escherichia coli* by carnitine. *J. Appl. Microbiol.* 85, 1036–1046. doi: 10.1111/j.1365-2672.1998.tb05269.x

Veronese, N., Stubbs, B., Solmi, M., Ajnakina, O., Carvalho, A. F., and Maggi, S. (2018). Acetyl-L-carnitine supplementation and the treatment of depressive symptoms: a systematic review and meta-analysis. *Psychosom. Med.* 80, 154–159. doi: 10.1097/PSY.0000000000000537

Volkmer, B., and Heinemann, M. (2011). Condition-dependent cell volume and concentration of *Escherichia coli* to facilitate data conversion for systems biology modeling. *PLoS One* 6:e23126. doi: 10.1371/journal.pone.0023126

Wang, X., Jiang, Y., Wu, M., Zhu, L., Yang, L., and Lin, J. (2019). Semi-rationally engineered variants of *S*-adenosylmethionine synthetase from *Escherichia coli* with reduced product inhibition and improved catalytic activity. *Enzyme Microb. Technol.* 129:109355. doi: 10.1016/j.enzmictec.2019.05.012

Wargo, M. J., and Meadows, J. A. (2015). Carnitine in bacterial physiology and metabolism. *Microbiology* 161, 1161–1174. doi: 10.1099/mic.0.000080

Wendisch, V. F. (2020). Metabolic engineering advances and prospects for amino acid production. *Metab. Eng.* 58, 17–34. doi: 10.1016/j.ymben.2019.03.008

Ye, C., Luo, Q., Guo, L., Gao, C., Xu, N., Zhang, L., et al. (2020). Improving lysine production through construction of an *Escherichia coli* enzyme-constrained model. *Biotechnol. Bioeng.* 117, 3533–3544. doi: 10.1002/bit.27485

Zhang, M., Xu, J.-Y., Hu, H., Ye, B.-C., and Tan, M. (2018). Systematic proteomic analysis of protein methylation in prokaryotes and eukaryotes revealed distinct substrate specificity. *Proteomics* 18:1700300. doi: 10.1002/pmic.201700300

Conflict of Interest: The authors declare that the research was conducted in the absence of any commercial or financial relationships that could be construed as a potential conflict of interest.

frontiers in Bioengineering and Biotechnology

ORIGINAL RESEARCH
published: 24 June 2021
doi: 10.3389/fbioe.2021.695704

Enhanced Protocatechuic Acid Production From Glucose Using *Pseudomonas putida* 3-Dehydroshikimate Dehydratase Expressed in a Phenylalanine-Overproducing Mutant of *Escherichia coli*

*Oliver Englund Örn[1], Stefano Sacchetto[1], Ed W. J. van Niel[2] and Rajni Hatti-Kaul[1]**

[1] Division of Biotechnology, Department of Chemistry, Center for Chemistry and Chemical Engineering, Lund University, Lund, Sweden, [2] Division of Applied Microbiology, Department of Chemistry, Center for Chemistry & Chemical Engineering, Lund University, Lund, Sweden

OPEN ACCESS

Edited by:
K. Madhavan Nampoothiri, National Institute for Interdisciplinary Science and Technology (CSIR), India

Reviewed by:
Huaiwei Liu, Shandong University, China
Zhaojuan Zheng, Nanjing Forestry University, China

***Correspondence:**
Rajni Hatti-Kaul
Rajni.Hatti-Kaul@biotek.lu.se

Specialty section:
This article was submitted to Industrial Biotechnology, a section of the journal Frontiers in Bioengineering and Biotechnology

Received: *15 April 2021*
Accepted: *31 May 2021*
Published: *24 June 2021*

Citation:
Örn OE, Sacchetto S, van Niel EWJ and Hatti-Kaul R (2021) Enhanced Protocatechuic Acid Production From Glucose Using Pseudomonas putida 3-Dehydroshikimate Dehydratase Expressed in a Phenylalanine-Overproducing Mutant of Escherichia coli. Front. Bioeng. Biotechnol. 9:695704. doi: 10.3389/fbioe.2021.695704

Protocatechuic acid (PCA) is a strong antioxidant and is also a potential platform for polymer building blocks like vanillic acid, vanillin, muconic acid, and adipic acid. This report presents a study on PCA production from glucose via the shikimate pathway precursor 3-dehydroshikimate by heterologous expression of a gene encoding 3-dehydroshikimate dehydratase in *Escherichia coli*. The phenylalanine overproducing *E. coli* strain, engineered to relieve the allosteric inhibition of 3-deoxy-7-phosphoheptulonate synthase by the aromatic amino acids, was shown to give a higher yield of PCA than the unmodified strain under aerobic conditions. Highest PCA yield of 18 mol% per mol glucose and concentration of 4.2 g/L was obtained at a productivity of 0.079 g/L/h during cultivation in fed-batch mode using a feed of glucose and ammonium salt. Acetate was formed as a major side-product indicating a shift to catabolic metabolism as a result of feedback inhibition of the enzymes including 3-dehydroshikimate dehydratase by PCA when reaching a critical concentration. Indirect measurement of proton motive force by flow cytometry revealed no membrane damage of the cells by PCA, which was thus ruled out as a cause for affecting PCA formation.

Keywords: aromatic building block, protocatechuic acid, shikimate pathway, 3-dehydroshikimate dehydratase, allosteric inhibition, proton motive force

INTRODUCTION

Decoupling of plastic production from fossil feedstock requires the availability of carbon-neutral polymer building blocks from renewable resources that could be suitable replacements for the currently used materials and can fit into the established value chains (Hatti-Kaul et al., 2020). Only a limited number of biobased building blocks, primarily aliphatic, are currently produced at large

scale including lactic acid, succinic acid, 1,4-butanediol, and 1,3-propanediol. Finding economically viable biobased aromatic monomers constitutes an enormous challenge. Aromatic building blocks are essential components of many important plastic categories, the important examples being terephthalic acid (TPA) present in poly(ethylene terephthalate) (PET) and several other polyesters, and styrene used in polystyrene. The aromatic groups increase the durability and the possibility of recycling the polymers (Hatti-Kaul et al., 2020). There are ongoing research efforts to produce biobased aromatic building blocks that could be either drop-ins or substitutes for the existing products (Graglia et al., 2015; Noda and Kondo, 2017; Kucherov et al., 2021).

Lignin is the largest natural source of aromatic building blocks, however, separation of the monomers after lignin depolymerization is still a challenge. Several routes to produce biobased TPA have been proposed (Collias et al., 2014). On the other hand, a sugar-based furan building block 2,5-furandicarboxylic acid (FDCA) is being developed as an alternative to TPA (Eerhart et al., 2012; Sousa et al., 2015), and furanics-to-benzene conversion is also being investigated (Kucherov et al., 2021). Several recent publications report on the shikimate pathway used by organisms for production of aromatic amino acids, phenylalanine, tyrosine and tryptophan, as a promising route for obtaining aromatic building blocks for chemicals, and plastics (Rodriguez et al., 2014; Suástegui and Shao, 2016; Lee and Wendisch, 2017; Noda and Kondo, 2017; Averesch and Krömer, 2018; Huccetogullari et al., 2019; Li et al., 2020). Among the various aromatic molecules, protocatechuic acid (PCA; 3,4-dihydroxybenzoic acid) has been identified as a potential platform chemical for several other monomers such as vanillic acid, vanillin, muconic acid, and adipic acid (Pugh et al., 2014). The compound also possesses strong antioxidant and anti-inflammatory properties and has immense pharmacological potential (Kakkar and Bais, 2014). Two recombinant pathways have been described for PCA production (**Figure 1**). The first pathway uses the enzyme 3-dehydroshikimate dehydratase (DSD) (also abbreviated as 3dhsd, AroZ, AsbF, and QuiC1) to catalyze the dehydration of the intermediate 3-dehydroshikimate (3-DHS) to PCA. The second pathway requires two enzymes - chorismate pyruvate lyase (ubiC) for converting chorismate to *p*-hydroxybenzoate (pHBA) and a NADPH-dependent enzyme *p*-hydroxybenzoate hydroxylase (pobA) for converting pHBA to PCA making it stoichiometrically less favorable (Pugh et al., 2014).

The major metabolic bottleneck for the shikimate pathway has been identified in the synthesis of 3-deoxy-D-arabinoheptulosonate 7-phosphate (DAHP) from phosphoenolpyruvate (PEP) and erythrose-4-phosphate (E4P) coming from glycolysis and pentose phosphate pathways, respectively (**Figure 1**). The synthesis is constrained in two different ways: (i) the PEP flux to the phosphotransferase system (PTS) (Rodriguez et al., 2014), and (ii) the feedback inhibition of the three DAHP synthase enzymes AroG, AroF and AroH by phenylalanine, tyrosine and tryptophan, respectively (Johansson and Lidén, 2006). Further limitations of PCA production through the shikimate pathway are ascribed to the product toxicity to the cells and inhibition of the DSD enzyme, resulting in termination of the process (Pugh et al., 2014; Shmonova et al., 2020). Addition of 1.5 g/L PCA to *Escherichia coli* culture has been shown to completely impair cell growth (Pugh et al., 2014). The toxicity of PCA could be due to its insertion in the core of the cell membrane, increasing the membrane fluidity and decreasing the structural integrity, as has been observed for other aromatic compounds (Ramos et al., 2002). Studies on DSD of *Corynebacterium glutamicum* have shown the enzyme to be competitively and non-competitively inhibited by PCA (inhibition constants Ki $\sim$ 0.38 mM and Ki' $\sim$ 0.96 mM, respectively) (Shmonova et al., 2020). It is possible to minimize the inhibition by *in situ* removal of the product, which would have an additional benefit of shifting the reaction equilibrium toward product formation (Sayed et al., 2016).

This report presents a study on PCA production through dehydration of 3-dehydroshikimate using recombinant *Pseudomonas putida* DSD in an *E. coli* strain engineered for phenylalanine overproduction by removing the enzymes AroF and AroG, that are inhibited by tyrosine and phenylalanine, respectively, as well as the essential enzymes in the tyrosine and tryptophan biosynthesis pathway (Fox et al., 2008; Peek et al., 2017; Shmonova et al., 2020). The physiological and metabolic effect of PCA production was further evaluated to identify the probable mechanism involved.

MATERIALS AND METHODS

E. coli Strains and the Culture Media

Escherichia coli strain DH5α was used for construction and long-time storage of assembled plasmids. *E. coli* strains BL21(DE3) and ATCC 31882 (ΔaroF ΔaroG ΔtyrR ΔpheA ΔpheA ΔtyrA ΔtrpE) were used for protein expression and PCA production. LB medium containing per liter 5 g yeast extract, 10 g tryptone, and 5 g NaCl, was used to prepare precultures for batch and fed batch cultures, for growing cells before transformation, DNA and protein isolation and purification. M9 medium containing per liter: 8.5 g $Na_2HPO_4.2H_2O$, 3 g KH_2PO_4, 0.5 g NaCl, 1 g NH_4Cl, 2 mM $MgSO_4$, 0.01 mM $CaCl_2$, and 20 g glucose (Neidhardt et al., 1974), was used in initial batch cultivations, and was modified further for use in cultivations for PCA production. The modified M9 medium consisted (per liter) of: 8.5 g $Na_2HPO_4.2H_2O$, 3 g KH_2PO_4, 0.5 g NaCl, 2 g NH_4Cl, 1 mg thiamine, 2 mM $MgSO_4$, 0.1 mM $CaCl_2$, 28 μg $FeSO_4$, 36 μg $(NH_4)_6Mo_7O_{24}.4H_2O$, 248 μg H_3BO_3, 72 μg $CoCl_2$, 24 μg $CuSO_4$, 160 μg $MnCl_2$, 28 μg $ZnSO_4$, and 20 g glucose, unless otherwise specified. In case of nitrogen-limited cultivation, the NH_4Cl concentration was lowered to 0.2 g/L, while in the phosphate-limited cultivation $Na_2HPO_4.2H_2O$ was omitted and 0.3 g/L KH_2PO_4 was used, while maintaining the concentrations of the other components. In certain cultivations, concentrations of all the metal salts were increased four times. In fed-batch experiments, the cultivation was started in a batch mode in the modified M9 medium, and the feed composed of 50 mL of 200 g/L glucose or 50 mL of 200 g/L glucose and 5 mL 200 g/L NH_4Cl solution added at discrete time points.

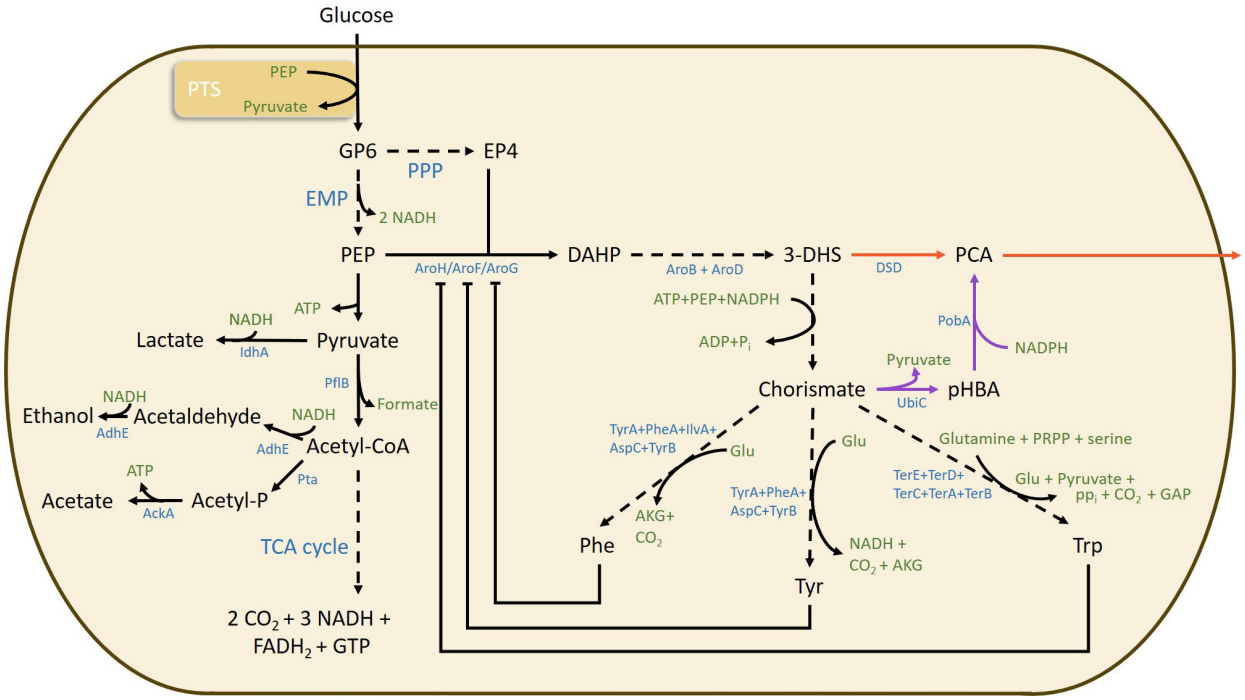

FIGURE 1 | Overview of relevant metabolic pathways, bottlenecks, metabolites, and enzymes involved in protocatechuic acid formation via both DSD (red arrow) and PobA/UbiC (purple arrow) from the shikimate pathway for aromatic amino acid metabolism in *E. coli*. Dashed arrows indicate a multistep enzymatic pathway. 3-dehydroshikimic acid, 3-DHS; acetate kinase, AckA; aldehyde/alcohol dehydrogenase, AdhE; α-ketoglutarate, AKG; 3-dehydroquinate synthase, AroB; 3-dehydroquinate dehydratase, AroD; 3-deoxy-7-phosphoheptulonate synthase, AroF, AroH, and AroG; aspartate aminotransferase, AspC; adenosine triphosphate, ATP; 3-dehydroshikimate dehydratase, DSD; erythrose 4-phosphate, E4P; 3-deoxy-D-arabino-heptulosonic acid 7-phosphate, DAHP; Embden–Meyerhof–Parnas, EMP; flavin adenine dinucleotide reduced form, $FADH_2$; glutamate, Glu; guanosine triphosphate, GTP; nicotinamide adenine dinucleotide reduced form, NADH; nicotinamide adenine dinucleotide phosphate reduced form, NADPH; protocatechuic acid, PCA; phosphoenolpyruvate, PEP; pyruvate formate-lyase, pflB; p-hydroxybenzoic acid, pHBA; phenylalanine, Phe; phosphate, P_i; pyrophosphate, PP_i; pentose phosphate pathway, PPP; p-hydroxybenzoate hydroxylase, PobA; 5-phosphoribosyl 1-pyrophosphate, PRPP; phosphate acetyltransferase, Pta; tricarboxylic acid cycle, TCA cycle; tryptophan, Trp; tyrosine, Tyr; tyrosine aminotransferase, TyrB; chorismate lyase, UbiC.

Strain Construction

Pseudomonas putida KT2440 was used as a source of the gene coding for DSD. The primers used for gene amplification are described in **Supplementary Table 1**. The genomic DNA from *P. putida* was extracted using an E.Z.N.A bacterial extraction kit and amplification of the *DSD* gene was done using Phusion High-Fidelity DNA Polymerase (Thermo Fisher Scientific, Waltham, MA, United States) according to the manufacturer's specifications. The primers also added overhang sequences for two restriction enzymes, *Eco*RI and *Hin*dIII (Thermo Fisher Scientific, Waltham, MA, United States), used for ligation to the plasmid pCDFDuet-1. Ligation was performed using T4 DNA ligase (Thermo Fisher Scientific, Waltham, MA, United States) with 50 ng of linearized vector and five times excess of insert and incubation at 4°C for 16 h, followed by 15°C for 30 min and 25°C for 30 min prior to transformation into competent DH5α cells prepared as described earlier (Hanahan, 1983). Transformation was performed by mixing 50 μL competent cell culture with 2 μL DNA (concentration of 3.5 ng/μL) and incubation on ice for 30 min, after which the cells were subjected to heat-shock for 45 s at 42°C in a water bath and cooled on ice for 2 min before addition of 1 mL LB medium. The cells were incubated for 1 h at 37°C and then 200 μL suspension was plated on LB agar plates supplemented with 50 μg/mL streptomycin. The ligation of *DSD* to the plasmid was confirmed using colony PCR with primers Duet1 Fw/Rev (**Supplementary Table 1**). Plasmid *pCDFDuet-DSD* was transformed into *E. coli* strains BL21(DE3) and ATCC 321882, respectively, using the method described above. Expression of DSD was confirmed using SDS-PAGE. BL21(DE3) and BL21(DE3)-DSD were grown overnight in 50 mL LB medium at 37°C or 30°C until reaching OD_{600} of approximately 5. The cell pellet obtained after centrifugation at 13,000 × *g* at room temperature was re-suspended in TE buffer (100 mM Tris–HCl, 1 mM EDTA, pH 8) and sonicated for 2 min at 24 kHz in a sonicator (Hielscher GmbH, UP 400). The soluble and insoluble fractions were separated by centrifugation at 13,000 × *g*; the insoluble fraction was re-suspended in the same volume of TE buffer, and 10 μL of each sample was loaded on 12% precast acrylamide gel for electrophoresis (Mini-PROTEAN TGX, Biorad).

Gene Expression and Growth Conditions

Escherichia coli DH5α, BL21(DE3), and ATCC 321882 cells were propagated in LB medium, and for growing the cells transformed

with pCDFDuet-*DSD* the medium was supplemented with 50 mg/L streptomycin. For production of PCA using BL21(DE3) or ATCC 31882 recombinant strains, M9 or modified M9 medium was used. Batch cultivations in shake flasks and cultivations of the inoculum for batch and fed-batch cultivation were performed at 37°C and 200 rpm, while cultivations in 3 L bioreactors (Applikon Biotechnology, Delft, Netherlands) were maintained at constant temperature of 37°C, pH 7, air flow 1 vvm, and stirring rate of 600 rpm. The pH was controlled by pumping 5 M NaOH solution. In fed-batch cultivations, the conditions were the same except that the stirring rate increased when the dissolved oxygen tension (DOT) value dropped below 40%. Protein expression was induced by addition of 0.1 mM IPTG at the start of the cultivation, unless otherwise specified. Two milliliter culture samples were collected at defined time intervals for monitoring the formation of products and consumption of glucose. In fed-batch experiments, glucose levels were monitored using MQuant glucose test strips (Merek Millipore, MA, United States). *In situ* adsorption of PCA was performed in a normal batch cultivation in the modified M9 medium by suspending 4 g/L of Amberlite 401 IRA (Cl) contained in a Spectra/Por^{TM} 4 (MWCO 12–14 kD) dialysis membrane (Spectrum Chemical Mfg., Corp., NJ, United States).

Adsorption of PCA

Screening of ion exchange resins Amberlite 400 IRA (Cl), Amberlite 401 IRA (Cl), and Amberlite 904 IRA (Cl) for adsorption and subsequent desorption of PCA was performed using 100 mg resin (pre-swollen in 10 mL water for one-hour) in 10 mL water with PCA (1–10 g/L) and as mixtures with other organic acids (succinic acid and acetic acid at concentrations of 0.1 or 1 g/L each) in 15 mL tubes on a rocking table at room temperature. Subsequently, the resin was washed twice with 10 mL MQ water, and desorption of the adsorbed compounds was tested with 3 × 10 mL eluting solutions (with different concentrations of acetic acid, NaCl and ethanol, respectively) for 30 min each at room temperature. Elution of PCA from Amberlite 401 IRA (Cl) after *in situ* adsorption experiment was performed by treating the resin with 3 × 10 mL of 0.3 M acetic acid solution for 30 min each at room temperature.

Analytical Methods

Cell Dry Weight

The cell dry weight (CDW) of *E. coli* BL21(DE3) was determined by filtering 5 mL cell suspension through a dried and pre-weighed 0.45 μm filter paper (Pall Corp.) in triplicates and then drying overnight at 105°C. The ratio 0.5479 g CDW/OD_{600} and an approximation of the cellular molecular weight of 22.90 g CDW/cmol based on an elemental composition of $CH_{1.74}N_{0.24}O_{0.34}S_{0.006}P_{0.005}$ (Taymaz-Nikerel et al., 2010) was used in the conversion of measured OD_{600} values to cmol.

HPLC Analysis of Substrate and Metabolites

Protocatechuic acid was analyzed using a Dionex HPLC system equipped with a UV/VIS detector and a Phenomenex kinetex 2.6 μm Biphenyl 100 A (50 × 2.1 mm) column for separation using a mobile phase consisting of 93% Solution A containing methanol: acetic acid: water (10:2:88) and 7% Solution B made of methanol: acetic acid: water (90:2:8), at a flow rate of 0.3 mL/min. Glucose, organic acids, and alcohols were analyzed by separation in a Jasco HPLC system equipped with RI detector using a BioRad Aminex HPX87H (Fast Acid) (100 × 7.8 mm) column. The mobile phase was 0.5 mM sulfuric acid used at a flow rate of 0.6 mL/min. The sample injection volume was 10 μL and all samples were filtered through a 0.2 μm filter, diluted 10 times in MQ water to a final volume of 1 mL prior to injecting into the column. The concentration of PCA and other metabolites formed was calculated as gram per liter (g/L) of the medium. Yield of PCA with respect to glucose ($Y_{P/S}$) was calculated as mol/mol. Biomass concentration was calculated as dry weight in cmol/L. The yield of PCA with respect to biomass ($Y_{P/B}$) was calculated as cmol/cmol. The productivity (g/L/h) was calculated by dividing maximum PCA concentration (g/L) by the time in hours from induction.

Flow Cytometry

The effect of PCA on the proton motive force (PMF) of *E. coli* ATCC 31882-DSD was evaluated using a BD Accuri C6 flow cytometer Plus (San Jose, CA, United States) and the dye DiBAC(4)3, as described earlier (Buysschaert et al., 2016). The organism was grown in a bioreactor at pH 7 with or without induction using IPTG. Culture samples were withdrawn in the exponential/early stationary phase (17 h) and late stationary phase (46 h) for measurement of PMF. As positive controls, cells treated with the antibiotic gramicidin D (2, 8, and 20 μg/mL) and heat treatment (30 min at 100°C), respectively, were used. The cell samples were diluted to an OD_{600} of 0.02 and re-suspended in PBS buffer with or without 4 g/L PCA. To stain the cells, 1 μM DiBAC(4)3 was added followed by incubation for 30 min at 37°C. A blue laser of wavelength 480 nm was used for emission and a band filter of 530/30 was used for the excitation measurement. A gate on the forward scatter (FSC) at 20 000 was used to filter out the background noise and 20 000 events were collected for each sample.

RESULTS

DSD Gene Expression in *E. coli* BL21(DE3) and PCA Production

Cloning and transformation of the *P. putida DSD* gene in *E. coli* BL21(DE3) resulted in successful expression of the DSD protein with a His_6 tag in a soluble form after induction with 0.1 mM IPTG. This was confirmed by SDS-PAGE as a 70 kDa band (**Supplementary Figure 1**). Cultivation of the recombinant *E. coli* BL21(DE3)-DSD in the normal M9 medium in shake flasks resulted in low cell density (OD_{600} value of 2) and PCA titer (0.2 g/L). But when supplemented with trace metals and thiamine, the OD_{600} and PCA titer increased to 8 and 0.8 g/L, respectively (**Figure 2A**), and the culture turned black toward the end of the cultivation at 27 h compared to the pale-yellow color of the M9 culture. Such a color change could be attributed to the photochemical oxidation of PCA catalyzed by the metal ions like Fe^{3+} present in the medium (Guo et al., 2020). Yet another likely reason is that the DSD due to its high

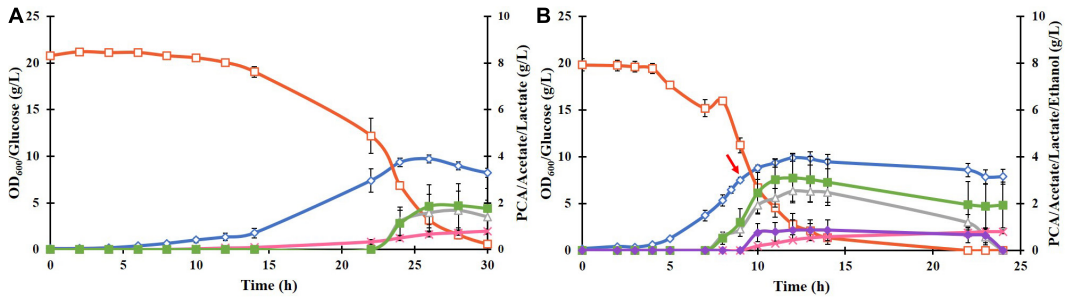

FIGURE 2 | (A) Culture parameters of *E. coli* BL21(DE3)-DSD during an aerobic batch cultivation in a bioreactor in modified M9 medium at constant temperature of 37°C, pH 7 and stirring rate of 600 rpm. Expression of DSD gene was done by addition of 0.1 mM IPTG at: **(A)** 0 h, and **(B)** at 9 h after the start of the cultivation shown by a red arrow. The cultivations were performed in duplicates. The symbols denote profiles of cell density measured as OD_{600} (◇), concentrations of glucose (□), PCA (x), acetate (△), lactate (■), and ethanol (♦).

sequence identity with hydroxyphenylpyruvate dioxygenase (HPPD), catalyzes conversion of 4-hydroxyphenylpyruvate in the tyrosine catabolism pathway to homogentisate (HGA), which undergoes a spontaneous oxidative dimerization, producing or orchronic pigments (Peek et al., 2017). Accumulation of both homogentisate and or orchronic pigments is known to lead to oxidative stress in human cells (Braconi et al., 2015). The color change was not seen in the normal M9 medium.

Cultivating the strain BL21(DE3)-DSD under anaerobic conditions (no air flow, 80 rpm) showed no color change, but led to slowing down of the growth rate and lower biomass formation as expected, and the PCA yield decreasing to 0.007 mol/mol glucose, which corresponds to a PCA concentration of 0.16 g/L, as compared to 0.06 mol/mol under aerobic conditions. Yet another major difference under anaerobic conditions was an increase in lactate formation from 1.6 to 15 g/L due to the fermentative metabolism of glucose (result not shown).

Regardless of the time of inducing the gene expression, whether right at the start of the cultivation or later when the cells were in the late exponential phase, the PCA formation started in the late exponential phase and continued into the stationary phase (**Figures 2A,B**, respectively). Late induction resulted in 55% increase in the PCA yield, *i.e.*, from 0.046 ± 0.013 to 0.083 ± 0.003 mol/mol glucose (**Figure 2B**), however, the final PCA titer was lowered from 0.804 ± 0.25 to 0.764 ± 0.117 g/L as less glucose was available during the PCA production phase. The PCA titer was deemed to be a more important variable to maximize compared to the yield, as the use of inducible promoters is impractical in industrial production and that the toxicity/inhibitory effect of PCA as a function of the titer was one of the major factors thought to limit its formation. Hence, in further experiments, cells were induced at the start of cultivations.

PCA Production Using *E. coli* ATCC 31882-DSD

The plasmid pCSFDuet-*DSD* was then transformed into *E. coli* ATCC 31882, a phenylalanine overproducing strain in which the feedback inhibited enzymes AroF and AroG were removed and so was also the ability to produce tyrosine and tryptophan. Growth under the same conditions as BL21(DE3)-DSD resulted in a higher PCA titer of 1.8 ± 0.28 g/L and yield of 0.13 ± 0.031 mol/mol (**Figure 3A**). There was also a difference between the strains in the amount of by-products formed; absence of lactate formation in *E. coli* ATCC 31882-DSD was especially notable.

Unlike BL21(DE3)-DSD, the strain ATCC 31882-DSD had what appeared to be two phases of growth (**Figure 3A**). The initial exponential phase was followed by a relatively long period during which there was no notable increase in biomass but PCA production followed by acetate formation was noticed. Subsequently, a more rapid glucose consumption and biomass increase was observed before cell growth leveled off. A similar pause in exponential phase was observed in the parental strain ATCC 31182 and formation of lactate was initiated (**Figure 3B**), indicating some kind of metabolic shift in this strain.

The effect of nitrogen and phosphorus limitation on cell growth and PCA production of ATCC 31882-DSD was also studied. The nitrogen-limited batch culture showed a large decrease in biomass formation, glucose consumption and PCA formation, while the strain grown under phosphorus limitation displayed nearly similar growth and PCA yields as under non-limited cultivation (0.124 ± 0.015 mol/mol compared to 0.128 ± 0.031) although at a slower rate and with increased acetate formation (**Supplementary Figure 2** and **Table 1**).

Fed Batch Cultivation of *E. coli* ATCC 31882-DSD

To improve the PCA titer, a fed-batch culture of ATCC 31882-DSD was performed using feed with glucose only or with glucose and NH_4Cl (**Figures 4A,B**). In the latter case, the PCA reached a maximum titer of 4.25 g/L after 54 h, with a yield of 0.182 mol/mol and a productivity of 0.079 g/L.h. In the absence of nitrogen in the feed, the PCA titer was 2.5 g/L after 110 h, with a final yield of 0.085 mol/mol and productivity of 0.02 g/L/h. Acetate was formed as a major side product in both cases starting at about 30 h of cultivation. In both cases the media turned black at the end of the cultivation.

The biomass formation ceased in both cultures after approximately 40 h, and even the PCA concentration remained almost constant after 54 h or dropped slightly. On the other

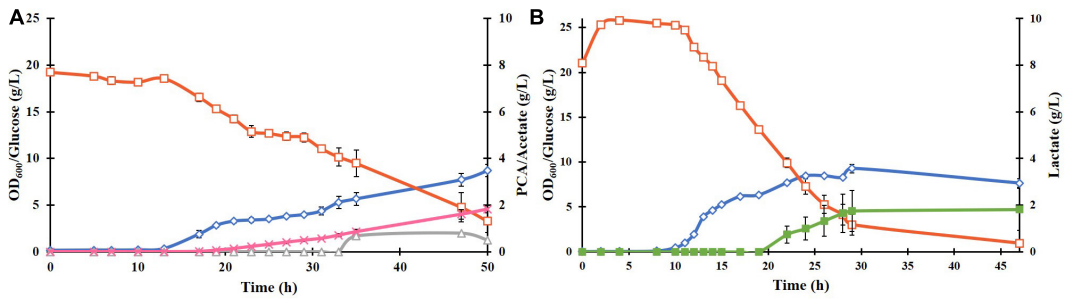

FIGURE 3 | Batch cultivation of *E. coli* ATCC 31882-DSD with the modified M9 medium in a bioreactor at pH 7, 37°C, and constant stirring rate at 600 rpm, with induction of gene expression at 0 h **(A)**. *E. coli* ATCC 31882 was grown as a control **(B)**. The cultivations were performed in duplicates. The symbols represent profiles of cell density measured as OD_{600} (◊), concentrations of glucose (□), PCA (x), acetate (△), and lactate (■).

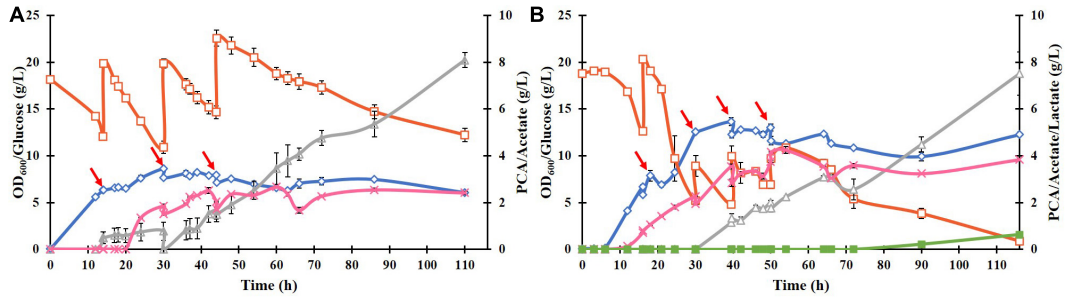

FIGURE 4 | Fed-batch cultivation of *E. coli* ATCC 31882-DSD in 1 liter of the modified M9 medium using a feed of: **(A)** glucose only, and **(B)** glucose and NH_4Cl. The cultivations were performed in duplicates. Symbols: cell density measured as OD_{600} (◊), concentrations of glucose (□), PCA (x), acetate (△), and lactate (■). The cells were induced for expression of DSD using 0.1 mM IPTG at the start of the cultivation. The feed of approximately 10 g glucose (and 2 g NH_4Cl) in 50 mL solution was added at discrete time points indicated by red arrows.

hand, glucose consumption continued for the duration of the cultivation, resulting in continued formation of acetate reaching the final concentration of 7.5 g/L after 110 h (**Figure 4B**). The acetate yield in the later phase of the cultivation, *i.e.*, after 54 h in **Figure 4B**, was 2.0 mol/mol glucose, corresponding to 5.3 g/L. As this is the theoretical maximal yield, it implies complete conversion of glucose to acetate and carbon dioxide during this time, which seems to suggest that the cells switched from running anabolic pathways to catabolic pathways.

Effect of Trace Metals Addition on Cell Growth and PCA Production by *E. coli* ATCC 31882-DSD

To investigate if the removal of metal ions due to chelation by PCA was linked to the observed stagnation of biomass and PCA formation and the significant increase in acetate formation (**Figure 4B**), *E. coli* ATCC 31882-DSD was cultivated in batch mode in the medium at four times higher trace metal concentration but not induced for PCA production. The culture showed an increase in acetate formation and decrease in lactate formation (**Figure 5B**). Cultivations were then performed by supplementation of 4 g/L PCA to the culture in the mid exponential phase that led to direct increase in acetate formation to 7.9 g/L (**Figure 5C**), and also formate and succinate to a lower degree. On the other hand, in the induced culture producing PCA in the medium containing higher content of trace metals, acetate formation was lower and PCA titers were similar to that with 1 × trace metals content (**Figure 5A**).

Effect of PCA on Proton Motive Force of *E. coli* ATCC 31882-DSD

The possible effect of PCA produced on the PMF of the cells was measured using flow cytometry. The method is based on the use of the fluorescent dye DiBAC(4)3 that enters the cell membrane when the membrane potential changes, which is an indication of a collapsed PMF. Comparison of *E. coli* ATCC 31882 and *E. coli* ATCC 31882-DSD showed that PCA production had no notable effect on the PMF of the cells (**Table 2**). Also, the addition of 4 g/L PCA to both ATCC 31882 and induced ATCC 31882-DSD cells (after washing) had no effect on the PMF. As a control, gradual addition of the antibiotic gramicidin D led to an increase in the percentage of permeabilized cells. Even the cells subjected to heat treatment did not maintain a PMF, resulting in permeabilization of 99.8% of total cells.

Adsorption of PCA to Ion Exchange Resin

Incubation of the PCA containing solution (1–10 g/L) with the ion exchange resins showed complete adsorption to occur within 20 min of incubation. The adsorption capacity of Amberlite 400

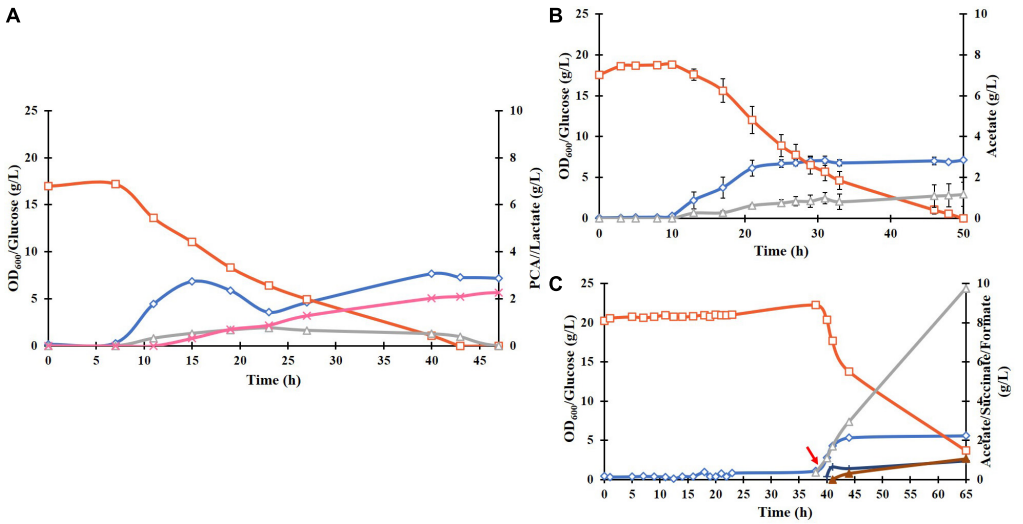

FIGURE 5 | Effect of trace metal concentration and PCA on cell growth and production of metabolites by *E. coli* ATCC 31882-DSD in the modified M9 medium: **(A)** supplemented with four times higher trace metal concentration and induction at 0 h with 0.1 mM IPTG, **(B)** non-induced culture with four times higher trace metal concentration, **(C)** culture as in B and with addition of PCA at 40 h of cultivation. The symbols denote the profiles of cell density measured as OD_{600} (◇), concentrations of glucose (□), PCA (×), acetate (△), succinate (▲), and formate (+).

IRA (Cl), Amberlite 401 IRA (Cl), and Amberlite 904 IRA (Cl) for PCA was found to be 436, 490, and 312 mg/g, respectively. Elution of the adsorbed PCA from the resins exposed to 10 g/L PCA showed highest degree of elution with 1 M NaCl, 0.3 M acetic acid and 0.5 M acetic acid from Amberlite IRA 400, 401, and 904, respectively. The highest amount of PCA eluted was 386 mg/g_{resin} from Amberlite IRA 401 (Cl) by 0.3 M acetic acid, corresponding to an elution yield of 82%.

Subsequently, 4 g/L of Amberlite IRA 401 (Cl) was added to the *E. coli* ATCC 31882-DSD batch culture in the modified M9 medium to study the possibility of *in situ* adsorption of PCA. no PCA adsorption was noted; the PCA concentration in the medium was 1.84 g/L and comparable to cultivation without the resin, and also no PCA could be eluted from the resin (data not shown). No adverse effect on the growth of the bacteria was observed.

DISCUSSION

Among the various metabolic and regulatory bottlenecks encountered in channeling the carbon flow to aromatic building blocks from the shikimate pathway for aromatic amino acids, this study focused on the effect of relieving allosteric control of DAHP synthesis on PCA production from glucose. Moreover, the route involving direct conversion of DAHP to PCA catalyzed by DSD was preferred over the alternative UbiC/PobA pathway, which is stoichiometrically less favorable and requires one mole each of ATP, NADPH and phosphoenol pyruvate (PEP) for the conversion of 3-DHS to chorismate and one more NADPH further downstream for reduction of *p*-hydroxybenzoic acid (pHBA) to PCA (**Figure 1**). Also, the use of an additional PEP to form chorismate might be more problematic since it is needed both for the formation of DAHP and for the transport of glucose via the phosphotransferase (PTS) system. Furthermore, UbiC is also allosterically inhibited by pHBA (Siebert et al., 1994). An earlier study making use of the overexpressed PobA/Ubic pathway in *E. coli* showed PCA production with a yield of 0.03 mol/mol glucose only in the strain in which the allosteric regulation was removed (Pugh et al., 2014; **Table 1**).

Dehydroshikimate dehydratase enzymes play a key role in the degradation of the aromatics quinate and shikimate by soil-associated bacteria (Peek et al., 2017). Multiple DSD variants from fungi, *Acinetobacter* species, *Bacillus* species, and *Pseudomonas* species have been identified. Earlier studies have reported the use of DSD from *Corynebacterium glutamicum*, *Podospora pauciseta,* and *Klebsiella pneumonia* (Hansen et al., 2009; Curran et al., 2013; Shmonova et al., 2020; **Table 1**). In this study, the *P. putida* DSD gene was cloned and expressed in *E. coli*. The structure of the enzyme has shown the protein to be a fusion of two modules comprising an N-terminal sugar phosphate isomerase like domain that is associated with the DSD activity and a C-terminal hydroxyphenylpyruvate dioxygenase-like domain (Peek et al., 2017). The N-terminal domain of the enzyme possesses limited sequence identity with fungal DSDs and 39.9% identity with the enzyme from *C. glutamicum* (Peek et al., 2017; Shmonova et al., 2020). The DSD from *P. putida* has been reported to have a favorable K_{cat}/K_m value of 494.3×10^3 M^{-1} s^{-1} (Peek et al., 2017), compared to the other characterized bacterial DSDs, such as 63.3×10^3 M^{-1} s^{-1} for *C. glutamicum* (Shmonova et al., 2020) and 28.9×10^3 M^{-1} s^{-1} for *Bacillus thuringiensis* (Fox et al., 2008).

Expression of *P. putida* DSD in *E. coli* BL21(DE3) yielded 0.8 g/L PCA when cultivated on glucose, which was comparable to the highest reported (**Table 1**). We further show that removal of allosteric control of the shikimate pathway resulted in over

TABLE 1 | Comparison of results on microbial PCA production obtained in this study with those from the literature.

Organism and strain	*E. coli* ATCC 31882	*E. coli* ATCC 31882	*E. coli* MG1655	*S. pombe*	*S. cerevisiae*, BY4741	*E. coli* BL21(DE3)	*C. glutamicum* ATCC 21420	*E. coli* NST74
Pathway determining intermediate	3-DHS	3-DHS	3-DHS	3-DHS	3-DHS	Chorismate	Chorismate	Chorismate
Overexpressed genes	*DSD*	*DSD*	*DSD*	*DSD*	*TKL1, aroY, CatA, DSD*	*Co-culture Strain A: pobA. Strain B: aroE, aroL, aroA, aroC, ubiC aroGfbr, aroB, aroD, and pobR*	*ubiC, pobA*	*ubiC, pobA*
Source of DSD if applicable	*P. putida*	*P. putida*	*C. glutamicum*	*P. pauciseta*	*K. pneumoniae*			
Genes knocked out	*aroF aroG tyrR pheA tyrA trpE*	*aroF aroG tyrR pheA pheAo tyrA trpE*	*aroE*	-	*aro3 aro4*	*xylA tyrA pheA*	-	*pheA*
Maximum titer (g/L)	4.25	1.82	3.9	0.364	0.300	0.641	1.17	0.454
Yield (mol/mol)	0.182	0.128	0.118	0.0104	0.006	0.110	0.008	0.028
Productivity (g/L/h)	0.079	0.036	0.089	0.008	0.004	0.013	0.010	0.005
Cultivation mode	Fed-batch in bioreactor	Batch in bioreactor	Batch in test tubes	Batch in bioreactor	Batch in shake flask	Batch co-culture	Fed-batch in bioreactor	Batch in bioreactor
References	This study	This study	Shmonova et al. (2020)	Hansen et al. (2009)	Curran et al. (2013)	Guo et al. (2020)	Okai et al. (2016)	Pugh et al. (2014)

aroA, 3-phosphoshikimate 1-carboxyvinyltransferase; aroB, aroC, chorismate synthase; 3-dehydroquinate synthase; aroD, 3- dehydroquinate dehydratase; aroE, shikimate dehydrogenase; aroL, shikimate kinase Gfbr, feedback-resistant 3-deoxy-7-phosphoheptulonate synthase; aro3, 3-deoxy-7-phosphoheptulonate synthase; aro4, 3-deoxy-7-phosphoheptulonate synthase; aroY, PCA decarboxylase; CatA, catechol 1,2-dioxygenase; TKL1, Transketolase; xylA, Xylose isomerase; ubiC, chorismate pyruvate lyase; pobA, p-hydroxybenzoate hydroxylase; pobR, p-hydroxybenzoate hydroxylase transcriptional activator; pheA, fused chorismate mutase/prephenate dehydratase; tyrR, Transcriptional regulatory protein; tyrA, fused chorismate mutase/prephenate dehydrogenase; trpE, anthranilate synthase subunit.

two-fold increase in PCA titer (1.8 g/L) produced by expression of DSD in *E. coli* ATCC 31882. We investigated the effect of nitrogen and phosphorus limitation on PCA synthesis, as these conditions can influence a shift from oxidative to overflow metabolism (Folsom and Carlson, 2015; Guevara-Martínez et al., 2015). Phosphorus limitation did not affect the PCA production significantly possibly due to the intracellular phosphate pools available. On the other hand, nitrogen limitation was detrimental for PCA production, primarily as a result of reduced biomass formation. Nitrogen is moreover a crucial component needed for production of amino acids and proteins.

Highest PCA titer of 4.25 g/L with a molar yield of 18% from glucose and productivity of 0.079 g/L/h was achieved during fed-batch cultivation of *E. coli* ATCC 31882-DSD using a feed containing glucose and nitrogen in the form of NH_4Cl. Also, the final cell density was increased from an OD_{600} of 6.1 to 12.3. With the feed containing glucose only, PCA and biomass formation leveled off despite the glucose being continually consumed, and $Y_{P/B}$ remained similar to the cultivation with nitrogen in the feed, *i.e.,* 0.60 cmol/cmol vs. 0.64 cmol/cmol (**Supplementary Table 2**). A likelihood of the PCA production being inhibited by the removal of Ni^{2+}, Mn^{2+}, Mg^{2+}, and Co^{2+} present in the medium due to chelation by PCA was considered (Yang et al., 2014), as these metal ions are known to increase the activity of *P. putida* DSD (Peek et al., 2017). However, increasing the trace metal concentration four-fold in the medium did not increase the yield of PCA or decrease acetate formation (**Figure 5A**). On the other hand, the recent report on *C. glutamicum* DSD showed an increased PCA production to 3.9 g/L in the medium supplemented with 10 μM $CoCl_2$ (Shmonova et al., 2020).

Once the PCA synthesis ceased in the fed-batch cultivation, the glucose consumption continued and was totally metabolized to acetate. This could be a result of the inhibition of the TCA-cycle or the electron transport chain (ETC) by PCA, resulting in lowered yield of ATP and biomass. Acetate formation, unlike lactate or ethanol, provides an extra ATP, which could be useful as a form of stress response, for example for the efflux of

TABLE 2 | Percentage of cells with collapsed proton motive force as seen by increase of fluorescence by DiBAC(4)3 of *E. coli* ATCC 31882 and *E. coli* ATCC 31882-DSD exposed to 4 g/L PCA, gramicidin and heat, respectively.

Time	Culture	Permeabilized cells (%)	
		PBS	PBS + PCA
19 h	ATCC 31882	2.6	3.1
19 h	ATCC 31882-DSD	4.6	1.9
43 h	ATCC 31882	7.2	4.7
43 h	ATCC 31882-DSD	7.6	15.0
	Gramicidin (2 μg/mL)	25.7	
	Gramicidin (8 μg/mL)	37.3	
	Gramicidin (20 μg/mL)	43.7	
	Heat treated	99.8	

Produced PCA at 19 h and 43 h for ATCC 31882-DSD was 0.49 g/L and 5.1 g/L, respectively.

PCA from the cells. Acetate formation was also induced by external supplementation of PCA to the culture. The possibility of PCA interfering in the ETC by inserting itself into the cell membrane and thus increasing the permeability (Pugh et al., 2014), and disrupting the PMF was shown not to be the case as measured by flow cytometry. This suggests that while PCA has an effect on either the TCA or ETC, it is not through metal chelation or lowered PMF.

Hence, while PCA is formed as a metabolite in anabolic metabolism its formation causes a shift to catabolic metabolism in *E. coli*, resulting in the termination of its own production (**Figure 4B**). The metabolic effect seems to be that acetyl-CoA is preferentially converted through a less energetically favorable route to form acetate rather than through the TCA-cycle although some amounts of the intermediate product succinate were observed. It is clear from **Figure 5C** that the rise in acetate formation is almost immediate upon addition of PCA, suggesting the mechanism of action is through regulation at the protein level and not through genetic regulation, which would have required a lag period of at least 30 min for the new proteins to be transcribed. PCA inhibition of DSD activity has been reported earlier (Shmonova et al., 2020). However, how PCA mediated enzyme inhibition and effect on glucose metabolism are related is not yet clear and would require further studies to map the metabolism and protein expression to evaluate how the shift to catabolic metabolism is regulated to find means for increasing the tolerance toward the inhibitory product.

While *in situ* product removal is a useful alternative to alleviate the product inhibition, our results showed that while the ion exchanger Amberlite IRA 401 (Cl) was able to adsorb PCA in aqueous solution, it showed no adsorption of the metabolite when included in the culture medium. This could be due to the interference by metal ions and other compounds present in the medium. Nevertheless, our observations are not in agreement with the study that reported a very high PCA titer of 71 g/L when a similar resin AG-1 × 8 was added during production of PCA using *E. coli* modified with DSD (Li et al., 2005). Even without the resin, production of 40 g/L PCA equivalent to 49% mol/mol glucose was reported, which is surprising considering that the growth of *E. coli* is inhibited by 1.5 g/L PCA (Pugh et al., 2014). Our results are more in agreement with the highest yields in *E. coli* reported for aromatic molecules that are not known to be toxic, e.g., 0.27 mol phenylalanine, 0.13 mol tryptophan, 0.43 mol tyrosine, and 0.40 mol salicylate per mol glucose (Zhou et al., 2010; Juminaga et al., 2012; Noda et al., 2016; Chen and Zeng, 2017; Noda and Kondo, 2017).

In conclusion, the study shows that expression of *P. putida* DSD gene in the *E. coli* strain engineered to relieve the allosteric inhibition and grown in a fed-batch mode gave among the highest PCA yield from glucose reported so far. It strongly pinpoints to PCA effectuating product inhibition rather than initiating alterations in the bacterial cell membrane. As a consequence, the inhibition caused a metabolic shift inherent to acetate production. The reduction of acetate formation will most likely be accomplished through applying efficient means for *in situ* removal of PCA to keep it below the critical inhibitory level. Formation of lactate as a by-product, although not significant, can perhaps be avoided by maintaining a high dissolved oxygen tension during the cultivation.

DATA AVAILABILITY STATEMENT

The original contributions presented in the study are included in the article/supplementary material, further inquiries can be directed to the corresponding author/s.

AUTHOR CONTRIBUTIONS

OÖ conceived the project, designed and performed the experiments, and wrote the manuscript. SS designed and performed the experiments. EN directed the project. RH-K conceived and directed the project and wrote the manuscript. All the authors were involved in revising the manuscript.

FUNDING

The work was performed within the framework of the research program Sustainable Plastics and Transition Pathways (STEPS; grant no. 2016/1489) supported by the Swedish Foundation for Strategic Environmental Research (Mistra).

ACKNOWLEDGMENTS

We acknowledge Arne Hagman for help with the flow cytometry set up and Carl Gray and Roya Sardari for help with the analytical method for PCA quantification.

SUPPLEMENTARY MATERIAL

The Supplementary Material for this article can be found online at: https://www.frontiersin.org/articles/10.3389/fbioe.2021.695704/full#supplementary-material

REFERENCES

Averesch, N. J., and Krömer, J. O. (2018). Metabolic engineering of the shikimate pathway for production of aromatics and derived compounds—present and future strain construction strategies. *Front. Bioeng. Biotechnol.* 6:32. doi: 10.3389/fbioe.2018.00032

Braconi, D., Millucci, L., Bernardini, G., and Santucci, A. (2015). Oxidative stress and mechanisms of ochronosis in alkaptonuria. *Free Radic. Biol. Med.* 88, 70–80. doi: 10.1016/j.freeradbiomed.2015.02.021

Buysschaert, B., Byloos, B., Leys, N., Van Houdt, R., and Boon, N. (2016). Reevaluating multicolor flow cytometry to assess microbial viability. *Appl. Microbiol. Biotechnol.* 100, 9037–9051. doi: 10.1007/s00253-016-7837-5

Chen, L., and Zeng, A.-P. (2017). Rational design and metabolic analysis of *Escherichia coli* for effective production of L-tryptophan at high concentration. *Appl. Microbiol. Biotechnol.* 101, 559–568. doi: 10.1007/s00253-016-7772-5

Collias, D. I., Harris, A. M., Nagpal, V., Cottrell, I. W., and Schultheis, M. W. (2014). Biobased terephthalic acid technologies: a literature review. *Ind. Biotechnol.* 10, 91–105. doi: 10.1089/ind.2014.0002

Curran, K. A., Leavitt, J. M., Karim, A. S., and Alper, H. S. (2013). Metabolic engineering of muconic acid production in *Saccharomyces cerevisiae*. *Metab. Eng.* 15, 55–66. doi: 10.1016/j.ymben.2012.10.003

Eerhart, A., Faaij, A., and Patel, M. K. (2012). Replacing fossil based PET with biobased PEF; process analysis, energy and GHG balance. *Energy Environ. Sci.* 5, 6407–6422. doi: 10.1039/C2EE02480B

Folsom, J. P., and Carlson, R. P. (2015). Physiological, biomass elemental composition and proteomic analyses of *Escherichia coli* ammonium-limited chemostat growth, and comparison with iron-and glucose-limited chemostat growth. *Microbiology* 161, 1659–1670. doi: 10.1099/mic.0.000118

Fox, D. T., Hotta, K., Kim, C.-Y., and Koppisch, A. T. (2008). The missing link in petrobactin biosynthesis: asbF encodes a (−)-3-dehydroshikimate dehydratase. *Biochemistry* 47, 12251–12253. doi: 10.1021/bi801876q

Graglia, M., Kanna, N., and Esposito, D. (2015). Lignin refinery: towards the preparation of renewable aromatic building blocks. *ChemBioEng Rev.* 2, 377–392. doi: 10.1002/cben.201500019

Guevara-Martínez, M., Gällnö, K. J., Sjöberg, G., Jarmandr, J., Perez-Zabaleta, M., Quillaguamán, J., et al. (2015). Regulating the production of (R)-3-hydroxybutyrate in *Escherichia coli* by N or P limitation. *Front. Microbiol.* 6:844. doi: 10.3389/fmicb.2015.00844

Guo, X., Wang, X., Chen, T., Lu, Y., and Zhang, H. (2020). Comparing *E. coli* mono-cultures and co-cultures for biosynthesis of protocatechuic acid and hydroquinone. *Biochem. Eng. J.* 156:107518. doi: 10.1016/j.bej.2020.107518

Hanahan, D. (1983). Studies on transformation of *Escherichia coli* with plasmids. *J. Mol. Biol.* 166, 557–580. doi: 10.1016/s0022-2836(83)80284-8

Hansen, E. H., Möller, B. L., Kock, G. R., Bünner, C. M., Kristensen, C., Jensen, O. R., et al. (2009). De novo biosynthesis of vanillin in fission yeast (*Schizosaccharomyces pombe*) and baker's yeast (*Saccharomyces cerevisiae*). *Appl. Environ. Microbiol.* 75, 2765–2774. doi: 10.1128/AEM.02681-08

Hatti-Kaul, R., Nilsson, L. J., Zhang, B., Rehnberg, N., and Lundmark, S. (2020). Designing biobased recyclable polymers for plastics. *Trends Biotechnol.* 38, 50–67. doi: 10.1016/j.tibtech.2019.04.011

Huccetogullari, D., Luo, Z. W., and Lee, S. Y. (2019). Metabolic engineering of microorganisms for production of aromatic compounds. *Microb. Cell Fact.* 18:41. doi: 10.1186/s12934-019-1090-4

Johansson, L., and Lidén, G. (2006). Transcriptome analysis of a shikimic acid producing strain of *Escherichia coli* W3110 grown under carbon-and phosphate-limited conditions. *J. Biotechnol.* 126, 528–545. doi: 10.1016/j.jbiotec.2006.05.007

Juminaga, D., Baidoo, E. E. K., Redding-Johanson, A. M., and Keasling, J. D. (2012). Modular engineering of L-tyrosine production in *Escherichia coli*. *Appl. Environ. Microbiol.* 78, 89–98. doi: 10.1128/AEM.06017-11

Kakkar, S., and Bais, S. (2014). A review on protocatechuic acid and its pharmacological potential. *Int. Sch. Res. Notices* 2014:952943. doi: 10.1155/2014/952943

Kucherov, F. A., Romashov, L. V., Averochkin, G. M., and Ananikov, V. P. (2021). Biobased C6-furans in organic synthesis and industry: cycloaddition chemistry as a key approach to aromatic building blocks. *ACS Sustain. Chem. Eng.* 9, 3011–3042. doi: 10.1021/acssuschemeng.0c09229

Lee, J.-H., and Wendisch, V. F. (2017). Biotechnological production of aromatic compounds of the extended shikimate pathway from renewable biomass. *J. Biotechnol.* 257, 211–221. doi: 10.1016/j.jbiotec.2016.11.016

Li, W., Xie, D., and Frost, J. (2005). Benzene-free synthesis of catechol: interfacing microbial and chemical catalysis. *J. Am. Chem. Soc.* 127, 2874–2882. doi: 10.1021/ja045148n

Li, Z., Wang, H., Ding, D., Liu, Y., Fang, H., Chang, Z., et al. (2020). Metabolic engineering of *Escherichia coli* for production of chemicals derived from the shikimate pathway. *J. Ind. Microbiol. Biotechnol.* 47, 525–535. doi: 10.1007/s10295-020-02288-2

Neidhardt, F. C., Bloch, P. L., and Smith, D. F. (1974). Culture medium for enterobacteria. *J. Bacteriol.* 119, 736–747. doi: 10.1128/JB.119.3.736-747.1974

Noda, S., and Kondo, A. (2017). Recent advances in microbial production of aromatic chemicals and derivatives. *Trends Biotechnol.* 35, 785–796. doi: 10.1016/j.tibtech.2017.05.006

Noda, S., Shirai, T., Oyama, S., and Kondo, A. (2016). Metabolic design of a platform *Escherichia coli* strain producing various chorismate derivatives. *Metab. Eng.* 33, 119–129. doi: 10.1016/j.ymben.2015.11.007

Okai, N., Miyoshi, T., Takeshima, Y., Kuwahara, H., Ogino, C., and Kondo, A. (2016). Production of protocatechuic acid by *Corynebacterium glutamicum* expressing chorismate-pyruvate lyase from *Escherichia coli*. *Appl. Microbiol. Biotechnol.* 100, 135–145. doi: 10.1007/s00253-015-6976-4

Peek, J., Roman, J., Moran, G. R., and Christendat, D. (2017). Structurally diverse dehydroshikimate dehydratase variants participate in microbial quinate catabolism. *Mol. Microbiol.* 103, 39–54. doi: 10.1111/mmi.13542

Pugh, S., McKenna, R., Osman, M., Thompson, B., and Nielsen, D. R. (2014). Rational engineering of a novel pathway for producing the aromatic compounds p-hydroxybenzoate, protocatechuate, and catechol in *Escherichia coli*. *Process Biochem.* 49, 1843–1850. doi: 10.1016/j.procbio.2014.08.011

Ramos, J. L., Duque, E., Gallegos, M.-T., Godoy, P., Ramos-Gonzalez, M. I., Rojas, A., et al. (2002). Mechanisms of solvent tolerance in gram-negative bacteria. *Ann. Rev. Microbiol.* 56, 743–768. doi: 10.1146/annurev.micro.56.012302.161038

Rodriguez, A., Martnez, J. A., Flores, N., Escalante, A., Gosset, G., and Bolivar, F. (2014). Engineering *Escherichia coli* to overproduce aromatic amino acids and derived compounds. *Microb. Cell Fact.* 13:126. doi: 10.1186/s12934-014-0126-z

Sayed, M., Dishisha, T., Sayed, W. F., Salem, W. M., Temerk, H. A., and Pyo, S.-H. (2016). Selective oxidation of trimethylolpropane to 2, 2-bis (hydroxymethyl) butyric acid using growing cells of *Corynebacterium* sp. ATCC 21245. *J. Biotechnol.* 221, 62–69. doi: 10.1016/j.jbiotec.2016.01.022

Shmonova, E. A., Voloshina, O. V., Ovsienko, M. V., Smirnov, S. V., Nolde, D. E., and Doroshenko, V. G. (2020). Characterization of the *Corynebacterium glutamicum* dehydroshikimate dehydratase QsuB and its potential for microbial production of protocatechuic acid. *PLoS One* 15:e0231560. doi: 10.1371/journal.pone.0231560

Siebert, M., Severin, K., and Heide, L. (1994). Formation of 4-hydroxybenzoate in *Escherichia coli*: characterization of the ubiC gene and its encoded enzyme chorismate pyruvate-lyase. *Microbiology* 140, 897–904. doi: 10.1099/00221287-140-4-897

Sousa, A. F., Vilela, C., Fonseca, A. C., Matos, M., Freire, C. S. R., Gruter, G.-J. M., et al. (2015). Biobased polyesters and other polymers from 2, 5-furandicarboxylic acid: a tribute to furan excellency. *Polym. Chem.* 6, 5961–5983. doi: 10.1039/C5PY00686D

Suástegui, M., and Shao, Z. (2016). Yeast factories for the production of aromatic compounds: from building blocks to plant secondary metabolites. *J. Ind. Microbiol. Biotechnol.* 43, 1611–1624. doi: 10.1007/s10295-016-1824-9

Taymaz-Nikerel, H., Borujeni, A. E., Verheijen, P. J., Heijnen, J. J., and van Gulik, W. M. (2010). Genome-derived minimal metabolic models for *Escherichia coli* MG1655 with estimated in vivo respiratory ATP stoichiometry. *Biotechnol. Bioeng.* 107, 369–381. doi: 10.1002/bit.22802

Yang, J., Stuart, M. A. C., and Kamperman, M. (2014). Jack of all trades: versatile catechol crosslinking mechanisms. *Chem. Soc. Rev.* 43, 8271–8298. doi: 10.1039/C4CS00185K

Zhou, H., Liao, X., Wang, T., Du, G., and Chen, J. (2010). Enhanced L-phenylalanine biosynthesis by co-expression of pheA(fbr) and aroF(wt). *Bioresour. Technol.* 101, 4151–4156. doi: 10.1016/j.biortech.2010.01.043

Conflict of Interest: The authors declare that the research was conducted in the absence of any commercial or financial relationships that could be construed as a potential conflict of interest.

frontiers in Bioengineering and Biotechnology

ORIGINAL RESEARCH
published: 28 June 2021
doi: 10.3389/fbioe.2021.686319

Evaluation of Heterologous Biosynthetic Pathways for Methanol-Based 5-Aminovalerate Production by Thermophilic *Bacillus methanolicus*

*Luciana Fernandes Brito[1†], Marta Irla[1†], Ingemar Nærdal[2], Simone Balzer Le[2], Baudoin Delépine[3], Stéphanie Heux[3] and Trygve Brautaset[1]**

[1] Department of Biotechnology and Food Science, Norwegian University of Science and Technology, Trondheim, Norway, [2] Department of Biotechnology and Nanomedicine, SINTEF Industry, Trondheim, Norway, [3] Toulouse Biotechnology Institute, Université de Toulouse, CNRS, INRA, INSA, Toulouse, France

OPEN ACCESS

Edited by:
K. Madhavan Nampoothiri, National Institute for Interdisciplinary Science and Technology (CSIR), India

Reviewed by:
Jing Wu, Jiangnan University, China
Nico Betterle, University of Verona, Italy

***Correspondence:**
Trygve Brautaset
trygve.brautaset@ntnu.no

[†] These authors have contributed equally to this work

Specialty section:
This article was submitted to Industrial Biotechnology, a section of the journal Frontiers in Bioengineering and Biotechnology

Received: 26 March 2021
Accepted: 18 May 2021
Published: 28 June 2021

Citation:
Brito LF, Irla M, Nærdal I, Le SB, Delépine B, Heux S and Brautaset T (2021) Evaluation of Heterologous Biosynthetic Pathways for Methanol-Based 5-Aminovalerate Production by Thermophilic Bacillus methanolicus. Front. Bioeng. Biotechnol. 9:686319. doi: 10.3389/fbioe.2021.686319

The use of methanol as carbon source for biotechnological processes has recently attracted great interest due to its relatively low price, high abundance, high purity, and the fact that it is a non-food raw material. In this study, methanol-based production of 5-aminovalerate (5AVA) was established using recombinant *Bacillus methanolicus* strains. 5AVA is a building block of polyamides and a candidate to become the C5 platform chemical for the production of, among others, δ-valerolactam, 5-hydroxy-valerate, glutarate, and 1,5-pentanediol. In this study, we test five different 5AVA biosynthesis pathways, whereof two directly convert L-lysine to 5AVA and three use cadaverine as an intermediate. The conversion of L-lysine to 5AVA employs lysine 2-monooxygenase (DavB) and 5-aminovaleramidase (DavA), encoded by the well-known *Pseudomonas putida* cluster *davBA*, among others, or lysine α-oxidase (RaiP) in the presence of hydrogen peroxide. Cadaverine is converted either to γ-glutamine-cadaverine by glutamine synthetase (SpuI) or to 5-aminopentanal through activity of putrescine oxidase (Puo) or putrescine transaminase (PatA). Our efforts resulted in proof-of-concept 5AVA production from methanol at 50°C, enabled by two pathways out of the five tested with the highest titer of 0.02 g l^{-1}. To our knowledge, this is the first report of 5AVA production from methanol in methylotrophic bacteria, and the recombinant strains and knowledge generated should represent a valuable basis for further improved 5AVA production from methanol.

Keywords: *Bacillus methanolicus*, thermophile, methanol, 5-aminovalerate, alternative feedstock

INTRODUCTION

The worldwide amino acid market is progressively growing at 5.6% annual rate and is estimated to reach US$25.6 billion by 2022, with amino acids used for animal feed production being its largest component (Wendisch, 2020). The growing demand for amino acid supply confronts the biotechnological industry with an unprecedented challenge of identifying suitable feedstocks,

especially in terms of replacing sugars and agricultural products, use whereof deteriorates food supply and threatens biodiversity (Cotton et al., 2020). Methanol, together with other one-carbon (C1) compounds, is considered a very promising substitute for feedstock that are conventionally used in biotechnological processes. The major advantages of using methanol as carbon source are its low production cost (e.g., methanol from steam reforming of methane), ease of transport and storage, and complete miscibility that bypasses the mass transfer barrier and potentially supports improvement in microbial productivities. However, what seems to cause a considerable difficulty in propagation of methanol as biotechnological feedstock is the limited selection of microorganisms capable to be used as their carbon and energy source. One of the compelling candidates to become a workhorse for the methanol-based production of amino acids is *Bacillus methanolicus*, a thermophilic methylotroph isolated from freshwater marsh soil by Schendel et al. (1990). The wild-type strain MGA3 naturally overproduces L-glutamate in methanol-controlled fed-batch fermentations with volumetric titers reaching up to 60 g l^{-1} (Heggeset et al., 2012; **Table 1**). Furthermore, thanks to recent developments in the toolbox for gene overexpression, it was engineered for production of different amino acid derivatives such as γ-aminobutyric acid and cadaverine (Nærdal et al., 2015; Irla et al., 2017; **Table 1**). MGA3 produces 0.4 g l^{-1} of L-lysine in high cell density fed-batch fermentations (Brautaset et al., 2010; **Table 1**); this titer was improved nearly 30-fold up to 11 g l^{-1} by plasmid-based overexpression of a gene coding for aspartokinase, a key enzyme controlling the synthesis of aspartate-derived amino acids (Jakobsen et al., 2009). Through application of a classical mutagenesis technique, a derivative of *B. methanolicus* MGA3 (M168-20) was constructed, which produces 11 g l^{-1} of L-lysine in high cell density methanol-controlled fed-batch fermentations (Brautaset et al., 2010); the L-lysine overproduction being caused among others by mutation in the *hom*-1 gene coding for homoserine dehydrogenase (Hom) and in the putative lysine 2,3-aminomutase gene (locus tag BMMGA3_02505). The mutation in *hom*-1 leads to the loss of catalytic activity of homoserine dehydrogenase and redirection of metabolic flux toward the L-lysine pathway and therefore its accumulation (Nærdal et al., 2011, 2017).

5-Aminovalerate (5AVA) is a product of L-lysine degradation, and it is mainly synthesized in a two-step process catalyzed by a lysine monooxygenase (DavB) and a δ-aminovaleramide amidohydrolase (DavA) (Revelles et al., 2005). 5AVA is a non-proteogenic five-carbon amino acid that could potentially be used as building block for producing biobased polyamides (Adkins et al., 2013; Park et al., 2014; Wendisch et al., 2018). It is also a promising precursor for plasticizers and chemicals that are intermediates for bioplastic preparation: δ-valerolactam (Chae et al., 2017), 5-hydroxy-valerate (Sohn et al., 2021), glutarate (Adkins et al., 2013; Pérez-García et al., 2018), and 1,5-pentanediol (Cen et al., 2021). As summarized in **Table 1**, diverse approaches have been made at the establishment of microbial 5AVA production. *Pseudomonas putida* KT2440, which possesses *davBA* in its genome, can synthesize 20.8 g l^{-1} 5AVA from 30 g l^{-1} L-lysine in 12 h (Liu et al., 2014). Production of 5AVA was established in *Corynebacterium glutamicum* by heterologous overexpression of the DavB- and DavA-encoding genes (*davBA*) from *P. putida* with a final titer up to 39.9 g l^{-1} in a sugar-based fed-batch fermentation (Rohles et al., 2016; Shin et al., 2016; Joo et al., 2017). 5AVA can be also produced in a process of bioconversion of L-lysine supplemented to the growth medium with molar yields of up to 0.942 achieved by *Escherichia coli* strains overproducing DavBA (Park et al., 2014; Wang et al., 2016). Moreover, when the recombinant *E. coli* strain expressing *davAB* genes was cultured in a medium containing 20 g l^{-1} glucose and 10 g l^{-1} L-lysine, 3.6 g l^{-1} 5AVA was produced, representing a molar yield of 0.45 (Park et al., 2013). Disruption of native lysine decarboxylase (CadA and LdcC) activity in *E. coli* strains overexpressing *davBA* limited cadaverine by-product formation, enabling increased accumulation of L-lysine following 5AVA production, with 5AVA yield of 0.86 g l^{-1} in glucose-based shaking flask fermentation (Adkins et al., 2013). Furthermore, Cheng et al. (2018) reported that the oxidative decarboxylation of L-lysine catalyzed by a L-lysine α-oxidase (RaiP) from *Scomber japonicus* led to 5AVA production. The production of RaiP was enhanced by the addition of 4% (v/v) ethanol and 10 mM H_2O_2, which increased the 5AVA titer to 29.12 g l^{-1} by an *E. coli* host strain in a fed-batch fermentation (Cheng et al., 2018). Recently, in a similar L-lysine bioconversion strategy, an *E. coli* whole-cell catalyst producing RaiP was developed, converting 100 g l^{-1} of L-lysine hydrochloride to 50.62 g l^{-1} 5AVA representing a molar yield of 0.84 (Cheng et al., 2020).

Recent efforts have employed novel metabolic routes toward 5AVA. In *Pseudomonas aeruginosa* PAO1, the set of enzymes composed of glutamylpolyamine synthetase, polyamine:pyruvate transaminase, aldehyde dehydrogenase, and glutamine amidotransferase is essential for the degradation of diamines through the γ-glutamylation pathway (Yao et al., 2011), which may lead to 5AVA production when cadaverine is degraded (Luengo and Olivera, 2020). Jorge et al. (2017) established a three-step 5AVA biosynthesis pathway consisting of the conversion of L-lysine to cadaverine by the activity of the enzyme LdcC, followed by cadaverine conversion to 5AVA through consecutive transamination, by a putrescine transaminase (PatA), and oxidation by a PatD. The heterologous overexpression of the genes *ldcC*, *patA*, and *patD* led to 5AVA production to a final titer of 5.1 g l^{-1} by an engineered *C. glutamicum* strain in a shake flask fermentation (Jorge et al., 2017). This pathway has served as basis for the establishment of a new three-step pathway toward 5AVA using the monooxygenase putrescine oxidase (Puo), which catalyzes the oxidative deamination of cadaverine, instead of PatA (Haupka et al., 2020).

Critical factors that can affect 5AVA accumulation in a production host are the presence of a native 5AVA degradation pathway in its genome and the end product-related inhibition. In some bacterial species, such as *P. putida* KT2440, *Pseudomonas syringae*, *Pseudomonas stutzeri*, and *C. glutamicum*, 5AVA is degraded by a GABAse (**Figure 1**), composed of two enzymes γ-aminobutyric acid aminotransferase (GabT) and succinic

TABLE 1 | Comparison of the 5AVA production by different engineered microbial strains and production of amino acids by *B. methanolicus*.

Organism	Approach	5AVA titer [g l^{-1}]	References
Pseudomonas putida KT2440	DavBA-based biocatalytic production of 5AVA from 30 g l^{-1} L-lysine	20.80	Liu et al., 2014
Corynebacterium glutamicum	Heterologous expression of *davBA*; sugar-based fed-batch fermentation	33.10	Shin et al., 2016
		28.00	Rohles et al., 2016
		39.93	Joo et al., 2017
	Heterologous expression of *ldcC* and *patAD*; shake flask fermentation	5.10	Jorge et al., 2017
	Heterologous expression of *puo* and *patD*, deletion of *gabTD*; microbioreactor fermentation	3.70	Haupka et al., 2020
Escherichia coli	Heterologous expression of *davBA* and deletion of *cadA*; glucose-based shaking flasks fermentation	0.86	Adkins et al., 2013
	Heterologous expression of *davBA*; sugar-based fermentation; 10 g l^{-1} lysine provided	3.60	Park et al., 2013
	Heterologous expression of *davBA*; sugar-based fed-batch fermentation	0.50	Park et al., 2013
	Heterologous expression of *davBA*; glucose-based fed- batch fermentation; 120 g l^{-1} L-lysine provided	90.59	Park et al., 2014
	Heterologous expression of *davBA*; fed-batch whole-cell bioconversion of L-lysine maintained at 120 g l^{-1}	240.70	Wang et al., 2016
	Heterologous expression of *raiP*; whole-cell bioconversion; addition of 4% ethanol, 10 mM H_2O_2 and 100 g l^{-1} lysine	29.12	Cheng et al., 2018
	Heterologous expression of *raiP*; whole-cell bioconversion; 4% ethanol pretreatment, 10 mM H_2O_2 and 100 g l^{-1} lysine	50.62	Cheng et al., 2020
Organism	**Product in methanol-controlled fed-batch fermentation**	**Titer [g L^{-1}]**	**References**
Bacillus methanolicus	L-Glutamate	60.00	Heggeset et al., 2012
	L-Lysine	11.00	Brautaset et al., 2010
	γ-Aminobutyric acid	9.00	Irla et al., 2017
	Cadaverine	11.30	Nærdal et al., 2015

semialdehyde dehydrogenase (GabD) (Park et al., 2013; Rohles et al., 2016; Pérez-García et al., 2018); for example, GABAse from *Pseudomonas fluorescens* KCCM 12537 retains 47.7% activity when 5AVA is used as its substrate in comparison to when GABA is used (So et al., 2013). Based on the previous research, *B. methanolicus* seems a feasible candidate for 5AVA production because it does not possess the necessary genetic background for GABAse-based 5AVA degradation, lacking the *gabT* gene in its genome (Irla et al., 2017). It was reported that 5AVA does not supports growth of *B. methanolicus* neither as sole carbon source nor as sole nitrogen source (Haupka et al., 2021). However, *B. methanolicus* displays low tolerance to 5AVA, with growth being impaired by addition of 1.17 g l^{-1} 5AVA to the culture broth (Haupka et al., 2021).

Even though the application of diverse 5AVA biosynthetic pathways has led to significant improvement in titers and yields of 5AVA production in bacterial hosts, the most efficient processes rely on raw materials that contain sugar and/or agricultural products. Addressing shortages of global resources and food requires a replacement of the current mode of industrial biotechnology, which results in the need for novel biosynthetic pathways that utilize alternative raw materials such as methanol. Hence, in the present study we have selected five different pathways to establish methanol-based 5AVA production in the methylotrophic bacterium *B. methanolicus*. For two of the five pathways, proof-of-principle 5AVA production was achieved and our results should represent a valuable basis of knowledge and strains for further improved 5AVA production from methanol at 50°C.

MATERIALS AND METHODS

Retrosynthesis Analysis

Retrosynthesis analysis was conducted with RetroPath 2 (Delépine et al., 2018) (v6) and RetroRules (Duigou et al., 2019) (1.0.2, with hydrogens, in reversed direction) that translated reactions from MetaNetX (Moretti et al., 2016) into reaction rules, and KNIME (3.6.1). The "source" used in this analysis was 5AVA [InChI = 1S/C5H11NO2/c6-4-2-1-3-5(7)8/h1-4,6H2,(H,7,8)], and "sink" was the set of all metabolites from *E. coli* genome-scale model iJO1366 (Orth et al., 2011). We used at most four reaction steps and a diameter of eight chemical bonds around the reaction center. Those conservative parameters were used to limit the strength of the substrate promiscuity hypothesis and to limit our results to pathways most likely to compete with known pathways.

Strains, Genomic DNA, Plasmids, and Primers

Bacterial strains and plasmids used in this study are listed in **Table 2**. The *E. coli* strain DH5α was used as general cloning host, and *B. methanolicus* strains MGA3 and M168-20 were used as expression hosts. The following strains were the source of genetic material for cloning of the 5AVA synthesis pathways: *E. coli* MG1655, *Rhodococcus qingshengii* DSM45257, *Paenarthrobacter aurescens* DSM20116, *Kocuria rosea* DSM20447, *Peribacillus simplex* DSM1321, and *P. putida* KT2440. The L-lysine-α-oxidase-coding regions from *Trichoderma viride* (GenBank

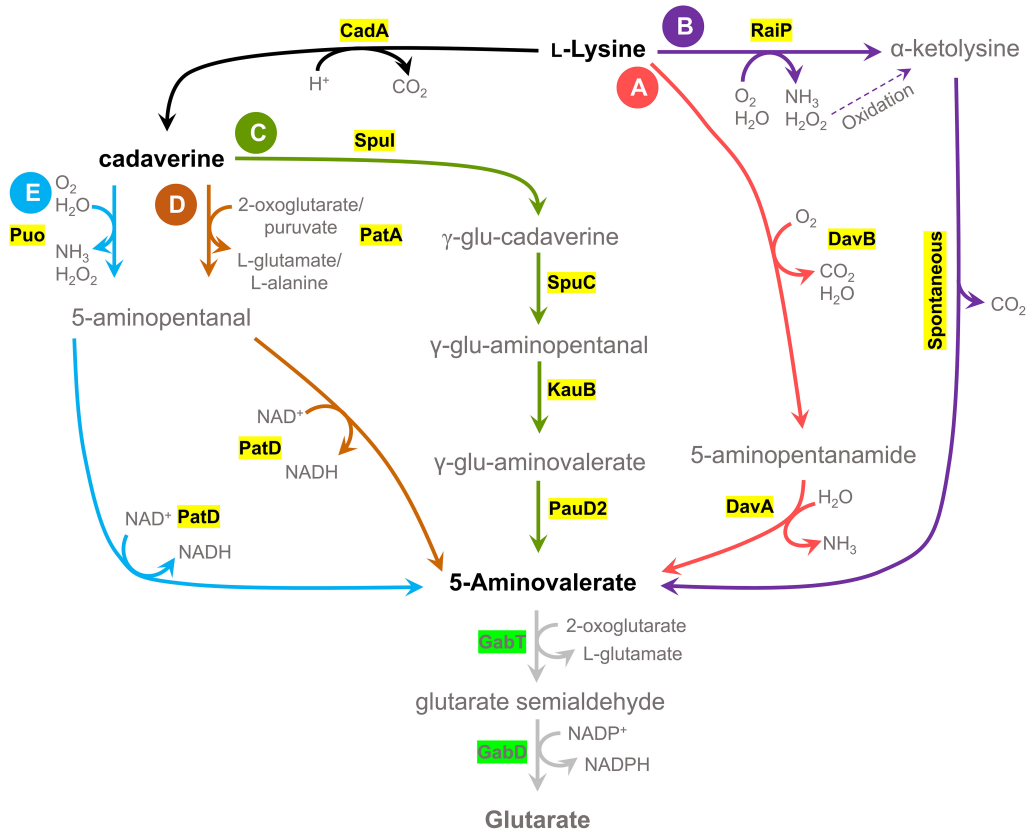

FIGURE 1 | Schematic view of five 5AVA biosynthesis pathways and a 5AVA degradation pathway. Five different pathways for potential 5AVA production in *Bacillus methanolicus* were tested; two pathways have L-lysine as precursor, and three pathways have cadaverine as an intermediate metabolite, obtained by conversion of L-lysine by a lysine decarboxylase (CadA). **(A)** DavBA pathway: L-lysine conversion to 5AVA by lysine 2-monooxygenase (DavB) and 5-aminovaleramidase (DavA). **(B)** RaiP pathway: conversion of L-lysine to α-ketolysine by a L-lysine α-oxidase (RaiP) and spontaneous decarboxylation of α-ketolysine in the presence of hydrogen peroxide. **(C)** SpuI pathway: cadaverine to γ-glutamine-cadaverine (γ-glu-cadaverine) by glutamylpolyamine synthetase (SpuI), with subsequent activity of polyamine:pyruvate transaminase (SpuC), aldehyde dehydrogenase (KauB), and glutamine amidotransferase class I (PauD2); γ-glu-aminopentanal: γ-glutamine-aminopentanal, γ-glu-aminovalerate: γ-glutamine-aminovalerate. **(D)** PatA pathway: cadaverine to 5-aminopentanal through activity of putrescine aminase (PatA) and 5-aminopentanal conversion to 5AVA by 5-aminopentanal dehydrogenase (PatD). **(E)** Puo pathway: cadaverine to 5-aminopentanal through activity of putrescine oxidase (Puo), followed by 5AVA formation by PatD. 5AVA is degraded to glutarate by GABAse activity, a combination of γ-aminobutyrate aminotransferase (GabT) and succinate semialdehyde dehydrogenase (GabD), although this activity was not found in *B. methanolicus* (Irla et al., 2017).

AB937978.1) and *S. japonicus* (GenBank AB970726.1) were codon-optimized for *B. methanolicus* MGA3 expression and synthesized by Twist Biosciences (**Supplementary Table S1** and **Supplementary Material**). The *davBA* operons from alternative hosts *Williamsia sterculiae* CPCC 203464, *Roseobacter denitrificans* OCh 114 strain DSM 7001, and *Parageobacillus caldoxylosilyticus* B4119 (*davA* only) were codon-optimized for expression in *B. methanolicus*, synthesized and provided in the pUC57 plasmid from GenScript (**Supplementary Table S1** and **Supplementary Material**). Isolated genomic DNA of *Bacillus megaterium* DSM32 was purchased from German Collection of Microorganisms and Cell Cultures GmbH (DSMZ). All primers (Sigma-Aldrich) used in this research are listed in **Table 2**.

Molecular Cloning

The *E. coli* DH5α competent cells were prepared according to the calcium chloride protocol as described in Green and Rogers (2013) or purchased as chemically competent NEB 5-α *E. coli* cells (New England Biolabs). All standard molecular cloning procedures were carried out as described in Sambrook and Russell (2001) or according to manuals provided by producers. Chromosomal DNA was isolated as described in Eikmanns et al. (1994). PCR products were amplified using CloneAmp HiFi PCR Premix (Takara) and purified using a QIAquick PCR Purification Kit from Qiagen. DNA fragments were separated using 8 g l^{-1} SeaKem LE Agarose gels (Lonza) and isolated using a QIAquick Gel Extraction Kit (Qiagen). The colony PCR was performed using GoTaq DNA Polymerase (Promega). The sequences of cloned DNA fragments were confirmed by Sanger sequencing (Eurofins). *B. methanolicus* MGA3 was made electrocompetent and transformed by electroporation as described previously (Jakobsen et al., 2006). Recombinant DNA was assembled *in vitro* by means of the isothermal DNA assembly method (Gibson et al., 2009), employing the NEBuilder HiFi DNA Assembly Kit or ligation with T4 DNA ligase.

TABLE 2 | Bacterial strains, plasmids, and primers used in this study.

Strain name	Relevant characteristics	References
Escherichia coli DH5α	General cloning host, F-*thi*-1 *endA*1 *hsdR*17(r-,m-) *supE*44 *_lacU*169 (_80*lacZ*_M15) *recA*1 *gyrA*96 *relA*1	StrataGene
E. coli MG1655	Wild-type strain	ATCC 47076
Bacillus methanolicus MGA3	Wild-type strain	ATCC 53907
Bacillus methanolicus M160-20	1st-generation S-(2-aminoethyl) cysteine-resistant mutant of MGA3; L-lysine overproducer	Brautaset et al., 2010
Rhodococcus qingshengii DSM45257	Wild-type strain	DSM45257
Paenarthrobacter aurescens DSM20116	Wild-type strain	DSM20116
Kocuria rosea DSM20447	Wild-type strain	DSM20447
Peribacillus simplex DSM1321	Wild-type strain	DSM1321
Pseudomonas putida KT2440	Wild-type strain	DSM6125
Genomic DNA	**Relevant characteristics**	**References**
Bacillus megaterium DSM32	Wild-type strain	DSM32
Plasmid	**Relevant characteristics**	**References**
pBV2xp	Kan^R; derivative of pHCMC04 for gene expression under control of the xylose-inducible promoter.	Drejer et al., 2020
pTH1mp	Cm^R; derivative of pTH1mp-*lysC* for gene expression under control of the *mdh* promoter. The *lysC* gene was replaced with multiple cloning site.	Irla et al., 2016
pMI2mp	Cm^R; Low copy number derivative (in *E. coli*) of pTH1mp	Drejer et al., 2020
pBV2xp-*davBA*^{Pp}	Kan^R; pBV2xp derivative for expression of the *P. putida davBA* operon under control of the xylose-inducible promoter.	This study
pBV2xp-*davBA*^{Ws}	Kan^R; pBV2xp derivative for expression of the *W. sterculiae davBA* operon under control of the inducible xylose-inducible ose promoter.	This study
pBV2xp-*davBA*Rd	Kan^R; pBV2xp derivative for expression of the *R. denitrificans davBA* operon under control of the xylose-inducible promoter.	This study
pBV2xp-*davB*^{Ws}-*davA*^{Pc}	Kan^R; pBV2xp derivative for expression of the synthetic operon containing *davB* from *W. sterculiae* and *davA* from *P. caldoxylosilyticus*. Expression under control of the xylose-inducible promoter.	This study
pBV2xp-*davA*^{Pc}-*davB*Rd	Kan^R; pBV2xp derivative for expression of the synthetic operon containing *davA* from *P. caldoxylosilyticus* and *davB* from *R. denitrificans*. Expression under control of the xylose-inducible promoter.	This study
pBV2xp-*davB*^{Pp}	Kan^R; pBV2xp derivative for expression of the *P. putida davB* gene under control of the xylose-inducible promoter.	This study
pBV2xp-*davB*^{Ws}	Kan^R; pBV2xp derivative for expression of the *W. sterculiae davB* gene under control of the xylose-inducible promoter.	This study
pMI2mp-*davA*^{Pc}	Cm^R; Derivative of pMI2mp for expression of *P. caldoxylosilyticus davA* gene under control of the constitutive *mdh* promoter.	This study
pMI2mp-*davA*^{Pp}	Cm^R; Derivative of pMI2mp for expression of *P. putida davA* gene under control of the constitutive *mdh* promoter.	This study
pBV2xp-*raiP*^{Ps}	Kan^R; pBV2xp-derived expression of *raiP* gene from *P. simplex*, under control of the xylose-inducible promoter	This study
pBV2xp-*raiP*^{Sj}	Kan^R; pBV2xp-derived expression of codon-optimized *raiP* gene from *S. japonicus*, under control of the xylose-inducible promoter	This study
pBV2xp-*raiP*^{Tv}	Kan^R; pBV2xp-derived expression of codon-optimized *raiP* gene from *T. viride*, under control of the xylose-inducible promoter	This study
pTH1mp-*cadA*	Cm^R; Derivative of pTH1mp for expression of *E. coli* MG1655-derived *cadA* gene under control of the constitutive *mdh* promoter.	Nærdal et al., 2015
pTH1mp-*katA*	Cm^R; Derivative of pTH1mp for expression of *B. methanolicus*-derived *katA* gene under control of the constitutive *mdh* promoter.	This study
pBV2xp-AVA^{Ec}	Kan^R; pBV2xp derivative for expression of the *E. coli* MG1655-derived genes *patDA* under control of the xylose-inducible promoter.	This study
pBV2xp-AVA^{Bm}	Kan^R; pBV2xp derivative for expression of the *B. megaterium* DSM32-derived genes *patDA* under control of the xylose-inducible promoter.	This study
pBV2xp-AVA^{Pp}	Kan^R; pBV2xp derivative for expression of *P. putida* KT2440-derived *spuI, spuC, kauB,* and *pauD2* genes under control of the xylose-inducible promoter.	This study
pBV2xp-AVA^{Rq}	Kan^R; pBV2xp derivative for expression of the *R. qingshengii* DSM45257-derived *puo* and *E. coli* MG1655-derived *patD* genes under control of the xylose-inducible promoter.	This study

(Continued)

TABLE 2 | Continued

Plasmid	Relevant characteristics	References
pBV2xp-AVA^{Pa}	Kan^{R}; pBV2xp derivative for expression of the *P. aurescens* DSM20116-derived *puo* and *E. coli* MG1655-derived *patD* genes under control of the xylose-inducible promoter.	This study
pBV2xp-AVA^{Kr}	Kan^{R}; pBV2xp derivative for expression of the *K. rosea* DSM20447-derived *puo* and *E. coli* MG1655-derived *patD* genes under control of the xylose-inducible promoter.	This study
Primer	**Sequence 5′ → 3′**	**Characteristics**
davBA_Pp_F1	atagttgatggataaacttgttcacttaaggaggtagtacatatgaacaagaagaaccgcc	*davBA* from *P. putida;* fw
davBA_Pp_R1	aacgacggccagtgaattcgagctcactagttatcagcctttacgcaggtg	*davBA* from *P. putida;* rv
davB_Pp_F1	gatggataaacttgttcacttaagg	*davB* from *P. putida for* pBV2xp-*davB*^{Pp}*;* fw
davB_Pp_R1	acggccagtgaattcgagctcaatccgccagggcgatc	*davB* from *P. putida for* pBV2xp-*davB*^{Pp}*;* rv
davA_Pc_F1	ccagattagcatttaaactagttttgtaaacaattacataaataggaggtagtacatatg-gaaacatcatatgaaattgcac	*davA* from *P. caldoxylosilyticus for* pMI2mp-*davA*^{Pc}*;* fw
davA_Pc_R1	tctagacctatggcgggtaccttaataaacatctgttcttctttcattcatc	*davA* from *P. caldoxylosilyticus for* pMI2mp-*davA*^{Pc}*;* rv
davB_Ws_F1	ggataaacttgttcacttaaggaggtagtacatatgagagttacaacatcagttgg	*davB* from *W. sterculiae for* pBV2xp-*davB*^{Ws}*;* fw
davB_Ws_R1	acggccagtgaattcgagctcttataatccaatatcaagtggtcc	*davB* from *W. sterculiae for* pBV2xp-*davB*^{Ws}*;* rv
davA_Pp_F1	ccagattagcatttaaactagttttgtaaacaattacataaataggaggtagtacatatgcgcatcgctctgtacc	*dava* from *P. putida for* pMI2mp-*dava*^{Pp}*;* fw
davA_Pp_R1	tctagacctatggcgggtacctcagcctttacgcaggtgc	*dava* from *P. putida for* pMI2mp-*dava*^{Pp}*;* rv
raippsfw	cttgttcacttaaggggaaatggctatgctcgctgtgatcagaaatggccttgg	*raiP* from *P. simplex* fw
raippsrv	gccagtgaattcgagctcatggtacggatcttaaaaaggctcactcaatgttctaggc	*raiP* from *P. simplex* rv
raipsjfw	cttgttcacttaaggggaaatggctatggaacatttagcagattgtttagaag	*raiP* from *S. japonicus* fw
raipsjrv	gccagtgaattcgagctcatggtacggatcttataattcatcttttgtatgttcaattg	*raiP* from *S. japonicus* rv
raiptvfw	cttgttcacttaaggggaaatggctatggataatgttgattttgcagaatctg	*raiP* from *T. viride* fw
raiptvrv	gccagtgaattcgagctcatggtacggatcttaaattttaacttgatattcttttgg	*raiP* from *P. viride* rv
Katafw	gtaaacaattacataaataggaggtagtagtacatgaccacaaataagaaaaaacttactacaagc	*katA* from *B. methanolicus* fw
katarv	ggatccccgggaattcaagctttaaacatgttaaactttctttttgtacaggtaaacctagac	*katA* from *B. methanolicus* rv
AVA1	ttcacttaaggggaaatggcaaatggatcgtacagtcgttaaaa	*patDA* from *B. megaterium;* fw
AVA2	acgacggccagtgaattcgagctttattggtggttcagctcatt	*patDA* from *B. megaterium;* fw
AVA3	ttcacttaaggggaaatggcaaatgtcggtacccccgcgtgccgttcagcttaac	*spuI* from *P. putida*; fw
AVA4	ttacacggtatgcaggtaccag	*spuI* from *P. putida*; rv
AVA5	tggtacctgcataccgtgtaatacataaataggaggtagtaagaatgagcgtcaacaacccgcaaacccgtgaatg	*spuC* from *P. putida*; fw
AVA6	ttattgaatcgcctcaagggtcaggtccag	*spuC* from *P. putida*; rv
AVA7	acccttgaggcgattcaataatacataaataggaggtagtaagaatgaccaccctgacccgtgcggactgggaacaa	*kauB* from *P. putida*; fw
AVA8	ttacagcttgatccaggtcgccttcagctcgg	*kauB* from *P. putida*; rv
AVA9	cgacctggatcaagctgtaatacataaataggaggtagtaagaatgtcgttacgcatctgcatcc	*pauD2* from *P. putida*; fw
AVA10	acgacggccagtgaattcgagctttacgcggcgctgtcgccggcctttga	*pauD2* from *P. putida*; rv
AVA11	ttcacttaaggggaaatggcaaatgcaacataagttactgattaacggagaactggttag	*patD* from *E. coli*; fw
AVA12	ttaatgtttaaccatgacgtggcggacga	*patD* from *E. coli*; rv
AVA13	cacgtcatggttaaacattaatacataaataggaggtagtaagaatgaacaggttaccttcgagcgcatcggctttag	*patA* from *E. coli*; fw
AVA14	acgacggccagtgaattcgagctttacgcttcttcgacacttactcgcatgg	*patA* from *E. coli*; rv
AVA23	ttcacttaaggggaaatggcaaatgaacctaattcattttagtgtgaagg	*puo* from *Kocuria rosea*; fw
AVA29	tcttactacctcctatttatgtaattgtttactcatcgctccgcgcccgtca	*puo* from *Kocuria rosea*; rw
AVA25	ttcacttaaggggaaatggcaaatgcagaatcttgatcgcgacgttgtgatcgtcgg	*puo* from *P. aurescens*; fw
AVA30	tcttactacctcctatttatgtaattgtttactcaggcgacaggtacagaagccaacttgtt	*puo* from *P. aurescens*; rv
AVA27	ttcacttaaggggaaatggcaaatgcctactctccagagagacgttgcaatcgt	*puo* from *R. qingshengii*; fw
AVA31	tcttactacctcctatttatgtaattgtttactcaggccttgctgcgagcgatgatgt	*puo* from *R. qingshengii*; rv
AVA32	gtaaacaattacataaataggaggtagtaagaatgcaacataagttactgattaacggagaactggttag	*patD* from *E. coli* (for *puo-patD*); fw
AVA33	acgacggccagtgaattcgagctttaatgtttaaccatgacgtggcggacga	*patD* from *E. coli* (for *puo-patD*); rv
MI09	gataccaaatactgtccttctagtgtagccg	SDM of *ori* pUC9; fw
MI10	cggctacactagaaggacagtatttggtatc	SDM of *ori* pUC9; rv

Cm^{R}, chloramphenicol resistance; Kan^{R}, kanamycin resistance.

pMI2mp plasmid was obtained *via* site-directed mutagenesis (SDM) of pTH1mp performed as previously described with CloneAmp HiFi PCR Premix (Liu and Naismith, 2008). The detailed description of plasmid creation is presented in **Supplementary Material**.

Media and Conditions for Shake Flask Cultivations

E. coli and *P. putida* strains were cultivated at 37°C in Lysogeny Broth (LB) or on LB agar plates supplemented with antibiotics when necessary. *P. aurescens* DSM2011 and *K. rosea* DSM20447 were cultivated at 30°C and 225 rpm in medium 53 (casein peptone, tryptic digest, 10.0 g l^{-1}, yeast extract, 5.0 g l^{-1}, glucose, 5.0 g l^{-1}, NaCl, 5.0 g l^{-1}; pH adjusted to 7.2–7.4); *R. qingshengii* DSM45257 was grown at 28°C and 225 rpm in medium 65 (glucose, 4.0 g l^{-1}, yeast extract, 4.0 g l^{-1}, malt extract, 10.0 g l^{-1}; adjusted to pH to 7.2); and *P. simplex* DSM1321 was cultivated in nutrient medium (peptone 5 g l^{-1} and meat extract 3 g l^{-1}; pH adjusted to 7.0) at 30°C and 200 rpm. For preparation of crude extracts, electrocompetent cells and transformation *B. methanolicus* strains were cultured at 50°C in SOB medium (Difco) supplemented with antibiotics when necessary. For 5AVA production experiments, recombinant *B. methanolicus* strains were cultivated in 250-ml baffled shake flasks at 50°C and 200 rpm in 40 or 50 ml MVcM medium containing 200 mM methanol. The MVcM medium contained the following, in 1 l of distilled water: K_2HPO_4, 4.09 g; $NaH_2PO_4{*}H_2O$, 1.49 g; $(NH_4)_2SO_4$, 2.11 g; it was adjusted to pH 7.2 before autoclaving. The MVcM medium was supplemented with 1 ml 1 M $MgSO_4{*}7H_2O$ solution, 1 ml trace element solution, and 1 ml vitamin solution (Schendel et al., 1990). One mole of $MgSO_4{*}7H_2O$ solution contained 246.47 g of $MgSO_4{*}7H_2O$ in 1 l of distilled water. The trace element solution contained the following, in 1 l of distilled water: $FeSO_4{*}7H_20$, 5.56 g; $CuSO_4{*}2H_2O$, 27.28 mg; $CaCl_2{*}2H_2O$, 7.35 g; $CoCl_2{*}6H_2O$, 40.50 mg; $MnCl_2{*}4H_2O$, 9.90 g; $ZnSO_4{*}7H_2O$, 287.54 mg; $Na_2MoO_4{*}2H_2O$, 48.40 mg; H_3BO_3, 30.92 mg; and HCl, 80 ml. The vitamin solution contained the following, in 1 l of distilled water: biotin, thiamine hydrochloride, riboflavin, D-calcium pantothenate, pyridoxine hydrochloride, nicotinamide, 0.1 g each; p-aminobenzoic acid, 0.02 g; folic acid, vitamin B_{12} and lipoic acid, 0.01 g each (Schendel et al., 1990). When needed, 10 g l^{-1} xylose (v/v) was added for induction. For precultures, a minimal medium supplemented with 0.25 g l^{-1} yeast extract, designated MVcMY, was used. Antibiotics (chloramphenicol, 5 μg ml^{-1} and/or kanamycin, 25 μg ml^{-1}) were supplemented as necessary. Cultivations were performed in triplicates with start OD_{600} of 0.1–0.2. Growth was monitored by measuring OD_{600} with a cell density meter (WPA CO 8000 Biowave).

Determination of Amino Acid Concentration

For the analysis of amino acid concentrations, 1 ml of the culture sample was taken from the bacterial cultures and centrifuged for 10 min at 11,000 rpm. Extracellular amino acids were quantified by means of high-pressure liquid chromatography (HPLC, Waters Alliance e2695 Separations Module). The samples underwent FMOC-Cl (fluorenylmethyloxycarbonyl chloride) derivatization before the analysis, according to the protocol described before (Haas et al., 2014), and were separated on a column (Symmetry C18 Column, 100 Å, 3.5 μm, 4.6 mm × 75 mm, Waters) according to the gradient flow presented in **Table 3**, where A is an elution buffer 50 mM Na-acetate pH = 4.2 and B is an organic solvent, acetonitrile. The detection was performed with a Waters 2475 HPLC Multi Fluorescence Detector (Waters), with excitation at 265 nm and emission at 315 nm.

TABLE 3 | Determined parameters of mobile phase gradient conditions in a HPLC separation of FMOC-derivatized amino acids.

Program time [min]	Flow rate [ml min^{-1}]	%A	%B
	1.3	62.0	38.0
5	1.3	62.0	38.0
12	1.3	43.0	57.0
14	1.3	24.0	76.0
15	1.3	43.0	57.0
18	1.3	620	38.0

Mobile phase consists of elution buffer 50 mM Na-acetate pH = 4.2 (A) and organic solvent acetonitrile (B).

Enzyme Assays

In order to determine enzymatic activity, crude extracts of recombinant *B. methanolicus* cells were prepared according to Drejer et al. (2020). *B. methanolicus* strains were inoculated in SOB medium and grown to exponential phase (OD_{600} = 0.8). Recombinant expression was induced by addition of 10 g l^{-1} xylose 2 h after inoculation. A total amount of 50 ml culture broth was harvested by centrifugation at 7,500 rpm and 4°C for 15 min and washed twice in ice-cold buffer used for specific enzyme assay before storing at −80°C. The cells were thawed in ice and disrupted by sonication using a Fisherbrand Sonic Dismembrator (FB-505) with 40% amplitude with 2 s on and 1 s off-pulse cycles for 7 min. Cell debris was then removed by centrifugation (at 14, 000 rpm and 4°C for 1 h). Protein concentrations were determined by Bradford assay (Bradford, 1976), using bovine albumin serum (Sigma) as standard.

L-Lysine α-oxidase activity was assayed by measuring the rate of hydrogen peroxide formation, as described elsewhere (Tani et al., 2015a). The reaction was initiated by adding crude extracts from *B. methanolicus* strains to the reaction media (50°C) consisting of 100 mM L-lysine and 50 mM pH 7 phosphate buffer, resulting in a total volume of 1 ml. Next, the sample was quenched by addition of 50 μl 2 M HCl. After neutralization with 50 μl 2 M NaOH, 200 μl of the mixture was withdrawn and transferred to 800 μl of a second reaction mixture containing 50 mM pH 6 phosphate buffer, 30 mM phenol, 2 units ml^{-1} peroxidase from horseradish (Sigma) and 0.5 mM 4-aminoantipyrine. Formation of quinoneimine dye from oxidative coupling of phenol and 4-aminoantipyrine (Job et al., 2002) was determined by measuring absorbance at 505 nm using a Cary 100 Bio UV-visible spectrophotometer (Varian). One unit (U) of RaiP activity was defined as the amount of enzyme that catalyzes the formation of 1 μmol hydrogen peroxide per minute.

Catalytic activities of PatA and PatD or putrescine oxidase and PatD were measured by using a coupled reaction, and

cadaverine was used as substrate instead of putrescine, as previously described elsewhere, with modifications (Jorge et al., 2017). The 1-ml assay mix contained 0.1 M Tris–HCl pH 8.0, 1.5 mM α-ketoglutarate, 2.5 mM cadaverine, 0.1 mM pyridoxal-5′-phosphate, and 0.3 mM NAD. In this coupled reaction, cadaverine was converted to 5AVA *via* 5-aminopentanal and one unit of coupled enzyme activity was defined as the amount of the enzyme that formed 1 μmol of NADH (ε340 nm = 6.22 mM^{-1} cm^{-1}) per minute at 50°C.

The coupled DavAB assay was performed as described in Liu et al. (2014) with some modifications. Five hundred microliters of crude extract was added into 50-ml Falcon tubes filled with 4 ml 100 mM phosphate buffer pH 7.0 supplemented with 10 g l^{-1} L-lysine. The tubes were incubated for 40 h at 30 or 50°C with stirring at 200 rpm. The samples for quantification of 5AVA concentration through HPLC (see section "Determination of Amino Acid Concentration") were taken at the beginning of incubation, after 16 h and after 40 h.

RESULTS AND DISCUSSION

Selection, Design, and Construction of Heterologous Biosynthetic Pathways for 5AVA Biosynthesis in *B. methanolicus*

Due to the fact that *B. methanolicus* is a thermophile, a typical issue concerning implementation of biosynthetic pathways from heterologous hosts is the lack of thermostability of the transferred enzymes. It was shown before that a screening of diverse donor organisms allows to identify pathways active at 50°C and leads to increased product titers (Irla et al., 2017; Drejer et al., 2020). In order to extend the scope of our screening, we have constructed 26 strains with five different 5AVA biosynthetic pathways, which are presented in **Figure 1**, derived from diverse donors. Two pathways that directly convert L-lysine to 5AVA were chosen: the DavBA pathway (**Figure 1A**) and the RaiP pathway (**Figure 1B**), as well as three pathways that use cadaverine as an intermediate: the SpuI pathway (**Figure 1C**), the PatA pathway (**Figure 1D**), and the Puo pathway (**Figure 1E**).

The genes encoding the core part of those pathways are cloned into a θ-replication, low copy number derivative of pHCMC04 plasmid, pBV2xp, under control of a *B. megaterium*-derived, xylose-inducible promoter, and the genes encoding any ancillary enzymes are cloned into pTH1mp or pMI2mp plasmids, which are compatible to pBV2xp, under control of the *mdh* promoter (Irla et al., 2016). The plasmids with genes encoding desired pathways were constructed as described fully in the **Supplementary Material** and then used to transform *B. methanolicus* cells leading to formation of strains presented in **Table 4**.

With help of retrosynthesis analysis, we have considered two pathways that utilize L-lysine directly as precursor and that utilize either DavB (EC 1.13.12.2) and DavA (EC 3.5.1.30) activity (DavBA pathway, **Figure 1A**) or RaiP (EC 1.4.3.14) in the presence of H_2O_2 (RaiP pathway, **Figure 1B**) for further conversion into 5AVA. For DavBA production, three different *davBA* operons from the following mesophilic organisms were applied: *P. putida*, *W. sterculiae*, and *R. denitrificans*. We could not identify a complete *davBA* operon from a thermophilic host; however, thermophilic *P. caldoxylosilyticus* possesses a putative *davA* gene and was also included in this study. All selected *davBA* operons were codon-optimized and cloned into the pBV2xp vector under control of the xylose-inducible promoter as described in the **Supplementary Material**. The finished vectors were used to create the following *B. methanolicus* strains: MGA3_DavBA^{Pp}, MGA3_DavBA^{Ws}, MGA3_DavBARd, MGA3_DavB^{Ws}A^{Pc}, and MGA3_DavA^{Pc}BRd (**Table 4**). Furthermore, selected *davBA* operons were expressed as single genes using compatible pBV2xp and pMI2mp plasmids for gene expression (**Supplementary Material**). The *davB* genes from *P. putida* and *W. sterculiae* were cloned under control of the xylose-inducible promoter in plasmid pBV2xp, while the *davA* gene from *P. caldoxylosilyticus* was cloned into the pMI2mp plasmid under control of the *mdh* promoter constitutively active in methylotrophic conditions. The combination of two plasmids (2p) expressing single genes resulted in creation of the following *B. methanolicus* strains: MGA3_DavB^{Pp}A^{Pc}(2p) and MGA3_DavB^{Ws}A^{Pc}(2p) (**Table 4**).

For expression of the RaiP pathway, the *B. methanolicus* strains MGA3_RaiP^{Ps}, MGA3_RaiP^{Sj}, and MGA3_RaiP^{Tv} (**Table 4**) carried heterologous *raiP* gene sequences from the prokaryote *P. simplex* and from the eukaryotic genetic donors

TABLE 4 | List of *B. methanolicus* strains used in this study with abbreviated strain names.

Abbreviated strain name	Recombinant *B. methanolicus* strains created in this study
MGA3_EV	MGA3(pBV2xp)
MGA3_DavBA^{Pp}	MGA3(pBV2xp-*davBA*^{Pp})
MGA3_DavBA^{Ws}	MGA3(pBV2xp-*davBA*^{Ws})
MGA3_DavBARd	MGA3(pBV2xp-*davBA*Rd)
MGA3_DavB^{Ws}A^{Pc}	MGA3(pBV2xp-*davB*^{Ws}-*davA*^{Pc})
MGA3_DavA^{Pc}BRd	MGA3(pBV2xp-*davA*^{Pc}-*davB*Rd)
MGA3_DavB^{Pp}A^{Pc}(2p)	MGA3(pMI2mp-*davA*^{Pc})(pBV2xp-*davB*^{Pp})
MGA3_DavB^{Ws}A^{Pc}(2p)	MGA3(pMI2mp-*davA*^{Pc})(pBV2xp-*davB*^{Ws})
M168-20_EV	M168-20(pBV2xp)
M168-20_DavBA^{Pp}	M168-20(pBV2xp-*davBA*^{Pp})
M168-20_DavA^{Pp}B^{Pp}(2p)	M168-20(pMI2mp-*davA*^{Pp})(pBV2xp-*davB*^{Pp})
M168-20_DavA^{Pp}B^{Ws}(2p)	M168-20(pMI2mp-*davA*^{Pp})(pBV2xp-*davB*^{Ws})
MGA3_RaiP^{Ps}	MGA3(pBV2xp-*raiP*^{Ps})
MGA3_RaiP^{Sj}	MGA3(pBV2xp-*raiP*^{Sj})
MGA3_RaiP^{Tv}	MGA3(pBV2xp-*raiP*^{Tv})
M168-20_RaiP^{Ps}	M168-20 (pBV2xp-*raiP*^{Ps})
M168-20_RaiP^{Sj}	M168-20(pBV2xp-*raiP*^{Sj})
M168-20_RaiP^{Tv}	M168-20 (pBV2xp-*raiP*^{Tv})
MGA3_Cad	MGA3(pTH1mp-*cadA*)(pBV2xp)
MGA3_PatA^{Ec}	MGA3(pTH1mp-*cadA*)(pBV2xp-AVA^{Ec})
MGA3_PatA^{Bm}	MGA3(pTH1mp-*cadA*)(pBV2xp-AVA^{Bm})
MGA3_SpuI	MGA3(pTH1mp-*cadA*)(pBV2xp-AVA^{Pp})
MGA3_Kat	MGA3(pTH1mp-*katA*)(pBV2xp)
MGA3_Puo^{Kr}	MGA3(pTH1mp-*katA*)(pBV2xp-AVA^{Kr})
MGA3_Puo^{Pa}	MGA3(pTH1mp-*katA*)(pBV2xp AVA^{Pa})
MGA3_Puo^{Rq}	MGA3(pTH1mp-*katA*)(pBV2xp-AVA^{Rq})

S. japonicus and *T. viride*, respectively, the two latter with characterized RaiP activity (Arinbasarova et al., 2012; Tani et al., 2015a). The full length of codon-optimized sequences derived from *S. japonicus* and *T. viride* is present in the **Supplementary Table S1**. The original *S. japonicus* sequence encodes a protein with 617 amino acids and has a 52.2% GC content, while the sequence codon optimized for *B. methanolicus* has a GC content of 29%. The *T. viride*-derivative sequence was adjusted from the GC content of 42.5 to 28.6%. The substitution of nucleotides did not alter their coding amino acid sequences.

Among the pathways using cadaverine formed from L-lysine through activity of *E. coli*-derived lysine decarboxylase CadA (EC 4.1.1.18, encoded by *cadA*) as an intermediate, we considered a multistep diamine catabolic pathway of *P. aeruginosa* PAOI (SpuI pathway, **Figure 1C**) (Yao et al., 2011). In order to test this pathway for methanol-based 5AVA production, the MGA3_SpuI strain was constructed through transformation of *B. methanolicus* wild type with two vectors pTH1mp-*cadA* and pBV2xp-AVA^{Pp}, the first one carrying the *cadA* gene and the latter the genes encoding the SpuI pathway (**Table 4** and **Supplementary Material**). The SpuI pathway that converts cadaverine to 5AVA is composed of the following enzymes: glutamylpolyamine synthetase (EC 6.3.1.2, SpuI), polyamine:pyruvate transaminase (EC 2.6.1.113, SpuC), aldehyde dehydrogenase (EC 1.2.1.3, KauB), and glutamine amidotransferase class I (EC 6.3.5.2, PauD2) (Yao et al., 2011).

Another pathway, also predicted by our retrosynthesis analysis, potentially leading to production of 5AVA from L-lysine is a three-step pathway composed of CadA, PatA (EC 2.6.1.82, PatA), and 5-aminopentanal dehydrogenase (EC 1.2.1.19, PatD) (PatA pathway, **Figure 1D**). In order to test this pathway, two strains were constructed, MGA3_PatA^{Ec} and MGA3_PatA^{Bm}, through transformation *of B. methanolicus* with pTH1mp-*cadA* plasmid, and pBV2xp-AVA^{Ec} or pBV2xp-AVA^{Bm}, respectively (**Table 4**). As described in the **Supplementary Material**, the lysine decarboxylase-encoding gene (*cadA*) was placed under control of the *mdh* promoter in a rolling circle vector pTH1mp. The *E. coli*-derived *patAD* operon encoding previously characterized enzymes was placed under control of the xylose-inducible promoter in pBV2xp, resulting in pBV2xp-AVA^{Ec} (Samsonova et al., 2003). The genes of the *patAD* operon in *B. megaterium* were identified based on a BLAST search of its genome and were cloned into pBV2xp, yielding pBV2xp-AVA^{Bm} (Altschul et al., 1990). While the existence of prior art makes it a solid candidate, we knew that its second step catalyzed by PatA may suffer from an unfavorable thermodynamic (predicted close to 0 kJ mol^{-1}) (Noor et al., 2012).

In our study, we have also included a pathway confirmed through retrosynthesis analysis where the step of cadaverine transamination (PatA pathway, **Figure 1D**) is replaced by its oxidative deamination (Puo pathway, **Figure 1E**) because this reaction displays a more favorable thermodynamic (predicted close to −100 kl mol^{-1} in cell conditions) in comparison to PatA. While a cadaverine oxidase has not been identified before, it was shown that putrescine oxidase encoded by *puo* retains up to 14% of its maximal activity when cadaverine is used as a substrate (Okada et al., 1979; Ishizuka et al., 1993; van Hellemond et al., 2008; Lee and Kim, 2013). We have therefore decided to express three different versions of the *puo* gene derived from *K. rosea*, *P. aurescens*, and *R. qingshengii*, together with the *E. coli*-derived *patD* gene from the pBV2xp plasmid (for details see **Supplementary Material**), which led to creation of the following strains: MGA3_Puo^{Kr}, MGA3_Puo^{Pa}, and MGA3_Puo^{Rq}, respectively (**Table 4**). In order to prevent oxidative stress caused by H_2O_2 formation, a native gene encoding catalase was homologously expressed from pTH1mp plasmid in all constructed strains.

Testing Recombinant *B. methanolicus* Strains for 5AVA Production From Methanol

The plasmids designed and built as described in the above Section were used for transformation of wild-type *B. methanolicus* cells and resulted in the creation of 26 different strains (**Table 4**) which were then tested for their ability to synthetize 5AVA. All strains were cultivated in minimal medium supplemented with methanol as the sole carbon and energy source, and the 5AVA titer was evaluated after the strains had reached the stationary growth phase as described in the following sections.

Expression of the DavAB-Encoding Genes Resulted in no 5AVA Biosynthesis in *B. methanolicus*

In the first attempt, we heterologously expressed genes encoding the DavBA pathway in *B. methanolicus* MGA3 (**Figure 1A**). In addition to the well-known *davBA* operon from *P. putida* (gamma-proteobacteria), the alternative *davBA* operon from *W. sterculiae* (actinobacteria) and *davAB* from *R. denitrificans* (alpha-proteobacteria) were tested for 5AVA formation in *B. methanolicus* MGA3. Moreover, the only enzyme identified from a thermophilic host, DavA from *P. caldoxylosilyticus* (bacilli), was combined with the before mentioned lysine 2-monooxygenases (DavB). *P. caldoxylosilyticus* has a reported optimum growth temperature from 50 to 65°C (Fortina et al., 2001).

Several considerations were made with regard to strain design, namely, adjusting the GC content and the types of codons present in the open reading frames in the genomic DNA of a donor and designing suitable expression cassettes. In total, seven different *B. methanolicus* strains were constructed: MGA3(pBV2xp-*davBA*^{Pp}) named MGA3_DavBA^{Pp}, MGA3(pBV2xp-*davBA*^{Ws}) named MGA3_DavBA^{Ws}, MGA3(pBV2xp-*davBA*Rd) named MGA3_DavBARd, MGA3(pBV2xp-*davB*^{Ws}-*davA*^{Pc}) named MGA3_DavB^{Ws}A^{Pc}, MGA3(pBV2xp-*davA*^{Pc}-*davB*Rd) named MGA3_DavA^{Pc}BRd, MGA3(pMI2mp-*davA*^{Pc})(pBV2xp-*davB*^{Pp}) named MGA3_DavB^{Pp}A^{Pc}(2p), MGA3(pMI2mp-*davA*^{Pc}) (pBV2xp-*davB*^{Ws}) named MGA3_DavB^{Ws}A^{Pc}(2p) (**Table 4**). However, in none of the tested strains (MGA3_DavBA^{Pp}, MGA3_DavBA^{Ws}, MGA3_DavBARd, MGA3_DavB^{Ws}A^{Pc}, MGA3_DavA^{Pc}BRd), the active pathway was expressed; and followingly no 5AVA accumulation was observed during shake flask cultivations in any constructed strain (data not shown).

The first reaction step from L-lysine to 5-aminopentanamide requires O_2 (**Figure 1A**), and due to the high O_2 demand to facilitate the assimilation of methanol, we also tested 5AVA formation from the alternative carbon source mannitol. Neither was this strategy successful. Furthermore, the DavAB pathway was also tested in the genetic background of L-lysine-overproducing *B. methanolicus* strain M160-20. Specifically, the following strains were constructed: M168-20_DavBA^{Pp}, M168-20_DavA^{Pp}B^{Pp}(2p), and M168-20_DavA^{Pp}B^{Ws}(2p); however, none of them produced any detectable 5AVA (data not shown). Taken together, the DavBA pathway did not enable 5AVA formation. It is not clear whether this was caused by low enzymatic stability at 50°C (only *P. caldoxylosilyticus* is known to be thermophilic among the organisms found to be source organisms for the two genes). In order to exclude the effect of elevated temperature on the DavAB activity, we tested enzymatic activity at 30°C for selected strains (MGA3_DavBA^{Pp}, MGA3_DavBA^{Ws}, MGA3_DavBARd, MGA3_DavB^{Ws}A^{Pc}, and MGA3_DavA^{Pc}BRd); however, no DavAB activity was detected (data not shown). The reason why the functional DavAB pathway was not expressed in *B. methanolicus* remains unknown.

RaiP Pathway Is Functional in *B. methanolicus* and Supports 5AVA Production

Methanol-based 5AVA biosynthesis was attempted *via* heterologous expression of RaiP encoding gene *raiP* in MGA3. The strains MGA3(pBV2xp-*raiP*^{Ps}) named MGA3_RaiP^{Ps}, MGA3(pBV2xp-*raiP*^{Sj}) named MGA3_RaiP^{Sj}, and MGA3(pBV2xp-*raiP*^{Tv}) named MGA3_RaiP^{Tv} (**Table 4**) carry the *raiP* gene from the bacterium *P. simplex* and *raiP* genes with codon-optimized sequences from the eukaryotic donors *S. japonicus* and *T. viride*, respectively. The *T. viride*-derived RaiP was shown to be stable at temperatures up to 50°C (Arinbasarova et al., 2012). It is reported that the RaiP protein from *S. japonicus* is thermally stable for at least 1 h in temperatures up to 60°C, with its highest activity registered at 70°C (Tani et al., 2015b). Moreover, although there is no kinetic characterization of RaiP from *P. simplex* available, this bacterium is classified as mesophilic, with growth optimum at 30°C (Yumoto et al., 2004). To examine the activity of RaiP in the constructed *B. methanolicus* strains, L-lysine α-oxidase activity was measured at 50°C. While the empty vector control strain has shown no RaiP activity, the highest RaiP specific activity was observed in crude extracts from strain MGA3_RaiP^{Tv}, being 62.1 ± 1.4 mU mg^{-1} (**Figure 2A**). The values of RaiP activity for strains MGA3_RaiP^{Ps} and MGA3_RaiP^{Sj} were 1.4 ± 0.3 mU mg^{-1} and 12.0 ± 4.4 mU mg^{-1}, respectively (**Figure 2A**). It is not clear if the poor activity of heterologous RaiP from genetic donors *S. japonicus* and *P. simplex* was caused by low enzymatic stability at 50°C, and the reason for that remains to be investigated.

HPLC analysis of supernatant from MGA3_RaiP^{Tv} strain cultivated in minimal medium revealed 16.15 ± 1.62 mg L^{-1} 5AVA and 0.27 ± 0.04 mg L^{-1} L-lysine. In contrast, the L-lysine level in the MGA3 strain harboring the empty vector plasmid pBV2xp (MGA3_EV) was 37.8 ± 7.2 mg L^{-1} (**Figure 2B**). Even though a slight RaiP activity was observed in crude extract of the strains MGA3_RaiP^{Ps} and MGA3_RaiP^{Sj}, no 5AVA production was observed for those strains (data not shown). Let us note here that the 5AVA titer in the methanol-based shaking flask fermentation of strain MGA3_RaiP^{Tv} was significantly inferior to that in previously reported glucose-based fermentations in *E. coli* (Cheng et al., 2018).

The value of the Michaelis–Menten constant for *T. viride*-derived RaiP for L-lysine has been estimated (K_m = 5.85 mg L^{-1}) (Kusakabe et al., 1980). Therefore, the precursor levels in the *B. methanolicus* strains should not be a limiting factor for production of 5AVA. The RaiP-mediated production is mainly utilized in the L-lysine bioconversion approach, utilizing *E. coli* strains as whole-cell biocatalysts (Cheng et al., 2018, 2020, 2021) where high concentrations of the precursor were used; for example, the molar yield of 0.942 was obtained from 120 g l^{-1} L-lysine (Park et al., 2014). However, construction and testing of the *B. methanolicus* strains M168-20_RaiP^{Sj}, M168-20_RaiP^{Ps}, and M168-20_RaiP^{Tv} (**Table 4**), based on the L-lysine-over producing mutant M168-20 (Brautaset et al., 2010), did not result in any improved 5AVA production (data not shown).

The lack of 5AVA production in MGA3_RaiP^{Ps} and MGA3_RaiP^{Sj}, as well as low 5AVA titer produced by strain MGA3_RaiP^{Tv}, might be related to the spontaneous conversion step that follows RaiP activity. This could be a limiting factor for the RaiP-mediated production of 5AVA. Three compounds are produced in a reaction catalyzed by RaiP: α-ketolysine, NH_3, and H_2O_2 (Mai-Prochnow et al., 2008; Cheng et al., 2018). In a second spontaneous step of 5AVA synthesis, the intermediate α-ketolysine is oxidatively decarboxylated to form 5AVA in the presence of H_2O_2 as an oxidizing agent. It was shown that the addition of H_2O_2 into the culture broth has led to an 18−fold increase of 5AVA titers in comparison with the control condition without H_2O_2 (final titer 29.12 g l^{-1}) in a 5–l fermenter (Cheng et al., 2018). The RaiP-mediated 5AVA production may be increased by enzymatic conversion of α-ketolysine in an approach different to ours, where spontaneous reaction of oxidative decarboxylation occurs. Recently, an artificial synthetic pathway for the biosynthesis of 5AVA in *E. coli* was developed, consisting of three steps: conversion of L-lysine to α-ketolysine *via* RaiP, decarboxylation of α-ketolysine to produce 5-aminopentanal *via* α-ketoacid decarboxylase, and oxidation of 5-aminopentanal to 5AVA *via* aldehyde dehydrogenase. The expression of the artificial pathway resulted in a yield increase of 774% compared to the single gene pathway (Cheng et al., 2021). This approach is potentially a feasible strategy we have shown in our study that *E. coli*-derived PatD is active as a 5-aminopentanal dehydrogenase in *B. methanolicus* and participates in 5AVA biosynthesis (see Section "The PatA Pathway Supports 5AVA Accumulation in *B. methanolicus*).

Use of the SpuI Pathway Does Not Lead to 5AVA Production in *B. methanolicus*

Three different pathways that use cadaverine as an intermediate product have been tested for their feasibility for production of 5AVA in *B. methanolicus*. Cadaverine biosynthesis in *B. methanolicus* cells was enabled through the activity of lysine decarboxylase encoded by a heterologously expressed *cadA*

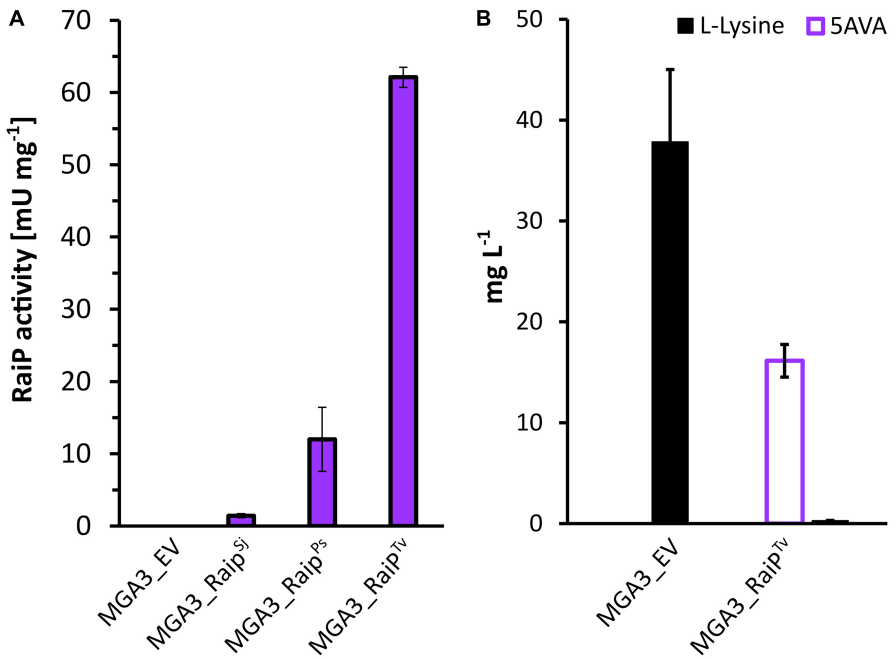

FIGURE 2 | Evaluation of RaiP enzyme activity **(A)** and amino acids production **(B)** in recombinant *B. methanolicus* strains. *B. methanolicus* strains MGA3_EV, MGA3_RaiP^{Sj}, MGA3_RaiP^{Ps}, or MGA3_RaiP^{Tv} were cultivated in a shaking flask culture. The grown cells were harvested, washed twice with 50 mM phosphate buffer (pH 7.0), and disrupted by sonication. After centrifugation, the crude extracts were directly used for the RaiP assay. MGA3_EV and MGA3_RaiP^{Tv} were cultivated for 27 h, and supernatants were obtained by centrifugation for HPLC analysis. The error bars represent standard deviation of technical triplicates.

(Nærdal et al., 2015). Cadaverine can be converted to 5AVA through activity of a multistep diamine catabolic pathway derived from *P. aeruginosa* PAOI (SpuI pathway, **Figure 1C**) (Yao et al., 2011). The MGA3(pTH1mp-*cadA*)(pBV2xp-AVA^{Pp}) strain called MGA3_SpuI (**Table 4**) did not accumulate any 5AVA during methanol-based growth in minimal medium, despite the accumulation of the precursor, cadaverine, at the level of 118.8 ± 5.1 mg l^{-1} similar to the empty vector control strain (130.0 ± 5.3 mg l^{-1}) (**Table 5**). The cadaverine titers of 130.0 ± 5.3 mg l^{-1} achieved by MGA3_Cad are higher than the L-lysine titer of 37.8 ± 7.2 mg L^{-1} achieved by MGA3_EV in this study (**Figure 2B**). This is in accordance with previous findings of Nærdal et al. (2011, 2015) who attributed high cadaverine titers for production strain in relation to L-lysine titer in empty vector

TABLE 5 | Growth rates, enzyme activities and L-lysine, cadaverine, and 5AVA final titers accumulated in growth media of recombinant MGA3 strains.

Strain	Growth rate [h^{-1}]	Coupled activity of PatAD or Puo-PatD [mU mg^{-1}]	Lysine [mg l^{-1}]	Cadaverine [mg l^{-1}]	5AVA [mg l^{-1}]
MGA3_Cad	0.37 ± 0.01	0 ± 0	Not detected	123.0 ± 5.3	0.0 ± 0.0
MGA3_SpuI	0.33 ± 0.01	N.A.	Not detected	118.82 ± 5.1	0.0 ± 0.0
MGA3_PatA^{Ec}	0.12 ± 0.02	7 ± 4	Not detected	1.47 ± 0.17	23.7 ± 2.7
MGA3_PatA^{Bm}	0.15 ± 0.03	170 ± 37	Not detected	0.71 ± 0.11	8.3 ± 4.1
MGA3_Cad	0.35 ± 0.01	0 ± 0	Not detected	Supplemented (500 mg L^{-1})	0.0 ± 0.0
MGA3_SpuI	0.32 ± 0.00	N.A.	Not detected	Supplemented (500 mg L^{-1})	0.0 ± 0.0
MGA3_PatA^{Ec}	0.14 ± 0.02	7 ± 4	Not detected	Supplemented (500 mg L^{-1})	31.8 ± 2.3
MGA3_PatA^{Bm}	0.17 ± 0.04	170 ± 37	Not detected	Supplemented (500 mg L^{-1})	77.7 ± 5.5
MGA3_Kat	0.32 ± 0.00	0 ± 0	3.1 ± 0.5	Supplemented (500 mg L^{-1})	0.0 ± 0.0
MGA3_Puo^{Ec}	0.28 ± 0.01	0 ± 0	5.0 ± 0.7	Supplemented (500 mg L^{-1})	0.0 ± 0.0
MGA3_Puo^{Pa}	0.29 ± 0.01	0 ± 0	4.9 ± 0.9	Supplemented (500 mg L^{-1})	0.0 ± 0.0
MGA3_Puo^{Rq}	0.29 ± 0.00	0 ± 0	3.7 ± 0.2	Supplemented (500 mg L^{-1})	0.0 ± 0.0

The B. methanolicus strains expressing pathways that use cadaverine as an intermediate (SpuI, PatA, or Puo pathways) were cultivated for 24 h, and supernatants were obtained by centrifugation for HPLC analysis. Catalytic activities of PatA and PatD or Puo and PatD were measured by using a coupled reaction, and cadaverine was used as substrate (see Section "Enzyme Assays"). The standard deviation of technical triplicates is shown. NB: RaiP activity and 5AVA production for the RaiP pathway is shown ***Figure 2****.*

control strain to a metabolic pull which deregulated flux through the L-lysine biosynthesis pathway.

The PatA Pathway Supports 5AVA Accumulation in *B. methanolicus*

In the next step, two versions of the PatA pathway (**Figure 1D**) derived from either *E. coli* or *B. megaterium* were tested in strains MGA3(pTH1mp-*cadA*)(pBV2xp-AVA^{Ec}) named MGA3_PatA^{Ec} and MGA3(pTH1mp-*cadA*)(pBV2xp-AVA^{Bm}) named MGA3 _PatA^{Bm} (**Table 4**), respectively. The optimal temperature of PatA derived from *E. coli* is 60°C, which means that it is a thermostable enzyme that should be active at 50°C, which is a temperature used for the production experiment. PatA was shown to have a broad substrate range including cadaverine and, in lower extent, spermidine, but not ornithine (Samsonova et al., 2003). This property was used by Jorge et al. (2017) who have shown in their study that it is possible to use PatA and PatD derived from *E. coli* to establish conversion of cadaverine to 5AVA, confirming experimentally the broad substrate range of those two enzymes. The *B. megaterium*-derived PatA was characterized only superficially with regard to its substrate spectrum and not optimal temperature or thermostability (Slabu et al., 2016); however, its host organism is known to have a wide temperature range for growth up to 45°C (Vary et al., 2007). The multiple-sequence alignment with *E. coli*-derived enzymes showed identity of 63 and 38% for PatA and PatD, respectively (Okada et al., 1979). Both *E. coli* and *B. megaterium*-derived versions of the pathway are functional in *B. methanolicus*, with the combined PatAD activity of 7 ± 4 mU and 170 ± 37 mU mg^{-1} (**Table 5**). Final 5AVA titers of 23.7 ± 2.7 and 8.3 ± 4.1 mg L^{-1} (**Table 5**) were achieved, which is considerably lower than 5AVA titers of 0.9 g l^{-1} obtained by wild-type *C. glutamicum* strain transformed with plasmids for expression of *ldcC* (coding for lysine decarboxylase) and *patDA* (Jorge et al., 2017). For both producer strains, the concentration of unconverted cadaverine is similar: 1.7 ± 0.1 mg l^{-1} and 1.5 ± 0.2 mg l^{-1} for MGA3_PatA^{Ec} and MGA3_PatA^{Bm}, respectively (**Table 5**). While K_m for cadaverine has not been assessed, it has been shown to be 811 mg l^{-1} for putrescine for *E. coli*-derived PatA; assuming similar K_m for cadaverine, it may explain why full conversion of cadaverine has not occurred (Samsonova et al., 2003). Due to relatively high K_m for putrescine of PatA, we decided to test how supplementation with external cadaverine affects 5AVA accumulation. In fact, for both MGA3_PatA^{Ec} and MGA3_PatA^{Bm}, 5AVA titers increased to 31.8 ± 2.3 and 77.7 ± 5.5, respectively, when the growth medium was supplemented with 500 mg l^{-1} cadaverine (**Table 5**). These results indicate that the enhancement of precursor supply is one potential target for subsequent metabolic engineering efforts to increase 5AVA titers. Another important consideration for activity of transaminase is availability of keto acid that acts as amino group acceptor. It was shown that *E. coli* and *B. megaterium*-derived PatA can use either pyruvate or 2-oxoglutarate as amino group acceptors (Slabu et al., 2016); the intracellular concentrations of those compounds in *B. methanolicus* MGA3 cells are 3.2 and 2.7 mM, respectively (Brautaset et al., 2003). Knowing that K_m for 2-oxoglutarate for *E. coli*-derived PatA is 19.0 mM (Samsonova et al., 2003), recovery of the keto acids may be a limitation for 5AVA accumulation. This issue could be potentially solved by heterologous production of alanine dehydrogenase or L-glutamate oxidase which catalyzes reactions where pyruvate or 2-oxoglutarate is produced (Böhmer et al., 1989; Sakamoto et al., 1990; Slabu et al., 2016).

Use of the Puo Pathway Leads to 5AVA Production in *B. methanolicus*

Lastly, a pathway that relies on an activity of the monooxygenase putrescine oxidase (Puo, EC 1.4.3.10) was tested (**Figure 1E**). Puo catalyzes the oxidative deamination of cadaverine *in lieu* of cadaverine transamination catalyzed by PatA. It was shown that different putrescine oxidases can use cadaverine as their substrate with 9–14% of their maximal activity shown when putrescine is a substrate (Desa, 1972; Okada et al., 1979; van Hellemond et al., 2008; Lee et al., 2013). Moreover, putrescine oxidases derived from *K. rosea* (*Micrococcus rubens*) and *Rhodococcus* are thermostable and optimal activity of *P. aurescens*-derived Puo is at 50°C (Desa, 1972; van Hellemond et al., 2008; Lee et al., 2013). The disadvantage of this pathway is that it requires O_2, the supply of which may be difficult to control. Furthermore, due to formation of hydrogen peroxide in the reaction catalyzed by Puo, the oxidative stress may increase when this pathway is active. In order to avoid detrimental effect of hydrogen peroxide accumulation, catalase was overproduced in the recombinant strains containing the Puo pathway: MGA3(pTH1mp-*katA*)(pBV2xp-AVA^{Kr}) named MGA3_Puo^{Kr}, MGA3(pTH1mp-*katA*)(pBV2xp AVA^{Pa}) named MGA3_Puo^{Pa}, and MGA3(pTH1mp-*katA*)(pBV2xp-AVA^{Rq}) named MGA3_Puo^{Rq} (**Table 4**). To achieve sufficient levels of the pathway precursor, cadaverine, we have decided not to rely on plasmid-based production of lysine decarboxylase and to add cadaverine to the growth medium, instead. The tested recombinant strains with the Puo pathway did not produce 5AVA, which is consistent with no Puo-PatD activity detected in crude extracts (**Table 5**). The Puo pathway was shown to be active in *C. glutamicum* where titer of 0.1 ± 0.0–0.4 ± 0.0 g l^{-1} 5AVA was achieved (Haupka et al., 2020).

CONCLUSION

In the search for 5AVA production from the sustainable feedstock methanol, we have screened five pathways toward 5AVA biosynthesis in *B. methanolicus*. No 5AVA production was observed for DavBA, Puo, and SpuI pathways. However, the pathways relying on RaiP and PatA activities were functional in shake flask cultures of *B. methanolicus*, which led to 5AVA production from methanol for the first time, respectively, up to 16.15 ± 1.62 mg l^{-1} or 23.7 ± 2.7. RaiP and PatA pathways are targets for further optimizations which could increase the 5AVA titers in the constructed strains. For instance, the improvement of substrate utilization and H_2O_2 availability or decomposition efficiency might contribute to the increase in the yield of 5AVA. Moreover, our study shows that the availability of supplemented

cadaverine has high impact on 5AVA titer when the PatA pathway is employed. Another factor that needs to be considered is tolerance to 5AVA, which was shown to be low (Haupka et al., 2021). Recently, adaptative laboratory evolution experiments resulted in the selection of a mutant strain of *B. methanolicus* that displays tolerance to approximately 46 g l^{-1} 5AVA (Haupka et al., 2021), which could be employed as a platform to develop high-titer 5AVA production strains. This shows that methanol has the potential to become a sustainable feedstock for the production of 5AVA.

DATA AVAILABILITY STATEMENT

The original contributions generated for this study are included in the article/**Supplementary Material**, further inquiries can be directed to the corresponding author.

AUTHOR CONTRIBUTIONS

LB, MI, IN, and SL: study design and experimental work. BD: bioinformatic analysis. LB and MI: writing—original draft preparation. TB: writing—review and editing and project administration. SH, TB, MI, and IN: funding acquisition. All authors have read and agreed to the published version of the manuscript.

FUNDING

This research was funded by The Research Council of Norway within ERA CoBioTech, an ERA-Net Cofund Action under H2020, grant number 285794 ERA-NET.

ACKNOWLEDGMENTS

We thank Tonje Marita Bjerkan Heggeset from SINTEF Industry for technical assistance.

SUPPLEMENTARY MATERIAL

The Supplementary Material for this article can be found online at: https://www.frontiersin.org/articles/10.3389/fbioe.2021.686319/full#supplementary-material

REFERENCES

Adkins, J., Jordan, J., and Nielsen, D. R. (2013). Engineering *Escherichia coli* for renewable production of the 5-carbon polyamide building-blocks 5-aminovalerate and glutarate. *Biotechnol. Bioeng.* 110, 1726–1734. doi: 10.1002/bit.24828

Altschul, S. F., Gish, W., Miller, W., Myers, E. W., and Lipman, D. J. (1990). Basic local alignment search tool. *J. Mol. Biol.* 215, 403–410. doi: 10.1016/S0022-2836(05)80360-2

Arinbasarova, A. Y., Ashin, V. V., Makrushin, K. V., Medentsev, A. G., Lukasheva, E. V., and Berezov, T. T. (2012). Isolation and properties of L-lysine-α-oxidase from the fungus *Trichoderma* cf. *aureoviride* RIFAI VKM F-4268D. *Microbiology* 81, 549–554. doi: 10.1134/S0026261712050037

Böhmer, A., Müller, A., Passarge, M., Liebs, P., Honeck, H., and Müller, H.-G. (1989). A novel L-glutamate oxidase from *Streptomyces endus*. *Eur. J. Biochem.* 182, 327–332. doi: 10.1111/j.1432-1033.1989.tb14834.x

Bradford, M. M. (1976). A rapid and sensitive method for the quantitation of microgram quantities of protein utilizing the principle of protein-dye binding. *Anal. Biochem.* 72, 248–254. doi: 10.1006/abio.1976.9999

Brautaset, T., Jakobsen, Ø. M., Degnes, K. F., Netzer, R., Nśrdal, I., Krog, A., et al. (2010). *Bacillus methanolicus* pyruvate carboxylase and homoserine dehydrogenase I and II and their roles for L-lysine production from methanol at 50°C. *Appl. Microbiol. Biotechnol.* 87, 951–964. doi: 10.1007/s00253-010-2559-6

Brautaset, T., Williams, M. D., Dillingham, R. D., Kaufmann, C., Bennaars, A., Crabbe, E., et al. (2003). Role of the *Bacillus methanolicus* citrate synthase II gene, *citY*, in regulating the secretion of glutamate in L-lysine-secreting mutants. *Appl. Microbiol. Biotechnol.* 69, 3986–3995. doi: 10.1128/AEM.69.7.3986-3995.2003

Cen, X., Liu, Y., Chen, B., Liu, D., and Chen, Z. (2021). Metabolic engineering of *Escherichia coli* for de novo production of 1,5-pentanediol from glucose. *ACS Synth. Biol.* 10, 192–203. doi: 10.1021/acssynbio.0c00567

Chae, T. U., Ko, Y.-S., Hwang, K.-S., and Lee, S. Y. (2017). Metabolic engineering of *Escherichia coli* for the production of four-, five- and six-carbon lactams. *Metab. Eng.* 41, 82–91. doi: 10.1016/j.ymben.2017.04.001

Cheng, J., Luo, Q., Duan, H., Peng, H., Zhang, Y., Hu, J., et al. (2020). Efficient whole-cell catalysis for 5-aminovalerate production from L-lysine by using engineered *Escherichia coli* with ethanol pretreatment. *Sci. Rep.* 10:990. doi: 10.1038/s41598-020-57752-x

Cheng, J., Tu, W., Luo, Z., Gou, X., Li, Q., Wang, D., et al. (2021). A high-efficiency artificial synthetic pathway for 5-aminovalerate production from biobased L-lysine in *Escherichia coli*. *Front. Bioeng. Biotechnol.* 9:633028. doi: 10.3389/fbioe.2021.633028

Cheng, J., Zhang, Y., Huang, M., Chen, P., Zhou, X., Wang, D., et al. (2018). Enhanced 5-aminovalerate production in *Escherichia coli* from L-lysine with ethanol and hydrogen peroxide addition. *J. Chem. Technol. Biotechnol.* 93, 3492–3501. doi: 10.1002/jctb.5708

Cotton, C. A., Claassens, N. J., Benito-Vaquerizo, S., and Bar-Even, A. (2020). Renewable methanol and formate as microbial feedstocks. *Curr. Opin. Biotechnol.* 62, 168–180. doi: 10.1016/j.copbio.2019.10.002

Delépine, B., Duigou, T., Carbonell, P., and Faulon, J. L. (2018). RetroPath2.0: a retrosynthesis workflow for metabolic engineers. *Metab. Eng.* 45, 158–170. doi: 10.1016/j.ymben.2017.12.002

Desa, R. J. (1972). Putrescine oxidase from *Micrococcus rubens*. *J. Biol. Chem.* 247, 5527–5534. doi: 10.1016/s0021-9258(20)81137-5

Drejer, E. B., Chan, D. T. C., Haupka, C., Wendisch, V. F., Brautaset, T., and Irla, M. (2020). Methanol-based acetoin production by genetically engineered *Bacillus methanolicus*. *Green Chem.* 22, 788–802. doi: 10.1039/c9gc03950c

Duigou, T., Du Lac, M., Carbonell, P., and Faulon, J. L. (2019). Retrorules: a database of reaction rules for engineering biology. *Nucleic Acids Res.* 47, D1229–D1235. doi: 10.1093/nar/gky940

Eikmanns, B. J., Thum-schmitz, N., Eggeling, L., Ludtke, K., and Sahm, H. (1994). Nucleotide sequence, expression and transcriptional analysis of the *Corynebacterium glutamicum gltA* gene encoding citrate synthase. *Microbiology* 140, 1817–1828. doi: 10.1099/13500872-140-8-1817

Fortina, M. G., Mora, D., Schumann, P., Parini, C., Manachini, P. L., and Stackebrandt, E. (2001). Reclassification of *Saccharococcus caldoxylosilyticus* as *Geobacillus caldoxylosilyticus* (Ahmad et al. 2000) comb. nov. *Int. J. Syst. Evol. Microbiol.* 51(Pt 6), 2063–2071. doi: 10.1099/00207713-51-6-2063

Gibson, D., Young, L., Chuang, R. Y., Venter, J. C., Hutchison, C. A. III, and Smith, H. O. (2009). Enzymatic assembly of DNA molecules up to several hundred kilobases. *Nat. Methods* 6, 343–345. doi: 10.1038/nmeth.1318

Green, R., and Rogers, E. J. (2013). Transformation of chemically competent *E. coli*. *Methods Enzymol.* 529, 329–336. doi: 10.1016/B978-0-12-418687-3.00028-8

Haas, T., Poetter, M., Pfeffer, J. C., Kroutil, W., Skerra, A., Lerchner, A., et al. (2014). *Oxidation and Amination of Secondary Alcohols. Patent number EP2734631B1*. Munich: European Patent Office.

Haupka, C., Delépine, B., Irla, M., Heux, S., and Wendisch, V. F. (2020). Flux enforcement for fermentative production of 5-aminovalerate and glutarate by *Corynebacterium glutamicum*. *Catalysts* 10:1065. doi: 10.3390/catal10091065

Haupka, C., Fernandes de Brito, L., Busche, T., Wibberg, D., and Wendisch, V. F. (2021). Genomic and transcriptomic investigation of the physiological response of the methylotroph *Bacillus methanolicus* to 5-aminovalerate. *Front. Microbiol.* 12:664598. doi: 10.3389/fmicb.2021.664598

Heggeset, T. M. B., Krog, A., Balzer, S., Wentzel, A., Ellingsen, T. E., and Brautaset, T. (2012). Genome sequence of thermotolerant *Bacillus methanolicus*: features and regulation related to methylotrophy and production of L-lysine and L-glutamate from methanol. *Appl. Environ. Microbiol.* 78, 5170–5181. doi: 10.1128/AEM.00703-12

Irla, M., Heggeset, T. M. B., Nærdal, I., Paul, L., Haugen, T., Le, S. B., et al. (2016). Genome-based genetic tool development for *Bacillus methanolicus*: theta- and rolling circle-replicating plasmids for inducible gene expression and application to methanol-based cadaverine production. *Front. Microbiol.* 7:1481. doi: 10.3389/fmicb.2016.01481

Irla, M., Nærdal, I., Brautaset, T., and Wendisch, V. F. (2017). Methanol-based γ-aminobutyric acid (GABA) production by genetically engineered *Bacillus methanolicus* strains. *Ind. Crops Prod.* 106, 12–20. doi: 10.1016/j.indcrop.2016.11.050

Ishizuka, H., Horinouchi, S., and Beppu, T. (1993). Putrescine oxidase of *Micrococcus rubens*: primary structure and *Escherichia coli*. *J. Gen. Microbiol.* 139, 425–432. doi: 10.1099/00221287-139-3-425

Jakobsen, Ø. M., Benichou, A., Flickinger, M. C., Valla, S., Ellingsen, T. E., and Brautaset, T. (2006). Upregulated transcription of plasmid and chromosomal ribulose monophosphate pathway genes is critical for methanol assimilation rate and methanol tolerance in the methylotrophic bacterium *Bacillus methanolicus*. *J. Bacteriol.* 188, 3063–3072. doi: 10.1128/JB.188.8.3063

Jakobsen, Ø. M., Brautaset, T., Degnes, K. F., Heggeset, T. M. B., Balzer, S., Flickinger, M. C., et al. (2009). Overexpression of wild-type aspartokinase increases L-lysine production in the thermotolerant methylotrophic bacterium *Bacillus methanolicus*. *Appl. Environ. Microbiol.* 75, 652–661. doi: 10.1128/AEM.01176-08

Job, V., Marcone, G. L., Pilone, M. S., and Pollegioni, L. (2002). Glycine oxidase from *Bacillus subtilis*: characterization of a new flavoprotein. *J. Biol. Chem.* 277, 6985–6993. doi: 10.1074/jbc.M111095200

Joo, J. C., Oh, Y. H., Yu, J. H., Hyun, S. M., Khang, T. U., Kang, K. H., et al. (2017). Production of 5-aminovaleric acid in recombinant *Corynebacterium glutamicum* strains from a *Miscanthus* hydrolysate solution prepared by a newly developed *Miscanthus* hydrolysis process. *Bioresour. Technol.* 245, 1692–1700. doi: 10.1016/j.biortech.2017.05.131

Jorge, J. M. P., Pérez-García, F., and Wendisch, V. F. (2017). A new metabolic route for the fermentative production of 5-aminovalerate from glucose and alternative carbon sources. *Bioresour. Technol.* 245, 1701–1709. doi: 10.1016/j.biortech.2017.04.108

Kusakabe, H., Kodama, K., Kuninaka, A., Yoshino, H., Misono, H., and Soda, K. (1980). A new antitumor enzyme, L-lysine alpha-oxidase from *Trichoderma viride*. Purification and enzymological properties. *J. Biol. Chem.* 255, 976–981. doi: 10.1016/S0021-9258(19)86128-8

Lee, J.-I., Jang, J.-H., Yu, M.-J., and Kim, Y.-W. (2013). Construction of a bifunctional enzyme fusion for the combined determination of biogenic amines in foods. *J. Agric. Food Chem.* 61, 9118–9124. doi: 10.1021/jf403044m

Lee, J. I., and Kim, Y. W. (2013). Characterization of amine oxidases from *Arthrobacter aurescens* and application for determination of biogenic amines. *World J. Microbiol. Biotechnol.* 29, 673–682. doi: 10.1007/s11274-012-1223-y

Liu, H., and Naismith, J. H. (2008). An efficient one-step site-directed deletion, insertion, single and multiple-site plasmid mutagenesis protocol. *BMC Biotechnol.* 8:91. doi: 10.1186/1472-6750-8-91

Liu, P., Zhang, H., Lv, M., Hu, M., Li, Z., Gao, C., et al. (2014). Enzymatic production of 5-aminovalerate from L-lysine using L-lysine monooxygenase and 5-aminovaleramide amidohydrolase. *Sci. Rep.* 4:5657. doi: 10.1038/srep05657

Luengo, J. M., and Olivera, E. R. (2020). Catabolism of biogenic amines in *Pseudomonas* species. *Environ. Microbiol.* 22, 1174–1192. doi: 10.1111/1462-2920.14912

Mai-Prochnow, A., Lucas-Elio, P., Egan, S., Thomas, T., Webb, J. S., Sanchez-Amat, A., et al. (2008). Hydrogen peroxide linked to lysine oxidase activity facilitates biofilm differentiation and dispersal in several Gram-negative bacteria. *J. Bacteriol.* 190, 5493–5501. doi: 10.1128/JB.00549-08

Moretti, S., Martin, O., van Du Tran, T., Bridge, A., Morgat, A., and Pagni, M. (2016). MetaNetX/MNXref - reconciliation of metabolites and biochemical reactions to bring together genome-scale metabolic networks. *Nucleic Acids Res.* 44, D523–D526. doi: 10.1093/nar/gkv1117

Nærdal, I., Netzer, R., Ellingsen, T. E., and Brautaset, T. (2011). Analysis and manipulation of aspartate pathway genes for L-lysine overproduction from methanol by *Bacillus methanolicus*. *Appl. Environ. Microbiol.* 77, 6020–6026. doi: 10.1128/AEM.05093-11

Nærdal, I., Netzer, R., Irla, M., Krog, A., Heggeset, T. M. B., Wendisch, V. F., et al. (2017). L-lysine production by *Bacillus methanolicus*: genome-based mutational analysis and L-lysine secretion engineering. *J. Biotechnol.* 244, 25–33. doi: 10.1016/j.jbiotec.2017.02.001

Nærdal, I., Pfeifenschneider, J., Brautaset, T., and Wendisch, V. F. (2015). Methanol-based cadaverine production by genetically engineered *Bacillus methanolicus* strains. *Microb. Biotechnol.* 8, 342–350. doi: 10.1111/1751-7915.12257

Noor, E., Bar-Even, A., Flamholz, A., Lubling, Y., Davidi, D., and Milo, R. (2012). An integrated open framework for thermodynamics of reactions that combines accuracy and coverage. *Bioinformatics* 28, 2037–2044. doi: 10.1093/bioinformatics/bts317

Okada, M., Kawashima, S., and Imahori, K. (1979). Substrate specificity and reaction mechanism of putrescine oxidase. *J. Biochem.* 86, 97–104.

Orth, J. D., Conrad, T. M., Na, J., Lerman, J. A., Nam, H., Feist, A. M., et al. (2011). A comprehensive genome-scale reconstruction of *Escherichia coli* metabolism-2011. *Mol. Syst. Biol.* 7:535. doi: 10.1038/msb.2011.65

Park, S. J., Kim, E. Y., Noh, W., Park, H. M., Oh, Y. H., Lee, S. H., et al. (2013). Metabolic engineering of *Escherichia coli* for the production of 5-aminovalerate and glutarate as C5 platform chemicals. *Metab. Eng.* 16, 42–47. doi: 10.1016/j.ymben.2012.11.011

Park, S. J., Oh, Y. H., Noh, W., Kim, H. Y., Shin, J. H., Lee, E. G., et al. (2014). High-level conversion of L-lysine into 5-aminovalerate that can be used for nylon 6,5 synthesis. *Biotechnol. J.* 9, 1322–1328. doi: 10.1002/biot.201400156

Pérez-García, F., Jorge, J. M. P., Dreyszas, A., Risse, J. M., and Wendisch, V. F. (2018). Efficient production of the dicarboxylic acid glutarate by *Corynebacterium glutamicum* via a novel synthetic pathway. *Front. Microbiol.* 9:2589. doi: 10.3389/fmicb.2018.02589

Revelles, O., Espinosa-Urgel, M., Fuhrer, T., Sauer, U., and Ramos, J. L. (2005). Multiple and interconnected pathways for L-lysine catabolism in *Pseudomonas putida* KT2440. *J. Bacteriol.* 187, 7500–7510. doi: 10.1128/JB.187.21.7500-7510.2005

Rohles, C. M., Gießelmann, G., Kohlstedt, M., Wittmann, C., and Becker, J. (2016). Systems metabolic engineering of *Corynebacterium glutamicum* for the production of the carbon-5 platform chemicals 5-aminovalerate and glutarate. *Microb. Cell Fact.* 15:154. doi: 10.1186/s12934-016-0553-0

Sakamoto, Y., Nagata, S., Esaki, N., Tanaka, H., and Soda, K. (1990). Gene cloning, purification and characterization of thermostable alanine dehydrogenase of *Bacillus stearothermophilus*. *J. Ferment. Bioeng.* 69, 154–158. doi: 10.1016/0922-338X(90)90038-X

Sambrook, J., and Russell, D. W. (2001). *Molecular Cloning: A Laboratory Manual*, 3rd Edn. Cold Spring Harbor, NY: Cold Spring Laboratory Press.

Samsonova, N. N., Smirnov, S. V., Altman, I. B., and Ptitsyn, L. R. (2003). Molecular cloning and characterization of *Escherichia coli* K12 *ygjG* gene. *BMC Microbiol.* 3:2. doi: 10.1186/1471-2180-3-2

Schendel, F. J., Bremmon, C. E., Flickinger, M. C., and Guettler, M. (1990). L-lysine production at 50°C by mutants of a newly isolated and characterized methylotrophic *Bacillus* sp. *Appl. Environ. Microbiol.* 56, 963–970. doi: 10.1128/AEM.56.4.963-970.1990

Shin, J. H., Park, S. H., Oh, Y. H., Choi, J. W., Lee, M. H., Cho, J. S., et al. (2016). Metabolic engineering of *Corynebacterium glutamicum* for enhanced production of 5-aminovaleric acid. *Microb. Cell Fact.* 15:174. doi: 10.1186/s12934-016-0566-8

Slabu, I., Galman, J. L., Weise, N. J., Lloyd, R. C., and Turner, N. J. (2016). Putrescine transaminases for the synthesis of saturated nitrogen heterocycles from polyamines. *ChemCatChem* 8, 1038–1042. doi: 10.1002/cctc.201600075

So, J. H., Lim, Y. M., Kim, S. J., Kim, H. H., and Rhee, I. K. (2013). Co-expression of gamma-aminobutyrate aminotransferase and succinic semialdehyde dehydrogenase genes for the enzymatic analysis of gamma-aminobutyric acid in *Escherichia coli*. *J. Appl. Biol. Chem.* 56, 89–93. doi: 10.3839/jabc.2013.015

Sohn, Y. J., Kang, M., Baritugo, K.-A., Son, J., Kang, K. H., Ryu, M.-H., et al. (2021). Fermentative high-level production of 5-hydroxyvaleric acid by metabolically engineered *Corynebacterium glutamicum*. *ACS Sustain. Chem. Eng.* 9, 2523–2533. doi: 10.1021/acssuschemeng.0c08118

Tani, Y., Miyake, R., Yukami, R., Dekishima, Y., China, H., Saito, S., et al. (2015a). Functional expression of L-lysine α-oxidase from *Scomber japonicus* in *Escherichia coli* for one-pot synthesis of L-pipecolic acid from DL-lysine. *Appl. Microbiol. Biotechnol.* 99, 5045–5054. doi: 10.1007/s00253-014-6308-0

Tani, Y., Omatsu, K., Saito, S., Miyake, R., Kawabata, H., Ueda, M., et al. (2015b). Heterologous expression of L-lysine α-oxidase from *Scomber japonicus* in *Pichia pastoris* and functional characterization of the recombinant enzyme. *J. Biochem.* 157, 201–210. doi: 10.1093/jb/mvu064

van Hellemond, E. W., van Dijk, M., Heuts, D. P. H. M., Janssen, D. B., and Fraaije, M. W. (2008). Discovery and characterization of a putrescine oxidase from *Rhodococcus erythropolis* NCIMB 11540. *Appl. Microbiol. Biotechnol.* 78, 455–463. doi: 10.1007/s00253-007-1310-4

Vary, P. S., Biedendieck, R., Fuerch, T., Meinhardt, F., Rohde, M., Deckwer, W.-D., et al. (2007). *Bacillus megaterium*-from simple soil bacterium to industrial protein production host. *Appl. Microbiol. Biotechnol.* 76, 957–967. doi: 10.1007/s00253-007-1089-3

Wang, X., Cai, P., Chen, K., and Ouyang, P. (2016). Efficient production of 5-aminovalerate from L-lysine by engineered *Escherichia coli* whole-cell biocatalysts. *J. Mol. Catal. B Enzym.* 134, 115–121. doi: 10.1016/j.molcatb.2016.10.008

Wendisch, V. F. (2020). Metabolic engineering advances and prospects for amino acid production. *Metab. Eng.* 58, 17–34. doi: 10.1016/j.ymben.2019.03.008

Wendisch, V. F., Mindt, M., and Pérez-García, F. (2018). Biotechnological production of mono- and diamines using bacteria: recent progress, applications, and perspectives. *Appl. Microbiol. Biotechnol.* 102, 3583–3594. doi: 10.1007/s00253-018-8890-z

Yao, X., He, W., and Lu, C. D. (2011). Functional characterization of seven γ-glutamylpolyamine synthetase genes and the *bauRABCD* locus for polyamine and β-alanine utilization in *Pseudomonas aeruginosa* PAO1. *J. Bacteriol.* 193, 3923–3930. doi: 10.1128/JB.05105-11

Yumoto, I., Hirota, K., Yamaga, S., Nodasaka, Y., Kawasaki, T., Matsuyama, H., et al. (2004). *Bacillus asahii* sp. nov., a novel bacterium isolated from soil with the ability to deodorize the bad smell generated from short-chain fatty acids. *Int. J. Syst. Evol. Microbiol.* 54, 1997–2001. doi: 10.1099/ijs.0.03014-0

Conflict of Interest: The authors declare that the research was conducted in the absence of any commercial or financial relationships that could be construed as a potential conflict of interest.

frontiers in Bioengineering and Biotechnology

ORIGINAL RESEARCH
published: 02 July 2021
doi: 10.3389/fbioe.2021.628569

Reconstruction of Secondary Metabolic Pathway to Synthesize Novel Metabolite in *Saccharopolyspora erythraea*

Chong-Yang Ren[1†], Yong Liu[2,3†], Wen-Ping Wei[2], Junbiao Dai[3] and Bang-Ce Ye[1,2]**

[1] Institute of Engineering Biology and Health, Collaborative Innovation Center of Yangtze River Delta Region Green Pharmaceuticals, College of Pharmaceutical Sciences, Zhejiang University of Technology, Hangzhou, China, [2] Laboratory of Biosystems and Microanalysis, State Key Laboratory of Bioreactor Engineering, East China University of Science and Technology, Shanghai, China, [3] Guangdong Provincial Key Laboratory of Synthetic Genomics, Shenzhen Key Laboratory of Synthetic Genomics and Center for Synthetic Genomics, Shenzhen Institute of Synthetic Biology, Shenzhen Institutes of Advanced Technology, Chinese Academy of Sciences, Shenzhen, China

OPEN ACCESS

Edited by:
Liming Liu,
Jiangnan University, China

Reviewed by:
Mingji Li,
Cornell University, United States
Liang Quanfeng,
Shandong University, China

***Correspondence:**
Bang-Ce Ye
bcye@ecust.edu.cn
Junbiao Dai
junbiao.dai@siat.ac.cn

[†] These authors have contributed equally to this work

Specialty section:
This article was submitted to Industrial Biotechnology, a section of the journal Frontiers in Bioengineering and Biotechnology

Received: *12 November 2020*
Accepted: *16 April 2021*
Published: *02 July 2021*

Citation:
Ren C-Y, Liu Y, Wei W-P, Dai J and Ye B-C (2021) Reconstruction of Secondary Metabolic Pathway to Synthesize Novel Metabolite in Saccharopolyspora erythraea. Front. Bioeng. Biotechnol. 9:628569. doi: 10.3389/fbioe.2021.628569

Natural polyketides play important roles in clinical treatment, agriculture, and animal husbandry. Compared to natural hosts, heterologous chassis (especially Actinomycetes) have many advantages in production of polyketide compounds. As a widely studied model Actinomycete, *Saccharopolyspora erythraea* is an excellent host to produce valuable heterologous polyketide compounds. However, many host factors affect the expression efficiency of heterologous genes, and it is necessary to modify the host to adapt heterologous production. In this study, the CRISPR-Cas9 system was used to knock out the erythromycin biosynthesis gene cluster of Ab (erythromycin high producing stain). A fragment of 49491 bp in genome (from SACE_0715 to SACE_0733) was deleted, generating the recombinant strain AbΔ*ery* in which erythromycin synthesis was blocked and synthetic substrates methylmalonyl-CoA and propionyl-CoA accumulated enormously. Based on AbΔ*ery* as heterologous host, three genes, AsCHS, RgTAL, and Sc4CL, driven by strong promoters Pj23119, PermE, and PkasO, respectively, were introduced to produce novel polyketide by L-tyrosine and methylmalonyl-CoA. The product (*E*)-4-hydroxy-6-(4-hydroxystyryl)-3,5-dimethyl-2H-pyrone was identified in fermentation by LC-MS. High performance liquid chromatography analysis showed that knocking out *ery* BGC resulted in an increase of methylmalonyl-CoA by 142% and propionyl-CoA by 57.9% in AbΔ*ery* compared to WT, and the yield of heterologous product in AbΔ*ery*:AsCHS-RgTAL-Sc4CL was higher than WT:AsCHS-RgTAL-Sc4CL. In summary, this study showed that AbΔ*ery* could potentially serve as a precious heterologous host to boost the synthesis of other valuable polyketone compounds using methylmalonyl-CoA and propionyl-CoA in the future.

Keywords: CRISPR-Cas9, *Saccharopolyspora erythraea*, polyketide, Acyl-CoA, heterologous expression, metabolic pathway

INTRODUCTION

Knockout and cloning of long fragment DNA, especially those containing large gene clusters, is particularly important for synthetic biology and chemical biology research (El-Sayed et al., 2017; Shao et al., 2018). Although homologous recombination has been applied to knock out single or multiple genes in the genome, it is difficult to remove long fragment DNA sequences in the genome, such as biosynthetic gene clusters, before the emergence of CRISPR-Cas9 technology (Komor et al., 2016; Park et al., 2016; Su et al., 2016). For example, a new yeast strain with a single chromosome was created by using CRISPR-Cas9 that achieved the deletion of long redundant repetitive sequences in chromosome and the accuracy of chromosome fusions (Shao et al., 2019). And then CRISPR-Cas9 was applied in *Streptomyces* as a more efficient tool for genome editing (Cobb et al., 2015; Tong et al., 2015). Researchers established a highly efficient CRISPR-Cas9 genome editing plasmid pKCcas9dO for the genetic manipulation of *Streptomyces*, with an editing efficiency of 60–100%. The system has been applied for single gene deletions such as actII-orf4 *redD*, *glnR*, and knocking out large gene clusters such as antibiotic biosynthetic gene clusters (ACT, 21.3 kb), red pigment synthesis gene clusters (31.6 kb), and Ca^{2+}-dependent antibiotics (82.8 kb) (Huang et al., 2015). The advances of genetic engineering tools and strategies accelerated the programs that introduce designed metabolic pathways in the strains for industrial production. Novel and efficient DNA splicing methods including BioBrick assembly (Storch et al., 2015), Gibson assembly (Gibson et al., 2009; Arturo et al., 2013), TAR clone (Ross et al., 2014), etc., facilitate multi-fragment, large gene cluster assembly (Zhang W. et al., 2017) and the manipulation of genes involved in metabolic pathways (Guo et al., 2015).

Saccharopolyspora erythraea is a Gram-positive bacterium and a model representative of Actinobacteria. It is widely used in industry for large-scale production of Erythromycin A (ErA), and has great value of research (Moffitt, 1998; Kim and Cerniglia, 2005). At the end of the last century, scholars discovered the location of erythromycin biosynthetic gene clusters, from SACE_0713 to SACE_0734, with a total length of about 56 kb and containing 21 erythromycin synthesis-related genes (Thompson et al., 1982; Tomich, 1988; Reeves et al., 1999). After the whole genome sequencing of *S. erythraea* finished in 2007 (Oliynyk et al., 2007), its genetic modification has become more convenient. Traditional genetic modification relies on its own homologous recombination machinery, and the genes are knocked in or out through homology arms mediated double exchange (Ferain et al., 1996; Tsai et al., 2011). However, it is difficult and inefficient to edit the gene in *S. erythraea* which has high GC content. With the emergence and continuous optimization of the CRISPR-Cas9 system, we have better tools for gene editing. In previous work, we have successfully applied CRISPR-Cas9 in *S. erythraea* (Liu W. et al., 2018; Liu et al., 2019).

Heterologous production of natural products has attracted more attention in terms of microbial technology and the discovery of new active compounds (Cleto and Lu, 2017; Liu Y. et al., 2018; Huo et al., 2019). Not only can it produce more valuable compounds and higher yield in more suitable heterologous hosts (Horbal and Luzhetskyy, 2016; Tan et al., 2017), but it can also dig out new compounds through biosynthetic engineering and metabolic engineering (Zhang et al., 2016; Lopatniuk et al., 2017; Reynolds et al., 2017). Due to the differences of transcription and metabolic regulation, precursor supply, etc. between different hosts, the yield of heterologous expression is not sufficient (Zhang J. J. et al., 2017; Horbal et al., 2018). Therefore, it can be increased by various methods such as medium optimization, precursor feeding, adding strong promoter (Cortina et al., 2012), and deleting some known metabolic biosynthetic gene clusters (Mao et al., 2017). There are abundant propionyl-CoA (PP-CoA) or methylmalonyl-CoA (MM-CoA) in *S. erythraea* which can be used to synthesize valuable compounds (Li et al., 2013; Karničar et al., 2016; Cho et al., 2018). Polyketides are widely found in bacteria, fungi, and plants and have a variety of biological activities, such as antibiotics (Erythromycin), immunosuppressants (Rapamycin) (Calne et al., 1989), anti-tumor (Doxorubicin), and insecticidal Agent (Nanchangmycin) (Sun et al., 2003), etc. In recent years, studies on polyketone compounds increased (Yu et al., 2012; Lim et al., 2016; Parvez et al., 2018). Chalcone synthase (CHS) (EC2.3.1.74), a plant-derived type III polyketide synthase, can use malonyl-CoA or MM-CoA and 4-coumaryl-CoA, 4-Hydroxyphenylpropionyl-CoA, or benzoyl-CoA as substrates to produce phlorizin and chalcone (Morita et al., 2001). Because of its broad substrate specificity, it has been widely expressed in heterologous hosts such as *Escherichia coli* (Wu et al., 2013) and *Saccharomyces cerevisiae* (Lyu et al., 2017; Wang et al., 2019).

In this study, we constructed a temperature-sensitive plasmid pKECas9-erysgRNAII-HA, using two sgRNAs to specifically target SACE_0715 and SACE_0733 sites of the erythromycin biosynthetic gene cluster, and knocking out about 49.5 kb genomic sequence by providing a homologous repair template spanning the two targets, which blocked the synthesis of erythromycin. It was detected by HPLC that the erythromycin synthesis precursor MM-CoA was accumulated in a large amount compared with the WT. On this basis, a secondary metabolic pathway was constructed by introducing the heterologous genes CHS from *Aquilaria sinensis* (Gao et al., 2015), TAL from *Rhodotorula glutinis* (Wu et al., 2014), and 4CL from *Streptomyces coelicolor* (Hsiao and Kirby, 2008). These genes were constructed in integrative plasmid pSET152 by tandem, and driven by stronger promoters Pj23119, PermE, and PkasO to increase the heterologous expression. The route of research is shown in **Figure 1**, using L-tyrosine as the starting substrate and MM-CoA accumulated in the AbΔ*ery* to synthesize a new secondary metabolite (*E*)-4-hydroxy-6-(4-hydroxystyryl)-3,5-dimethyl-2H-pyrone (BNY-type pyrone), a kind of non-natural small molecule with novel structure catalyzed by plant polyketone polymerase. It can be used as a precursor to synthesize pyrone drugs and has a broad application prospect in the future (Abe et al., 2002; Gao et al., 2015).

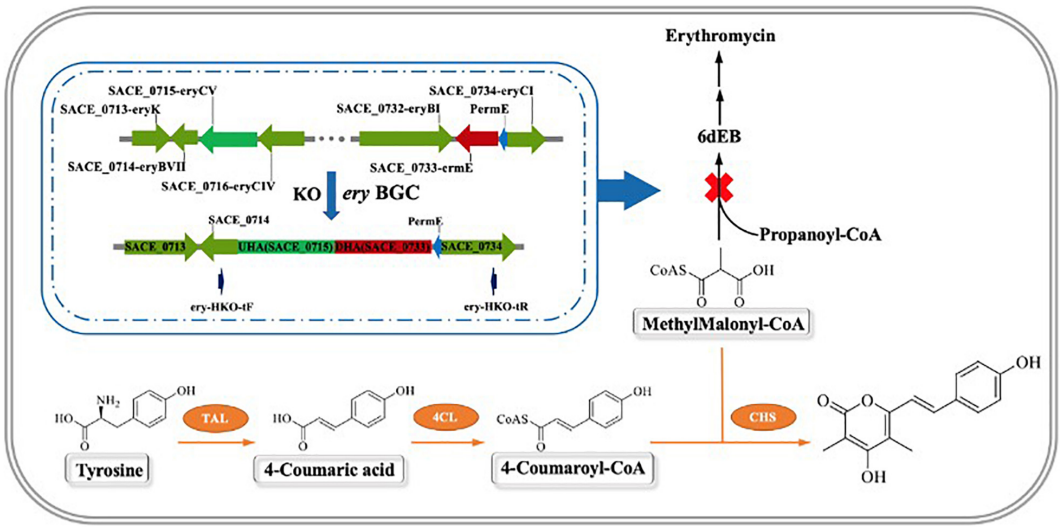

FIGURE 1 | Schematic diagram of the reconstruction of secondary metabolic pathway and the synthesize route of novel metabolites BNY-type pyrone.

MATERIALS AND METHODS

Strains, Plasmids, and Growth Conditions

All recombinant strains and plasmids used in this study are listed in **Supplementary Table 2**. *E. coli* DH5α was used for construction of recombinant plasmids. *E. coli* were cultured at 30 or 37°C in Luria-Bertani broth (LB) medium (Tryptone 10 g/L, Yeast extract 5 g/L, NaCl 10 g/L), and apramycin (50 μg/mL) was added for plasmid cloning when required. In order to select the apramycin-resistant mutant strain of *S. erythraea* after transformation, 25 μg/mL or 50 μg/mL apramycin was used. The *S. erythraea* wild-type strain (NRRL23338), the erythromycin high-yield strain (Ab), and the AbΔ*ery* strain were grown on R2YE agar plates (Liao et al., 2015). For seed stock preparation, the strain was cultivated in a 250 mL flask containing 30 mL tryptic soy broth (TSB), shaken at 220 rpm for 48 h at 30°C. With the same culture conditions, 0.5 mL of the seed culture was inoculated into a 500 mL flask containing 100 mL of TSB medium with 0.5 g glycine, and strain samples were harvested for preparation of protoplast at the indicated time points (48 h). PEG-mediated transformations of protoplasts were performed as previously described (Liu Y. et al., 2018).

Recombinant plasmid construction was performed using a Hieff Clone Multi One Step Cloning Kit (Yeasen, Shanghai, China). Plasmid extraction was performed using an Endofree Mini Plasmid Kit II (Tiangen, Beijing, China). *S. erythraea* mutant was verified by colony polymerase chain reaction (PCR). Sequencing validation of all plasmid constructs (support information) was performed using Phanta Max SupperFidelity DNA polymerase (Vazyme, Nanjing China) and was confirmed by sequencing (Majorbio, Shanghai, China). Restriction enzymes, polymerases, and kits were used according to the supplier's instructions (Takara, Japan).

Construction of *ery* BGC Knock-Out and Heterologous Expression Plasmids

The analysis of sgRNA in the *ery* BGCs knock-out plasmid was referred to previous studies (Doench et al., 2014). Two sgRNAs were selected to target *ery* BGC and their transcription were driven by Pj23119 and PkasO promoters, respectively. The gRNA backbone was added to form sgRNAII, which was constructed into pUC57 vector for preparation.

The knock-out element was recombined and cloned into the *Xba*I + *Hin*dIII restriction site, and pKECas9 vector was used as a backbone (Liu Y. et al., 2018). The complete knock-out cassette consisting of *ery* BGC sgRNAII and the homology arms (KOery-UHA, KOery-DHA) flanking the target was obtained by overlapping PCR, and the cloning kit was used to construct the *ery* BGC knockout vector by the following steps: (1) The pUC57-erysgRNAII plasmid was used as a template to obtain the (*Xba*I) H-erysgRNAII-O fragment; the O-UHA-O and O-DHA-*Hin*dIII-H fragment were amplified from *S. erythraea* genomic DNA. (2) The (*Xba*I) H-erysgRNAII-O and O-UHA-O fragments were used to generated (*Xba*I) H-erysgRNAII-UHA-O by the first round of overlapping PCR. Then the (*Xba*I) H-erysgRNAII-UHA-O and O-DHA-*Hin*dIII-H were used to the second round of overlapping PCR, amplified to obtain the H-*Xba*I-erysgRNA-UHA-DHA-*Hin*dIII-H fragment. (3) The pKECas9 plasmid was digested with *Xba*I + *Hin*dIII to obtain the linear vector, homologous recombination with (*Xba*I) H-erysgRNAII-UHA-DHA-H (*Hin*dIII) fragment to construct the pKECas9-erysgRNAII-UHA-DHA plasmid (**Supplementary Figure 3a**). The positive clones were confirmed by PCR using the pKECas9-test-F, pKECas9-test-R primer pair.

The heterologous genes AsCHS, RgTAL, and Sc4CL were driven by the Pj23119 (Huang et al., 2015), PermE (Bibb et al., 1985), and PkasO (Wang et al., 2013; Phelan et al., 2017), respectively, and promoters were cloned into the

*Xba*I + *Eco*RV site of the pSET152 vector. Firstly, three fragments including Pj23119-AsCHS commercially synthesized by Ruimian (Shanghai, China), PermE-RgTAL, and PkasO-Sc4CL maintained in our laboratory were amplified and their sequences were provided in Supporting Information. Next, Pj23119-AsCHS and PermE-RgTAL were fused by overlapping PCR to obtain Pj23119-AsCHS-PermE-RgTAL, then combining with PkasO-Sc4CL to generate (*Xba*I) H-Pj23119-CHS-PermE-TAL-PkasO-4CL-H (*Eco*RV). Finally, the (*Xba*I) H-Pj23119-AsCHS-PermE-RgTAL-PkasO-Sc4CL-H (*Eco*RV) linear fragment was cloned into pSET152 (*Xba*I, *Eco*RV) to complete construction, see schematic (**Supplementary Figure 3b**). Six positive clones were screened with M13 primer pairs and the No. 2 was selected for expansion culture to extract plasmid (**Supplementary Figure 6a**). Then corresponding primers were used to confirm that all three gene expression cassettes were present; the fragment Pj23119-AsCHS was 1235 bp, PermE-RgTAL was 2273 bp, and PkasO-Sc4CL was 1696 bp (**Supplementary Figure 6b**). The primers used to amplify DNA fragments are shown in **Supplementary Table 3**.

Ab∆*ery* Erythromycin Bioactivity Analysis

Growth trends were analyzed by a microplate reader (BioTek Reader) (Liu et al., 2019). Cell density measurements at OD_{600} were acquired every 8 or 12 h and were analyzed using GraphPad Prism 7 software package (GraphPad Software). According to the previous method, the titer of erythromycin in Ab∆*ery* and control Ab fermentation were quickly analyzed by turbidimetry of antibiotic microorganisms. Ab∆*ery* and Ab were inoculated into 500 mL shake flasks containing 30 mL of ABPM8 industrial medium at 30°C, 220 rpm for 7 days. After fermentation was completed, broth was centrifuged at 12000 × *g*, 10 min, and the supernatant was extracted for subsequent analysis. *Bacillus subtilis* was inoculated in LB medium and cultured overnight at 37°C, 220 rpm, then transferred to new LB medium growth to OD_{580} was 0.4. Then, 200 μL above *B. subtilis* was added to a sterile 90 mm dish containing 20 mL of bioactivity assay medium (Supporting methods), then distributed to a 96-well cell culture plate by an 8-channel pipette, and each well was 135 μL. Adding 15 μl erythromycin standard and fermentation supernatant to the 96-well plate incubated at 37°C, 200 rpm for 2.5–3 h, set three replicates for each sample and measurement of OD_{580} was analyzed by microplate reader. Making sure the OD_{580} of blank control was not more than 0.5 and fitting the curve with OD_{580}-logC to determine the linear range and standard curve.

The above fermentation was filtered through a 0.22 μm disposable organic phase filter, and the filtrate was accurately analyzed by HPLC to calculate the titer of erythromycin. The analysis conditions were following: solvent B phase (55% acetonitrile) and solvent A phase (1L Milli-Q H_2O, 8.7 g K_2HPO_4, pH 8.2), the flow rate was 1.0 mL/min, and the column maintained at 40°C. UV spectra were acquired at 215 nm (Liu Y. et al., 2018). The peak area value and the standard concentration value were used to fit the standard curve, then the ErA titer of the sample was calculated.

Determination of Three Intracellular CoAs Concentration

Intracellular PP-CoA and MM-CoA of Ab∆*ery*, Ab, and WT strains were extracted and assayed by HPLC. Strains were inoculated into 30 mL TSB medium at 30°C and cultured at 220 rpm for 48 h. The cells were washed twice with PBS and collected by centrifugation at 12000 × *g*, 10 min, then resuspended in 800 μL lysate (10% trichloroacetic acid and 90% 2 mM dithiothreitol). The mixture was freeze-thawed 2–3 times at −80°C and 4°C, centrifuged at 15,000 × *g* for 10 min, then the supernatant was transferred to an activated, equilibrated Sep-Pak column (1 ml, 50 mg tC18; Milford, MA, United States). After 3–5 min for adsorption, the column was washed with 1 ml ddH_2O and eluted with 400 μL of 40% acetonitrile. SpeedVac (Thermo Fisher, Waltham, MA, United States) was used for lyophilization. It was dissolved by 100 μL of pure acetonitrile for HPLC analysis. The analytical conditions were mobile phase A (75 mM KH_2PO_4, pH 5.5) and mobile phase B (80% 75 mM aqueous KH_2PO_4, pH 5.0, mixed with 20% acetonitrile). Separation using a reversed-phase C18 column, flow rate 1 mL/min, column temperature 30°C, detector 254 nm, mobile phase distribution as follows: 4 min (when Buffer B reached 11% from 10%), 7 min (Buffer B reached 13% from 11%), 10 min (Buffer B reaches 15% from 13%), 15 min (Buffer B reaches 18% from 15%), 20 min (Buffer B reaches 23% from 18%), 23 min (Buffer B Results 28% from 23%), 28 min (Buffer B reaches 33% from 28%), 30 min (Buffer B reaches 39% from 33%), 50 min (Buffer B reaches 48% from 39%), 55 min (Buffer B reached 54% from 48%), and 65 min (Buffer B decreased from 54 to 10%), maintaining 10% phase B for 5 min, and stopping data collection at 70 min (Xu et al., 2017). Three independent experiments were performed to calculate the standard deviation.

RNA Extraction and qRT-PCR Analysis

The strain was grown in 30 mL TSB medium to the late stage of the exponential phase, and collected by centrifugation at 12,000 × *g* for 10 min at 4°C. Total RNA was isolated and purified from the strain by RNA Prep Pure Cell/Bacteria Kit DP430 (TIANGEN) kit, and the RNA quality was assessed by 1% agarose gel electrophoresis and concentration was quantified by Synergy Mx multi-plate reader (BioTek, Winooski, VT, United States). Then, 1.0 μg total RNA with PrimeScript RT Reagent Kit and gDNA Eraser (Takara, Japan) kit were performed to synthesize cDNA which has removed genomic DNA. The resulting cDNA was diluted to final concentration of 50 ng/μL as the template, and real-time quantitative PCR analysis of mRNA levels was performed with 10 μL SYBR Premix Ex Taq GC (Takara) and the volume was 20 μL. All samples were prepared in triplicate to obtain CT values, and the relative gene expression levels were calculated using the comparative CT method ($2^{-\Delta\Delta Ct}$) (Jinek et al., 2012; Liu et al., 2019). The qPCR assays were carried out by CFX96 Real-Time System (Bio-Rad) under conditions as following: 95°C for 5 min, then 40 cycles (95°C for 10 s, 60°C for 20 s, 72°C for 30 s), with a final extension cycle at 72°C for 10 min with *sigA* (SACE_1801) as the reference gene (Liao et al., 2015). The transcription levels of heterologous genes were determined by absolute quantification, and the copy

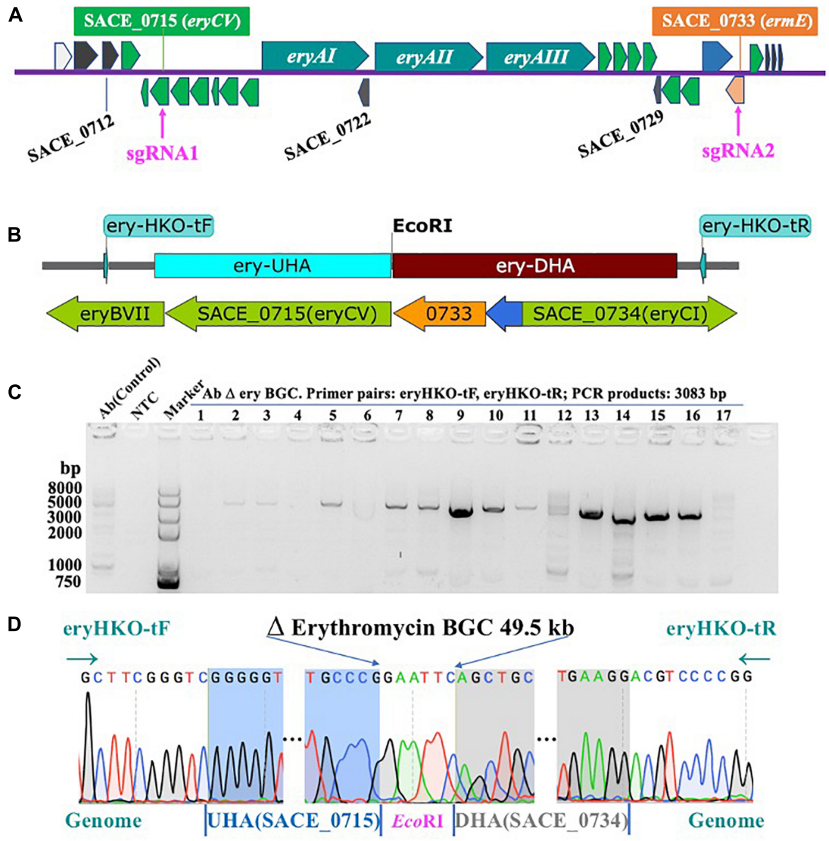

FIGURE 2 | Knock-out of erythromycin biosynthetic gene cluster. **(A)** Erythromycin Biosynthetic Gene cluster (from SACE_0713 to SACE_0734) and the target of sgRNAs (SACE_0715 and SACE_0733). **(B)** Schematic of knock-out Erythromycin biosynthetic gene cluster. **(C)** Agarose gel electrophoresis of PCR products from Ab Δ*ery* using test primer pairs (eryHKO-tF, eryHKO-tR). The size of PCR products is 3083 bp. **(D)** Sequencing of Ab Δ*ery* BGC recombinant strain. 49491 bp sequence in *ery* BGC is knocked out.

number of constructed plasmid was diluted into gradient of 2×10^7, 2×10^6, 2×10^5, 2×10^4, 2×10^3, 2×10^2, 2×10^1, 2×10^0 as template for Q-PCR. Three replicates were set for each sample, and the copy number of heterologous genes were calculated by plotting the standard curve with the Ct value and the copy number logarithm as the horizontal and vertical coordinates. All primers in this work were described in **Supplementary Table 3**.

HPLC and LC-MS Analysis of Fermentation

Ab Δ*ery*:CT4, WT:CT4, Ab Δ*ery*, and WT strains were transferred to a 250 mL flask containing 30 mL TSB medium and cultured at 37°C, 220 rpm for 7 days. The fermentations were centrifuged at 8000 × *g* to collect the supernatant, and concentrated. Then, 2 ml of the concentrate was filtered through a 0.22 μm disposable organic phase filter, and the filtrate was analyzed by HPLC. The analysis conditions were as follows: HPLC system (Waters 2695, water 2489 UV/visible light detector) equipped with a Thermo Hypersil BDS C18 column maintained at 35°C. The productions were analyzed at 277 nm, respectively, with mobile phase A (25 mM $HCOONH_4$, pH 3.0) and mobile phase B (acetonitrile) at a flow rate 1.0 mL/min, mobile phase distribution as follows: 5 min (when Buffer B reached 10% from 2%), 20 min (Buffer B reached 40% from 10%), 25 min (Buffer B reached 2% from 10%). LC-ESIMS spectra were measured with a HPLC system (Agilent 1260) coupled to a 6530C Q-TOF LC-MS System (Agilent, Waldbronn, Germany). LC separation was carried out with a ZORBAX SB-C18 column (4.6 × 250 mm, 5 μm) at 30°C. For elution, H_2O (solvent A) and acetonitrile (solvent B) were applied as the mobile phases at a flow rate of 1 mL/min. A gradient was used that the amount of solvent B as follows: 0–7 min (reached 60% from 5%), 9.5–12 min (reached 5% from 60%), 12–20 min (maintained 5%). The mass spectrometer was operated in the positive electrospray ionization (ESI) mode, the gas temperature and voltage were 300°C and 3.5 KV, nebulizer was 35 psig, collision energy 20 V.

RESULTS

CRISPR-Cas9 Strategy for *ery* BGC Knock Out

Firstly, we used the Ape software to choose all sgRNAs that score more than 0.5 in sequence of *ery* BGC. In order to

TABLE 1 | Details of two sgRNAs for knock-out of *ery* BGC.

No.	*ery*-sgRNA (Seq.)	PAM	Loc	Dir	Score	5′G	3′GG	Matches	>15nt
1	GGCGAGGTCGGCGAGCCGGG	cGG	3513	>	0.692	0	1	1	1
2	GCACCGGCTTGAACAGCCGG	cGG	52743	>	0.856	1	1	1	1

Seq, sgRNA sequence 5′ to 3′; Loc, location. Dir, direction, >indicates sgRNA on the sense strand, <indicates sgRNA on the antisense strand.

reduce the possibility of off-target as much as possible, two optimal sgRNAs were selected after using the BLAST function at the NCBI to confirm no sequence matches were found in the whole genome. The targets of the erythromycin biosynthesis gene cluster (*ery* cluster, SACE_0713-SACE_0734) were shown in **Figure 2A**, and provided details information of the entire *ery* BGC (**Supplementary Figure 1** and **Supplementary Table 1**). The details of sgRNAs were shown in **Table 1**. Subsequently, we combined the two sgRNAs to sgRNAII under the control of Pj23119 and PkasO promoters, respectively, cloned into the PKEcas9 vector with the homology arms (KOery-UHA, KOery-DHA) on both sides of the target, and then the plasmid was transferred into *E. coli* DH5α. The primer pairs pKECas9-test-F, pKECas9-test-R were used to screen positive clones by colony PCR, and the results were shown in **Supplementary Figure 2a**. We expanded the positive clone and extracted plasmids for further verification using different primer pairs. The results of agarose gel electrophoresis indicated that the size of each band was correct (**Supplementary Figure 2b**) and the construction of plasmid pKECas9-erysgRNAII-HA was succeeded (**Supplementary Figure 2c**).

After we transformed plasmid into Ab protoplasts, a single colony growing on the selective plates was randomly selected and subjected to PCR analysis to verify whether *ery* BGC has been knocked out. Successful deletion of the 49.5 kb DNA fragment will result in an amplification product at size 3083 bp; otherwise, no band should show up since it is too big to amplify. As shown in **Figure 2C**, among 17 clones, we found several PCR products at the right size. To further confirm, the PCR products were subjected to DNA sequencing. In **Figure 2D**, the sequencing results of No.9 showed that all core genes from SACE_0716 (*eryCIV*) to SACE_0732 (*eryBI*) in *ery* BGC were knocked out, and the 3′ end of the *eryCV* was 310 bp, and the 5′ end of *ermE* was 670 bp, which deleted 49491 bp sequence in *ery* BGC. In conclusion, using CRISPR-Cas9, we are able to successfully construct the *S. erythraea* strain in which the entire *ery* BGC has been removed (**Figures 2B,D**). This strain was designated Ab1*ery* and cultured at 42°C several times, and lost the temperature-sensitive gene editing plasmid, which is convenient for subsequent research. Growth curves showed that knocked-out BGC reduced the metabolic pressure of Ab1*ery* and made it grow better before 120 h, but biomass decreases slightly in later stages of culture (**Supplementary Figure 4**).

Strain Ab1*ery* Lost the Ability of Erythromycin Synthesis

In order to test whether deletion of *ery* BGC will lead to the loss of erythromycin synthesis, 12 colonies from the subcultured Ab1*ery* strain were cultured (**Figure 3A**), and the biological activity method was used to determine the ability of erythromycin production with Ab as a control (**Supplementary Table 8**). The erythromycin synthesized by *S. erythraea* was not a single compound but included six isomers, ErA, ErB, ErC, ErD, ErE, and ErF, of which ErA was the highest antibacterial activity and the most widely used element. The biological activity method cannot determine the yield of ErA and the measurement results were not accurate which can only function as a reference, so the lowest yield Ab1*ery* and Ab(control) were chosen and cultured in industrial fermentation medium for 7 days. Then the culture was sampled and centrifuged to collect the supernatant. The high-performance liquid chromatography (HPLC) was used to determine the yield of ErA (**Figure 3B**), which is nearly 1.5 g/L in Ab and barely detectable in Ab1*ery*. Therefore, these data indicated that Ab1*ery* has lost ability to synthesize ErA.

To further prove, we analyzed the transcription level of erythromycin biosynthetic gene cluster in Ab1*ery*. The total RNA was extracted at 48 h and reverse-transcribed into cDNA as a template, after which the transcription level of *ery* BGC was determined by QPCR. The sigA (SACE_1801) was selected as reference gene and Ab was used as control. The primers designed from SACE_0713 to SACE_0734 in *ery* BGC were used to detect the transcription levels of each gene, information of primers in **Supplementary Table 3**. The results of the transcription level analysis were shown in **Figure 3C** and **Supplementary Table 4**, which indicate that the transcripts of genes for SACE_0713 to SACE_0734 were all downregulated. Furthermore, we found that a few gene transcriptions were still detected. The situation of contamination with wild type *S. erythraea* or cells that still contain *ery* BGC was ruled out by repeated experiments. We speculated that there were background signal errors or non-specific binding of primers and several genes such as SACE_0727 and SACE_0731 had multiple copies in genome of Ab compared to WT (Karničar et al., 2016), so there was still a small amount of transcription.

Accumulation of MM-CoA and PP-CoA in Ab1*ery* Strain

The biosynthesis of erythromycin is divided into two stages, the synthesis of 6-dEB (6-deoxyerythromycin-B) and post-synthesis modification. The 6-dEB was synthesized by a series of polyketide synthase using one unit of PP-CoA and six units of MM-CoA (Zhang J. J. et al., 2017). *S. erythraea* produced abundant MM-CoA and PP-CoA, which were used for the synthesis of erythromycin and maintaining own metabolism. When *ery* BGC was knocked out, synthesis of erythromycin will be blocked, and cells will accumulate a large amount of MM-CoA and PP-CoA. To verify that, we

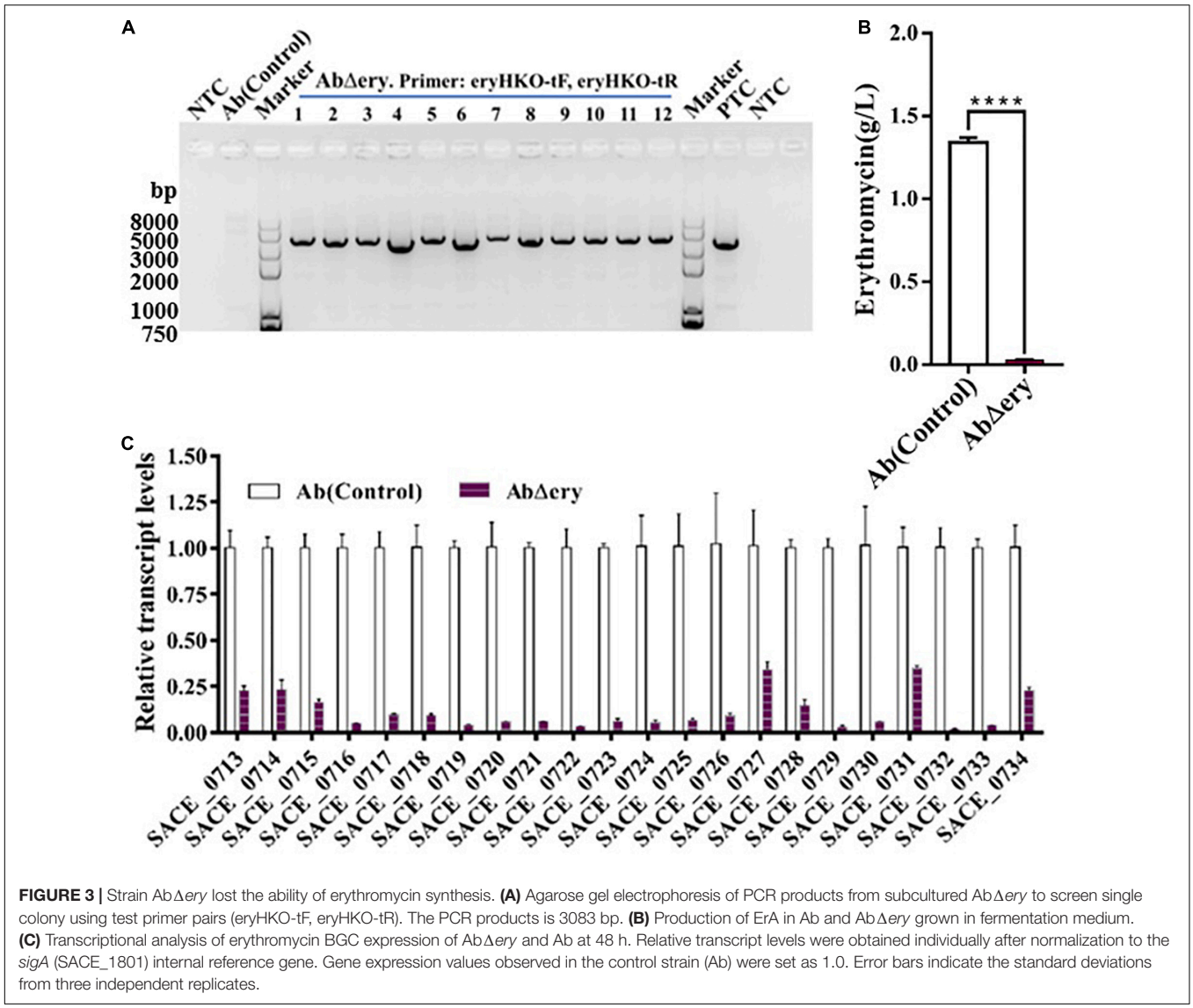

FIGURE 3 | Strain Ab*Δery* lost the ability of erythromycin synthesis. **(A)** Agarose gel electrophoresis of PCR products from subcultured Ab*Δery* to screen single colony using test primer pairs (eryHKO-tF, eryHKO-tR). The PCR products is 3083 bp. **(B)** Production of ErA in Ab and Ab*Δery* grown in fermentation medium. **(C)** Transcriptional analysis of erythromycin BGC expression of Ab*Δery* and Ab at 48 h. Relative transcript levels were obtained individually after normalization to the *sigA* (SACE_1801) internal reference gene. Gene expression values observed in the control strain (Ab) were set as 1.0. Error bars indicate the standard deviations from three independent replicates.

cultured Ab*Δery*, Ab, and WT in TSB for 48 h before extracting intracellular CoAs and determining concentration by HPLC. We measured the contents of MM-CoA and PP-CoA in the recombinant strain. The HPLC results (**Figure 4A** and **Supplementary Figure 5**) showed that compared with WT and Ab, MM-CoA and PP-CoA were significantly accumulated in Ab*Δery*. The concentration of MM-CoA in Ab*Δery* was about 1.5 times of Ab (162%) and WT (142%), whereas the concentration of PP-CoA increased 220 and 57.9% than Ab and WT (**Figure 4B**).

Heterologous Genes Were Introduced Into Ab*Δery* to Reconstruct Secondary Metabolic Pathways

The above experiments indicated that the mutant strain Ab*Δery* was successfully constructed, in which the entire *ery* BGC has been deleted and the substrate CoAs were accumulated. Next, we would like to use Ab*Δery* as a heterologous host to synthesize BNY-type pyrone using MM-CoA and L-tyrosine as substrates. RgTAL encodes tyrosine ammonia lyase which catalyzed L-tyrosine to 4-coumaric acid, Sc4CL encodes 4-coumarate-CoA ligase which synthesized to 4-coumaroyl-CoA, and AsCHS encoded chalcone synthase which catalyzed 1 unit of 4-coumaryl-CoA and 2 units of MM-CoA to BNY-type pyrone. In order to improve the efficiency of heterologous expression and ensure that AsCHS, RgTAL, and Sc4CL can be independently and completely expressed, they were driven by three strong promoters respectively, and constructed into the pSET152 vector (**Figure 5A** and **Supplementary Figure 6d**). According to the synthetic route, chalcone synthase catalyzing 4-coumaryl-CoA and MM-CoA to BNY-type pyrone was the rate-limiting step, therefore AsCHS was driven by the strongest promoter Pj23119, then Sc4CL was driven by PkasO and PermE for RgTAL. The sequencing results showed that the plasmid was successfully constructed (**Supplementary Figure 6e**).

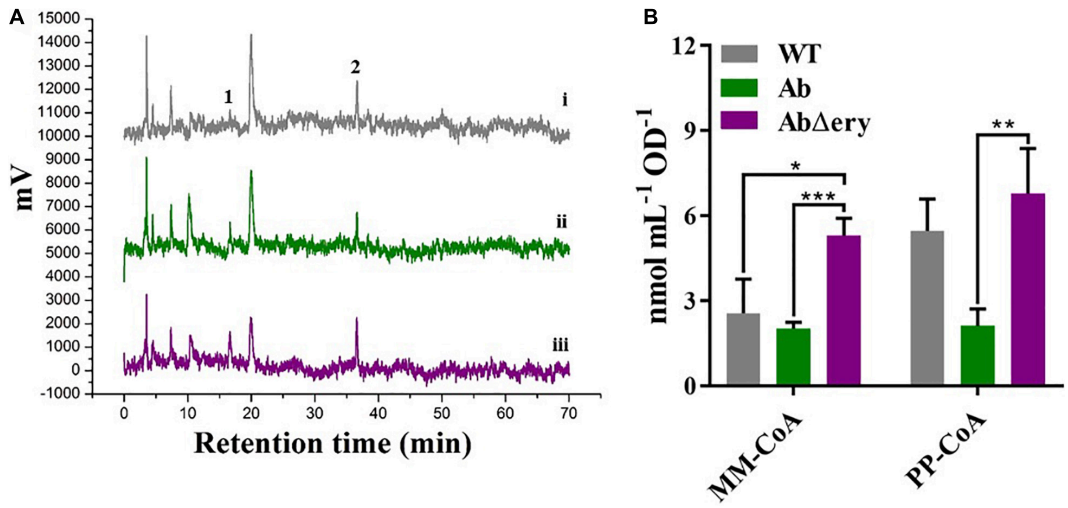

FIGURE 4 | Determination of CoAs concentration by HPLC. **(A)** HPLC analysis of intracellular coenzyme A in WT (i), Ab (ii), and Ab*Δery* (iii). The peak 1 is MM-CoA (methylmalonyl-CoA) which peak time in spectrum is 17.6 min, and 2 is PP-CoA (propionyl-CoA) which peak time is 35.9 min. **(B)** Comparison of peak area of MM-CoA and PP-CoA between Ab*Δery* (purple), Ab (green), and WT (gray).

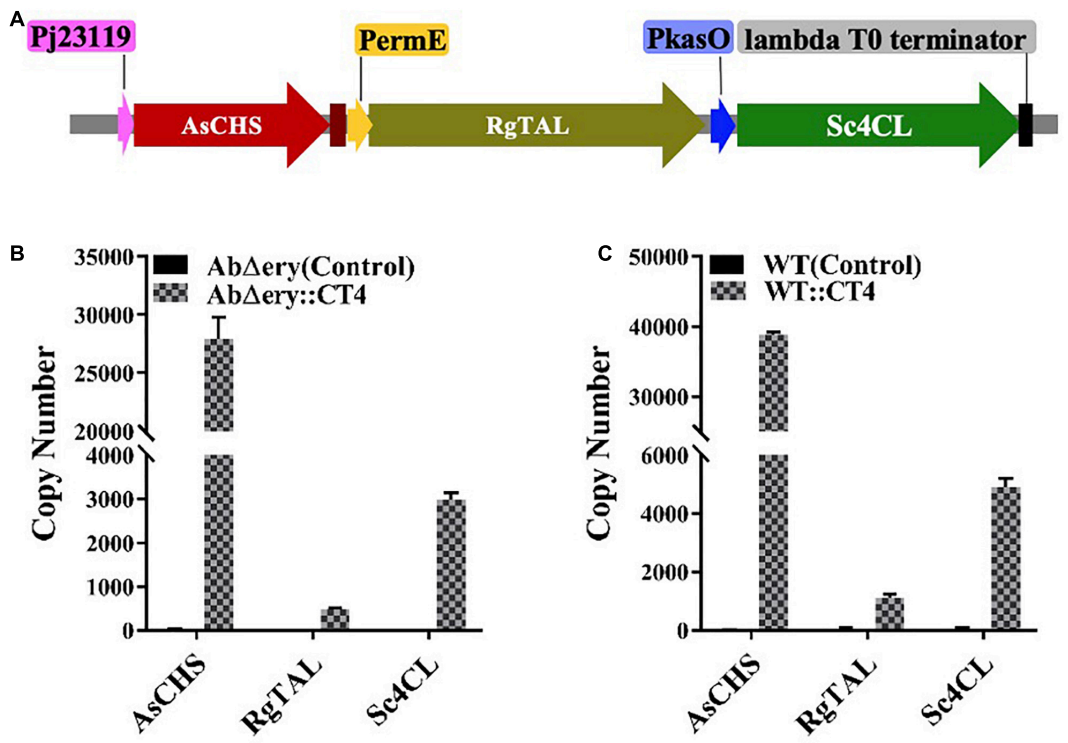

FIGURE 5 | Confirm of pSET152-Pj23119-AsCHS-PermE-RgTAL-PkasO-Sc4CL plasmids. **(A)** Schematic diagram of heterologous genes expression cassette (Pj23119-AsCHS-PermE-RgTAL-PkasO-Sc4CL) in pSET152. **(B)** qRT-PCR analysis expression of AsCHS, RgTAL, and Sc4CL in Ab*Δery*:CT4 with Ab*Δery* as control. **(C)** qRT-PCR analysis expression of AsCHS, RgTAL, and Sc4CL in WT:CT4 with WT as control. Transcript levels were obtained individually after drawing a standard curve using Ct value and copy number logarithm as the horizontal and vertical coordinates with a serial copy number gradient plasmid as a control. Error bars indicate the standard deviations from three independent replicates.

The plasmid pSET152-Pj23119-AsCHS-PermE-RgTAL-PkasO-Sc4CL was transformed into Ab*Δery* and WT protoplasts. Positive colonies Ab*Δery*:AsCHS-RgTAL-Sc4CL (Ab*Δery*:CT4), WT:AsCHS-RgTAL-Sc4CL(WT:CT4) were identified (**Supplementary Figure 6c**). The expression of heterologous genes was confirmed by reverse-transcription PCR

using AbΔ*ery* and WT as control. The copy numbers of the three genes were calculated by absolute quantification (**Figures 5B,C**). This analysis showed that AbΔ*ery*:CT4 had the AsCHS copy number about 28000, the RgTAL copy number about 500, and the Sc4CL copy number about 3000, while WT:CT4 had the AsCHS copy number about 39000, the RgTAL copy number about 1100, and the Sc4CL copy number about 5000, the copy number of gene was consistent with the strength of its promoter. These data indicated that all genes were successfully transcribed.

BNY-Type Pyrone Was Synthesized in Reconstructed Strain

Agarose gel electrophoresis and QPCR analysis showed that three heterologous genes were successfully transferred into the AbΔ*ery* and had a high level of transcription. To further prove the role of heterologous genes, we analyzed the metabolites. AbΔ*ery*:CT4, WT:CT4, AbΔ*ery*, and WT were inoculated in TSB medium fermentation for 7 days, cultures were centrifuged to collect the supernatant, then it was concentrated by a freeze dryer and measured by HPLC (**Figure 6A** and **Supplementary Figure 8a**). The results showed that compared with the negative control, three new peaks were observed in the HPLC spectrum of AbΔ*ery*:CT4 and WT:CT4, and the peaks at 7.5 and 9.6 min were intermediate products 4-coumaric acid and cinnamic acid, 8.5 min was the target product, of which the yield in AbΔ*ery*:CT4 was much higher than WT:CT4. *In vitro* enzyme activity experiments showed that AsCHS can synthesize two products using MM-CoA and 4-coumaroyl-CoA, but it may be different *in vivo*. Therefore, we analyzed the structure of the target product by LC-MS, which the LC-ESIMS spectrum gave a molecular ion peak $[M + H]^+$ at m/z 259 and was synthesized by two MM-CoA and 4-Coumaroyl-CoA (**Figure 6B** and **Supplementary Figure 8c**). Besides, their growth phenotypes were analyzed in TSB medium and growth curves showed that heterologous genes had no significant effect on their growth (**Figure 6C**). In summary, exogenous genes can play a role in AbΔ*ery*, and AbΔ*ery* can use the large amount of MM-CoA accumulated in the cell after knocking out *ery* BGC to produce more products, which has greater advantage than WT strains.

DISCUSSION

Heterologous expression of natural product biosynthetic pathways is widely used in synthetic biology field. It can not only dig hidden metabolites, identify the function of genome biosynthetic gene clusters (BGCs), but also enhance yield of valuable compounds in more suitable hosts (Huo et al., 2019). In addition to the level of expression of heterologous genes, the choice of host and its genetic background are critical

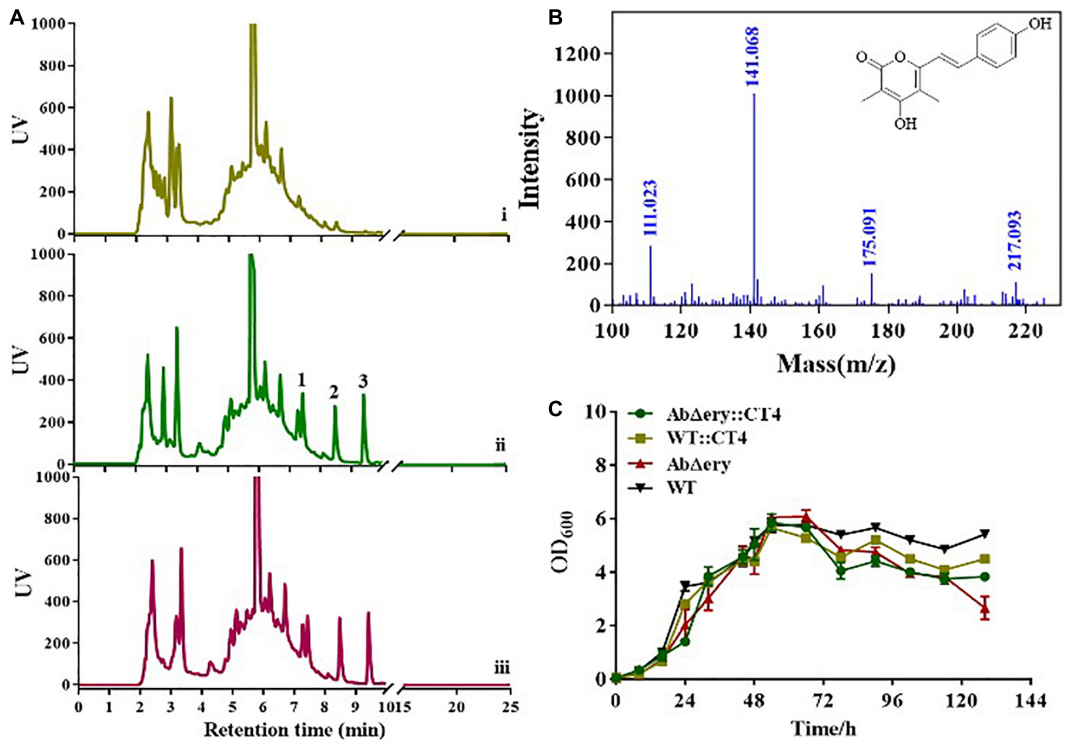

FIGURE 6 | HPLC and LC-MS determination of heterologous gene expression products. **(A)** HPLC spectra of AbΔ*ery* **(i)**, WT:CT4 **(ii)**, and AbΔ*ery*:CT4 **(iii)**. Compared with control, three new peaks appeared after introduction of the heterologous genes, 1 is intermediate product 4-coumaric acid, 2 is the target product, and 3 is the by-product cinnamic acid (b) LC-ESIMS spectrum of 2 and the molecular ion peak $[M + H]^+$ is m/z 259.0956. **(C)** Growth curve for the AbΔ*ery* (control), WT (control), AbΔ*ery*:CT4, and WT:CT4.

for heterologous pathways to work (Zhang et al., 2010). By inhibiting competitive pathways, knocking out non-essential genes, or removing the toxicity of byproducts, the metabolic pathways of heterologous hosts can be altered, and precursor supply can be increased to achieve higher yields (Liu W. et al., 2018). The rapid development of molecular engineering technologies, including CRISPR-Cas9 and the advancement of synthetic biotechnology (Guo et al., 2015; Zhang W. et al., 2017), have effectively promoted the optimization of heterologous hosts.

Many secondary metabolites in actinomycetes belong to polyketones, which have a variety of biological activities. As a representative of engineering actinomycetes, *S. erythraea* has been widely studied, contains a large amount of PP-CoA and MM-CoA, and is suitable as a heterogeneous host for polyketides production. Therefore, we modified *S. erythraea* through chassis engineering, applied the CRISPR-Cas9 strategy to knock out large fragments of the genome to change its metabolic pathways. Two sgRNAs were designed to target SACE_0715 and SACE_0733 respectively. Q-PCR analysis of transcription level and HPLC analysis of fermentation showed that AbΔ*ery* lost the ability to synthesize erythromycin, and we found that the concentration of MM-CoA in AbΔ*ery* increased 220% and PP-CoA increased 162%. Therefore, AbΔ*ery* has advantages as a host to synthesize heterogenous polyketide.

For further verification, we introduced heterologous genes in AbΔ*ery* to reconstruct metabolic pathway. We selected type III polyketide synthase AsCHS, RgTAL, and Sc4CL, cloned into pSET152 plasmid, and used three constitutive strong promoters to enhance expression. New polyketide compounds were synthesized using MM-CoA and L-tyrosine as substrates in new metabolic pathway. The absolute quantification was used to analyze the transcription level of heterologous genes, the result showed all three genes were successfully expressed both in AbΔ*ery*:CT4 and WT:CT4. HPLC and LC-MS data showed that the yield of product in AbΔ*ery*:CT4 is higher than WT:CT4 (**Figure 6A** and **Supplementary Figure 8b**). Combined with the growth curve analysis, the biomass of AbΔ*ery* decreases faster than AbΔ*ery*:CT4 in later stages (**Figure 6C**). We speculate it may be due to blocking the *ery* BGC that initiates synthesis at the later stage, resulting in substrate accumulation. When the exogenous synthesis pathway is introduced, the substrate (PP-CoA and MM-CoA) accumulation pressure is reduced. Therefore, the growth of the reconstituted strain AbΔ*ery*:CT4 in the later stage returned to a state approximately to the original strain, and also produced more products. AbΔ*ery* have great advantages in production of polyketone compounds with MM-CoA as the substrate. Genome sequence analysis suggests that PCC pathway play a main role in providing MM-CoA and there are multiple loci such as SACE_0026-0028 and SACE_3398-3400 encode biotin-dependent carboxylases catalyzing carboxylation of PP-CoA to MM-CoA in *S. erythraea*. In future research, we want to enhance the metabolic pathway from PP-CoA to MM-CoA to improve the accumulation of MM-CoA. Besides, heterologous expression of other valuable polyketide such as spinosad which used both PP-CoA and MM-CoA as precursor in AbΔ*ery* is a feasible idea or activate silent gene clusters in its genome to discover new products.

In this study, we used the CRISPR-Cas9 system to achieve knock-out of long fragment gene clusters in *S. erythraea*, deleting the erythromycin biosynthesis gene clusters and accumulating precursor CoAs. Hence, *S. erythraea* became an excellent heterologous host that was beneficial for production of polyketides. We introduced heterologous genes type III polyketide synthase AsCHS, RgTAL and Sc4CL to reconstruct secondary metabolic pathway and synthesize new products which characterizes the ability of AbΔ*ery* as a heterologous host. Our results highlight the advantages of AbΔ*ery* as a heterologous host and the potential to produce more valuable exogenous polyketides.

DATA AVAILABILITY STATEMENT

The original contributions presented in the study are included in the article/**Supplementary Material**, further inquiries can be directed to the corresponding author/s.

AUTHOR CONTRIBUTIONS

C-YR and YL contributed equally, were responsible for experimental design, investigation, analysis, interpretation of data, and writing the original draft. JD and B-CY were responsible for the study's conception and design, data analysis, and final approval of the manuscript. All the authors read and approved the final manuscript.

FUNDING

This study was supported by grants from the National Key Research and Development Program of China (2018YFA0900404), the National Natural Science Foundation of China (31730004), Shenzhen Key Laboratory of Synthetic Genomics (ZDSYS201802061806209), Shenzhen Science and Technology Program (Grant No. KQTD20180413181837372), Guangdong Provincial Key Laboratory of Synthetic Genomics (2019B030301006), and China Postdoctoral Science Foundation (2020M682974).

SUPPLEMENTARY MATERIAL

The Supplementary Material for this article can be found online at: https://www.frontiersin.org/articles/10.3389/fbioe.2021.628569/full#supplementary-material

REFERENCES

Abe, I., Takahashi, Y., and Noguchi, H. (2002). Enzymatic formation of an unnatural c6-c5 aromatic polyketide by plant type III polyketide synthases. *Org. Lett.* 4, 3623–3626. doi: 10.1021/ol0201409

Arturo, C., Macdonald, J. T., Joachim, D. J., Georgia, C., Freemont, P. S., Baldwin, G. S., et al. (2013). One-pot DNA construction for synthetic biology: the Modular Overlap-Directed Assembly with Linkers (MODAL) strategy. *Nucleic Acids Res.* 42:e7. doi: 10.1093/nar/gkt915

Bibb, M. J., Janssen, G. R., and Ward, J. M. (1985). Cloning and analysis of the promoter region of the erythromycin resistance gene (ermE) of Streptomyces erythraeus. *Gene* 38, 215–226. doi: 10.1016/0378-1119(85)90220-3

Calne, R. Y., Lim, S., Samaan, A., Collier, D. S. J., Pollard, S. G., White, D. J. G., et al. (1989). Rapamycin for immunosuppression in organ allografting. *Lancet* 334:227. doi: 10.1016/S0140-6736(89)90417-0

Cho, S., Shin, J., and Cho, B. (2018). Applications of CRISPR/Cas system to bacterial metabolic engineering. *Int. J. Mol. Sci.* 19:1089. doi: 10.3390/ijms19041089

Cleto, S., and Lu, T. K. (2017). An engineered synthetic pathway for discovering nonnatural nonribosomal peptides in *escherichia coli*. *mBio* 8, e01474–17. doi: 10.1128/mBio.01474-17

Cobb, R. E., Wang, Y., and Zhao, H. (2015). High-efficiency multiplex genome editing of Streptomyces species using an engineered CRISPR/Cas system. *ACS Synth. Biol.* 4, 723–728. doi: 10.1021/sb500351f

Cortina, N. S., Krug, D., Plaza, A., Revermann, O., and Müller, R. (2012). Myxoprincomide: a Natural Product from Myxococcus xanthus Discovered by Comprehensive Analysis of the Secondary Metabolome. *Angew. Chem. Int. Ed. Engl.* 51, 811–816. doi: 10.1002/anie.201106305

Doench, J. G., Hartenian, E., Graham, D. B., Tothova, Z., Hegde, M., Smith, I., et al. (2014). Rational design of highly active sgRNAs for CRISPR-Cas9–mediated gene inactivation. *Nat. Biotechnol.* 32, 1262–1267. doi: 10.1038/nbt.3026

El-Sayed, A. S. A., Abdel-Ghany, S. E., and Ali, G. S. (2017). Genome editing approaches: manipulating of lovastatin and taxol synthesis of filamentous fungi by CRISPR/Cas9 system. *Appl. Microbiol. Biotechnol.* 101, 3953–3976. doi: 10.1007/s00253-017-8263-z

Ferain, T., Hobbs, J. N. Jr., Richardson, J., Bernard, N., Garmyn, D., Hols, P., et al. (1996). Knockout of the two ldh genes has a major impact on peptidoglycan precursor synthesis in Lactobacillus plantarum. *J. Bacteriol.* 178, 5431–5437. doi: 10.1128/jb.178.18.5431-5437.1996

Gao, B., Wang, X., Liu, X., Shi, S., and Tu, P. (2015). Rapid preparation of (methyl)malonyl coenzyme a and enzymatic formation of unusual polyketides by type III polyketide synthase from Aquilaria sinensis. *Bioorg. Med. Chem. Lett.* 25, 1279–1283. doi: 10.1016/j.bmcl.2015.01.045

Gibson, D., Young, L., Chuang, R. Y., Venter, J. C., Hutchison, C. I. I. I., and Smith, H. O. (2009). Enzymatic assembly of DNA molecules up to several hundred kilobases. *Nat. Methods* 6, 341–343. doi: 10.1038/nmeth.1318

Guo, Y., Dong, J., Zhou, T., Auxillos, J., Li, T., Zhang, W., et al. (2015). YeastFab: the design and construction of standard biological parts for metabolic engineering in Saccharomyces cerevisiae. *Nucleic Acids Res.* 43:e88. doi: 10.1093/nar/gkv464

Horbal, L., and Luzhetskyy, A. (2016). Dual control system - a novel scaffolding architecture of an inducible regulatory device for the precise regulation of gene expression. *Metab. Eng.* 37, 11–23. doi: 10.1016/j.ymben.2016.03.008

Horbal, L., Siegl, T., and Luzhetskyy, A. (2018). A set of synthetic versatile genetic control elements for the efficient expression of genes in Actinobacteria. *Sci. Rep.* 8:491. doi: 10.1038/s41598-017-18846-1

Hsiao, N., and Kirby, R. (2008). Comparative genomics of Streptomyces avermitilis, Streptomyces cattleya, Streptomyces maritimus and Kitasatospora aureofaciens using a Streptomyces coelicolor microarray system. *Antonie van Leeuwenhoek* 93, 1–25. doi: 10.1007/s10482-007-9175-1

Huang, H., Zheng, G., Jiang, W., Hu, H., and Lu, Y. (2015). One-step high-efficiency CRISPR/Cas9-mediated genome editing in Streptomyces. *Acta Biochim. Biophys. Sin.* 47, 231–243. doi: 10.1093/abbs/gmv007

Huo, L., Hug, J. J., Fu, C., Bian, X., Zhang, Y., and Müller, R. (2019). Heterologous expression of bacterial natural product biosynthetic pathways. *Nat. Prod. Rep.* 36, 1412–1436. doi: 10.1039/c8np00091c

Jinek, M., Chylinski, K., Fonfara, I., Hauer, M., Doudna, J. A., and Charpentier, E. (2012). A programmable dual-RNA-guided DNA endonuclease in adaptive bacterial immunity. *Science* 337, 816–821. doi: 10.1126/science.1225829

Karničar, K., Drobnak, I., Petek, M., Magdevska, V., Horvat, J., and Vidmar, R. (2016). Integrated omics approaches provide strategies for rapid erythromycin yield increase in Saccharopolyspora erythraea. *Microb. Cell Fact.* 15:93. doi: 10.1186/s12934-016-0496-5

Kim, Y. H., and Cerniglia, C. E. (2005). Influence of erythromycin a on the microbial populations in aquaculture sediment microcosms. *Aquat. Toxicol.* 73, 230–241. doi: 10.1016/j.aquatox.2005.03.013

Komor, A., Badran, A., and Liu, D. (2016). CRISPR-Based technologies for the manipulation of eukaryotic genomes. *Cell* 168, 20–36. doi: 10.1016/j.cell.2016.10.044

Li, Y., Chang, X., Yu, W., Li, H., Ye, Z. Q., Yu, H., et al. (2013). Systems perspectives on erythromycin biosynthesis by comparative genomic and transcriptomic analyses of s. Erythraea e3 and nrrl23338 strains. *BMC Genomics* 14:523. doi: 10.1186/1471-2164-14-523

Liao, C. H., Yao, L., Xu, Y., Liu, W., Zhou, Y., and Ye, B. C. (2015). Nitrogen regulator GlnR controls uptake and utilization of non-phosphotransferase-system carbon sources in actinomycetes. *Proc. Natl. Acad. Sci. U. S. A.* 112, 15630–15635. doi: 10.1073/pnas.1508465112

Lim, Y. P., Go, M. K., and Yew, W. S. (2016). Exploiting the biosynthetic potential of type III polyketide synthases. *Molecules* 21:806. doi: 10.3390/molecules21060806

Liu, W., Luo, Z., Wang, Y., Pham, N. T., Tuck, L., Pérez-Pi, I., et al. (2018). Rapid pathway prototyping and engineering using in vitro and in vivo synthetic genome SCRaMbLE-in methods. *Nat. Commun.* 9, 1–12. doi: 10.1038/s41467-018-04254-0

Liu, Y., Ren, C. Y., Wei, W. P., You, D., Yin, B. C., and Ye, B. C. (2019). A CRISPR-Cas9 strategy for activating theSaccharopolyspora erythraea erythromycin biosynthetic gene cluster with knock-in bidirectional promoters. *ACS Synth. Biol.* 8, 1134–1143. doi: 10.1021/acssynbio.9b00024

Liu, Y., Wei, W. P., and Ye, B. C. (2018). High GC content Cas9-Mediated Genome-Editing and biosynthetic gene cluster activation in saccharopolyspora erythraea. *ACS Synth. Biol.* 7, 1338–1348. doi: 10.1021/acssynbio.7b00448

Lopatniuk, M., Myronovskyi, M., and Luzhetskyy, A. (2017). Streptomyces albus: a new cell factory for Non-Canonical ami-no acids incorporation into ribosomally synthetized natural products. *ACS Chem. Biol.* 12, 2362–2370. doi: 10.1021/acschembio.7b00359

Lyu, X., Ng, K. R., Lee, J. L., Mark, R., and Chen, W. N. (2017). Enhancement of Naringenin Biosynthesis from Tyrosine by Metabolic Engineering ofSaccharomyces cerevisiae. *J. Agr. Food Chem.* 65, 6638–6646. doi: 10.1021/acs.jafc.7b02507

Mao, D., Bushin, L. B., Moon, K., Wu, Y., and Seyedsayamdost, M. R. (2017). Discovery of scmR as a global regulator of secondary metabolism and virulence in Burkholderia thailandensis E264. *Proc. Natl. Acad. Sci. U. S. A.* 114, E2920–E2928. doi: 10.1073/pnas.1619529114

Moffitt, C. M. (1998). Field trials of investigational new animal drugs. *Vet. Hum. Toxicol.* 40, 48–52.

Morita, H., Noguchi, H., Schroder, J., and Abe, I. (2001). Novel polyketides synthesized with a higher plant stilbene synthase. *Eur. J. Biochem.* 268, 3759–3766. doi: 10.1046/j.1432-1327.2001.02289.x

Oliynyk, M., Samborskyy, M., Lester, J. B., Mironenko, T., Scott, N., DIckens, S., et al. (2007). Complete genome sequence of the erythromycin-producing bacterium Saccharopolyspora erythraea NRRL23338. *Nat. Biotechnol.* 25, 447–453. doi: 10.1038/nbt1297

Park, C. Y., Jin, J. S., and Kim, D. W. (2016). Genome editing of structural variations: modeling and gene correction. *Trends Biotechnol.* 34, 548–561. doi: 10.1016/j.tibtech.2016.02.011

Parvez, A., Giri, S., Giri, G. R., Kumari, M., Bisht, R., Saxena, P., et al. (2018). Novel type III polyketide synthases biosynthesize methylated polyketides in mycobacterium marinum. *Sci. Rep.* 8:6529. doi: 10.1038/s41598-018-24980-1

Phelan, R. M., Sachs, D., Petkiewicz, S. J., Barajas, J. F., Blake-hedges, J. M., Thompson, M. G., et al. (2017). Development of next generation synthetic biology tools for use in streptomyces venezuelae. *ACS Synth. Biol.* 6, 159–166. doi: 10.1021/acssynbio.6b00202

Reeves, A. R., English, R. S., Lampel, J. S., Post, D. A., and Boom, T. J. V. (1999). Transcriptional organization of the erythromycin biosynthetic gene cluster of

saccharopolyspora erythraea. *J. Bacteriol.* 181, 7098–7106. doi: 10.1128/jb.181.22.7098-7106.1999

Reynolds, K. A., Luhavaya, H., Li, J., Dahesh, S., Nizet, V., Yamanaka, K., et al. (2017). Isolation and structure elucidation of lipopeptide antibiotic taromycin B from the activated taromycin biosynthetic gene cluster. *J. Antibiot.* 71, 333–338. doi: 10.1038/ja.2017.146

Ross, A. C., Gulland, L. E. S., Dorrestein, P. C., and Moore, B. S. (2014). Targeted capture and heterologous expression of the pseudoalteromonas alterochromide gene cluster in *escherichia coli* represents a promising natural product exploratory platform. *ACS Synth. Biol.* 4, 414–420. doi: 10.1021/sb500280q

Shao, Y., Lu, N., Wu, Z., Cai, C., Wang, S., Zhang, L., et al. (2018). Creating a functional single-chromosome yeast. *Nature* 560, 331–335. doi: 10.1038/s41586-018-0382-x

Shao, Y., Lu, N., Xue, X., and Qin, Z. (2019). Creating functional chromosome fusions in yeast with CRISPR–Cas9. *Nat. Protoc.* 14, 2521–2545. doi: 10.1038/s41596-019-0192-0

Storch, M., Casini, A., Mackrow, B., Fleming, T., Trewhitt, H., Ellis, T., et al. (2015). BASIC: a new biopart assembly standard for idempotent cloning provides accurate, Single-Tier DNA assembly for synthetic biology. *ACS Synth. Biol.* 4, 781–787. doi: 10.1021/sb500356d

Su, T., Liu, F., Gu, P., Jin, H., Chang, Y., Wang, Q., et al. (2016). A CRISPR-Cas9 assisted Non-Homologous End-Joining strategy for one-step engineering of bacterial genome. *Sci. Rep.* 6:37895. doi: 10.1038/srep37895

Sun, Y., Zhou, X., Dong, H., Tu, G., Wang, M., Wang, B., et al. (2003). A Complete Gene Cluster from Streptomyces nanchangensis NS3226 Encoding Biosynthesis of the Polyether Ionophore Nanchangmycin. *Chem. Biol.* 10, 431–441. doi: 10.1016/S1074-5521(03)00092-9

Tan, G. Y., Deng, K., Liu, X., Tao, H., Chang, Y., Chen, J., et al. (2017). Heterologous biosynthesis of spinosad: an Omics-Guided large polyketide synthase gene cluster reconstitution in streptomyces. *ACS Synth. Biol.* 6, 995–1005. doi: 10.1021/acssynbio.6b00330

Thompson, C. J., Kieser, T., Ward, J. M., and Hopwood, D. A. (1982). Physical analysis of antibiotic-resistance genes from Streptomyces and their use in vector construction. *Gene* 20, 51–62. doi: 10.1016/0378-1119(82)90086-5

Tomich, P. K. (1988). Streptomyces cloning: possible construction of novel compounds and regulation of antibiotic biosynthetic genes. *Antimicrob. Agents Chemother.* 32, 1472–1476. doi: 10.1128/aac.32.10.1472

Tong, Y., Charusanti, P., Zhang, L., Weber, T., and Lee, S. Y. (2015). CRISPR-Cas9 based engineering of actinomycetal genomes. *ACS Synth. Biol.* 4, 1020–1029. doi: 10.1021/acssynbio.5b00038

Tsai, Y. K., Fung, C. P., Lin, J. C., Chen, J. H., Chang, F. Y., Chen, T. L., et al. (2011). *Klebsiella pneumoniae* outer membrane porins OmpK35 and OmpK36 play roles in both antimicrobial resistance and virulence. *Antimicrob. Agents Chemother.* 55, 1485–1493. doi: 10.1128/AAC.01275-10

Wang, R., Cress, B. F., Yang, Z., Hordines, J. C., Zhao, S., Jung, G. Y., et al. (2019). Design and characterization of biosensors for the screening of modular assembled naringenin biosynthetic library in Saccharomyces cerevisiae. *ACS Synth. Biol.* 8, 2121–2130. doi: 10.1021/acssynbio.9b00212

Wang, W., Li, X., Wang, J., Xiang, S., Feng, X., and Yang, K. (2013). An engineered strong promoter for streptomycetes. *Appl. Environ. Microbiol.* 79, 4484–4492. doi: 10.1128/AEM.00985-13

Wu, J., Du, G., Zhou, J., and Chen, J. (2013). Metabolic engineering of *Escherichia coli* for (2S)-pinocembrin production from glucose by a modular metabolic strategy. *Metab. Eng.* 16, 48–55. doi: 10.1016/j.ymben.2012.11.009

Wu, J., Zhou, T., Du, G., Zhou, J., and Chen, J. (2014). Modular optimization of heterologous pathways for de novo synthesis of (2S)-naringenin in *Escherichia coli*. *PLoS One* 9:e101492. doi: 10.1371/journal.pone.0101492

Xu, Z., Wang, M., and Ye, B. C. (2017). The TetR family transcriptional regulator PccD negatively controls propionyl coenzyme a assimilation in Saccharopolyspora erythraea. *J. Bacteriol.* 199, 217–281. doi: 10.1128/jb.00281-17

Yu, D., Xu, F., Zeng, J., and Zhan, J. (2012). Type III polyketide synthases in natural product biosynthesis. *IUBMB Life* 64, 285–295. doi: 10.1002/iub.1005

Zhang, G., Zhang, W., Saha, S., and Zhang, C. (2016). Recent advances in discovery, biosynthesis and genome mining of medicinally relevant polycyclic tetramate macrolactams. *Curr. Top. Med. Chem.* 16, 1727–1739. doi: 10.2174/1568026616666151012112818

Zhang, H., Boghigian, B. A., Armando, J., and Pfeifer, B. A. (2010). Methods and options for the heterologous production of complex natural products. *Cheminform* 28, 125–151. doi: 10.1039/c0np00037j

Zhang, J. J., Tang, X., Zhang, M., Nguyen, D., and Moore, B. S. (2017). Broad-Host-Range expression reveals native and host regulatory elements that influence heterologous antibiotic production in Gram-Negative bacteria. *mBio* 8, e01291–17. doi: 10.1128/mBio.01291-17

Zhang, W., Zhao, G., Luo, Z., Lin, Y., Wang, L., Guo, Y., et al. (2017). Engineering the ribosomal DNA in a megabase synthetic chromosome. *Science* 355:eaaf3981. doi: 10.1126/science.aaf3981

Conflict of Interest: The authors declare that the research was conducted in the absence of any commercial or financial relationships that could be construed as a potential conflict of interest.

frontiers in Bioengineering and Biotechnology

ORIGINAL RESEARCH
published: 16 September 2021
doi: 10.3389/fbioe.2021.726126

Coproduction of 5-Aminovalerate and δ-Valerolactam for the Synthesis of Nylon 5 From L-Lysine in *Escherichia coli*

Jie Cheng[1], *Wenying Tu*[1,2], *Zhou Luo*[1,3], *Li Liang*[1], *Xinghua Gou*[1], *Xinhui Wang*[1], *Chao Liu*[2]* *and Guoqiang Zhang*[3]*

[1]Key Laboratory of Medicinal and Edible Plants Resources Development of Sichuan Education Department, Sichuan Industrial Institute of Antibiotics, Chengdu University, Chengdu, China, [2]Key Laboratory of Industrial Biotechnology, Ministry of Education, Jiangnan University, Wuxi, China, [3]National Engineering Laboratory for Cereal Fermentation Technology, Jiangnan University, Wuxi, China

The compounds 5-aminovalerate and δ-valerolactam are important building blocks that can be used to synthesize bioplastics. The production of 5-aminovalerate and δ-valerolactam in microorganisms provides an ideal source that reduces the cost. To achieve efficient biobased coproduction of 5-aminovalerate and δ-valerolactam in *Escherichia coli*, a single biotransformation step from L-lysine was constructed. First, an equilibrium mixture was formed by L-lysine α-oxidase RaiP from *Scomber japonicus*. In addition, by adjusting the pH and H_2O_2 concentration, the titers of 5-aminovalerate and δ-valerolactam reached 10.24 and 1.82 g/L from 40 g/L L-lysine HCl at pH 5.0 and 10 mM H_2O_2, respectively. With the optimized pH value, the δ-valerolactam titer was improved to 6.88 g/L at pH 9.0 with a molar yield of 0.35 mol/mol lysine. The ratio of 5AVA and δ-valerolactam was obviously affected by pH value. The ratio of 5AVA and δ-valerolactam could be obtained in the range of 5.63:1–0.58:1 at pH 5.0–9.0 from the equilibrium mixture. As a result, the simultaneous synthesis of 5-aminovalerate and δ-valerolactam from L-lysine in *Escherichia coli* is highly promising. To our knowledge, this result constitutes the highest δ-valerolactam titer reported by biological methods. In summary, a commercially implied bioprocess developed for the coproduction of 5-aminovalerate and δ-valerolactam using engineered *Escherichia coli*.

Keywords: 5-aminovalerate, δ-valerolactam, L-lysine HCl, equilibrium mixture, H_2O_2

OPEN ACCESS

Edited by:
Yi-Rui Wu,
Shantou University, China

Reviewed by:
Bin Zhang,
Jiangxi Agricultural University, China
Shuke Wu,
University of Greifswald, Germany

***Correspondence:**
Chao Liu
histliuchao@163.com
Guoqiang Zhang
gqzhang@jiangnan.edu.cn

Specialty section:
This article was submitted to Industrial Biotechnology, a section of the journal Frontiers in Bioengineering and Biotechnology

Received: *16 June 2021*
Accepted: *04 August 2021*
Published: *16 September 2021*

Citation:
Cheng J, Tu W, Luo Z, Liang L, Gou X, Wang X, Liu C and Zhang G (2021) Coproduction of 5-Aminovalerate and δ-Valerolactam for the Synthesis of Nylon 5 From L-Lysine in Escherichia coli. *Front. Bioeng. Biotechnol. 9:726126. doi: 10.3389/fbioe.2021.726126*

INTRODUCTION

Over the years, mounting global environmental, climate change, economic concerns, and fossil fuel sources are leading to a shift in the production of traditional bulk chemicals toward more green, renewable, economic, and sustainable routes (Wang A. et al., 2020; Gordillo Sierra and Alper, 2020; Wendisch, 2020). In many cases, the need has been partially met by biorefineries, in which microbial cell factories convert renewable feedstock resources into high-value and useful chemicals (Gao et al., 2020; Klenk et al., 2020; Youn et al., 2020; Zhang et al., 2021). While many chemicals are being developed via biotechnology, polyamide monomers are an important class of compounds (Li et al., 2020; Prell et al., 2020; Osire et al., 2021). 5-Aminovalerate (5AVA) and δ-valerolactam are attractive monomers for the production of biopolyamides, serving as raw materials for clothes, architecture, and disposable goods.

Plastics are mainly derived from petroleum feedstock. Bioplastics have attracted enormous interest because of their main degradability (Ben Abdallah et al., 2020). The annual output of bioplastics is predicted to exceed 2.43 million tons in 2024 (Haupka et al., 2020). Among microbial bioplastics, biopolyamides are widely applied in chemical, automotive, and textile industries (Ligon et al., 2017). The monomers of polyamides are primarily dicarboxylic acids, diamines, lactams, and ω-amino acids (Radzik et al., 2019). Examples of these main platform chemicals range from succinate (Zhang et al., 2009), glutarate (Zhao et al., 2018), to adipate (Wang F. et al., 2020) for dicarboxylic acids; from putrescine, cadaverine (Rui et al., 2020; Xue et al., 2020), to 1,6-hexanediamine for diamines; from δ-valerolactam (Zhang et al., 2017a), to ε-caprolactam (Thompson et al., 2020) for lactams; from 3-hydroxybutyrate (Atakav et al., 2021; Mierziak et al., 2021; Schmid et al., 2021), 2-hydroxybutyrate (Tian et al., 2021), to 3-hydroxyhexanoate (Harada et al., 2021) for hydroxyl acids; and from 4-aminobutyrate, 5AVA (Cheng et al., 2021b), to 6-aminocaproate (Turk et al., 2016) for ω-amino acids. In this respect, also 5AVA (Adkins et al., 2013) and δ-valerolactam (Xu et al., 2020) are attractive C5 platform chemicals for the production of biopolyamides from renewable biomass.

Four metabolic routes of 5AVA from L-lysine have been developed so far. The first route is the 5-aminovaleramide–mediated pathway that involves L-lysine 2-monooxygenase (DavB) and δ-aminovaleramidase (DavA) (Joo et al., 2017). The engineering WL3110 strain with overexpression of DavA and DavB generated 3.6 g/L 5AVA (Park et al., 2013). Shin et al. reported that 33.1 g/L of 5AVA was successfully formed by promoter optimization (Shin et al., 2016). The second route is the cadaverine-mediated pathway that does not require oxygen involves L-lysine decarboxylase (LdcC), putrescine transaminase (PatA), and γ-aminobutyraldehyde dehydrogenase (PatD) (Haupka et al., 2020). Haupka et al. reported that 3.7 g/L 5AVA was reached, with a yield of 0.09 g/g in shake flasks (Haupka et al., 2020). The third route is 2-keto-6-aminocaproate (2K6AC)–mediated pathway that involves L-lysine α-oxidase (RaiP) from *Scomber japonicus* (*S. japonicus*) and H_2O_2 (Pukin et al., 2010). Pukin et al. found that 13.4 g/L 5AVA was enzymatically produced by RaiP from *Trichoderma viride* (Pukin et al., 2010). Interestingly, Cheng et al. proposed that the titer of 5AVA could be improved to 29.12 g/L by adding 4% (v/v) ethanol and 10 mM H_2O_2 (Cheng et al., 2018b). Independently, a three-step route based on RaiP, α-ketoacid decarboxylase (KivD) from *Lactococcus lactis*, and aldehyde dehydrogenase (PadA) from *Escherichia coli* (*E. coli*) was established in *E. coli* with 5AVA titer up to about 52.24 g/L (Cheng et al., 2021b).

Lactams are important chemicals used in the manufacture of commercial polyamides. However, there are few reports on the direct bioproduction of lactams from engineered microorganisms. Zhang et al. confirmed that 1.1 g/L γ-butyrolactam was formed from L-glutamate by identifying a newly 2-pyrrolidone synthase ORF26 from *Streptomyces aizunensis*, with a yield of 0.14 g/g (Zhang et al., 2016). Then, Zhang et al. further revealed the catalytic promiscuity of ORF26, which cyclized ω-amino acids to produce of γ-butyrolactam, δ-valerolactam, and ε-caprolactam (Zhang et al., 2017b). However, the titers of δ-valerolactam and ε-caprolactam achieved were relatively low; 705 mg/L δ-valerolactam and 2.02 mg/L ε-caprolactam were produced, respectively. Chae et al. reported that β-alanine CoA transferase could activate ω-amino acids to produce 54.14 g/L γ-butyrolactam, 29 mg/L δ-valerolactam, and 79.6 μg/L ε-caprolactam, respectively (Chae et al., 2017). In addition, a novel route for δ-valerolactam was discovered through the direct oxidative decarboxylation of L-pipecolic acid by DavB in Xu et al.'s research (Xu et al., 2020). 90.3 mg/L δ-valerolactam was achieved from L-pipecolic acid by DavB expressed in *E. coli* (Xu et al., 2020). However, the titer of δ-valerolactam generated was rather low (**Table 1**).

Escapin from *Aplysia californica* (*A. californica*) is an L-amino acid oxidase, which could oxidize L-lysine to produce an antimicrobial equilibrium mixture (Kamio et al., 2009). This equilibrium mixture contains cyclic form Δ^1-piperidine-2-carboxylase (P2C), 2-hydroxy-piperidine-2-carboxylase (2HP2C) and Δ^2-piperidine-2-carboxylase (^{2}P2C) and linear form 2K6AC, 6-amino-2-hydroxy-hex-2-enolate (6A2HH2E), and 6-amino-2,2-dihydroxy-caproate (6A2DHC) (Ko et al., 2008). P2C was proved to be the dominant component of this enzymatic product at any pH using mass spectroscopy and NMR. Interestingly, this equilibrium shifts to produce relatively more ^{2}P2C at more alkaline conditions, 2K6AC, 6A2HH2E, and 6A2DHC under more acidic conditions (Ko et al., 2008). The equilibrium mixture could react with H_2O_2 to produce 5AVA and δ-valerolactam, and its ratios are affected by pH (Kamio et al., 2009). However, the titers of 5AVA and δ-valerolactam and its ratios were not mentioned in their studies.

In this study, 5AVA and δ-valerolactam were coproduced from an equilibrium mixture by adjusting pH and H_2O_2 in *E. coli* (**Figure 1**). The α-amino group of L-lysine was oxidized by RaiP from *S. japonicus* to form the equilibrium mixture. 2K6AC, P2C, and ^{2}P2C in this equilibrium mixture were oxidized to generate 5AVA, δ-valerolactam, and δ-valerolactam, respectively. In addition, the ratio of 5AVA and δ-valerolactam could be regulated by pH. The route of coproduction of 5AVA and δ-valerolactam was first proposed in this study. As a result, a promising strategy for coproducing 5AVA and δ-valerolactam in a single biotransformation step by adjusting the pH and H_2O_2 was established.

MATERIALS AND METHODS

Strains and Plasmids

The strains and plasmids used in this work are listed in **Table 2**. The *raiP* from *S. japonicus* (Accession No. MG423617) was inserted into pET21a to generate plasmid pET21a-*raiP* with *Nde*I and *Bam*HI restriction sites (Cheng et al., 2018b). The gene *katE* from *E. coli* MG1655 (Accession No. AAT48137.1) was inserted into pET21a-*raiP* to generate plasmid pET21a-*raiP-katE* with *Sal*I and *Xho*I restriction sites. The engineered *E. coli* ML03 for knocking out lysine decarboxylase gene *cadA* was from our previous study (Cheng et al., 2018a). In addition, the plasmid

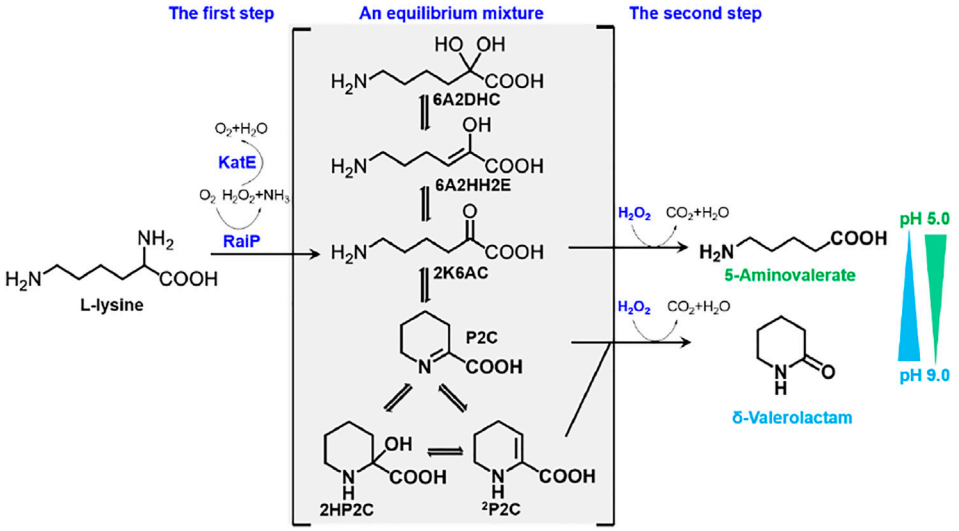

FIGURE 1 | Schematic diagram of coproduction routes of 5AVA and δ-valerolactam from L-lysine in this study. RaiP, L-lysine α-oxidase; 5AVA, 5-aminovalerate; P2C, Δ^1-piperidine-2-carboxylase; 2HP2C, 2-hydroxy-piperidine-2-carboxylase; ^{2}P2C, Δ^2-piperidine-2-carboxylase; 2K6AC, linear form 2-keto-6-aminocaproate; 6A2HH2E, 6-amino-2-hydroxy-hex-2-enolate; 6A2DHC, 6-amino-2,2-dihydroxy-caproate.

TABLE 1 | Production of 5AVA and δ-valerolactam in microbes.

Host strain	Strategy	5AVA titer (g/L)	Yield (g/g)	δ-Valerolactam (g/L)	Yield (g/g)	Substrate/feedstock	References
E. coli	Enzymatic catalysis	63.20	0.62	—	—	L-lysine	Li et al. (2016)
C. glutamicum	Fermentation	0.26	0.007	—	—	Rice straw hydrolysate	Sasikumar et al. (2021)
C. glutamicum	Fermentation	5.10	0.13	—	—	Glucose and alternative carbon sources	Jorge et al. (2017)
C. glutamicum	Fermentation	3.70	0.09	—	—	Glucose	Haupka et al. (2020)
C. glutamicum	Fed-batch fermentation	33.10	0.10	—	—	Glucose	Shin et al. (2016)
C. glutamicum	Fed-batch fermentation	12.51	0.10	—	—	*Miscanthus* hydrolysate	Joo et al. (2017)
E. coli	Whole-cell biotransformation	240.70	0.70	—	—	L-lysine	Wang et al. (2016)
E. coli	Whole-cell biotransformation	29.12	0.44	—	—	L-lysine HCl	Cheng et al. (2018b)
E. coli	Whole-cell biotransformation	52.24	0.38	—	—	L-lysine HCl	Cheng et al. (2021b)
E. coli	Whole-cell biotransformation	—	—	0.24	0.06	L-lysine	Xu et al. (2020)
E. coli	Whole-cell biotransformation	10.24	0.26	6.88	0.17	L-lysine HCl	This study

pET21a, pET21a-*raiP*, and pET21a-*raiP-katE* were transformed into *E. coli* BL21 (DE3) or *E. coli* ML03 to obtain the strains BL21-pET21a, BL21-*raiP*, BL21-*raiP-katE*, ML03-pET21a, ML03-*raiP*, and ML03-*raiP-katE*, respectively.

Cultivation Conditions

The engineering strains were streaked onto Luria–Bertani (LB) agar plates with 100 mg/L Amp at 37°C for overnight. Engineering strains used for biotransformation in the shake flask were cultured in LB medium with 100 mg/L Amp. After the OD_{600} reached 0.6, 0.2 mM of isopropyl β-D-thiogalactoside (IPTG) and 6.5 g/L of L-lysine HCl were added. The pH was controlled at 5.0, 6.0, 7.0, 8.0, and 9.0 by $NH_3{\cdot}H_2O$ and 10% H_2SO_4 at 30°C after 12 h. H_2O_2 was added after 12 h.

Enzyme Assays

RaiP activity was determined as Cheng et al. reported (Cheng et al., 2018b). Briefly, the reaction buffer contained 30 mM

TABLE 2 | Strains and plasmids used in this study.

Strain or plasmid	Description	Sources
Strains		
DH5α	Wild type	Novagen
BL21 (DE3)	Wild type	Novagen
ML03	*E. coli* BL21 (DE3) △*cadA*	Cheng et al. (2018a)
BL21-pET21a	*E. coli* BL21 (DE3) harboring plasmid pET21a	Cheng et al. (2018b)
BL21-*raiP*	*E. coli* BL21 (DE3) harboring plasmid pET21a-*raiP*	Cheng et al. (2018b)
BL21-*raiP-katE*	*E. coli* BL21 (DE3) harboring plasmid pET21a-*raiP-katE*	This study
ML03-pET21a	*E. coli* ML03 harboring plasmid pET21a	This study
ML03-*raiP*	*E. coli* ML03 harboring plasmid pET21a-*raiP*	Cheng et al. (2018b)
ML03-*raiP-katE*	*E. coli* ML03 harboring plasmid pET21a-*raiP-katE*	This study
Plasmids		
pET21a-*raiP*	pET21a carries an L-lysine α-oxidase gene (*raiP*) from *S. japonicus*, Amp^R	Cheng et al. (2018b)
pET21a-*raiP-katE*	pET21a carries an L-lysine α-oxidase gene (*raiP*) from *S. japonicus* and a catalase gene (*katE*) from *E. coli*, Kan^R	This study

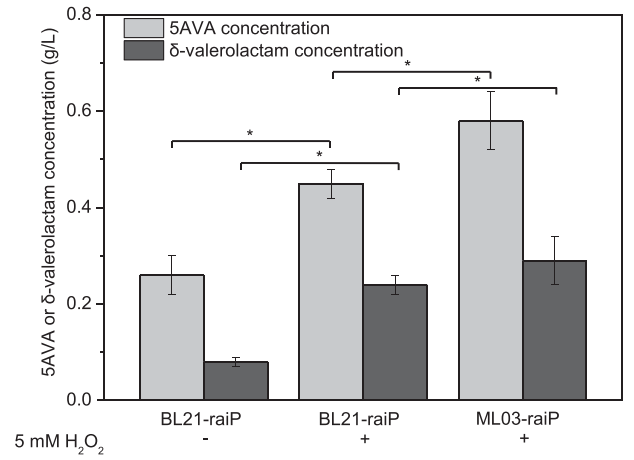

FIGURE 2 | Feasibility for the coproduction of 5AVA and δ-valerolactam in a single biotransformation step. pH was controlled at 7.0. 6.5 g/L of L-lysine HCl was added as the substrate. Statistics were performed by two-tailed Student's *t*-test. $^*p < 0.05$. All experiments were performed a minimum of three independent sets.

L-lysine, 26.5 mM phenol, 0.5 mM 4-aminoantipyrine, and 10 units/ml catalase. Quinoneimine dye formed was measured at 505 nm using SpectraMax M2e. One unit of enzyme activity was defined as the amount of enzyme that catalyzes the formation of 1 μM of H_2O_2 per minute (Cheng et al., 2018b). The activity of KatE was determined according to Liu et al. (2017); 0.1 ml diluted crude enzyme was incubated with 1 ml 60 mM H_2O_2 at 30°C for 10 min. The absorbance of a yellow complex formed by molybdate and H_2O_2 was immediately measured at 405 nm (Liu et al., 2017). One unit of catalase activity was defined as the amount of enzyme decomposing of 1 μmol H_2O_2 per min.

Biotransformation

Biotransformation was performed in a 5.0-L fermenter. The medium consisted of 55 g/L of glucose, 0.004 g/L of $CoCl_2{\cdot}6H_2O$, 0.02 g/L of Na_2SO_4, 1.6 g/L of $MgSO_4{\cdot}7H_2O$, 0.0064 g/L of $ZnSO_4$, 0.0006 g/L of $Cu_2SO_4{\cdot}5H_2O$, 1.6 g/L of $(NH_4)_2SO_4$, 0.00756 g/L of $FeSO_4{\cdot}7H_2O$, 2 g/L of citric acid, 7.5 g/L of $K_2HPO_4{\cdot}3H_2O$, and 250 μl of antifoam 289. The pH was controlled at 7.0 by the automatic addition of $NH_3{\cdot}H_2O$ and 10% H_2SO_4 at 30°C. After the OD_{600} reached 20, 0.2 mM IPTG was added to the broth. When the OD_{600} reached 80, the pH was controlled at 5.0, 6.0, 7.0, 8.0, and 9.0 by the automatic addition of $NH_3{\cdot}H_2O$ and 10% H_2SO_4. L-lysine HCl was added to at an initial concentration of 40 g/L. H_2O_2 was added after 24 h.

Lysine, 5-Aminovalerate, and δ-Valerolactam Analysis by High-Performance Liquid Chromatography

Lysine, 5AVA, and δ-valerolactam were monitored and quantitated by high-performance liquid chromatography (HPLC). For monitoring L-lysine and 5AVA, samples were derived with phenyl isothiocyanate (PITC) with an Agilent Eclipse XDB-C18 column (4.6 mm × 150 mm × 5 μm), as described by Cheng et al. (2018b). To monitor δ-valerolactam, a Chirex®3126 (D)-penicillamine LC column (4.6 × 250 mm, Phenomenex, USA) was used (Xu et al., 2020).

RESULTS AND DISCUSSION

Construction of a Synthetic Route for the Simultaneous Synthesis of 5-Aminovalerate and δ-Valerolactam in *E. coli*

A synthetic route for the concurrent synthesis of 5AVA and δ-valerolactam from L-lysine was constructed from an equilibrium mixture (**Figure 1**). The designed route for the coproduction of 5AVA and δ-valerolactam consists of two steps: 1) the deamination of α-amino group in L-lysine to generate an equilibrium mixture by RaiP from *S. japonicus*, with this equilibrium mixture containing P2C, 2HP2C, ^{2}P2C, 2K6AC, 6A2HH2E, and 6A2DHC; 2) the decarboxylation of 2K6AC, P2C, and ^{2}P2C in this equilibrium mixture to produce 5AVA and δ-valerolactam via H_2O_2, respectively. First, a plasmid pET21a–*raiP* was constructed and introduced into *E. coli* BL21(DE3) to obtain the strain BL21–*raiP*. As shown

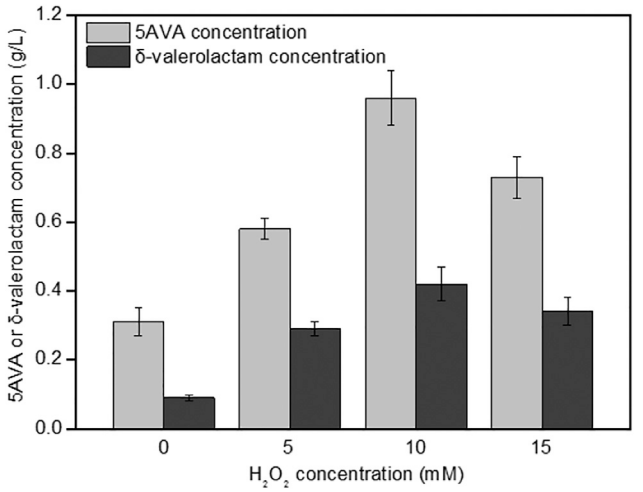

FIGURE 3 | Effect of H_2O_2 on the coproduction of 5AVA and δ-valerolactam by strain ML03-*raiP-katE* in flasks. pH was controlled at 7.0. 6.5 g/L of L-lysine HCl was added as the substrate. All experiments were performed a minimum of three independent sets.

in **Figure 2**, engineering strain BL21-*raiP* produced 0.26 g/L 5AVA and 0.08 g/L δ-valerolactam in the absence of H_2O_2, and 0.45 g/L 5AVA and 0.24 g/L δ-valerolactam in pH 7.0 and 5 mM H_2O_2, respectively. The specific activity of RaiP was 5.14 units/mg. These results demonstrated the feasibility of the coproduction of 5AVA and δ-valerolactam in *E. coli*. In addition, the strain ML03-raiP with cadA knocked out was constructed. The engineered strain ML03-*raiP* produced 0.58 g/L 5AVA and 0.29 g/L δ-valerolactam, nearly about 0.29-fold and 0.21-fold increase compared to control strain BL21-raiP at pH 7.0 and 5 mM H_2O_2 (**Figure 2**).

In the past, some studies of the concurrent bioproduction of bulk chemicals were investigated (Li et al., 2017). Few examples are the simultaneous synthesis of 5AVA and glutarate by *Corynebacterium glutamicum* (Rohles et al., 2016; Haupka et al., 2020), β-glucan and pullulan by engineering *Aureobasidium pullulans* (Wang G.-L. et al., 2020), acetoin and succinic acid by *Enterobacter cloacae* (Su et al., 2021), polyhydroxyalkanoates and exopolysaccharides by *Yangia* sp. ND199 (Romero Soto et al., 2021), and xylitol and ethanol by yeast strains (Shankar et al., 2020). Lopez-Hidalgo et al. reported that the engineered strain increased 30% the coproduction of ethanol and hydrogen used wheat straw and corn stover as feedstock (Lopez-Hidalgo et al., 2021). And 11.0 g/L polyhydroxybutyrate and 1.5 g/L violacein pigment were successfully co-synthesized in *Iodobacter* sp. PCH194 (Kumar et al., 2021). 7,12-dioxolithocholate and L-*tert*-leucine were simultaneously produced in a cofactor self-sufficient cascade system for enhancing the atom efficiency (You et al., 2021). Chae et al. found that only 29 mg/L δ-valerolactam was produced by β-alanine CoA transferase (Chae et al., 2017). Xu et al. reported that 90.3 mg/L δ-valerolactam was successfully obtained by an oxidative decarboxylase DavB (Xu et al., 2020). However, the low titers limit the prospect of industrial application.

The Effect of H_2O_2 on the Simultaneous Synthesis of 5-Aminovalerate and δ-Valerolactam

The effect of H_2O_2 on the simultaneous synthesis of 5AVA and δ-valerolactam in engineering strain ML03-*raiP-katE* at pH 7.0 is shown in **Figure 3**. It showed that the addition of H_2O_2 had a significant effect on the titers of 5AVA and δ-valerolactam. Engineering *E. coli* ML03-*raiP-katE* was cultured in LB medium to form an equilibrium mixture containing P2C, 2HP2C, ^{2}P2C, 2K6AC, 6A2HH2E, and 6A2DHC. At 5 mM H_2O_2 addition, recombinant ML03-*raiP-katE* produced 0.58 g/L 5AVA and 0.29 g/L δ-valerolactam after 24 h, respectively, increased about 0.87-fold and 2.22-fold compared to the control group without H_2O_2. With the continuous increase in H_2O_2 concentration to 10 mM, the titers of 5AVA and δ-valerolactam both were further increased to 0.96 g/L 5AVA and 0.42 g/L δ-valerolactam, with a yield increase of 2.13-fold and 3.67-fold compared to the control without H_2O_2 addition, respectively. However, with the increase in H_2O_2 concentration to 15 mM, the titers of 5AVA and δ-valerolactam decreased dramatically (**Figure 3**).

H_2O_2 is an important reactive oxygen species in organisms and is produced in response to signal transduction, growth, and development (Oldroyd, 2013; Sies and Jones, 2020). H_2O_2 enters cells to regulate signaling and cellular processes through aquaporin membrane proteins and covalently modifies cytoplasmic proteins (Sies and Jones, 2020). Wu et al. found that H_2O_2 sensor HPCAI is a receptor kinase (Wu et al., 2020). However, excess of H_2O_2 could inhibit cell growth and affect the production of target compounds, resulting in low OD_{600} (Cheng et al., 2018b). Therefore, in this study, a strategy was proposed that the H_2O_2 produced by RaiP was decomposed by overexpression of catalase in *E. coli* in the early stage, and then H_2O_2 was added in the later stage to produce 5AVA and δ-valerolactam. The specific activity of KatE was 23.58 units/mg. The H_2O_2 that is generated by RaiP can affect the cell growth and the titers of products (Cheng et al., 2021b). The coexpression of RaiP and KatE in *E. coli* might provide a more convenient and effective method for the production of 5AVA and δ-valerolactam. As shown in **Supplementary Figure S1**, the coexpressed *E. coli* BL21 (DE3) strain harboring pET21a-*raiP-katE* showed another distinct 84-kDa band on SDS-PAGE, which was consistent with the calculated molecular weight of catalase.

The Effect of pH on the Ratio of 5-Aminovalerate and δ-Valerolactam

The effect of pH on the ratio of 5AVA and δ-valerolactam in engineering strain ML03-*raiP-katE* with 10 mM H_2O_2 addition is shown in **Table 3**. It showed that the pH had a great effect on the ratio of 5AVA and δ-valerolactam; 1.12 g/L 5AVA and 0.25 g/L δ-valerolactam were generated at pH 5.0 after adding H_2O_2 for 12 h. The maximum ratio of 5AVA and δ-valerolactam was

TABLE 3 | Effect of pH on the ratio of 5AVA and δ-valerolactam in ML03-*raiP-katE*. Data are presented as means ± STDV calculated from three replicate biotransformation experiments. Statistics were performed by the two-tailed Student's *t*-test. *$p < 0.05$; ns, not significant.

pH	Time (h)	5AVA production (g/L)	Statistical analysis[a]	δ-Valerolactam (g/L)	Statistical analysis[a]	Ratio of 5AVA and δ-valerolactam
5.0	12	0.24 ± 0.02	—	0.07 ± 0.01	—	3.42:1
	24	1.12 ± 0.07	—	0.25 ± 0.03	—	4.48:1
6.0	12	0.28 ± 0.03	ns	0.09 ± 0.01	ns	3.11:1
	24	1.08 ± 0.04	ns	0.33 ± 0.03	ns	3.27:1
7.0	12	0.31 ± 0.03	ns	0.09 ± 0.01	ns	3.44:1
	24	0.96 ± 0.04	*	0.42 ± 0.03	*	2.29:1
8.0	12	0.30 ± 0.03	ns	0.08 ± 0.01	ns	3.75:1
	24	0.92 ± 0.05	ns	0.56 ± 0.04	*	1.64:1
9.0	12	0.27 ± 0.02	ns	0.06 ± 0.01	ns	4.50:1
	24	0.68 ± 0.05	*	0.75 ± 0.05	*	0.91:1

[a]*Statistical analysis of the 5AVA production was performed with every two separated lines. 6.5 g/L L-lys HCl and 0.2 mM IPTG were added. 10 mM H_2O_2 was added after 12 h.*

reached 4.48:1 at pH 5.0. With the increase in pH, the titer of δ-valerolactam increased gradually, resulting in a decrease in the ratio of 5AVA and δ-valerolactam; 1.08 g/L 5AVA and 0.33 g/L δ-valerolactam were obtained at pH 6.0. When the pH value was 7.0, recombinant ML03-*raiP-katE* could produce 0.96 g/L 5AVA and 0.42 g/L δ-valerolactam after 24 h from the equilibrium mixture. In addition, the titer of δ-valerolactam increased significantly to 0.56 g/L at pH 8.0, with a titer increase of 0.33-fold compared with pH 7.0. Interestingly, the titer of δ-valerolactam was higher than 5AVA at pH 9.0, and the ratio of 5AVA and δ-valerolactam was 0.91. As a result, the flux of the equilibrium mixture would shift to 5AVA under acidic condition and to δ-valerolactam under alkaline condition. These findings are consistent with Kamio's research (Kamio et al., 2009). However, their specific ratio has not been reported (Ko et al., 2008; Kamio et al., 2009).

Biotransformation for the Coproduction of 5-Aminovalerate and δ-Valerolactam

Time profiles for the simultaneous synthesis of 5AVA and δ-valerolactam were investigated by biotransformation of engineered strain ML03-*raiP-katE* at pH 5.0 (**Figure 4A**) and pH 9.0 (**Figure 4B**) in a 5-L fermenter. The catalase KatE was overexpressed to remove H_2O_2, which significantly improved OD_{600} and the titer of products in the 5-L fermenter (Cheng et al., 2021b). The titers of 5AVA and δ-valerolactam were very low before the addition of H_2O_2. In this process, the main accumulation was the equilibrium mixture produced by RaiP from lysine. Although H_2O_2 was produced by RaiP, its low concentration leads to low production of 5AVA and δ-valerolactam. After adding H_2O_2 for 12 h, the titers of 5AVA and δ-valerolactam increased significantly to 8.88 and 1.56 g/L at pH 5.0. Finally, 10.24 g/L 5AVA and 1.82 g/L δ-valerolactam were obtained, with a total molar yield of 0.52 mol/mol lysine, and its ratio was 5.63:1 at pH 5.0. The difference was that the titers of 5AVA and δ-valerolactam were 3.42 and 5.12 g/L after adding H_2O_2 for 12 h at pH 9.0. Finally, 3.98 g/L 5AVA and 6.88 g/L δ-valerolactam were obtained, with a total molar yield of 0.51 mol/mol lysine, and its ratio was 0.58:1 at pH 9.0. The previous results showed that the ratio of 5AVA and δ-valerolactam was significantly regulated by pH. δ-Valerolactam would be the main component in alkaline condition.

We have previously reported the production of 5AVA by overexpression of RaiP, but the titer and change in δ-valerolactam were not noticed in this process. At the same time, the addition of ethanol improved the expression level of RaiP, which increases the cost and leads to uneconomical (Cheng et al., 2018b; Cheng et al., 2020; Cheng et al., 2021a). Xu et al. reported that the expression of DavB from *P. putida* could synthesize 90.3 mg/L of δ-valerolactam from L-pipecolic acid (Xu et al., 2020). Interestingly, the coexpression of RaiP, glucose dehydrogenase GDH, P2C reductase DpkA, and LysP could produce more δ-valerolactam from lysine, up to 242 mg/L (Xu et al., 2020). This may be due to the fact that part of δ-valerolactam does not originate from the oxidative decarboxylation of L-pipecolic acid but from this equilibrium mixture in this study. Compared with other biotransformation for production of 5AVA, the advantage in this study was to realize the simultaneous synthesis of 5AVA and δ-valerolactam. In terms of biotransformation mechanism, the simultaneous synthesis of 5AVA and δ-valerolactam mainly includes two steps: 1) the formation of an equilibrium mixture by RaiP from lysine and 2) the oxidization of the equilibrium mixture to 5AVA and δ-valerolactam by H_2O_2 at different pH values.

CONCLUSION

Many important monomers of polyamides, such as adipate, cadaverine, and 3-hydroxybutyrate, have been extensively studied in microbes. The results presented here demonstrated that engineering *E. coli* also has the potential to be used as a promising alternative to produce monomers of polyamides derived from petrochemicals. In this study, the strategy for coproducing 5AVA and δ-valerolactam by adjusting the pH and H_2O_2 in *E. coli* was proposed. H_2O_2 was regulated to improve the synthesis efficiency of δ-valerolactam in *E. coli* in different

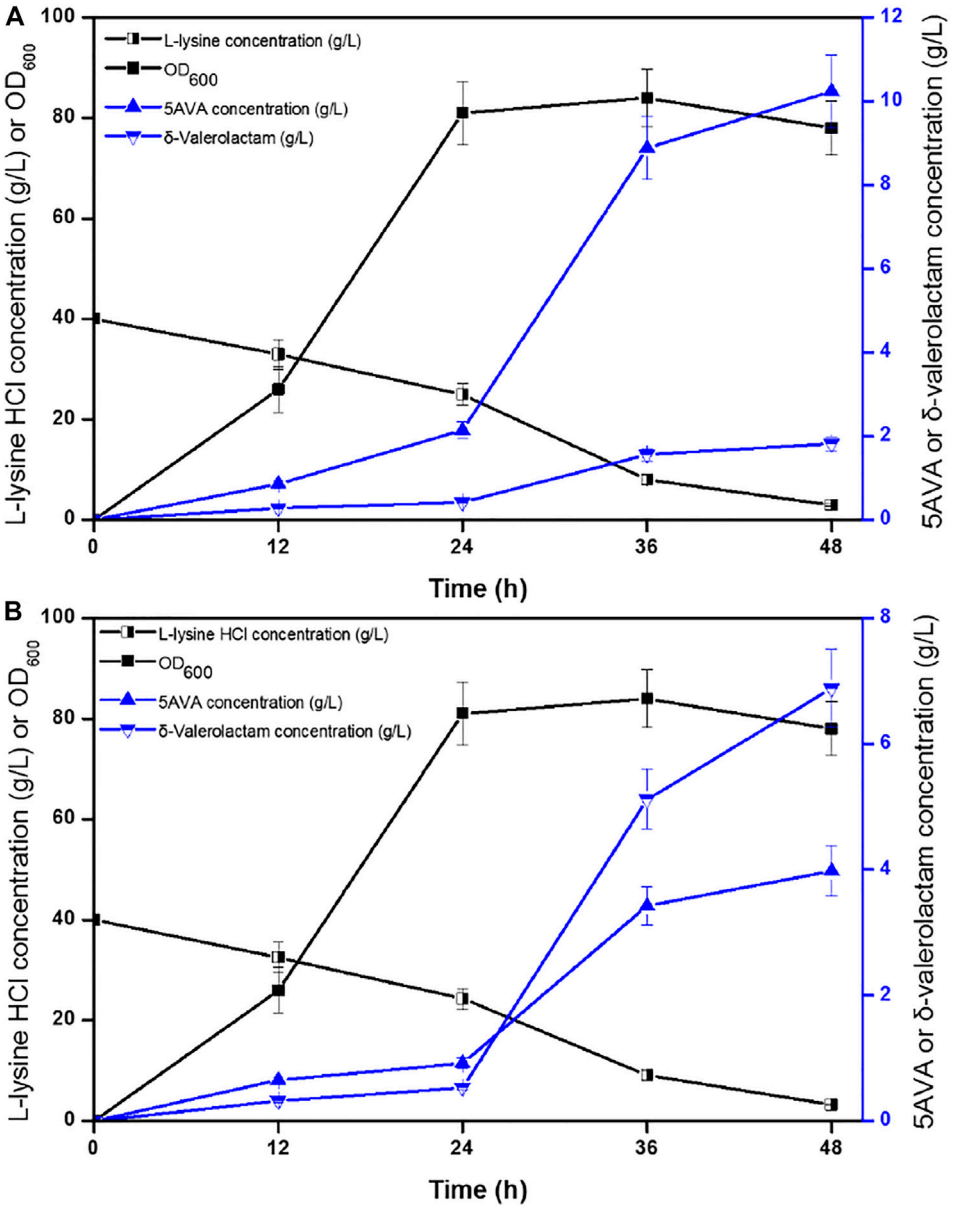

FIGURE 4 | Time profiles of 5AVA and δ-valerolactam production were investigated by biotransformation of engineered strain ML03-*raiP-katE* at pH 5.0 **(A)** or pH 9.0 **(B)** in a 5-L fermenter. The experiments were conducted at 40 g/L L-lysine HCl, 37°C and 250 rpm. 10 mM H_2O_2 was added after reaction 24 h. All experiments were performed a minimum of three independent sets.

pH environments, which also increased 5AVA accumulation. The ratio of 5AVA and δ-valerolactam was significantly affected by pH value. δ-Valerolactam would be the main component in alkaline condition. The titers of 5-aminovalerate and δ-valerolactam reached 3.98 and 6.88 g/L from 40 g/L L-lysine HCl at pH 9.0, with a total yield of 0.51 mol/mol lysine. The present findings indicated a promising strategy for the simultaneous synthesis of two commercial products in a single biotransformation step. These strategies could be widely applied for sustainable production of many commercially monomers of polyamides.

DATA AVAILABILITY STATEMENT

The original contributions presented in the study are included in the article/**Supplementary Material**; further inquiries can be directed to the corresponding authors.

AUTHOR CONTRIBUTIONS

JC, WT, and ZL performed the experiments and analyzed the data. LL, XG, and XW analyzed data. JC and CL drafted the

manuscript. JC, CL, and GZ coordinated the study and finalized the manuscript.

FUNDING

This work was financially supported by the National Key Research and Development Program of China (2019YFA0904900); the National Natural Science Foundation of China (2210081508); the Open Funding Project of Key Laboratory of Industrial Biotechnology, Ministry of Education, Jiangnan University (KLIB-KF202103); the Natural Science Foundation of Jiangsu Province (BK20190607); the Open Funding Project of the Key Laboratory of Medicinal and Edible Plants Resources Development of Sichuan Education Department (10Y202105).

SUPPLEMENTARY MATERIAL

The Supplementary Material for this article can be found online at: https://www.frontiersin.org/articles/10.3389/fbioe.2021.726126/full#supplementary-material

REFERENCES

Adkins, J., Jordan, J., and Nielsen, D. R. (2013). EngineeringEscherichia Colifor Renewable Production of the 5-carbon Polyamide Building-Blocks 5-aminovalerate and Glutarate. *Biotechnol. Bioeng.* 110 (6), 1726–1734. doi:10.1002/bit.24828

Atakav, Y., Pinar, O., and Kazan, D. (2021). Investigation of the Physiology of the Obligate Alkaliphilic Bacillus Marmarensis GMBE 72T Considering its Alkaline Adaptation Mechanism for Poly(3-Hydroxybutyrate) Synthesis. *Microorganisms* 9 (2), 462. doi:10.3390/microorganisms9020462

Ben Abdallah, M., Karray, F., and Sayadi, S. (2020). Production of Polyhydroxyalkanoates by Two Halophilic Archaeal Isolates from Chott El Jerid Using Inexpensive Carbon Sources. *Biomolecules* 10 (1), 109. doi:10.3390/biom10010109

Chae, T. U., Ko, Y.-S., Hwang, K.-S., and Lee, S. Y. (2017). Metabolic Engineering of *Escherichia coli* for the Production of Four-, Five- and Six-Carbon Lactams. *Metab. Eng.* 41, 82–91. doi:10.1016/j.ymben.2017.04.001

Cheng, J., Luo, Q., Duan, H., Peng, H., Zhang, Y., Hu, J., et al. (2020). Efficient Whole-Cell Catalysis for 5-aminovalerate Production from L-Lysine by Using Engineered *Escherichia coli* with Ethanol Pretreatment. *Sci. Rep.* 10 (1), 990. doi:10.1038/s41598-020-57752-x

Cheng, J., Huang, Y., Mi, L., Chen, W., Wang, D., and Wang, Q. (2018a). An Economically and Environmentally Acceptable Synthesis of Chiral Drug Intermediate L-Pipecolic Acid from Biomass-Derived Lysine via Artificially Engineered Microbes. *J. Ind. Microbiol. Biot* 45, 405–415. doi:10.1007/s10295-018-2044-2

Cheng, J., Luo, Q., Ren, Y., Luo, Z., Liao, W., Wang, X., et al. (2021a). Panorama of Intron Dynamics and Gene Rearrangements in the Phylum Basidiomycota as Revealed by the Complete Mitochondrial Genome of *Turbinellus Floccosus*. *Appl. Microbiol. Biotechnol.* 105 (5), 2017–2032. doi:10.1007/s00253-021-11153-w

Cheng, J., Tu, W., Luo, Z., Gou, X., Li, Q., Wang, D., et al. (2021b). A High-Efficiency Artificial Synthetic Pathway for 5-aminovalerate Production from Biobased L-Lysine in *Escherichia coli*. *Front. Bioeng. Biotechnol.* 9, 633028. doi:10.3389/fbioe.2021.633028

Cheng, J., Zhang, Y., Huang, M., Chen, P., Zhou, X., Wang, D., et al. (2018b). Enhanced 5-aminovalerate Production in *Escherichia coli* from L -lysine with Ethanol and Hydrogen Peroxide Addition. *J. Chem. Technol. Biotechnol.* 93 (12), 3492–3501. doi:10.1002/jctb.5708

Gao, S., Xu, X., Zeng, W., Xu, S., Lyv, Y., Feng, Y., et al. (2020). Efficient Biosynthesis of (2S)-Eriodictyol from (2S)-Naringenin in *Saccharomyces cerevisiae* through a Combination of Promoter Adjustment and Directed Evolution. *ACS Synth. Biol.* 9 (12), 3288–3297. doi:10.1021/acssynbio.0c00346

Gordillo Sierra, A. R., and Alper, H. S. (2020). Progress in the Metabolic Engineering of Bio-Based Lactams and Their ω-amino Acids Precursors. *Biotechnol. Adv.* 43, 107587. doi:10.1016/j.biotechadv.2020.107587

Harada, K., Kobayashi, S., Oshima, K., Yoshida, S., Tsuge, T., and Sato, S. (2021). Engineering of Aeromonas Caviae Polyhydroxyalkanoate Synthase through Site-Directed Mutagenesis for Enhanced Polymerization of the 3-Hydroxyhexanoate Unit. *Front. Bioeng. Biotechnol.* 9, 627082. doi:10.3389/fbioe.2021.627082

Haupka, C., Delépine, B., Irla, M., Heux, S., and Wendisch, V. F. (2020). Flux Enforcement for Fermentative Production of 5-aminovalerate and Glutarate by Corynebacterium Glutamicum. *Catalysts* 10 (9), 1065. doi:10.3390/catal10091065

Joo, J. C., Oh, Y. H., Yu, J. H., Hyun, S. M., Khang, T. U., Kang, K. H., et al. (2017). Production of 5-aminovaleric Acid in Recombinant *Corynebacterium Glutamicum* Strains from a Miscanthus Hydrolysate Solution Prepared by a Newly Developed Miscanthus Hydrolysis Process. *Bioresour. Technol.* 245 (Pt B), 1692–1700. doi:10.1016/j.biortech.2017.05.131

Jorge, J. M. P., Pérez-García, F., and Wendisch, V. F. (2017). A New Metabolic Route for the Fermentative Production of 5-aminovalerate from Glucose and Alternative Carbon Sources. *Bioresour. Technol.* 245 (Pt B), 1701–1709. doi:10.1016/j.biortech.2017.04.108

Kamio, M., Ko, K.-C., Zheng, S., Wang, B., Collins, S. L., Gadda, G., et al. (2009). The Chemistry of Escapin: Identification and Quantification of the Components in the Complex Mixture Generated by an L-Amino Acid Oxidase in the Defensive Secretion of the Sea SnailAplysia Californica. *Chem. Eur. J.* 15 (7), 1597–1603. doi:10.1002/chem.200801696

Klenk, J. M., Ertl, J., Rapp, L., Fischer, M.-P., and Hauer, B. (2020). Expression and Characterization of the Benzoic Acid Hydroxylase CYP199A25 from *Arthrobacter Sp. Mol. Catal.* 484, 110739. doi:10.1016/j.mcat.2019.110739

Ko, K.-C., Wang, B., Tai, P. C., and Derby, C. D. (2008). Identification of Potent Bactericidal Compounds Produced by Escapin, an L -Amino Acid Oxidase in the Ink of the Sea Hare *Aplysia californica*. *Antimicrob. Agents Chemother.* 52 (12), 4455–4462. doi:10.1128/aac.01103-08

Kumar, V., Darnal, S., Kumar, S., Kumar, S., and Singh, D. (2021). Bioprocess for Co-production of Polyhydroxybutyrate and Violacein Using Himalayan Bacterium Iodobacter Sp. PCH194. *Bioresour. Technol.* 319, 124235. doi:10.1016/j.biortech.2020.124235

Li, L., Zou, D., Ji, A., He, Y., Liu, Y., Deng, Y., et al. (2020). Multilevel Metabolic Engineering of Bacillus Amyloliquefaciens for Production of the Platform Chemical Putrescine from Sustainable Biomass Hydrolysates. *ACS Sustain. Chem. Eng.* 8 (5), 2147–2157. doi:10.1021/acssuschemeng.9b05484

Li, T., Elhadi, D., and Chen, G.-Q. (2017). Co-production of Microbial Polyhydroxyalkanoates with Other Chemicals. *Metab. Eng.* 43 (Pt A), 29–36. doi:10.1016/j.ymben.2017.07.007

Li, Z., Xu, J., Jiang, T., Ge, Y., Liu, P., Zhang, M., et al. (2016). Overexpression of Transport Proteins Improves the Production of 5-aminovalerate from L-Lysine in *Escherichia coli*. *Sci. Rep.* 6, 30884. doi:10.1038/srep30884

Ligon, S. C., Liska, R., Stampfl, J., Gurr, M., and Mülhaupt, R. (2017). Polymers for 3D Printing and Customized Additive Manufacturing. *Chem. Rev.* 117 (15), 10212–10290. doi:10.1021/acs.chemrev.7b00074

Liu, Q., Ma, X., Cheng, H., Xu, N., Liu, J., and Ma, Y. (2017). Co-expression of L-Glutamate Oxidase and Catalase in *Escherichia coli* to Produce α-ketoglutaric Acid by Whole-Cell Biocatalyst. *Biotechnol. Lett.* 39 (6), 913–919. doi:10.1007/s10529-017-2314-5

Lopez-Hidalgo, A. M., Magaña, G., Rodriguez, F., De Leon-Rodriguez, A., and Sanchez, A. (2021). Co-production of Ethanol-Hydrogen by Genetically Engineered *Escherichia coli* in Sustainable Biorefineries for Lignocellulosic Ethanol Production. *Chem. Eng. J.* 406, 126829. doi:10.1016/j.cej.2020.126829

Mierziak, J., Burgberger, M., and Wojtasik, W. (2021). 3-Hydroxybutyrate as a Metabolite and a Signal Molecule Regulating Processes of Living Organisms. *Biomolecules* 11 (3), 402. doi:10.3390/biom11030402

Oldroyd, G. E. D. (2013). Speak, Friend, and Enter: Signalling Systems that Promote Beneficial Symbiotic Associations in Plants. *Nat. Rev. Microbiol.* 11 (4), 252–263. doi:10.1038/nrmicro2990

Osire, T., Yang, T., Xu, M., Zhang, X., Long, M., Ngon, N. K. a., et al. (2021). Integrated Gene Engineering Synergistically Improved Substrate-Product Transport, Cofactor Generation and Gene Translation for Cadaverine Biosynthesis in *E. coli*. *Int. J. Biol. Macromolecules* 169, 8–17. doi:10.1016/j.ijbiomac.2020.12.017

Park, S. J., Kim, E. Y., Noh, W., Park, H. M., Oh, Y. H., Lee, S. H., et al. (2013). Metabolic Engineering of *Escherichia coli* for the Production of 5-aminovalerate and Glutarate as C5 Platform Chemicals. *Metab. Eng.* 16, 42–47. doi:10.1016/j.ymben.2012.11.011

Prell, C., Burgardt, A., Meyer, F., and Wendisch, V. F. (2020). Fermentative Production of L-2-Hydroxyglutarate by Engineered *Corynebacterium Glutamicum* via Pathway Extension of L-Lysine Biosynthesis. *Front. Bioeng. Biotechnol.* 8, 630476. doi:10.3389/fbioe.2020.630476

Pukin, A. V., Boeriu, C. G., Scott, E. L., Sanders, J. P. M., and Franssen, M. C. R. (2010). An Efficient Enzymatic Synthesis of 5-aminovaleric Acid. *J. Mol. Catal. B: Enzym* 65 (1-4), 58–62. doi:10.1016/j.molcatb.2009.12.006

Radzik, P., Leszczyńska, A., and Pielichowski, K. (2019). Modern Biopolyamide-Based Materials: Synthesis and Modification. *Polym. Bull.* 77 (1), 501–528. doi:10.1007/s00289-019-02718-x

Rohles, C. M., Giesselmann, G., Kohlstedt, M., Wittmann, C., and Becker, J. (2016). Systems Metabolic Engineering of *Corynebacterium Glutamicum* for the Production of the Carbon-5 Platform Chemicals 5-aminovalerate and Glutarate. *Microb. Cel Fact* 15 (1), 154. doi:10.1186/s12934-016-0553-0

Romero Soto, L., Thabet, H., Maghembe, R., Gameiro, D., Van-Thuoc, D., Dishisha, T., et al. (2021). Metabolic Potential of the Moderate Halophile Yangia Sp. ND199 for Co-production of Polyhydroxyalkanoates and Exopolysaccharides. *Microbiologyopen* 10 (1), e1160. doi:10.1002/mbo3.1160

Rui, J., You, S., Zheng, Y., Wang, C., Gao, Y., Zhang, W., et al. (2020). High-efficiency and Low-Cost Production of Cadaverine from a Permeabilized-Cell Bioconversion by a Lysine-Induced Engineered *Escherichia coli*. *Bioresour. Technol.* 302, 122844. doi:10.1016/j.biortech.2020.122844

Sasikumar, K., Hannibal, S., Wendisch, V. F., and Nampoothiri, K. M. (2021). Production of Biopolyamide Precursors 5-Amino Valeric Acid and Putrescine from Rice Straw Hydrolysate by Engineered *Corynebacterium Glutamicum*. *Front. Bioeng. Biotechnol.* 9, 635509. doi:10.3389/fbioe.2021.635509

Schmid, M., Raschbauer, M., Song, H., Bauer, C., and Neureiter, M. (2021). Effects of Nutrient and Oxygen Limitation, Salinity and Type of Salt on the Accumulation of Poly(3-Hydroxybutyrate) in *Bacillus Megaterium* Uyuni S29 with Sucrose as a Carbon Source. *New Biotechnol.* 61, 137–144. doi:10.1016/j.nbt.2020.11.012

Shankar, K., Kulkarni, N. S., Sajjanshetty, R., Jayalakshmi, S. K., and Sreeramulu, K. (2020). Co-production of Xylitol and Ethanol by the Fermentation of the Lignocellulosic Hydrolysates of Banana and Water Hyacinth Leaves by Individual Yeast Strains. *Ind. Crops Prod.* 155, 112809. doi:10.1016/j.indcrop.2020.112809

Shin, J. H., Park, S. H., Oh, Y. H., Choi, J. W., Lee, M. H., Cho, J. S., et al. (2016). Metabolic Engineering of *Corynebacterium Glutamicum* for Enhanced Production of 5-aminovaleric Acid. *Microb. Cel Fact* 15 (1), 174. doi:10.1186/s12934-016-0566-8

Sies, H., and Jones, D. P. (2020). Reactive Oxygen Species (ROS) as Pleiotropic Physiological Signalling Agents. *Nat. Rev. Mol. Cel Biol* 21 (7), 363–383. doi:10.1038/s41580-020-0230-3

Su, H.-Y., Li, H.-Y., Xie, C.-Y., Fei, Q., and Cheng, K.-K. (2021). Co-production of Acetoin and Succinic Acid by Metabolically Engineered *Enterobacter cloacae*. *Biotechnol. Biofuels* 14 (1), 26. doi:10.1186/s13068-021-01878-1

Thompson, M. G., Pearson, A. N., Barajas, J. F., Cruz-Morales, P., Sedaghatian, N., Costello, Z., et al. (2020). Identification, Characterization, and Application of a Highly Sensitive Lactam Biosensor from *Pseudomonas Putida*. *ACS Synth. Biol.* 9 (1), 53–62. doi:10.1021/acssynbio.9b00292

Tian, L., Zhou, J., Yang, T., Zhang, X., Xu, M., and Rao, Z. (2021). Cascade Biocatalysis for Production of Enantiopure (S)-2-hydroxybutyric Acid Using Recombinant *Escherichia coli* with a Tunable Multi-Enzyme-Coordinate Expression System. *Syst. Microbiol. Biomanuf* 1 (2), 234–244. doi:10.1007/s43393-020-00021-9

Turk, S. C. H. J., Kloosterman, W. P., Ninaber, D. K., Kolen, K. P. A. M., Knutova, J., Suir, E., et al. (2016). Metabolic Engineering toward Sustainable Production of Nylon-6. *ACS Synth. Biol.* 5 (1), 65–73. doi:10.1021/acssynbio.5b00129

Wang, A., Duncan, S. E., Whalley, N. W., and O'Keefe, S. F. (2020). Interaction Effect of LED Color Temperatures and Light-Protective Additive Packaging on Photo-Oxidation in Milk Displayed in Retail Dairy Case. *Food Chem.* 323, 126699. doi:10.1016/j.foodchem.2020.126699

Wang, F., Zhao, J., Li, Q., Yang, J., Li, R., Min, J., et al. (2020). One-pot Biocatalytic Route from Cycloalkanes to α,ω-dicarboxylic Acids by Designed *Escherichia coli* Consortia. *Nat. Commun.* 11 (1), 5035. doi:10.1038/s41467-020-18833-7

Wang, G.-L., Din, A. U., Qiu, Y.-S., Wang, C.-L., Wang, D.-H., and Wei, G.-Y. (2020c). Triton X-100 Improves Co-production of β-1,3-D-glucan and Pullulan by Aureobasidium Pullulans. *Appl. Microbiol. Biotechnol.* 104 (24), 10685–10696. doi:10.1007/s00253-020-10992-3

Wang, X., Cai, P., Chen, K., and Ouyang, P. (2016). Efficient Production of 5-aminovalerate from L -lysine by Engineered *Escherichia coli* Whole-Cell Biocatalysts. *J. Mol. Catal. B: Enzymatic* 134, 115–121. doi:10.1016/j.molcatb.2016.10.008

Wendisch, V. F. (2020). Metabolic Engineering Advances and Prospects for Amino Acid Production. *Metab. Eng.* 58, 17–34. doi:10.1016/j.ymben.2019.03.008

Wu, F., Chi, Y., Jiang, Z., Xu, Y., Xie, L., Huang, F., et al. (2020). Hydrogen Peroxide Sensor HPCA1 Is an LRR Receptor Kinase in *Arabidopsis*. *Nature* 578 (7796), 577–581. doi:10.1038/s41586-020-2032-3

Xu, Y., Zhou, D., Luo, R., Yang, X., Wang, B., Xiong, X., et al. (2020). Metabolic Engineering of *Escherichia coli* for Polyamides Monomer δ-valerolactam Production from Feedstock Lysine. *Appl. Microbiol. Biotechnol.* 104 (23), 9965–9977. doi:10.1007/s00253-020-10939-8

Xue, Y., Zhao, Y., Ji, X., Yao, J., Busk, P. K., Lange, L., et al. (2020). Advances in Bio-Nylon 5X: Discovery of New Lysine Decarboxylases for the High-Level Production of Cadaverine. *Green. Chem.* 22 (24), 8656–8668. doi:10.1039/d0gc03100c

You, Z.-N., Zhou, K., Han, Y., Yang, B.-Y., Chen, Q., Pan, J., et al. (2021). Design of a Self-Sufficient Hydride-Shuttling cascade for Concurrent Bioproduction of 7,12-dioxolithocholate and L-Tert-Leucine. *Green. Chem.* 23, 4125–4133. doi:10.1039/d1gc01120k

Youn, J.-W., Albermann, C., and Sprenger, G. A. (2020). *In Vivo* cascade Catalysis of Aromatic Amino Acids to the Respective Mandelic Acids Using Recombinant *E. coli* Cells Expressing Hydroxymandelate Synthase (HMS) from Amycolatopsis Mediterranei. *Mol. Catal.* 483, 110713. doi:10.1016/j.mcat.2019.110713

Zhang, J., Barajas, J. F., Burdu, M., Ruegg, T. L., Dias, B., and Keasling, J. D. (2017a). Development of a Transcription Factor-Based Lactam Biosensor. *ACS Synth. Biol.* 6 (3), 439–445. doi:10.1021/acssynbio.6b00136

Zhang, J., Barajas, J. F., Burdu, M., Wang, G., Baidoo, E. E., and Keasling, J. D. (2017b). Application of an Acyl-CoA Ligase from *Streptomyces Aizunensis* for Lactam Biosynthesis. *ACS Synth. Biol.* 6 (5), 884–890. doi:10.1021/acssynbio.6b00372

Zhang, J., Kao, E., Wang, G., Baidoo, E. E. K., Chen, M., and Keasling, J. D. (2016). Metabolic Engineering of *Escherichia coli* for the Biosynthesis of 2-pyrrolidone. *Metab. Eng. Commun.* 3, 1–7. doi:10.1016/j.meteno.2015.11.001

Zhang, S., Fang, Y., Zhu, L., Li, H., Wang, Z., Li, Y., et al. (2021). Metabolic Engineering of *Escherichia coli* for Efficient Ectoine Production. *Syst. Microbiol. Biomanufacturing*. doi:10.1007/s43393-021-00031-1

Zhang, X., Jantama, K., Moore, J. C., Jarboe, L. R., Shanmugam, K. T., and Ingram, L. O. (2009). Metabolic Evolution of Energy-Conserving Pathways for Succinate Production in *Escherichia coli*. *Proc. Natl. Acad. Sci.* 106 (48), 20180–20185. doi:10.1073/pnas.0905396106

Zhao, M., Li, G., and Deng, Y. (2018). Engineering *Escherichia coli* for Glutarate Production as the C5 Platform Backbone. *Appl. Environ. Microbiol.* 84 (16), e00814–18. doi:10.1128/AEM.00814-18

Conflict of Interest: The authors declare that the research was conducted in the absence of any commercial or financial relationships that could be construed as a potential conflict of interest.

Publisher's Note: All claims expressed in this article are solely those of the authors and do not necessarily represent those of their affiliated organizations, or those of the publisher, the editors, and the reviewers. Any product that may be evaluated in this article, or claim that may be made by its manufacturer, is not guaranteed or endorsed by the publisher.

Advantages of publishing in Frontiers

OPEN ACCESS
Articles are free to read for greatest visibility and readership

FAST PUBLICATION
Around 90 days from submission to decision

HIGH QUALITY PEER-REVIEW
Rigorous, collaborative, and constructive peer-review

TRANSPARENT PEER-REVIEW
Editors and reviewers acknowledged by name on published articles

Frontiers
Avenue du Tribunal-Fédéral 34
1005 Lausanne | Switzerland

Visit us: www.frontiersin.org
Contact us: frontiersin.org/about/contact

REPRODUCIBILITY OF RESEARCH
Support open data and methods to enhance research reproducibility

DIGITAL PUBLISHING
Articles designed for optimal readership across devices

FOLLOW US
@frontiersin

IMPACT METRICS
Advanced article metrics track visibility across digital media

EXTENSIVE PROMOTION
Marketing and promotion of impactful research

LOOP RESEARCH NETWORK
Our network increases your article's readership